Proceedings of the First MCEER Workshop on Mitigation of Earthquake Disaster by Advanced Technologies [MEDAT-1]

Edited by

M. Shinozuka
Department of Civil Engineering
University of Southern California

D.J. Inman
Mechanical Engineering Department
Virginia Polytechnic Institute and
State University

T.D. O'Rourke
School of Civil and Environmental
Engineering
Cornell University

MCEER
MULTIDISCIPLINARY CENTER FOR EARTHQUAKE ENGINEERING RESEARCH
A National Center of Excellence in Advanced Technology Applications

ISSN 1520-295X

Technical Report MCEER-00-0009
November 10, 2000

This workshop was held March 2-3, 2000 at the Radisson Hotel, Los Angeles, California, and was supported primarily by the Earthquake Engineering Research Centers Program of the National Science Foundation under Award number EEC-9701471.

NOTICE

This report was prepared by the University of Sourhern California, the Virginia Polytechnic Institute and State University, and Cornell University as a result of research sponsored by the Multidisciplinary Center for Earthquake Engineering Research (MCEER) through a grant from the Earthquake Engineering Research Centers Program of the National Science Foundation and other sponsors. Neither MCEER, associates of MCEER, its sponsors, [University], nor any person acting on their behalf:

a. makes any warranty, express or implied, with respect to the use of any information, apparatus, method, or process disclosed in this report or that such use may not infringe upon privately owned rights; or

b. assumes any liabilities of whatsoever kind with respect to the use of, or the damage resulting from the use of, any information, apparatus, method, or process disclosed in this report.

Any opinions, findings, and conclusions or recommendations expressed in this publication are those of the author(s) and do not necessarily reflect the views of MCEER, the National Science Foundation, or other sponsors.

Cover Photo/Illustration Credits

Landsat 5 Image of Izmit Bay taken on August 19, 1999, following the August 17, 1999 Marmara, Turkey earthquake. Note the fire and smoke plume originating from the Tupras Refinery, seen at the center of the figure. Image provided to EQE International by the European Space Agency under a cooperative research agreement established for this earthquake. Image details: RGB mapping of 721, replacing the red band with the far infrared band. A Gaussian filter was applied to maximize visibility of the smoke. Image taken from "The Marmara Earthquake: A View From Space" by R. T. Eguchi, C.K. Huyck, B. Houshmand, B. Mansouri, M. Shinozuka, F. Yamazaki, M. Matsuoka and S. Ulgen, pages 181-200.

City of Los Angeles Water System Pressure Zones taken from "Water Services Organization SCADA System" by James B. McDaniel, James G. Yannotta and Hampik Dekermenjian, pages 145-153.

SPOT/XS Band 3 satellite image of the Santo Thomas area after the Luzon earthquake, taken from "Remote Sensing Technologies for Earthquake Damage Detection: Examples for Kobe, Japan and Luzon, the Phillipines" by Masashi Matsuoka and Fumio Yamazaki, pages 201-210.

Proceedings of the First MCEER Workshop on Mitigation of Earthquake Disaster by Advanced Technologies (MEDAT-1)

Held at
Radisson Hotel, Midtown Los Angeles
Los Angeles, California
March 2-3, 2000

Edited by
M. Shinozuka[1], D.J. Inman[2] and T.D. O'Rourke[3]
with assistance from A. Rejaie[4]

Publication Date: November 10, 2000

Technical Report MCEER-00-0009

Task Number 00-2061

NSF Master Contract Number CMS 97-01471

Sponsored by MCEER, NSF, University of Southern California,
and the International Institute for Innovative Risk Reduction Research
on Civil Infrastructure Systems (I^3R^3CIS)

1 Fred Champion Professor of Civil Engineering and Director, I^3R^3CIS, Department of Civil Engineering, University of Southern California
2 G.R. Goodson Professor, Mechanical Engineering Department, Virginia Polytechnic Institute and State University
3 Thomas R. Briggs Professor of Engineering, School of Civil and Environmental Engineering, Cornell University
4 Research Assistant, I^3R^3CIS, Department of Civil Engineering, University of Southern California

MULTIDISCIPLINARY CENTER FOR EARTHQUAKE ENGINEERING RESEARCH
University at Buffalo, State University of New York
Red Jacket Quadrangle, Buffalo, NY 14261

Workshop Description

A *Workshop on Mitigation of Earthquake Disaster by Advanced Technologies (MEDAT)* was held, under the sponsorship of MCEER and the National Science Foundation (NSF), in Los Angeles at the Radisson Hotel Midtown, across from University of Southern California (USC) campus on March 2 (Thursday) and 3 (Friday), 2000. This workshop (MEDAT-1) consisted of all-plenary two day sessions and was the first in a new series of MCEER-sponsored workshops involving advanced technologies.

Workshop participants explored the state-of-the-art field applications of nondestructive inspection and health monitoring technology including remote sensing techniques, for the purpose of mitigating urban earthquake disasters. Innovative applications of the technologies, either actually implemented or having high potential of implementation in civil infrastructure systems, were emphasized. Two discussion sessions of generous duration provided a forum for critical review and exchange of ideas among all the participants for breakthrough applications of the technologies. Future MEDAT workshops will address additional applications of these and other advanced technologies.

This document was produced by Masanobu Shinozuka, Director, International Institute of Innovative Risk Reduction Research in Civil Infrastructures (I^3R^3onCIS), with the help of Mr. Ali Rejaie, University of Southern California.

MEDAT-1 Workshop Participants, Raddisson Hotel, Los Angeles, California, March 3, 2000.

Contents

Session 1

Condition Monitoring and Response Control

Chairs: M. Bruneau and M. Zako

Structural Performance and Advanced Energy Dissipation Technologies
By G. Lee, Z. Liang and M. Tong

Soil Reinforcement Systems for Construction and Retrofitting in Earthquake Zones
By I. Juran and S. Hanna

Advanced Sensors for Condition Monitoring and Damage Assessment of Civil Structures
By M. Feng and F. DeFlaviis

Structural Performance and Advanced Energy Dissipation Technologies

G. C. Lee[1], Z. Liang[2] and M. Tong[3]

[1] *Professor and Center Director, Multidisciplinary Center for Earthquake Engineering Research State University of New York at Buffalo, Buffalo, NY 14261 USA*
[2] *Research Associate Professor, Multidisciplinary Center for Earthquake Engineering Research State University of New York at Buffalo, Buffalo, NY 14261 USA*
[3] *Senior Research Scientist, Multidisciplinary Center for Earthquake Engineering Research State University of New York at Buffalo, Buffalo, NY 14261 USA*

Abstract

This paper is intended to address the general concerns associated with analysis and design approaches for structures with added energy dissipation technologies. First, the challenges of integrating energy dissipation devices with the current performance-based structural design approach are described. Then, several important issues related to the challenges are briefly summarized. Finally, energy dissipation technologies are briefly reviewed and a variable passive (a special type of semi-active system) vibration reduction technology is given as an example. Emphasis is given to the problem areas where, following traditional perceptions, modeling, analysis and design procedures, structural engineers will need additional information in order to achieve desired structural performances so that appropriate energy dissipation, both ordinary and advanced types, technologies can be selected for safe and cost-effective seismic protection of structures.

INTRODUCTION

Evolution in Earthquake Engineering Design

Today earthquake engineering design for structures is considered by many as a special professional pursuit, somewhat distinct from general structural design. This may be easily understood because design against strong earthquake ground motions requires extra consideration and application of structural dynamics principles and the random nature of earthquake magnitude, characteristics, location and frequency of occurrence.

Structural engineering as a major component of civil engineering professional activities was well organized in contents and design procedures during the last half of the 19th century and the first half of the 20th century primarily using "static" and "deterministic" approaches. Since the end of the Second World War, coupled with the development of physics, engineering mechanics and applied mathematics, structural engineering has been continuously refining and improving its design criteria and procedures. Today, due to the rapid development in digital computation, applied mathematics and numerical procedures, structural engineering enjoys unprecedented success in providing competent professional services to society for most structures that can be handled by the "static and deterministic" approach. This covers a majority of all the structures in the world that require structural engineering design.

Since the middle of the 20th century, earthquake hazards mitigation research activities were initiated. The maturity of structural dynamics, applied mechanics, and mechanics and

stochastic processes theory had enabled many earthquake engineers to use "dynamic" and "stochastic" knowledge to compliment the "static" and "deterministic" based structural design approaches such as utilization of large inelastic deformation of structures (ductility). Since the middle of the 20th century, earthquake engineering practice benefited from the development of design spectra. Although this approach is only based on the single degree-of-freedom model, it is an extremely useful method for earthquake engineering practice. This approach marked the beginning of designing structures based on principles of structural dynamics. It also marked the beginning of considering earthquake engineering as a specialty type in the general structural engineering profession.

During the last half of the 20th century, earthquake engineering research has gained significant momentum in the US and in the earthquake vulnerable countries of the world. Many significant developments and milestone accomplishments will not be elaborated in this paper. The present day state-of-the-art for earthquake engineering includes two major thrusts. The first is performance-based design and engineering, and the second is using seismic response reduction technologies to enhance or control the performance of structures.

Two Challenges Ahead

To continue the advancement of earthquake engineering practice, researchers and practitioners are faced with two major challenges:

1. Integration of performance-based design approach with structural response reduction technologies.

   The structural response reduction technology is the primary professional interest and responsibility of structural engineers who must also consider all other aspects of loading conditions and requirements in the design of complex large-scale MDOF structures. The performance-based design is the primary interest of manufacturers of materials and devices with most of their professional expertise in mechanical systems and devices, which ensures the device to deliver the performances as the specifications such as the strokes, force level, damping coefficients etc. In most cases, the device performances are verified through SDOF bench tests.

2. Integration of earthquake engineering special considerations with general structural engineering design practice.

   Although special design provisions must be developed to ensure earthquake performance, they should be part of the overall structural engineering design package. This challenge will have to be examined closely after the first challenge is satisfactorily addressed.

Purpose and Scope

The purpose of this workshop paper is to address certain general concerns associated with analysis and design approaches for structures with added energy dissipation technologies. We will raise a number of issues related to future research needs that may lead to the development of design provisions for using advanced energy dissipation technologies under the performance-based structural design approach.

There is a wide spectrum of advanced technologies, both materials and devices, that can be applied to enhance structural performances and to reduce vibrations. There is every reason to

believe that this list of various devices/systems will continue to expand. This paper, however, will limit its scope to passive energy dissipation technologies of the brace type presently applied in many retrofitted steel frame buildings, to illustrate the importance of understanding the issues raised. No attempt is made here to present a catalog of available materials and devices of various types and their characteristics. The basic approach taken is to define needs and challenges first from the viewpoint of a structural engineer and to invite solutions from the material/device manufacturers and experts who have experiences in developing and in applying energy dissipation technologies for other professional fields.

The scope of this workshop paper is limited compared to the comprehensive research at MCEER for a wide spectrum of structural protective systems. Various research tasks are being carried out on different passive, semi-active and active systems as they apply to buildings, bridges and lifeline systems as well as their application to protect nonstructural components in buildings and special structures (monuments, etc.). Many of these MCEER research tasks will result in reports, and monographs to be published by MCEER in addition to journal and conference papers by the individual researchers. The subject of this paper is the reflection of a proposed MCEER monograph presently under preparation by the researchers of a special task led by the senior author. This monograph will include the semi-active system by using viscous fluid dampers and a few other energy dissipation technologies. The driving motivation for such a monograph is to enhance structural engineers' abilities to more intelligently use the current NEHRP (and new codes to appear in year 2000) regarding the analysis and design of protective systems with added energy dissipation devices/systems. The major performance gains of such engineering practice include keeping the structural responses within the elastic range to achieving optimal life cycle economy.

STRUCTURAL PERFORMANCE AND ADVANCED ENERGY DISSIPATION TECHNOLOGIES

The essence of performance-based structural design is to control the behavior or responses of a structure to perform within prescribed levels. In this regard, earthquake engineering is very suitable by adapting such design philosophy. However, even for a structure without any added devices, design of the structural performances for various levels of loading conditions are complex. Nevertheless, it has been realized by the structural engineering profession that this design approach is superior in many instances.

When considering the performance of a structure with added energy dissipation devices, the meaning of performance becomes more complicated because there are a few new factors that must be included. For example, the failure modes of the control devices are not as accurately quantifiable as the structural material properties. This makes the integration of performance-based design approach with structural response reduction technologies more challenging.

On the practical side, in most applications using advanced technologies for structural seismic protections, the expected performance of the structure is higher than that of using traditional method such as stiffness enhancement (Chang et al, 1993). In addition, most of the energy dissipation devices are only used in retrofit projects for various reasons. Therefore, retrofit design is more restrictive than for a new building design (FEMA273, Lee, Tong and Wu, 2000). In considering these two typical characters of practical applications for advanced technologies, the structural engineers who are responsible to design the protective system are often faced with many issues they have not experienced in standard design procedures. For

example, they have major concerns today regarding the reliability of the design procedure and the long-term reliability of the protective system itself. They are now faced with the challenge of combining reliable performance of structural materials with much less proven energy dissipation devices. The net result is a combined building-device system with less confidence.

It is impossible to provide a complete solution to this problem. In fact, it is not even possible to provide a complete list of potential problems that may develop by adding energy dissipation technologies to a structure. What we intend to offer in this paper is to address a few issues which have surfaced and are currently addressed by the authors. These issues include:

- Selection of protective systems for a given structure for required performance
- Issue of increase damping vs. reduction of response levels
- Issue of related to supporting stiffness for energy dissipation devices
- Issue of related to additional column axial force due to added device
- Cross effects
- Failure modes of energy dissipation device

Selection of Protective Systems

The selection of a seismic protective system basically varies case by case. The dominant factors under considerations are performance levels, practical constraints and cost. For retrofit projects, the following choices are available in general:

Stiffness Modification
- Add bracing members
- Add rigid diaphragms (shear walls)
- Replace/add higher performance structural materials/components
- Add/rearrange structural components to change overall structural configuration

Damping Modification
- Increase energy dissipation by principally increasing the damping using material deformational capacity
- Increase damping by using added damping devices of various types and placed in various strategic locations
- Increased damping usually also modifies the stiffness

Weight Modification
- Adjust position of live load and use added masses
- TMD
- TLD

Modification of Dynamic Stiffness
- Avoid resonance
- Combination of stiffness, damping and mass modification

Input Energy Reduction

- Various base isolation technologies

To various degrees, all the above require a clear understanding of the role of damping, which is not thoroughly developed and formulated for retrofit applications by using energy dissipation systems to multiple degree-of-freedom (M-DOF) building structures.

Without added damping, a typical multiple degree-of-freedom (M-DOF) building structure can be decoupled into several single degree-of-freedom (S-DOF) systems, when the damping ratio is small (several percent). This approximation has been very useful not only because it results in much simplified computational procedure but also it simplifies the design concept and approach by concentrating on the first few modes that contain a major portion of the total vibration energy of otherwise a complex, M-DOF structure (Liang and Lee, 1991).

When we purposely add energy dissipation devices to a structure to increase the damping ratio, the structure can no longer have small damping. Instead, the damping force can be in the same order of inertia and spring forces. In this situation, how to model the damping becomes important. More accurate damping models are needed, which is likely to be based on certain quantitative description of the damping force. At least, it is necessary to establish the limits and conditions for which the approximation of decoupling in a M-DOF system can be introduced for developing building retrofit strategies with energy dissipation systems (Lee and Liang, 1998).

In addition, selection of device types may be influential to the performance of the structure. Depending on the damping force characteristics, devices may be classified as adaptive or non-adaptive damping. Based on the hystersis loops of energy dissipation, devices may display different energy dissipation efficiencies, often the ones with rectangular shaped loops provide higher dissipation efficiency (Lee, Liang and Tong, 1998; Lee, Wu, Tong and Liang, 1999).

Increased Energy Dissipation and Decreased Vibration Level

In many books, journal articles, technical reports and other publications, the concept and statements are often implied by many structural engineers that retrofit, by using earthquake protective systems such as the energy dissipation devices, is to increase damping, and therefore, the vibration level of the retrofitted building-device system with high damping will automatically be reduced.

This concept is not always valid unless qualified technical details are added. Such details have not been criticized by engineers in practice before the introduction of earthquake protective systems in earthquake engineering design. Today, they should understand that it is important to limit this concept to structures that can be approximated by S-DOF systems in addition to other limitations. Some examples in this paper will demonstrate this issue in specific terms.

To substantiate the above description, consider the relationship given by Uang-Bertero (1988):

$$E = E_k + E_s + E_h + E_d \qquad (1)$$

where,

E = absolute energy input from the ground motions

E_k = absolute kinetic energy

E_s = Recoverable elastic strain energy
E_h = irrecoverable energy dissipated by the inelastic or other forms of action
E_d = energy dissipated by added energy dissipation devices

From Eq (s), if E_d is increased, $(E_k + E_s)$ will be decreased for more or less constant E. Now consider the equation of motion

$$Mx'' + Cx' + Kx = - M \{1\} x''_g \qquad (2)$$

where M, C and K are, respectively, the mass, damping and stiffness matrices, and X", X' and X are, respectively, the acceleration, velocity and displacement relative to ground x_g" is the ground acceleration.

During an earthquake, the ground motion is often not affected by the structure, no matter how the structure deforms. That is, the excitation forcing M $\{1\}$ x_g" is not affected and the amplitude of which remains constant despite the variation of the left side quantities (X", X' and X, M, C and K in Eg.(1)). In the case, when the damping coefficient C changes, it is likely that the displacement x will be changed also. Therefore, the production of X^T M $\{1\}$ x_g" will not be a constant, that is

$$X^T M \{1\} x_g'' = \text{input energy} \neq \text{constant} \qquad (3)$$

The above equation indicates that to increase the damping ratio may not always yield a lower vibration level, because the input energy may also be increased if dampers are not properly configured. Comparing Eqs. (3) and (1), it shows that M-DOF system dynamics could be much more complicated than that of S-DOF systems.

On the other hand, if we define a "dynamic stiffness" for the structural system, it is possible to state that when the dynamic stiffness of the structure is increased, the vibration level will always be reduced. Rewriting Eq. (3),

$$\{M \frac{d^2}{dt^2} + C \frac{d}{dt} + K\} X = F = -M\{1\} x_\varepsilon'' \qquad (4)$$

and denoting the dynamic stiffness K_d by

$$\{M \frac{d^2}{dt^2} + C \frac{d}{dt} + K\} \qquad (5)$$

We have

$$K_d X = F \qquad (6)$$

in which the dynamic stiffness is a function of the damping matrix

$$K_d = K_d(C) \qquad (7)$$

With the above definition, the remaining problem is how to define the vibration level. From matrix Eq. (5), we can also realize that in certain cases, when the vibration level of a

certain portion of a structure is reduced, the vibration may be magnified at other locations of the structure. That is, the norm of:

$$X = \{ x_1 \ x_2 , \ldots , x_n \}^T \qquad (8)$$

is reduced and it is not necessarily that all the local displacements are reduced.

The above discussion suggests that, by using energy dissipation or supplemental damping devices in a M-DOF structure, a designer must consider the total dynamic responses of the structure and the configurations of the devices to target the critical locations for vibration reduction.

To illustrate the above statement, a four-story steel moment resistant structure is examined. This is an actual test frame in an experimental program. Eight linear viscous dampers are installed in different floors with four configurations. As shown in the Fig. 1, the first configuration uses eight dampers installed in the first and second floors, four dampers for each bay. The damping parameter is 0.15 kips second/inch. In the second configuration, the eight dampers are installed in the second and third floors. In the third and fourth configurations, the eight dampers are installed in the third and fourth floors, but in these cases, the damping parameter is 0.35 and 0.30 kips second/inch, respectively.

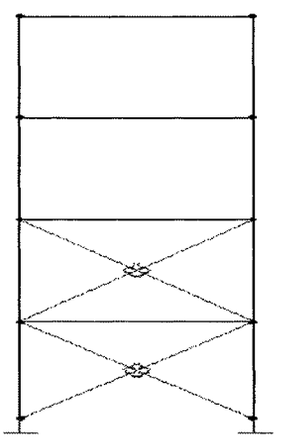

Fig. 1. Steel frame and damper configuration.

The seismic response is calculated by using the SAP2000 FEM model. Linear and non-linear analysis are performed to obtain damping ratio and dynamic response. In SAP2000, when linear analysis is selected, the damper will be treated as linear damper in the structure, after the non-diagonal damping element are eliminated, decoupled modal damping ratio and modal coordinate will be used to solve the response using the superposition method. Here, the damping ratio calculation is consistence with FEMA273. When the non-linear feature is selected, the damper will be treated as a non-linear damper element, and the direct time integral method is used to obtain the response.

For the four configurations, linear analysis gives the damping ratio for the first six modes as shown in Table 1. Then the non-linear time history analysis is used to obtain the seismic

response of the building under the El-central ground motion record. The responses are the relative displacement, relative velocity and absolute acceleration on the building roof. The maximum responses are shown in Table 2, in which the highest damping ratio is obtained for case 3, but the lowest response is obtained for case 2.

Table 1. The damping ratios.

% Damping	Mode 1 T=0.53	Mode 2 T=0.36	Mode 3 T=0.20	Mode 4 T=0.15	Mode 5 0.11	Mode 6 T=0.08
Case 1	0.14	0.21	0.08	0.11	0.21	0.17
Case 2	0.16	0.23	0.12	0.20	0.37	0.31
Case 3	0.18	0.25	0.55	0.21	0.99	0.89
Case 4	0.16	0.22	0.47	0.18	0.99	0.77

Table 2. The maximum seismic responses.

	Case 1	Case 2	Case 3	Case 4
Displacement (in)	1.063	1.018	1.108	1.225
Velocity (in/sec)	12.41	11.87	13.33	13.56
Acceleration (in/sec^2)	175.3	171.5	184.4	184.9

Thus, added passive energy dissipating devices can make the structure a highly non-proportional damped system. For the M-DOF non-proportional damping systems, the modal damping ratio is not a good index to reflect the effects. Higher value of the calculated damping may increase the seismic response.

In some high-rise building applications, this problem can be even more serious such that the highest damping configuration may be 20% - 30% higher than that of other configurations, whereas the differences between the best response reduction configuration and the highest damping configuration could be another 20%. This issue is strongly related to the damping effect for vibration reduction and the cost performance tradeoff.

Supporting Stiffness for Energy Dissipation Devices

For civil engineering structures, the design is primarily concerned with live and static loads. Dynamic forces are considered afterwards. Damping is mainly designed to withstand the dynamic forces. Most dampers, however, need supporting stiffness. (In Fig. 2, a damper c is needed to be supported by a stiffness s, different from the structural stiffness k.) Thus, it is necessary to know the effects of such stiffness on dead load resistance. A practical thought is, if the needed supporting stiffness must be very strong, why bother to use dampers? Why not simply increase the stiffness to resist horizontal dynamic forces?

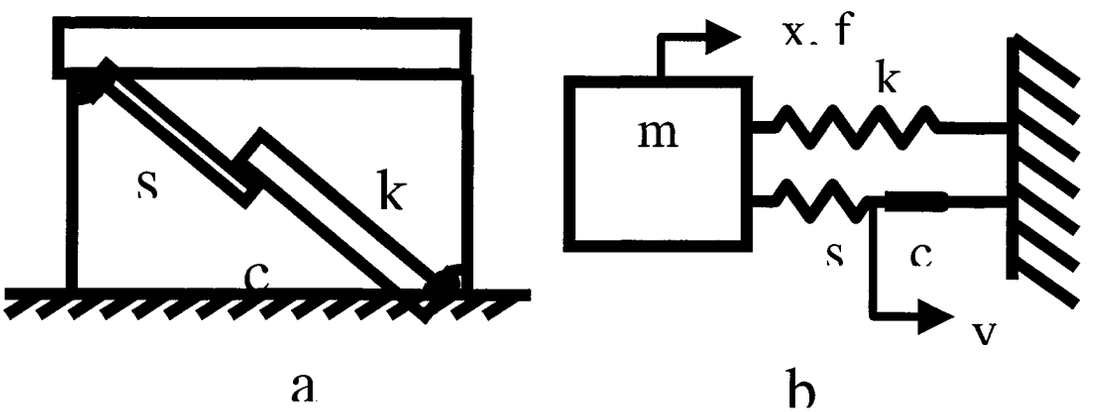

Fig. 2. Supporting stiffness for dampers.

It is understood that increasing a structure's natural frequency above the dominant driving frequency of the earthquake excitation could be an effect approach to reduce structural response. However, the vulnerability still exists, only in a higher frequency range. Using damping devices may lessen the overall vulnerability. The effectiveness of damping devices sometimes requires very strong support, even much stronger than that required to enhance the structure. Strong supporting stiffness often induces many other problems such as stress concentration. We shall briefly discuss the issues using the following mathematical model .

This single mass model shown in Fig. 2 can be modeled by:

$$mx'' + kx + s(x-y) = f \tag{9}$$

$$s(y - x) + cy' = 0 \tag{10}$$

where the finite-valued supporting stiffness adds an additional degree-of-freedom. Take the Laplace transform of the above equation and assume zero initial conditions and also let the Laplace variable be $j\omega$ (case in steady state) we have

$$-\omega^2 mX + kX + s(X-Y) - F \tag{11}$$

$$s(Y - X) + jc\omega Y = 0 \tag{12}$$

where X, Y and F are the Laplace pair of x, y and f, respectively. Let $X = x_o e^{j\omega t}$ and $Y = y_o e^{j\omega t}$ and $F = f_o e^{j\omega t}$, where, x_o, y_o and f_o are complex-valued amplitude of x, y and f, respectively, then we have,

$$x_o = \frac{f_o}{m} \frac{s + jc\omega}{-je\omega^3 - s\omega^2 + j\frac{k+s}{m} c\omega + \frac{ks}{m}} \tag{13}$$

and

$$y_o = \frac{s}{s + je\omega} x_o \tag{14}$$

With the help of the above notation, we can see that roughly for an originally S-DOF system, to achieve 10% of damping ratio, we need the supporting stiffness s to be the same value of k. That is,

$$s \geq k \tag{15}$$

To achieve 20% of damping ratio, we need roughly

$$s \geq 2k \tag{16}$$

Finite supporting will limit the damping capacity of energy dissipation system. It can change a viscous damper into a visoelastic damper. This issue cannot be ignored in design of energy dissipation systems. When dealing with a large scale structure with limited bays for added devices, the supporting stiffness issue becomes more severe since the required supporting stiffness is compared with the total stiffness of the floor. It may often end up at large local stress concentration.

Additional Axial Force due to Added Devices

For bracing type of energy dissipation devices, an often asked question by engineers using FEMA273 guidelines has been concerned with the additional vertical load increase due tothe damping force generated by the control device on the columns. As illustrated by Fig. 3, taken from FEMA274, when dampers are installed in the diagonal direction of the 3-story frame, the vertical components of the damper force may add to the axial force to the columns. This question can be answered by considering the frame as a whole where the axial force in the column due to earthquake ground motions consists of three parts:

- Force due to the dead load
- Live load
- Any other additional vertical load

The second contribution is the axial force due to the overturn moments because of the story shear force. If dampers or other stiffness-related devices are applied to the structure, the damper force or the device force will contribute to the column axial force. The total axial force of the column P is given by

$$P = P_d + P_l + P_o + P_x \tag{17}$$

where,

P_d The axial force due to dead load
P_l The axial force due to live load
P_o The axial force due to change of overturning moment (earthquake load)
P_x The increased axial force due to the damper force

P_d and P_l have the same value for dampered and original structure. If dampers or stiffness-related devices are added to the structure, the addition value of P_x will be added to P. But at the same time, the added devices will reduce the structural response, which include the total shear force and its overturning moments. The effect of such response reduction is the decrease of P_o. If the reduction of P_o is larger than the increase of P_x, the column total axial force will be reduced with the supplemental devices. For most of the regular buildings with a reasonable number of dampers or devices distributed, it can be shown that the column axial force is generally reduced. However, because of the multiple factors contributing to the total axial force, the change of column axial force with added devices may vary significantly.

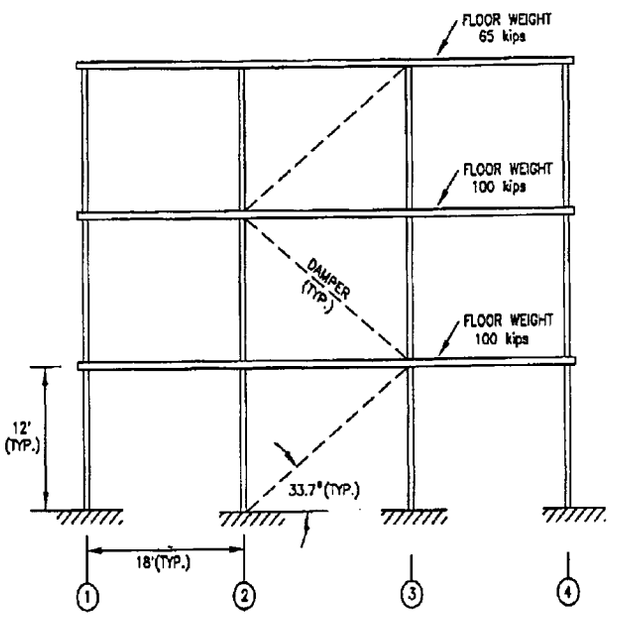

Fig. 3. Dampers installed in the diagonal direction of the 3-story frame.

Cross Effect

Cross effects have not been clearly defined in the literature. The authors choose cross effects to be a more general description of modal and directional couplings in dynamic responses due to all possible causes, including the traditionally defined orthogonal effects. For modal cross effect (or modal coupling), we generally mean that modes of a non-proportionally damped system are not orthogonal to each other in the physical space (Lee and Liang, 1998). However, this problem can be treated in the state space, where modes of a general linear dynamic system (including non-proportionally damped system) are decoupled. Therefore, we may consider that there is no modal cross effect in the state space.

Directional cross effect is the description of a phenomenon. We may intuitively consider it as the response in the normal direction of the input excitation. This phenomenon is not

uncommon. In fact, for most structures, there are only a few directions that have no directional cross effect. What is generally interesting to earthquake engineers is that for a geometrically symmetric structure (geometric shape is assumed to be the structural mesh without including the structural elements' material properties and sections, etc.), how to determine whether there could be a large directional cross effect in the two symmetric and perpendicular axes, because the strength of the structure is usually designed only in these two directions.

There are two major possible factors that may contribute to the directional cross effects: skewness of stiffness and eccentricity between mass center and shear center. In static analysis, as well as in linear analysis, if the mass center and shear center coincide, the directional cross response due to skewness of stiffness (be it acceleration, velocity or displacement) may be treated with the help of principal major and minor) axes. By projecting the input to the two principal axes, this portion of directional cross effect can be described by linear composition of the responses in the two principal directions. On the other hand, if the mass center and shear center do not coincide, then a torsion response will be introduced, which may also contribute to the directional cross effect depending on the location of interested point on the structure. In some sense, directional cross effects are unavoidable in civil engineering structures. Even in cases of purposely designed axially symmetrical structures with symmetrically placed dead load only, material inhomogeneity and construction misalignment can still introduce directional cross effects. Such effects have been accounted for in designs for static and static-equivalent loads and in situations where S-DOF dynamic models are appropriate. We raise the issue for M-DOF dynamic responses when the structure is complex and when damping is elevated by energy dissipation systems that make the structure device systems nonlinear. Even the differences of ground motion at various points of the building, may cause "directional effects". One important objective for raising the issue of cross effects is to at least make sure that the added energy dissipation devices does not amplify the responses of the structure in an unexpected manner when all the cross effects (directional, modal, etc.) are acting for a non-proportionally damped structure device system.

The authors have in recent years observed many amplified cross effects from experimental projects and from computer simulations in structures with improperly implemented earthquake protective systems (unsymmetrical arrangements, etc.). More recently, earthquake reconnaissance in Taiwan increased their belief that skewed stiffness arrangements (e.g. unsymmetrical stiffness configuration in the plan of low-rise buildings such as in-filled walls, etc. and in the vertical direction such as open space at the ground floor level, etc. can be a significant factor among the reasons of building collapse. These issues can only be classified by using generally damped, M-DOF models.

Failure Modes and Maintenance Issues

By using energy dissipation devices or other earthquake protective systems, a major concern of the structural engineer is safety. Controlling seismic vibrations is a relatively new approach with relatively little field experience in civil infrastructure systems. Furthermore, earthquakes are random events in terms of site, magnitude, frequency of occurrence and strong ground motion characteristics. It is believed that improperly configured damping and stiffness arrangements can result in amplified dynamic responses of structures. The issue of fail-safe strategy must be addressed before full implementation of energy dissipation systems in structural engineering practice (Lee and Liang, 1999). At least, the structural engineering profession

should be assured of two items: (1) when the devices fail, the seismic performance will not be worse than that without the added devices, and (2) there are limitations for using energy dissipation systems to retrofit so that no ill effects can result to the original structure.

As mentioned earlier, using energy dissipation systems (or other protective systems) can be cost effective from the viewpoint of the life cycle of the structure, if the performance of the structure is controlled to function in the elastic range of the material. However, this will require a high reliability for the safe and efficient function of the added energy dissipation devices.

The above discussions have been directed at raising some needed information for structural engineers to take advantages of energy dissipation technologies in performance-based design. The issues raised are general in nature. They are valid for most situations of structures implemented with earthquake protective systems, particularly the energy dissipation technologies. To address these problem areas for civil infrastructures, it is necessary to employ structural dynamics principles of M-DOF systems and to develop appropriate energy dissipation systems accordingly. In the following present-day seismic response reduction technologies will be briefly outlined and a special semi-active type of energy dissipation technology will be described.

SEISMIC RESPONSE REDUCTION TECHNOLOGIES

Structural Control Technologies

Structural control technologies today are classified into three general groups: passive systems, active/hybrid systems and semi-active systems. The general approaches for response reduction are based on properties of materials or mechanical/electromechanical devices, or their combinations. Although much of the control principles and technologies apply to both new structures and existing structures (retrofit), specific applications are and encouraged in buildings and bridge retrofit design practices. In practical, the passive base isolation systems have been used for some time for low-rise buildings and highway bridges in many earthquake regions in the world. The commonly recognized seismic response reduction technologies are given in Table 3. The basic idea for the three groups of control technologies are shown in Fig 4.

Table 3. Three general groups of structural control technologies.

Passive Systems	• Base isolation system • Energy dissipation systems • Tuned main systems • Others
Active/Hybrid Systems	• Active, adaptive system • Combined active-passive system • Others
Semi-Active Systems	• Negative feedback approach • Direct approach • Combined feedback and feedforward approach • Others

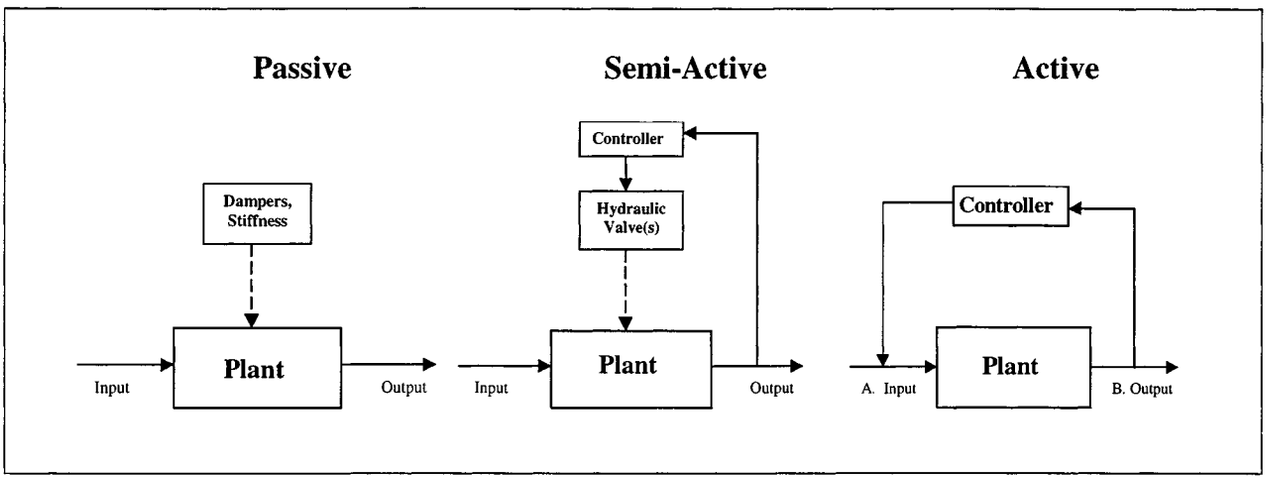

Fig. 4. Three groups of control technologies.

In Table 3, there are further classifications. For example, in base isolation systems there are rubber systems, rubber-lead systems and various sliding systems, etc.

Of the three general groups of seismic response reduction technologies, the active/hybrid control systems are considered to be appropriate for equipment and small structure/object protection. They will not be discussed further herein for civil infrastructures which are typically large and complex.

Semi-Active Controls

Semi-active has certain advantages over passive control. Since the structural parameters can be changed in real time, semi-active control has a wider working range. The vibration reduction under a given control force or an allowable deformation can be more optimal. In other words, to achieve the same vibration reduction, the control force, and/or supporting stiffness can be less than those required by using passive control. In addition, it is more capable to address fail-safe issues resulting from sudden failure of the control system.

Semi-Active Control Devices

There are basically two types of devices to provide semi-active actions:

1. Switching devices for variable stiffness and connecting/disconnecting to structural components/members and/or other devices.

The most commonly used switching devices are hydraulic cylinders with oil chambers, pistons and on/off valves. When the value is "on", the piston cannot travel freely, thus the device can connect to other structural members and/or devices or it will supply a certain amount of stiffness by itself. When the valve is "off", the piston can travel freely, thus the device cannot support any force (e.g. Kobori et al, 1990, 1991; Lee, Liang and Tong, 1994).

2. Variable damping devices for energy dissipation.

Electro-rheological and magneto-rheological fluid/grease are often used for variable dampers (e.g. Spencer and Sain, 1994; Inaudi, Kelly, Taniwangsa and Krunmme, 1993). With different amount of electric or magnetic fields, the viscosity of such fluid will be varied and thus the damping coefficient of the corresponding devices will be changed. Shape memory alloys can also be used to supply methods for variable damping. Piezo-electric materials, for example, can be used to generate electric changes (Inman, 1995). With different loading resistance, the materials can dissipate different amounts of energy in a given period. It is noted that, not all of the variable dampers can be used for structural control because their costs are not suitable for applications in civil engineering structures.

Control Algorithms

Semi-active control technologies can also be classified by the nature of control algorithms into three major types: Simulation of active control, Direct method and Real-Time structural parameters modifications.

1. Simulation of active control.

The simulation of optimal control approach can be found in many publications (e.g. Spencer; Constantinou, Soong and Dargush, 1996). Generally speaking, the design procedure of this kind of semi-active control will include the selection of cost functions, a typical step of optimal control. The selection of cost functions may be concerned with minimizing the response velocity and displacement, minimizing the control forces and the number of devices, etc. However, for semi-active control, devices are not actuators required in active control. They are not used to apply active forces to the structure. The end-up control force can be conceptually shown in Fig. 5 marked as a solid line, whereas the active control is marked by a dotted line. From Fig. 5, we can see the similarity and difference of these two control strategies.

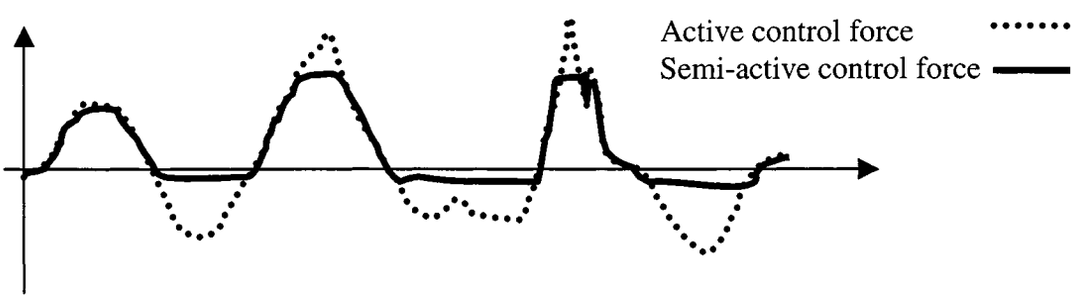

Fig. 5. Simulation of active control.

Another simulation is to use the idea of adaptive control. The end-up control force will have the same phenomenon as shown in Fig. 5.

2. Direct method.

The second semi-active control approach is established directly from various laws of physics as well as direct logic observation and reasoning. The first example of the direct method is to use a Lyapunov function as the control principle (e.g. Sack, Pattern and Ebrahimpour,

1994). If the Lyapunov function indicates that at the next time step a new combination of connecting/disconnecting for a switching control is beneficial, then the controller will issue such a switching combination to the control devices. Otherwise, the switching combination will remain unchanged.

The second example is the so-called Skyhook dampers (e.g Karnopp, 1990). The damping coefficient of a variable damper can be changed according to a special set-up of damper configuration, whose damper is "hooked" to the "sky" and thus provide the best energy dissipation. In real case, no damper can be hooked up to the sky. However, such a variable damper is used to simulate the corresponding damping coefficients. In fact, Fig. 5 shows the skyhook damping force with dotted line, whereas the variable damper can achieve the solid line if the driving frequency is reasonably low.

The third example can be found in papers by Feng, Shinozuka and Fujii (1992), as well as Constantinou and Symans (1993), where the damping coefficients are determined according to the amplitudes of excitation loading. There are many other methods, Symans (1995) summarized them in his Ph..D. dissertation.

3. Real-time structural parameters modifications.

In the remainder of this presentation, one type of advanced energy dissipation technology will be briefly described. It is referred to as the real-time structural parameter modification (RSPM) technology, which is based on a combined negative feedback and feedforward control scheme. This technology is a special type of semi-active system. The authors also refer to it as variable passive system, because it only utilizes passive control forces. Minimal external electrical power is needed only for on-and-off switching of viscous fluid devices (the action devices) and not for applying counter forces. It is the intention to use this example to illustrate the idea of using semi-active systems to expand the capacity and effectiveness of passive viscous fluid dampers.

To further explain the difference between the RSPM technology and other semi-active systems, Fig. 6 is given. In this figure, it is shown that the control strategy for the RSPM technology is established from both input and output signals that will be further elaborated.

From the viewpoint of systems components, RSPM and other semi-active systems require the same units as those of an active control system: sensors and information processing, decision-making (control schemes) and action devices. In the case of the RSPM system, the action device is a specially designed viscous fluid damper. However, each semi-active and active system has its own unique control scheme. For the RSPM technology, there are four levels of control:

Level I: Local control
Level II: Local control modifications
Level III: Global optimization
Level IV: Fail-safe mechanism

The hierarchical action diagram of the RSPM control algorithm is given in Fig. 7. The lowest level of command is issued for specific purposes such as changing the stiffness of a truss member or a diagonal bracing member, based on information (a sensor and decision module) obtained at that local region of the structure.

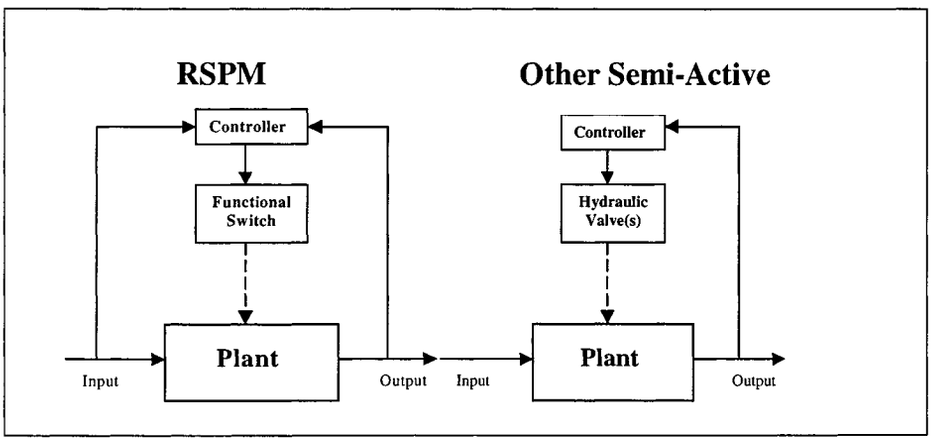

Fig. 6. RSPM system vs. other semi-active systems.

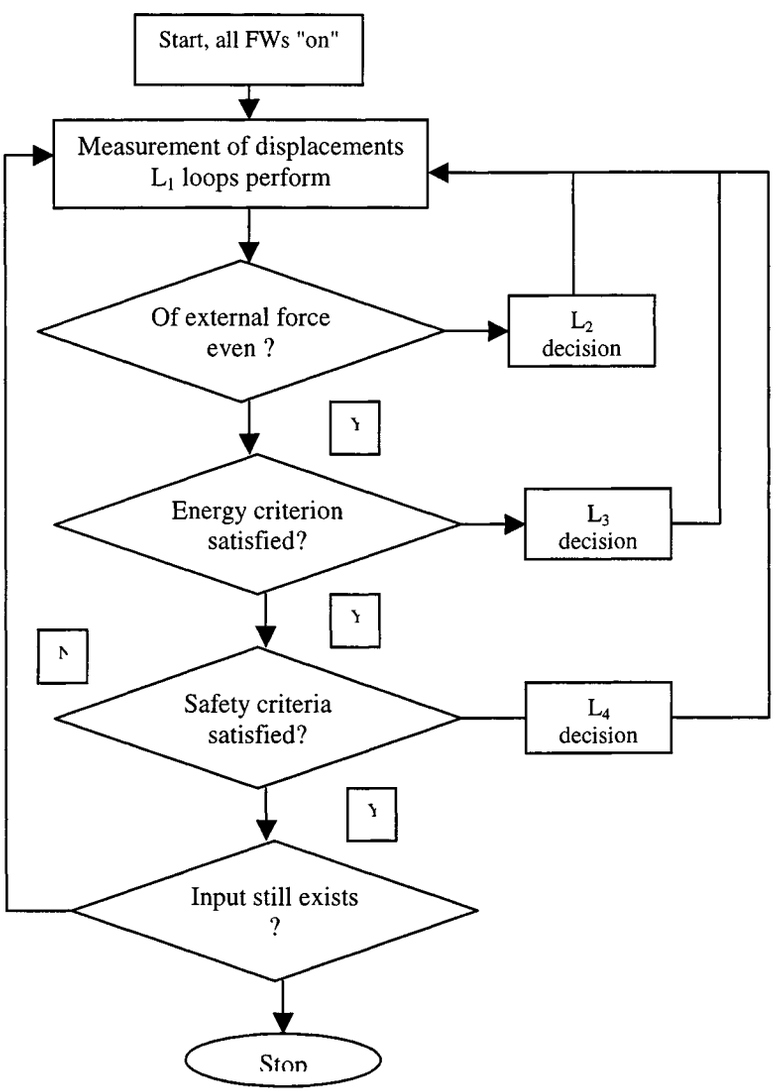

Fig. 7. RSPM control scheme

The next level of command is introduced to prevent or limit the development of unbalanced forces, which can develop after the stiffness is reduced at a local region acting in the direction of greater displacement (for reduced stiffness). The unbalanced force cannot be predetermined in the control algorithm under random earthquake ground motions. This special control loop is necessary in order to keep the stiffness from decreasing. It is an added feature of the RSPM control algorithm (see Fig. 8 for explanation of displacement overdraft). It is noted that both Levels I and II are local control loops.

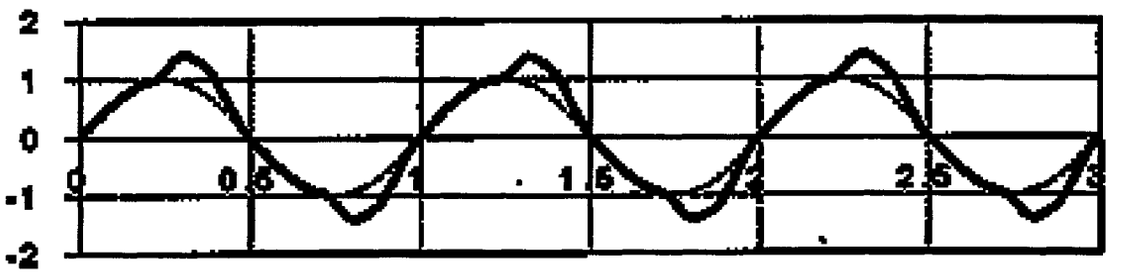

Fig. 8. RSPM control algorithm.

In a structure, there are many local control actions adjusting any of the three physical parameters (mass, damping and/or stiffness). Thus, a strategy for all the local action units of the structure has to be available which can override the lower level control actions. This is taken care of by Level III, which is a global control scheme based on a minimum conservative energy principle.

The highest level of RSPM control is the safety-check loop (Level IV). This level of command overrides decisions of all local action units and configures them to the most desirable mode of operation from the viewpoint of structure safety under the given input excitations or structure condition (e.g. unexpected failure of a structural member or a control device, etc.). A more detailed description can be found in Liang et al (1995, 1999, 1999).

Advanced Features of the RSPM System

As mentioned in the introductory section, the current state-of-the-art of structural engineering practice is challenged by the use of seismic response reduction technologies to retrofit buildings and bridges and to enhance the performance of the structure. The intention of this workshop paper is to highlight some difficult areas facing structural engineers as they attempt to introduce energy dissipation systems according to the design guidelines/codes. The approach of the authors is to be consistent with the current practice by first addressing the issues of passive energy dissipation technologies followed by an example of extending the capacity and effectiveness of passive systems with advanced control algorithms and devices (a semi-active or variable-passive system) that has a promise to be introduced to the world of structural engineering practice. The advanced features of the RSPM technology are further discussed in the following.

As shown in Fig. 4, active control has a complete, closed feedback loop. The switching type of semi-active control, on the other hand, does not possess a complete loop. Because a variable damper or a function switch often receives electric signal which is based on the

feedback from the structural responses and issued by the controller. It is the electric signal that commands the function switch to open/close or to vary the orifice of the fluid path, where no active force can be generated. Therefore, the device cannot actively affect the behavior of the structure. Thus, the semi-active control is fundamentally different from the active control. It is rather close to passive control since the force that is generated by the control device is passive in nature because the dynamic stiffness of the structure will be changed in real time. The authors prefer to call the RSPM technology a variable-passive control system.

Seismic response reduction by using RSPM technology has all the advantages of an active control system but without the demand for instant availability of power to operate large actuators to deliver counter forces to control the structural responses. This is an important and extremely desirable feature in earthquake engineering applications.

Stiffness modification is commonly used in most structural control applications because of its effectiveness and its good implementability. To illustrate the special feature of how RSPM can change passive stiffness to variable stiffness and therefore improve the effectiveness of a S-DOF model is shown in Fig. 9.

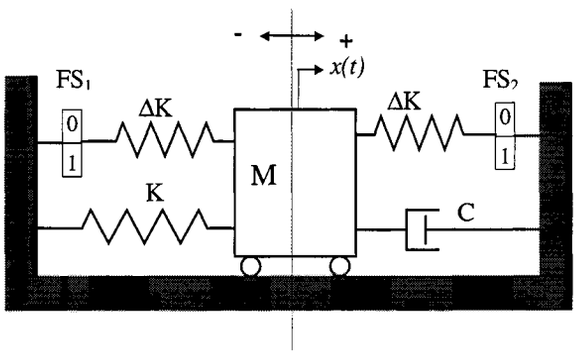

Fig. 9. Idealized S-DOF RSPM System.

In Fig. 7 the motion of the mass M of the structure such as a nuclear power plant is constrained by rollers so that it can move only in simple translation. Thus, the single displacement coordinate x(t) is suffice to define its position. The permanent and switched stiffness is represented by the weightless spring K and ΔK, respectively. The damping is represented by dashpot C. FS_1 and FS_2 are two function switches to realize the RSPM actions. (The sensors and decisionmaking unit are required but not shown.) Since earthquake ground motions are random in nature, adding the variable stiffness protective feature through RSPM action increases the effectiveness of using passive damping devices.

SUMMARY

Structural engineering as a professional discipline has a history of at least 150 years. The practice started from the "static and deterministic" approach. The design process and criteria improved incrementally as the knowledge base and technology (computing) increases. To account for dynamic effects due to wind gusts, moving traffic and earthquake ground motions, static equivalent forces have been used and extra safety factors are used to take care of the uncertainties of nature and man-made hazards that are dynamic in character. Today, structural

engineering is moving toward performance-based criteria in earthquake engineering design practice.

At the same time advancement in control technologies has offered attractive possible options to reduce seismic responses of structures and thus the implications of prolong life span of civil infrastructure systems. Much of these advanced technologies have been developed for applications in other fields of engineering applications. They are not necessarily suitable for civil engineering structures.

The major challenge today, for a structural engineer, is how to articulate his (her) needs so that the advanced technology side can develop the necessary characteristics into the device systems to help the structural engineers to satisfy the structural performance requirements in a cost effective and safe fashion.

For such a structural engineering-control system technology integration effort, several issues from the viewpoint of total system performance are presented in this paper. Admittedly, these are not the only issues requiring further research, and the authors are still feeling their way to expand their thoughts. Hopefully, a more comprehensive discussion and some solutions can be presented in the proposed monograph that is currently under preparation.

For those interested in research concerning the performance of structure-device systems from the structure's viewpoint (not device capacities' viewpoint), two important directions are recommended.

Aging Considerations

Advanced technologies thus far developed and used in other fields are expected to have a life span shorter than typical civil engineering structures. How they maintain their performance under hostile environmental conditions for a long time and how the devices can be easily replaced after earthquakes requires consideration research and development efforts, and particularly, a long time to study the aging effects on the expected performance of the structures. Additionally, many civil engineering structures are large in size and "one-of-a-kind", with little possibilities to repeat experimentation in the laboratory or in the field.

Thus, real-world demonstration projects and observations are important. In the interest of making long time observations of the aging process, real-world implementation of energy dissipation devices should be expanded and properly observed (Lee, Liang and Song, 1999).

Semi-Active Response Reduction Technologies

It is clear that due to the random nature of earthquakes, passive approaches cannot provide sufficient range of effectiveness. Semi-active or intelligent passive systems offer the best possible, and most likely, cost effective approach to accomplish the goal of response modification for structures to perform at the desirable levels.

SELECTED REFERENCES

Chang, K.C., Lai, M.C., Soong, T.T., Hao, D.S. and Yeh, Y.C. (1993). *Seismic Behavior and Design Guidelines for Steel Frame Structures with Added Viscoelastic Dampers*, NCEER Technical Report, 93-0009.

Constantinou, M. C. and Symans, M. D. (1993). "Experimental study of seismic Response of buildings with supplemental fluid dampers," *The Structural Design of Tall Buildings,* Vol. 2, 93-132.

Constantinou, M.C., Soong, T.T., Dargush, G.F. (1996). *Passive Energy Dissipation Systems for Structural Design and Retrofit*, An NCEER Monograph, Department of Civil Engineering, SUNY at Buffalo, NY 14260, June.

Federal Emergency Management Agency (1997). *NEHRP Commentary on the Guidelines for the Seismic Rehabilitation of Buildings.* FEMA-274, October 1997. Redwood City, CA: Applied Technology Council.

Federal Emergency Management Agency (1997*). NEHRP Guidelines for the Seismic Rehabilitation of Buildings.* FEMA-273, October 1997. Redwood City, CA: Applied Technology Council.

Feng, M. Q., Shimozuka, M. and Fujii, S. (1992). *Experimental and Analytical Study of a Hybrid Isolation System Using Friction Controllable Sliding Bearings*, Tech. Report NCEER-*92—0009*, NCEER, State University of New York at Buffalo.

Inaudi, J. A., Kelly, J. M., Taniwangsa, W. and Krunmme, R. (1993). "Analytical and experimental study of a mass damper using shape-memory alloys," *Proc. Damping'93*, San Francisco Cac x.

Inman, D. J. (1995). "Some design considerations for active/passive damping treatment," *Proc. 2nd Workshop on Smart Structures*, Maryland, September 1990, 448-455.

Karnopp, D. (1990). "Design principles for vibration control systems using semi-active dampers," *Transactions of the ASME*, Vol. 112, Sept. 1990, 448-455.

Kobori, T. et al (1990). "Rigidity Control system for Variable Rigidity Structure," U.S. Patent No. 4, 964,246.

Kobori, T. et al (1991). "Combined Variable Stiffness and Variable Damping Systems," U.S. Patent No. 5,036,633.

Lee, G. C. and Liang, L. (1998). "On cross effects of seismic responses of structures." *Engineering Structures*, Vol. 20, 4-6, 503-509.

Lee, G. C. and Liang, Z. (1999). "Development of a Bridge Monitoring System," *Proc. 2nd Workshop on Structural Health Monitoring*, Stanford University, Sept. 1999.

Lee, G. C., Liang, Z. and Song, J. W (1999). Development of a Condition Assessment Methodology for Highway Bridges, *Proc. International Workshop on Seismic Hazard Mitigation on Transportation Systems,* Taiwan.

Lee, C. G., Liang, Z. and Tong, M. (1994). "Innervated structures," *Proc. First World Conference on Structural Control*, Los Angeles, CA, Aug. 3-5, 1994.

Lee, G. C., Liang, Z. and Tong, M. (1998). "Some Damping Design Considerations for Structural Protective Systems," In C-H Loh and J-S Hwang (eds), *Proc. ASIA-Pacific Workshop on Seismic Design and Retrofit of Structures*, National Center for Research on Earthquake Engineering, Chinese Taipei, 83-95.

Lee, G. C., Tong, M. and Wu, Y. H. (to appear 2000). "Some design issues for building seismic retrofit using energy dissipation devices," *International Journal of Structural Engineering and Mechanics.*

Lee, G. C., Wu, Y.H. Tong, M. and Liang, Z. (1999). "Seismic Design Considerations of Structures with Supplemental Protective Devices: Effects of Damping Force on Column Strength," *Proc. Int. Workshop on Seismic Isolation, Energy Dissipation and Structural Control*, Quanzhou, May 1999.

Liang, Z. and Lee, G. C. (1991). *Damping of Structures: Part 1 - Theory of Complex Damping*, Technical Report NCEER-91-0004, NCEER, State University of New York at Buffalo.

Liang, Z., Tong, M. and Lee, G. C. (1995). *Real-Time Structural Parameter Modification (RSPM): Development of Innervated Structures*, NCEER Report #950012, April 1995.

Liang, Z., Tong, M., and Lee, G. C. (1999). "A Real-time Structural Parameter Modification (RSPM) Approach for Random Vibration Reduction: Part I – Principle," *Journal of Probabilistic Engineering*, June 1999, 349-362.

Liang, Z., Tong, M., and Lee, G. C. (1999). "A Real-time Structural Parameter Modification (RSPM) Approach for Random Vibration Reduction: Part II– Experimental Verification," *Journal of Probabilistic Engineering*, June 1999, 362-385.

Sack, R., Pattern, and Ebrahimpour, A. (1994). "Structural control for phase-related inputs," Report to Second Annual NSF Control Research Coordination Meeting, Aug. 6-7, 1994, Pasaena, CA.

Spencer, B. F., Jr. and Sain, M. K. (1994). "Reliability and safety of structures using hybrid and semi-active control." Informal report of Structural Control Workshop, Aug. 7, 1994, Pasadena, CA.

Symans, M. D. (1995). *Development of the Experimental Study of Semi-Active Fluid Damping Devices for Seismic Protection of Structures*, Unpublished Ph.D. Dissertation, State University of New York at Buffalo, Buffalo, NY.

Uang, C.-M. and Bertero, V. V. (1988). *Use of Energy as a Design Criterion in Earthquake-Resistant Design*, Report No. UCB/EERC-88/18, Earthquake Engineering Research Center, University of California, Berkeley

Soil Reinforcement Systems for Construction and Retrofitting in Earthquake Zones

By: Ilan Juran,[1] D.Sc., Member, ASCE
Sherif Hanna[2], Student Member, ASCE

ABSTRACT: Soil reinforcement systems have been increasingly used over the past decades representing cost-effective construction and retrofitting solutions in earthquake zones with significant performance advantages as compared with traditional systems. The use of soil reinforcement technologies can provide a high strength but more ductile and flexible structural elements. Furthermore, installation techniques can effectively be used with the advantageous of efficient load transfer with minimal displacement for retrofitting and underpinning in seismic zones. This paper illustrates and summarizes the benefits and current developments of using such systems including Texsol, soil nailing, and micropiles. Future developments and use of such systems in liquefied soils are also discussed.

[1] Professor, Polytechnic University, 6 MetroTech Center, Brooklyn, NY 11201
[2] Research Fellow, Polytechnic University, 6 MetroTech Center., Brooklyn, NY 11201

During the past decade post-earthquake observations on reinforced soil retaining structures consistently demonstrated that due to their composite behavior and energy absorption capacity these structures present high resistance to earthquake loading, the following comments will share some observations on (i) engineered fills, and (ii) in-situ ground reinforcement

(I) ENGINEERED FILLS

Figure (1) illustrates a typical example of the seismic performance of reinforced earth structures During the Hanshin earthquake, Japan, 27 km from the epicenter the reinforced earth structure has not suffered any damage whereas 200 meter away the road has completely collapsed.

For reinforced earth walls extensive research has been conducted on reduce scale models and full scale monitored structures to provide seismic design guidelines and predict structural displacements. The initial seismic design method proposed by Seed and Mitchell (1981), was modified by Bastick and Segrestin (1989) following finite element simulations and incorporated in design guide lines.

The seismic performance of Texsol was investigated in Japan by Fukuoka (1990) on (i) a series of shaking table tests on models of earth dam with reinforced facing, and (ii) a ten meter high test wall instrumented for performance monitoring under earthquakes. During the February 19, 1989 earthquake, 5.7 on the Richter scale, measured acceleration at the ground surface reached 95 gal with frequency spectrum from 2 to 8 Hz. Site observations illustrated that while the static safety of the wall was already at the critical state no damage was observed. Figure (2) illustrates the instrumentation of the wall and measured earth-pressure due to the seismic load compared with predicted values obtained from the Mononobe-Okabe formula. These results as well as the results of the model scale shaking table tests demonstrated the effectiveness of Texsol for earthquake design.

It is of interest at this point to share few comments on the potential use of 3-D fiber reinforcement. Texsol represents an industrialization of the fiber reinforcement concept, where continuos polyester thread 0 .1% to 0 .2% by weight, is injected together with sand in order to create in situ composite material with a friction angle of the native sand and "cohesion" due to the sand encapsulation by the continuos filament. With 100 to 250 kilometers of continuous thread per cubic meter, Texsol yields a substantial cohesion to the composite material. Major issues concern: deformation response, long term performance and, QC. It is of interest to indicate that in Japan

tests have been conducted to assess the feasibility of using low level cementation (up to 4%) for a better control of deformation response of Texsol.

3-D fiber reinforcement of both sand and clays have been reported in the literature as potentially effective tool for various civil engineering applications, including retaining structures, engineered fills, pavement design, volume change control of expensive clays, increasing liquefaction resistance of loose sands, and improving dynamic resistance and shear modules (Noorany et al, 1989; Mahar & Woods, 1990). However the mechanism between the fiber and soil particles is still a subject of research and no consensus has yet been reached with regard to the optimal aspect ratio in different types of soils. Furthermore the use of fibers to isotropically reinforce soils raises significant concerns with regard to the uniformity of compaction and quality control.

Fiber reinforcement has gained a significant interest with the current investigation and thrust on the potential use of recycled waste products such as shredded tires in highway construction. It is believed that in the next decade the use of recycle products often mandated in different countries, will raise new R&D in material design and quality control. The past experience with manufactured goesynthetics that in the 80's has escalated to a billion dollar industry could set forth a relevant model for turning processed waste materials into economically viable resource for infrastructure construction materials. Numerous examples already attest to this end raising challenging R&D needs as the emerging industry of processed waste material continues to grow and faces new engineering applications.

(II) IN-SITU GROUND REINFORCEMENT

Soil Nailing

For soil nailing the site observations by Felio et al. (1990) raised significant interest in the potential use of the technology for construction in earthquake zones. However only limited studies have to date been conducted to investigate the seismic response of soil nailed structures and evaluate the available pseudo-static limit equilibrium design methods Of particular interest with this regard is the centrifugal model study conducted by Vucetic et al. (1993). At this point it should be emphasized that while the centrifuge offers effective tools for modeling actual working load conditions it raises R&D challenges with regard to the difficulties involved in complying with scaling requirements, controlling the effect of boundary conditions for seismic loading, and simulating in flight

construction processes and installation of reinforcements. However, at this stage further centrifugal model studies on instrumented soil nailed wall as well as performance monitoring of full scale structure are required in order to establish a relevant database for the development and evaluation of reliable seismic design methods for soil nailed structures.

In particular the seismic loading effect on nail pull out resistance needs to be investigated. The potential use of innovative nail installation technologies in earthquake zone raises pertinent questions with this regard. Recent examples for such innovative construction technologies include Jet Nailing (Louis 1986) which combines vibro-percussion driving with high pressure jet grouting, and Nail Launching (Ingold & Miles 1996). The use of such innovative technologies raises the need to investigate the effect of the installation process on soil nail interaction under both static and seismic loading in different types of soils. Further, the use of these technologies for the reinforcement of clayey soils, raises various questions regarding creep potential at the interface and the effect of bending stiffness on structural displacements.

Soil nailed structures are systems that are coherent and flexible, offering inherent advantages in withstanding large deformations and, as illustrated by post-earthquake observations (Barar, 1990; Felio et al, 1990; Tatsuoka et al, 1996) they present high resistance to earthquake loading. However, to date the analysis of the available case histories and dynamic model tests results has been primarily limited to qualitative evaluation of the system performance and failure mechanisms.

The design methods most currently used for seismic stability analysis of soil nailed systems are derived from the pseudo-static Mononobe-Okabe analysis. Two fundamentally different pseudo-static design approaches have been developed: (i) limit equilibrium analysis (Schlosser, 1983; Koga et al, 1988; Calterance; 1990) which yields only a global safety factor with respect to a rotational or transitional failure of the reinforced soil mass and/or the surrounding ground along the potential sliding surface; and (ii) the working stress analysis using empirical correlations (Richardson and Lee, 1975), or numerically derived design assumptions (Seed and Mitchell, 1981; Dhouib, 1987; Bastick and Segrestin, 1989) to evaluate the seismically induced forces in the reinforcements. Displacement methods have also been incorporated in global limit equilibrium analysis (Bathrust and Cai, 1995), extending the sliding-block theory proposed by Newmark (1965) to predict the permanent horizontal displacements that may accumulate at the base of the structure during seismic events.

The limit equilibrium methods provide only a global safety factor with respect to the shear strength characteristics of the soil and/or the pull-out capacity of the reinforcements. They do not allow for an estimate of the seismic loading effect on the maximum tension and shear forces generated in the nails, and therefore cannot be used to evaluate the local seismic stability of the nailed soil at each reinforcement level. The requirement to evaluate the local pull-out stability of soil nailed retaining systems under both static and seismic loading conditions raises the need for the development and experimental evaluation of working stress design methods in order to estimate the seismic loading effect on the forces mobilized at each reinforcement level.

The KADRENSS working stress analysis code developed by Juran and Elias (1991) was extended (Choukeir et al, 1997) to allow for seismic pseudo static stability analysis of soil nailed retaining systems. The basic assumptions considered in this analysis implies that the seismic loading effect can be represented by a pseudo static self-weight inertia force due to the horizontal acceleration of the potentially sliding active zone limited by the locus of maximum tension forces in the nails. This pseudo static inertia force is equivalent to a uniform horizontal earth pressure acting along the potential sliding surface in the soil nailed mass. For a given earthquake acceleration, its magnitude is therefore directly related to the geometry of the active zone determined from the kinematical working stress analysis.

This pseudo static working stress analysis approach was evaluated (Choukeir et al, 1997) through the comparison of pullout failure simulations with experimental observations on centrifugal soil nailed model walls conducted by Vucetic et al., (1993) and numerical model simulations conducted by Choukeir (1996). Pullout failure observations on the centrifugal shaking table soil nailed model walls are illustrated in Figure (3).

Figure (4) illustrates the comparison of predicted and measured failure geometry in the centrifugal soil-nailed model walls for different acceleration levels of a_m/g = 0. 1, 0.28, and 0.43. This comparison illustrates that, the method predictions agree fairly well with the experimental values of L/H and with the numerical test simulations. The low L/H values obtained for a/g=0.1 can be probably related to the effect of the experimental technique (Choukeir et al, 1997).

However, it should be emphasized that further experimental research and particularly centrifugal and shaking table model testing is necessary in order to establish a statistically significant data base

for the seismic performance assessment as well as for the development and experimental evaluation of reliable seismic design methods for the engineering use of soil nailing in earthquake zones.

Micropiles

Micropiles have been reported (Bruce and Juran 1 997) to be successfully used for seismic retrofitting. However, the engineering use of micropile systems in earthquake zones requires better understanding of the seismic response of micropiles groups and networks as well as the development of relevant methods to predict the effect of seismic loading on structural displacements. A national research project "FOREVER" is presently being conducted in France in cooperation with the Federal Highway Administration to investigate the behavior of the micropile groups and networks, and establish engineering guidelines for their use in civil engineering applications. Within the framework of this project a cooperative study is conducted to evaluate the seismic response of micropile systems involving cyclic and dynamic calibration chamber tests by the ENPC in Paris, 1 -G shaking table model tests conducted by the University of Canterbury , New Zealand, and centrifugal model tests conducted by polytechnic University in the USA. The prime objectives are to evaluate the seismic response of micropile groups and networks to earthquake loading.

Figure 5 shows the micropile model system tested by Polytechnic University in the centrifuge. The instrumentation involved accelerometers to measure the pile head and free field accelerations in order to characterize the structural response of soil-micropile system, transducers (LVDT's) to monitor soil surface settlements, vertical and lateral pile cap displacements, and strain gauges to monitor both axial forces and bending moments and to assess seismic loading and vibration effect on the soil-micropile interaction.

The experimental program consisted of horizontally shaking the models in flight at 20g, using the RPI geotechnical centrifuge (Fig. 6). The horizontal shaking included sequences of 100 uniform cycles of sinusoidal accelerations at 2 Hz (prototype frequency). Prototype micropiles were 0.20 m diameter and 5 m length with bending stiffness of 30 MN.m^2. The models were first subjected to a prototype acceleration time history with amplitude of 0.3g with cap only and then under 50% and 90% of the estimated static failure load (Weltmann, 1980). Details of testing program and limitations were described by Benslimane et al, 1998 and Juran et al, 2000.

Soil – Micropile Interaction: Interaction parameters during base motion excitation at different vibration levels were determined using cyclic p-y curves derived from the single pile data using the procedure suggested by Ting (1987). Figure (7) compares the computed p-y curves under strong and low level of shaking with the cyclic p-y curves recommended by the existing API (1983) guidelines (using $\phi = 32$ $n_h = 6750$ kN/m^3) and the p-y curves reported by Gohl (1991) based on centrifuge tests on model piles with prototype bending stiffness of EI = 172 MN.m^2. It can be seen that for low level of shaking the secant lateral stiffness corresponds fairly well to the results obtained by Gohl (1991). For strong shaking, the API and Gohl (1991) p-y curves are considered stiffer compared to the experimental p-y curves.

Group Effect: Figure (8) displays the experimentally derived pile bending and displacement profiles for (i) single pile, (ii) 2x1 pile group configuration with s/D = 3 (test 7) and s/D = 5 (test 11), and 2x2 pile group (test 10). All these configurations are tested under 0.3g and subjected to 0.9Fl superstructure loading. The experimental results illustrated: (i) negligible interaction effect for 2x1 vertical pile group with s/D = 5. (ii) for the selected frequency of excitation, the experimental data illustrated a "positive" group effect, which results in smaller bending moment and displacement for the spacing to diameter ratio of 3 as compared to single and 2x1 vertical piles.

Network Effect: The experimental data of 2x1 and 3x2x1 networks with 10 and 30 degrees batter piles, displayed on figure (9), illustrate the bi-dimensional network effect results in a decrease of the bending moment as compared with vertical pile as well as in further reduction in lateral pile cap displacement as compared with 2x1 and 3x2x1 vertical pile groups. Furthermore, a substantial improvement is observed in the superstructure response with acceleration reduction to 40% of the values obtained in the case of vertical piles. Nevertheless, a considerable increase in shear and bending moments were observed at pile cap connections as result of changing the load transfer mechanism from bending moment to axial force. These results strongly suggest that further research is needed on the construct-ability of flexible connections for cap micropile systems.

Micropile Network systems for Liquefaction Control

The catastrophic impacts of lateral spreading on urban civil infrastructure systems and networks raise the critical need for innovative approaches to retrofit, rehab, and mitigate earthquake hazards (National Science Foundation – 9836; Japanese Geotechnical Society – JGS). Analysis and design

procedures, as well as performance of conventional piles in earthquake zones involving lateral spreading, are evident to be uncertain (Bardet et al, 1996) due to the lack of physical data, such as case histories, centrifuge tests or shaking table, against which they can be evaluated. Site observations (Herbs, 1994; Mason, 1993; Pearlman et al, 1993; Lizzi and Carnavle, 1981) have demonstrated that micropiles systems appear to provide innovative engineering solutions to earthquake disaster mitigation either for retrofitting or for new construction of infrastructure facilities.

The above critical needs instigated yet a more comprehensive research on the performance of micropile network systems in liquefied soil under lateral spreading. The ongoing liquefaction research at Polytechnic University is a continuation of the FOREVER program described above in collaboration with the Nikken Sekkei Nakase Geotechnical Institute of Japan and the University of Lille in France.

The focus and main objectives of the ongoing research is to investigate the effect of permanent lateral ground displacement due to seismically induced liquefaction and lateral spreading, on the load transfer mechanism between the superstructure – the soil – and the micropile network systems, using the centrifuge modeling and numerical analyses. The prime objective is to assess and develop our fundamental understanding of the effect of lateral spreading on 2-3 D reticulated friction micropile network creating a composite reinforced soil foundations. The specific objectives is to:

(i) Assess the seismic response of the composite micropile-reinforced soil system. The composite system response will be assessed in terms of the effect of micropile system on: a) the buildup of excess pore pressure in the composite reinforced soil foundation as compared with the free field; b) the acceleration profiles and ground motion amplification within the reinforced soil zones as compared with the free field; c) surface settlement profiles under superstructure and in the free filed; and d) the overall stiffness (apparent fundamental period) which significantly affects its dynamic response to the input motion.

(ii) Investigate the basic load transfer mechanism between the superstructure – soil – micropile network system under liquefaction induced lateral spreading in terms of: a) the loading conditions imposed on the micropile system including both inertial loading from the superstructure and kinematical loading from the liquefied ground; b) the resisting forces (e.g. shear, compression,

tension, and bending) mobilized in the micropiles; c) the relative soil micropile displacement during lateral spreading.

It is expected that this cooperative research will contribute to improve the state of practice and provide the engineering community with reliable tools to effectively mitigate and control the seismic induced damage to the critical urban infrastructures.

ACKNOWLEDGMENTS

The work presented herein was funded in part by The Federal Highway Administration and National Science Foundation. The authors are grateful to Mr. AL DiMillio of Federal Highway Administration for providing valuable comments and suggestions.

REFERENCES

API, American Petroleum Institute, 1983, Recommended Practice for Planning, Design, and Construction of Fixed Offshore Platforms, Washington, D.C.

Bardet J.P., Idriss, I.M., O'Rourke, Adachi, N., Hamda, M., and Ishihara, K., (1996) "North America – Japan Workshop on the Geotechnical Aspects of the Kobe, Loma Prieta, and Northridge Earthquake", Report No. 98-36 to National Science Foundation, Air Force Office of Scientific Research, and Japanese Geotechncial Society, Osaka, Japan.

Barar, P., (1990) " The Behavior of Five Soil Nailed Earth Retaining Structures During the Loma Prieta Earthquake of October 17, 1989", Technical Report Prepared by the University of California, Los Angeles.

Bathurst, M., and Cai, Z. (1995), "Pseudo-Static Seismic Analysis of Geosynthetics – Reinforced Segmental Retaining Walls", Geosynthetics International, Vol. 2, No. 5, 787-830.

Bastick, M.J., and Segrestin, P. (1989) " Seismic Design of Reinforced Earth Retaining Walls: the contribution of Finite Element Analysis", Proc. Int. Symp. On Theory and Practice of Earth Reinforcement, Kyushu, Japan, Oct.

Benslimane, A., Juran, I., Hanna, S., and Drabkin, S., (1998), " Seismic Behavior of Micropile Systems", ASCE Special Publications No. 81, Annual Convention, Boston.

Bruce, D.A., and Juran I., (1997) "Drilled and Grouted Micropiles State-of-Practice Review" Federal Highway Administration, Publication No FHW A-RD-96-0 17

CALTRANS (1990), A user manual for SNAIL program, V1.3. Obtained from K.A. Jackura, California Department of Transportation, Division of New Technology, Material and Research, Office of Geotechnical Engineering, Sacramento.

Choukeir, M., Juran, I., and Hanna, S. (1997), "Seismic Design of Reinforced-Earth and Soil-Nailed Structures", J of Ground Improvement, Vol I, No. 4, pp. 223-238

Choukeir, M., (1996), Finite Element Analysis of Reinforced Earth and Soil Nailed Structures under Seismic Loading, Ph.D. Thesis, Polytechnic University, New York.

Dhouib A., (1987) "Contribution a l'etude du comportement des sols renforces sous sollicitations statiques et dynamiques" These de Docteur-Ingeniuer, Universite des Science et Techniques de Lille Flandres Artois, France.

Fukuoka, M., "Stability of Retaining Wall Reinforced by Continuous Fibers During Earthquakes". Proceedings of The 4th International Congress on Geotextiles, the Hague, the Netherlands, I 990, pp. 546-558 I 990.

Felio, G. Y., Vucetic, M., Hudson, M, Barar, P., and Chapman, R. (1990) "Performance of Soil Nailed Walls during the October 17, 1989 Loma Prieta Earthquake" Proceedings, Forty-third Canadian Geotechnical Conference, Quebec, Oct.

French National Research Project CLOUTERRE, (1993) "Recommendations CLOUTERRE 1991-Soil Nailing Recommendations 1991 " Presses de l'Ecole National des Ponts et Clausseess, English Translation

Gohl, W. B., (1991) "Response of Pile Foundations to Simulate Earthquake Loading – Experimental-and Analytical Results", Ph.D. dissertation, University of British Columbia, Canda.

Herbst, T.F., (1994) "The GEWI-PILE, a micropile for retrofitting, seismic upgrading and difficult installation", Int. Conference on Design and Construction of Deep Foundations, Sponsored by the US Federal Highway Administration (FHWA), Vol. (2), 913-930.

Ingold, T S and Miles, B (1996) "Ballistic soil nailing Earth Reinforcemen1" *H. Ochiai, N. YasufiJku, and K Omine,* eds., Proceedings of The International Symposium on Earth Reinforcement, Japan.

Juran, I., Benslimane, A., and Hanna, S. (2000) "Engineering Analysis of the Dynamic Behavior of Micropile Systems", Transportation Research Board, Paper No. 00-0768, presented Jan 10.

Juran, I., Benslimane, A., Hanna, S., and Perlo, S., (1997) "Seismic Behavior of Micropile Systems - Centrifuge T est Results" Preliminary Report - FHWA Contract No DTFH61-96-00021

Juran I., and Elias, V. (1991), Ground Anchors and Soil Nails in Retaining Structures, In Foundation Engineering Handbook, 2nd edn. Hasai-Yang Fang, Chapter 26

Koga, Y., Ita, Y., Washida, S., and Shimazu, T. (PWRI, 1988), "Seismic Resistance of Reinforced Embankment by Model Shaking Table Tests" Int. Geotechnical Symp. On Theory and Practice of Earth Reinforcement, Balkema, Rotterdam, pp. 413-428

Lizzi, F., and Carnevale, G. (1981), "The static restoration of the leaning AL Habda Minaret in Mosul (Iraq)" Proceeding 3rd International Symposium on Babylon, Ashur and Haditha, Baghdad. November.

Louis, C. (1986) "Theory and practice in soil nailing temporary or permanent works" ASCE Annual Conference, Boston

Maher, M. H., and Woods, R. D. (1990) "Dynamic response of sand reinforced with randomly distributed fibers " J Geotech Engrg., ASCE, Vol. 116,No 7,pp 116-1131

Mason, J.A., (1993) "CALTRANS full scale lateral load test of a driven pile foundation in soft bay mud. Preliminary results", California Department of Transportation (CALTRANS), Division o f Structure, Sacramento, California, 31pp.

NSF - 9836, National Science Foundation (1997), US-Japan Cooperative Research in Urban Earthquake Disaster Mitigation, NSF joint program funding announcement number 9836, Division of Civil and Mechanical Systems, Virginia.

Newmark, N.M., (1965) "Effect of Earthquake on Dams and Embankments", Geotechnique, Vol 15, No. 2, 139-159.

Pearlman, S.L., Wolosick, J.R., and Groneck (1993) "Pinpiles for seismic rehabilitation of bridges", *Proceeding, 10th International Bridge Conference.* Pittsburg, Pennsylvania. June 14-16.

Richardson G.N., and Lee K.L. (1975), "Seismic Design of Reinforcement Earth Walls", J. Geotech. Engng Div., ASCE, 101 No. GT2, Feb., 167-188.

Schlosser, F., (1983) " Analogies et differences dans le comportment et par clouage du sol", Annales de l'Innstitute Technique du Batiment et des Travaux Publics, No. 418

Seed H B and Mitchell J.K. ,(1981) Earthquake resistant design of reinforced earth walls Internal study for the Reinforced Earth company. Progress Report Berkely, California

Tatsuoka, F., Tateyama, M., and Koseki, J., (1996) "Performance of Soil Retaining Walls for Railway Embankments", Soils and Foundations, Special Issue on Geotechnical Aspects of the Jan. 1995 Hyogoken-Nanbu Earthquake, pp. 311-324.

Vucetic, M, Tufenkjian, M, and Doroudian, M (1993) "Dynamic Centrifuge Testing of Soil-Nailed Excavations" ASTM Geotechnical Testing Journal, Vol. 16, No. 2 pp.172-187

Weltmann, A.J., (1980) "Pile Load Testing Procedure" Report PG 7, Construction Industry Research and Information Association (CIRIA), London, 53pp.

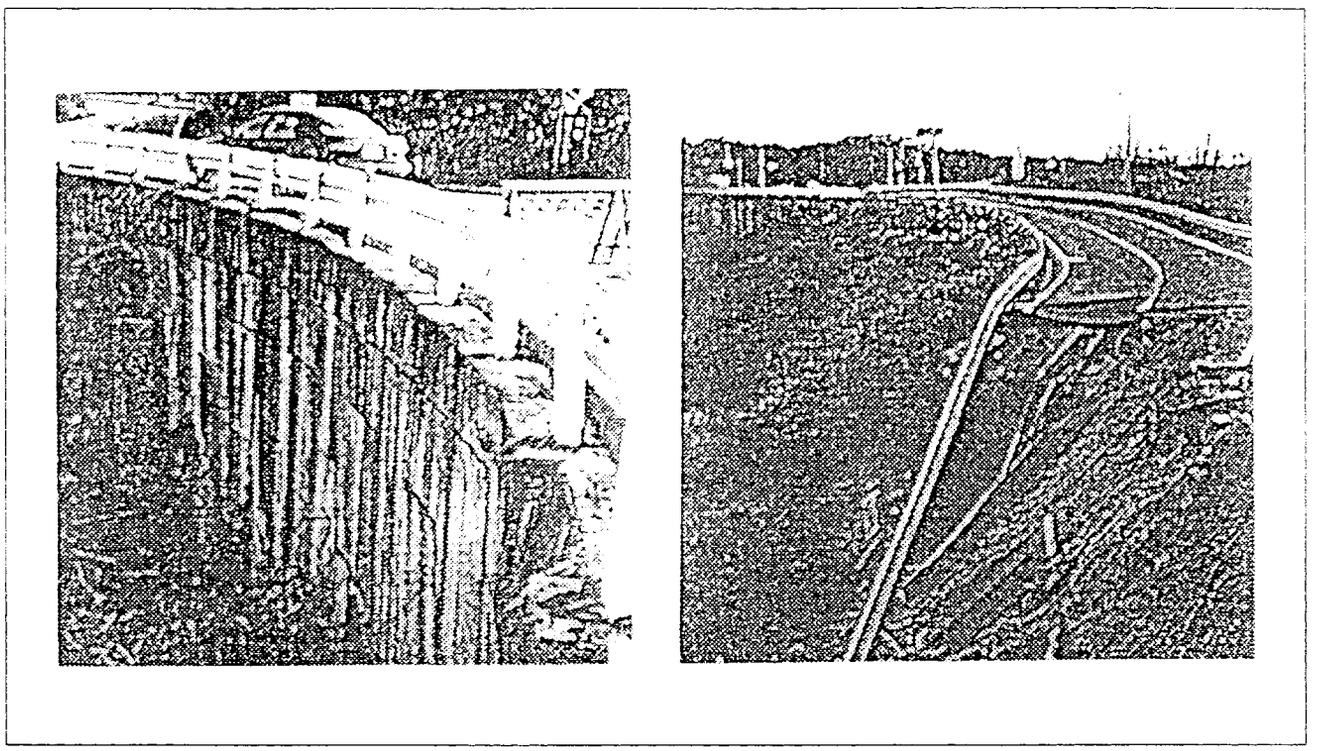

Fig. 1 — Reinforced earth structure performance after the Hanshin earthquake (1995)

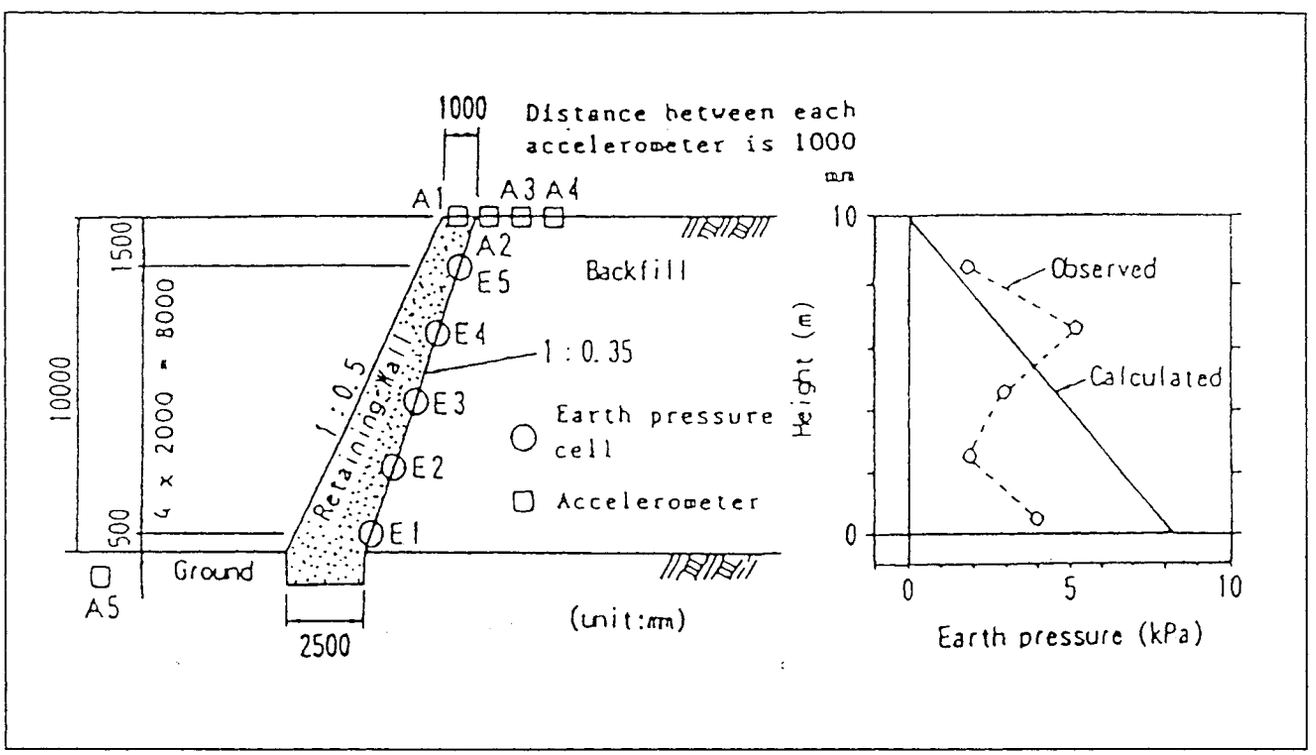

Fig. 2 — Model retaining wall and observation points: maximum increments of earth pressure due to earthquake (Fukuoka, 1990)

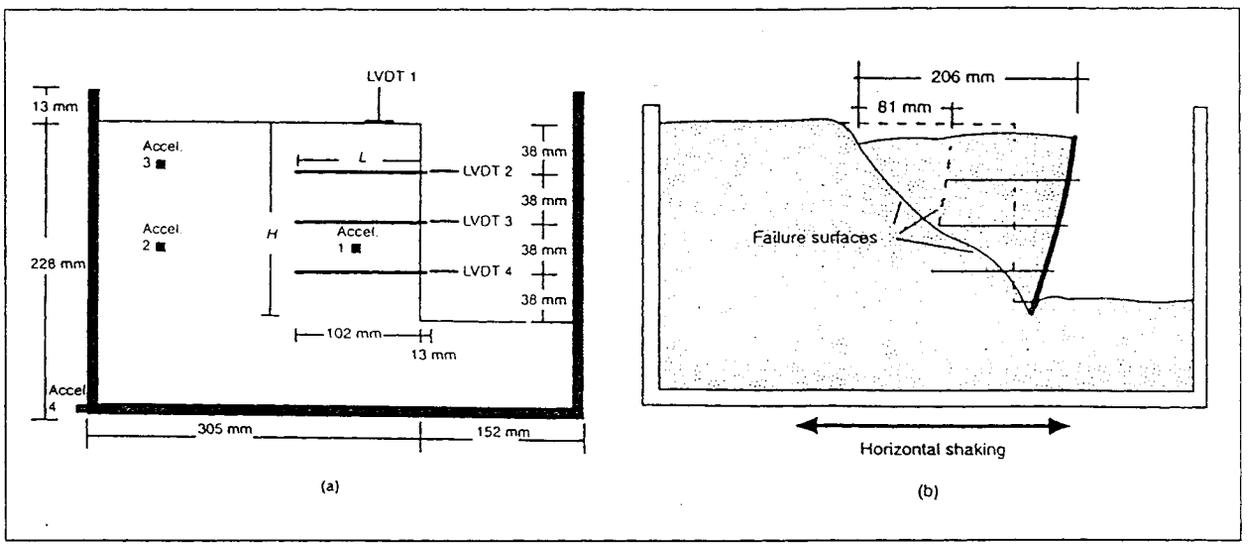

Fig. 3 — Configuration of centrifuge model wall (Vucetic et al, 1993), (a) Longitudinal view of the model box; (b) Failure surface

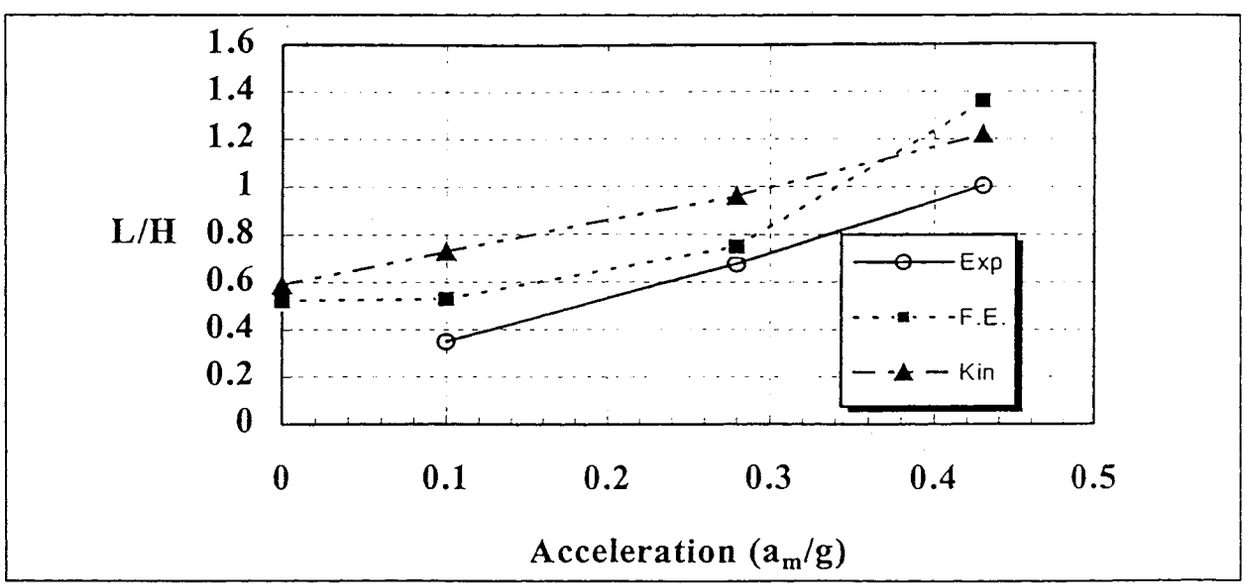

Fig. 4 — Comparison between experimental results (Exp.) of pullout failure (L/H values), and values obtained from the finite element simulations (FE) and from KADRENSS code predictions (KADR)

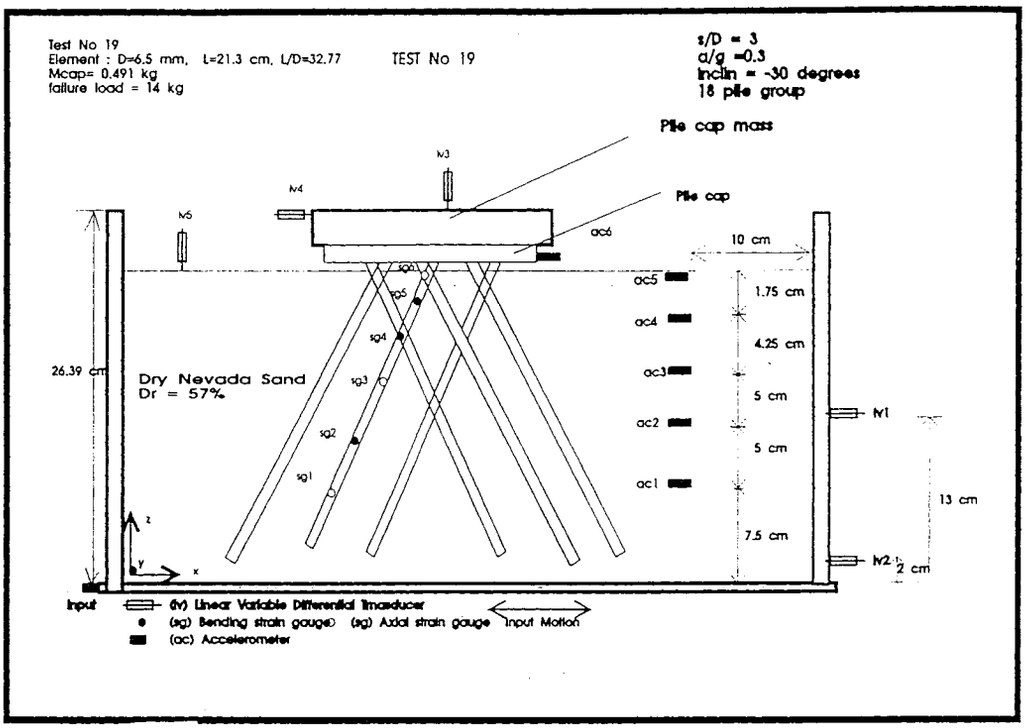

Figure 5a — Sketch of 18 pile network system investigated (Test Conf. 19)

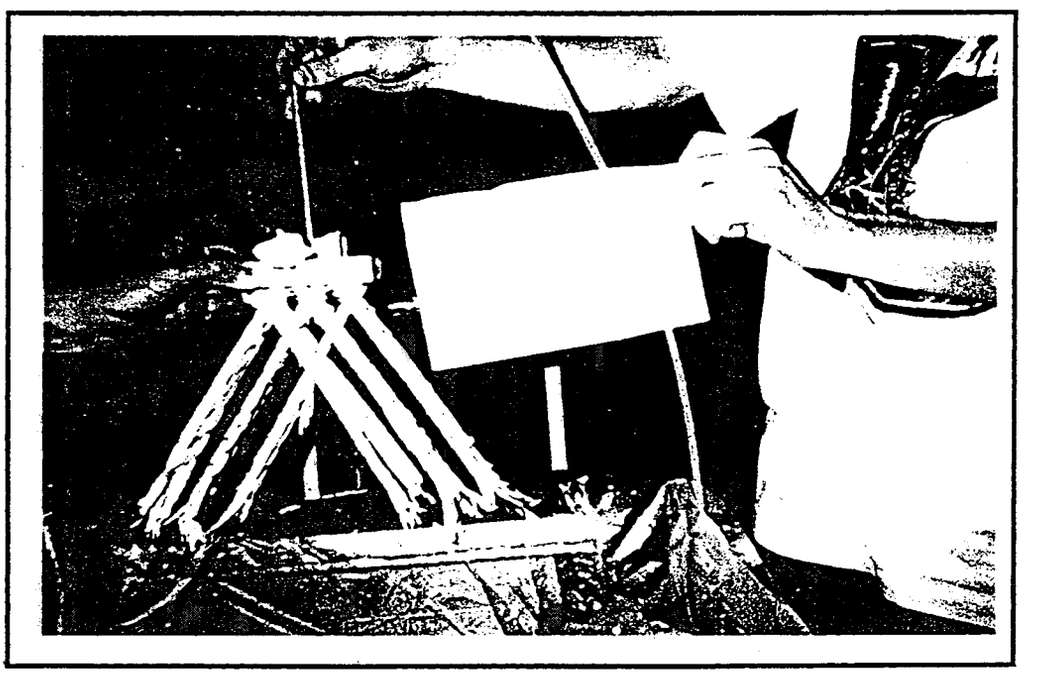

Figure 5b — Photograph of the adopted configuration in centrifuge Test Conf.19

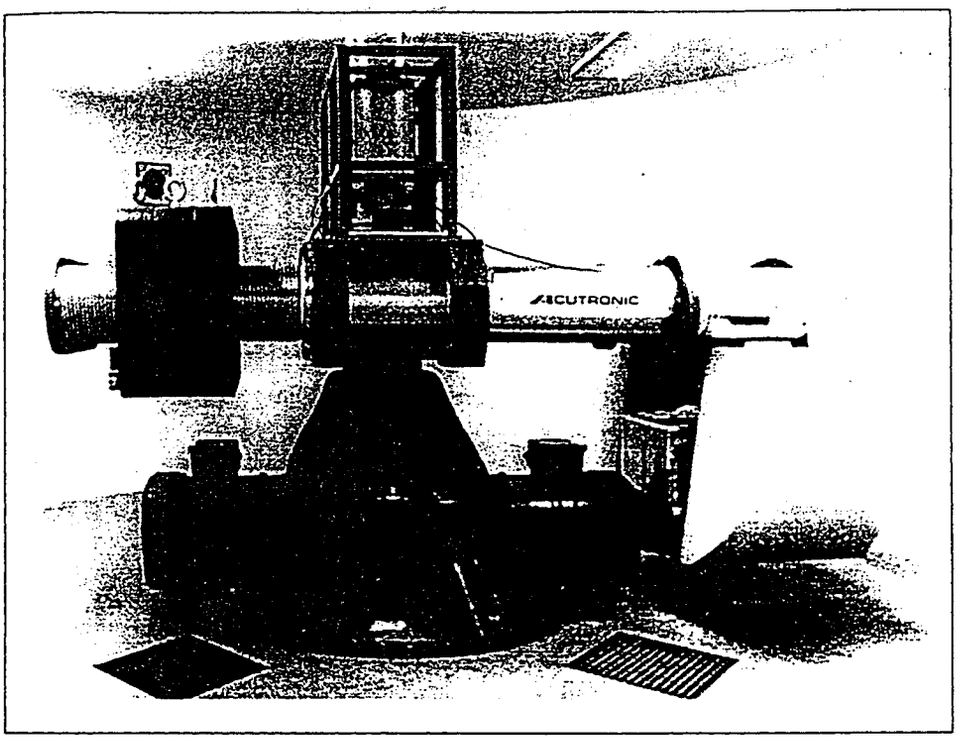

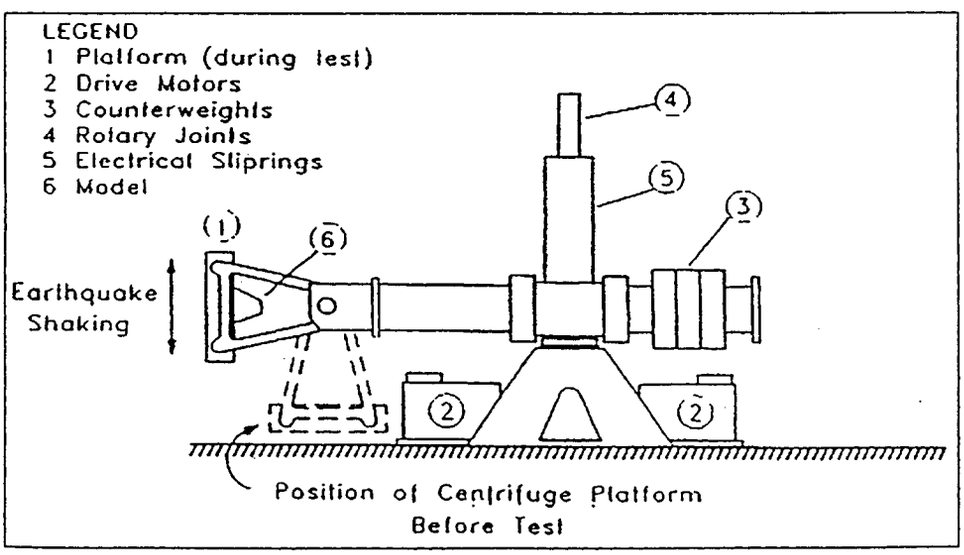

Figure 6 — Sketch and photograph of the RPI geotechnical centrifuge

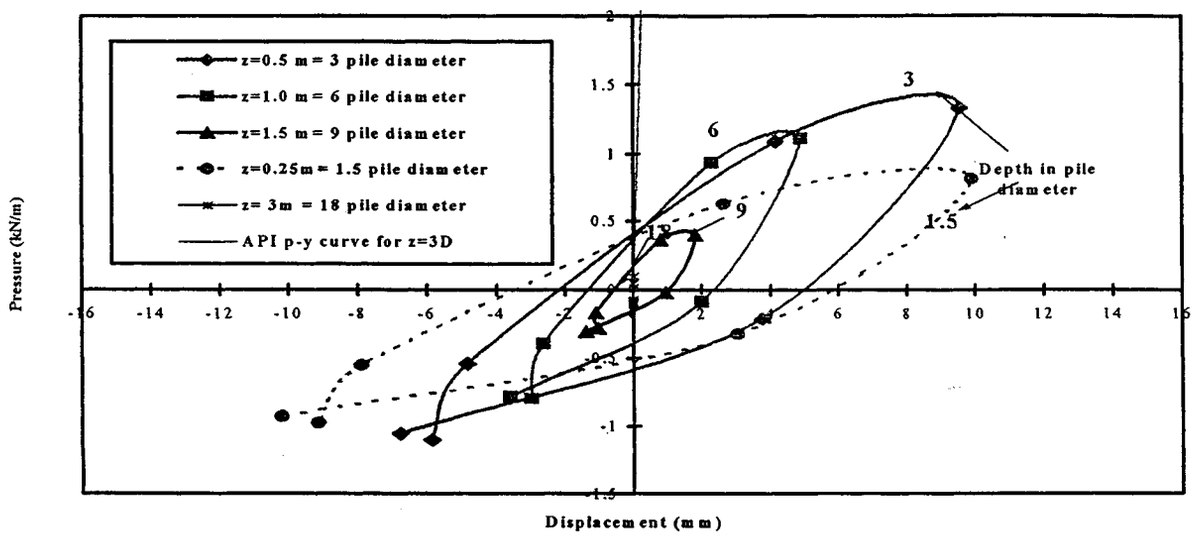

Figure 7a. Cyclic p-y curves at depths during steady state shaking cycle (t=30-30.5 sec) and comparison with API p-y curve – centrifuge test 1 (203) (a/g=0.03).

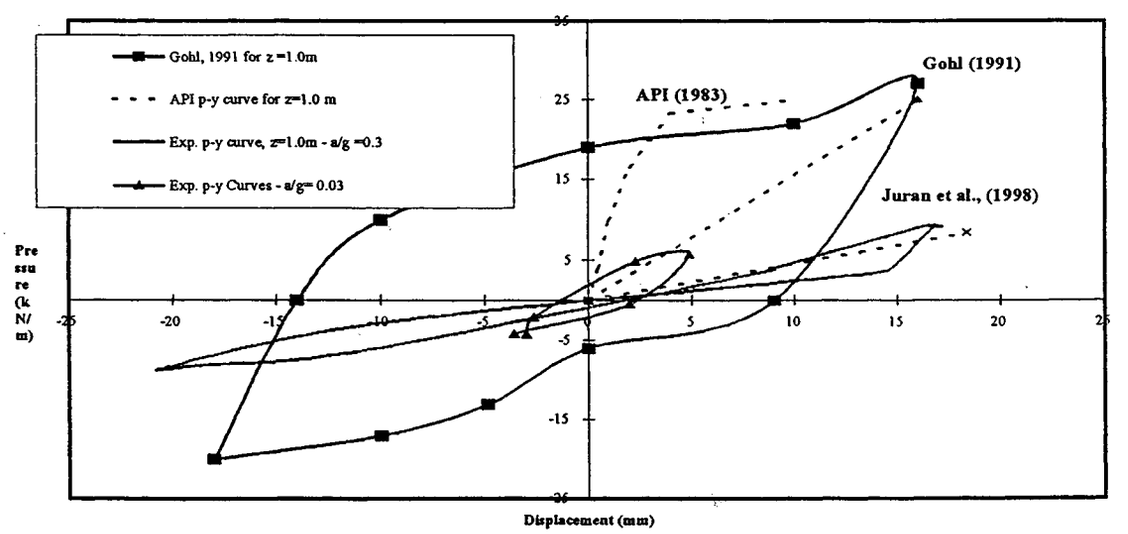

Figure 7b. Comparison of the experimentally derived cyclic p-y curves during steady state shaking cycle (t=30-30.5sec – centrifuge test 1-203 and P5) with API (1983) p-y curve, and Gohl, 1991

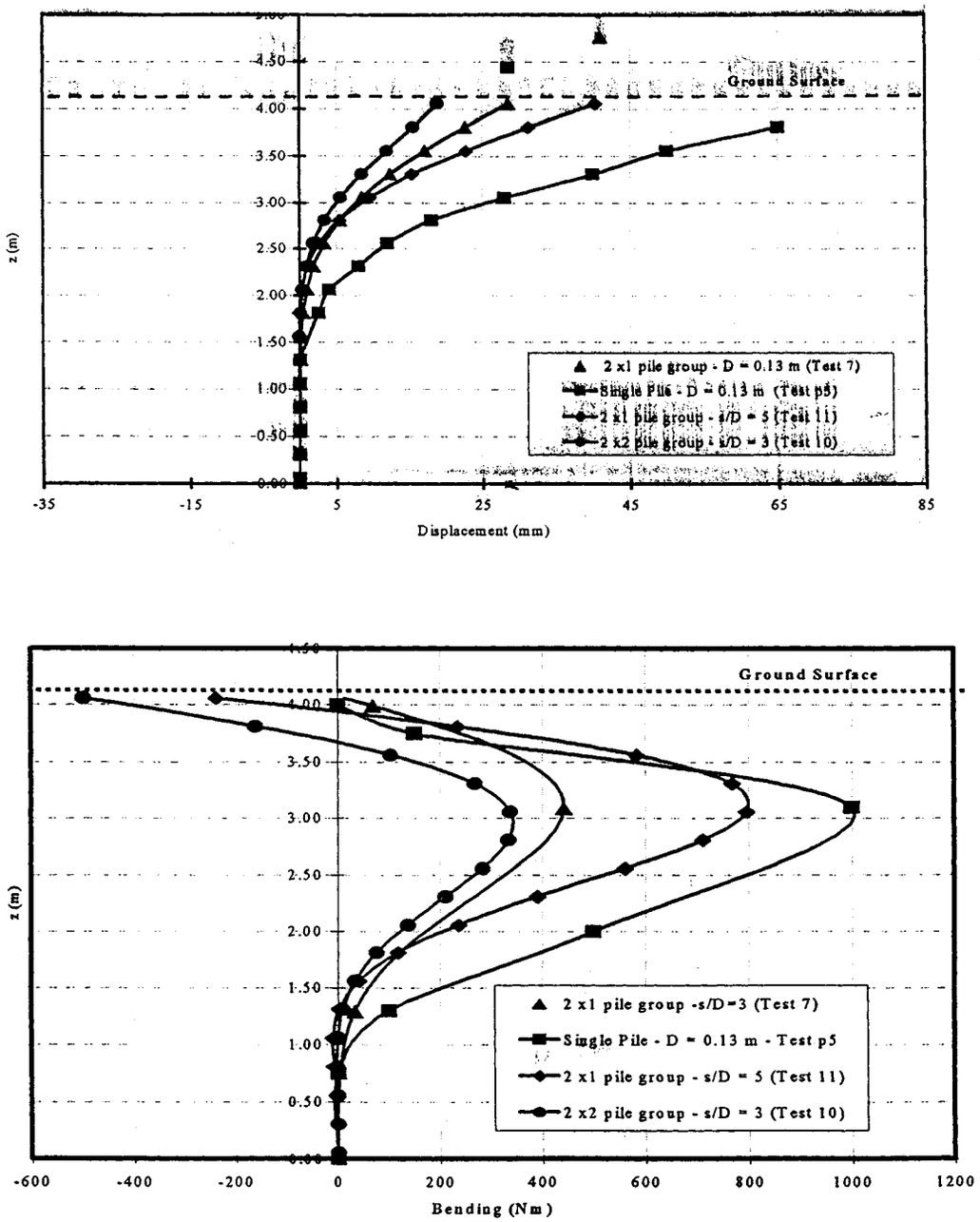

Figure 8. Effect of the spacing to diameter ratio (s/D) on the recorded a) displacement and b) bending moment profiles of micropile systems. (a/g_2= 0.3, D = 0.13m, 0.9FL)

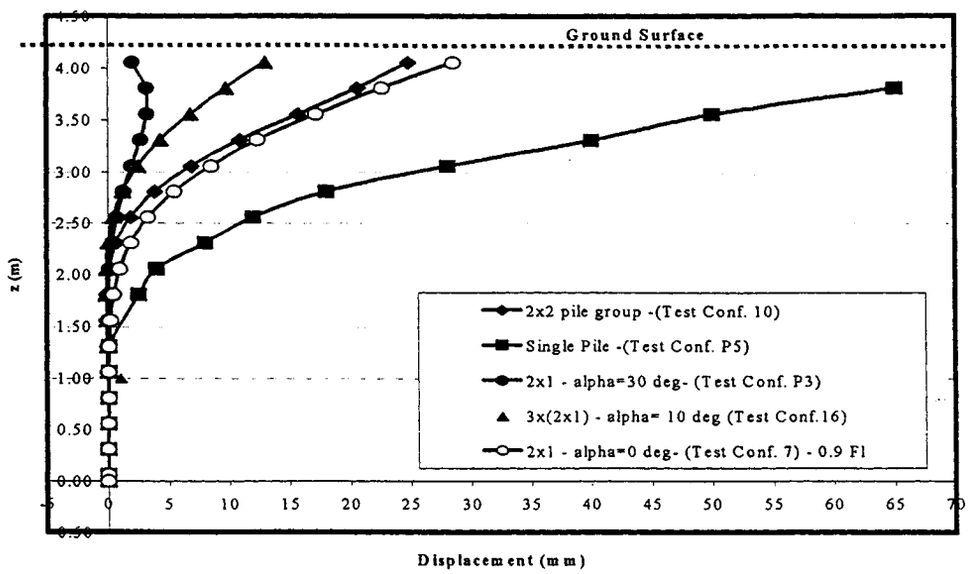

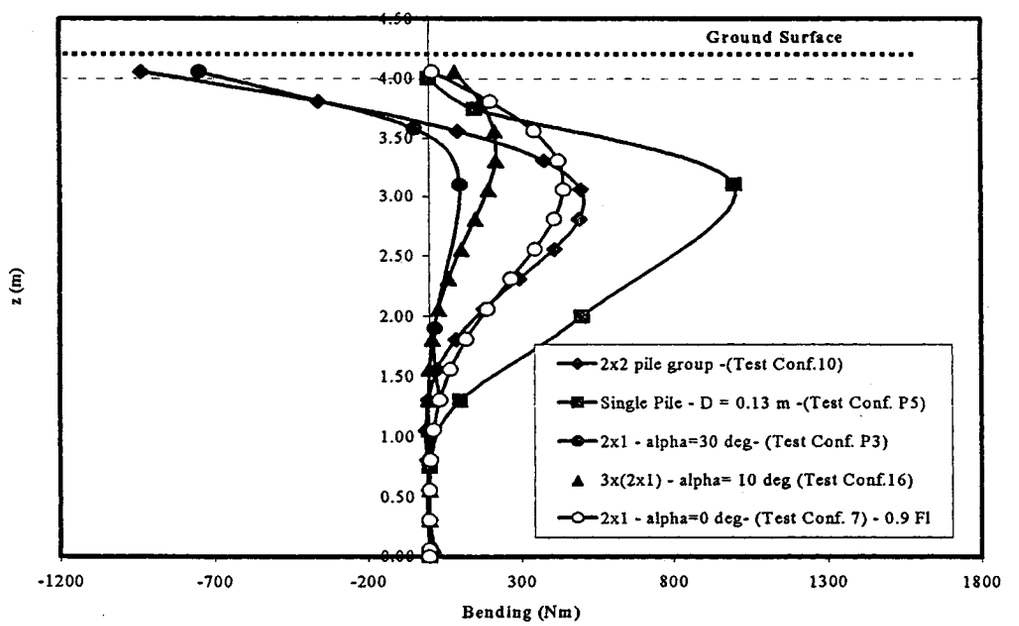

Figure 9. Effect of the pile inclination (□) on the recorded a) displacement and;
b) bending moment profiles of micropile systems. (a/g = 0.3, D = 0.13m, s/D = 3, 0.5FL)

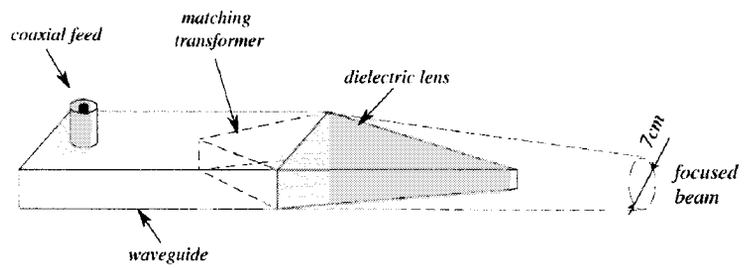

Fig. 8. Dielectric Lens

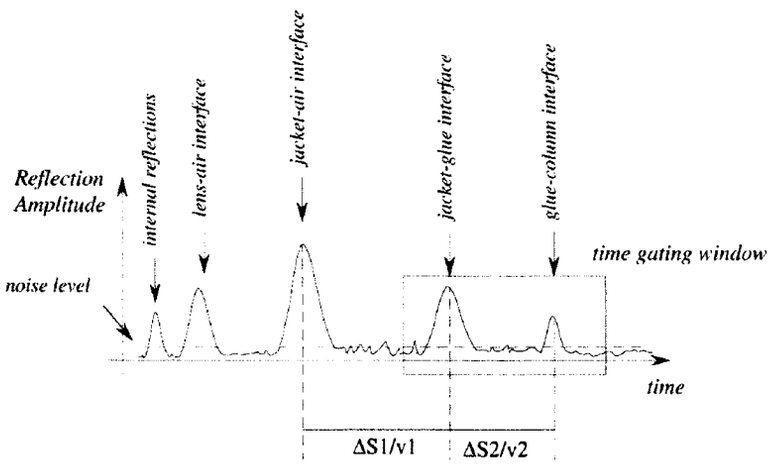

Fig. 9 Time Gating of Reflection Signal

In order to remove spurious signals, the time gating technique is used. This technique allows one to select a specified time frame in which the received or reflected signal is to be observed. In this way, unwanted reflections due to unavoidable obstacles different from air voids, such as the lens internal reflections and air to lens reflection, can be removed. The time gating concept is illustrated in Fig.9.

Measurement of Dielectric Properties

Accurate measurement of dielectric properties of different materials involved in an FRP-jacketed RC column was pursued in this study. Such properties, including dielectric constants and conductivity, are needed for the simulation analysis of the EM imaging technology. For the measurement, flat material sample sheets, each with an equal dimension of 25.5cm by 21.5cm, were made from glass fiber reinforced polymer, carbon fiber reinforced polymer, adhesive epoxy, and concrete, respectively. The complete experimental setup is shown in Fig. 10. A material sample sheet is inserted in a reflectometer which is connected to an automatic network analyzer (ANA), HP-8510, and further to a personal computer (PC).

The dielectric properties of each material are measured from the response of the material sample to plane wave excitation in the free space. There are usually two fundamental difficulties associated with the measurement of the free space reflection and transmission with respect to the material sample: First, it is difficult to generate a uniform plane wave and second, unwanted parasitic reflections and multiple reflections are produced in the measurement path. Fortunately, with its special design based on the use of hollow metal dielectric waveguide (HMDW) as the wave transmission line structure, the reflectometer used in this study virtually eliminates both of these problems.

As shown in Fig.10, the reflectometer has four ports. A microwave signal from port 1 of the ANA is fed into the small end of the tapered transition connected to port 1 of the HMDW cross directional coupler, and is converted from the TE mode to LM mode. The signal passes through the HMDW cross waveguide coupler at port 1. Part of the signal goes to the load at port 4, while most of the signal passed through, to the sample under test at port 3. The reflection from the sample returns through port 3 and in turn splits into a component that passes through to the source arm at port 1 and into a major component that is coupled to the receiver/detector arm at

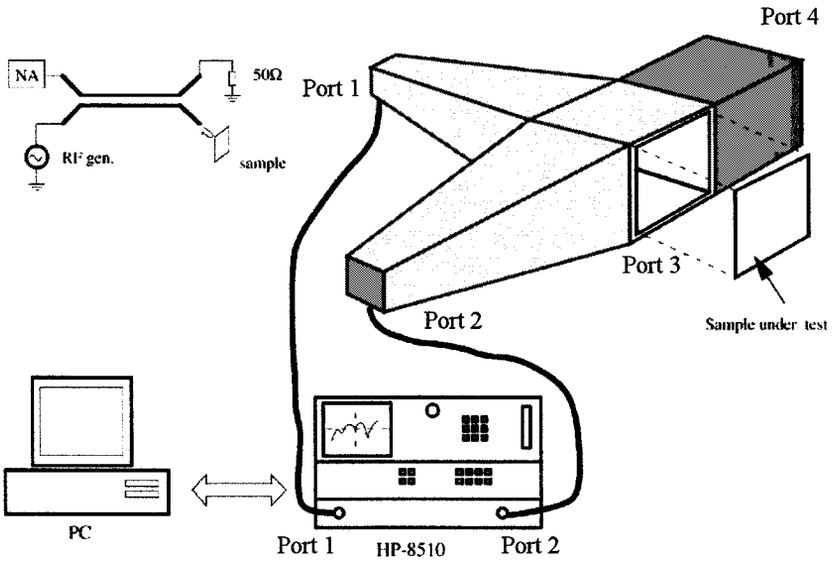

Fig. 10 Experimental Setup for Dielectric Property Measurement

port 2 of the HMDW coupler. The coupled signal passes through the waveguide transition of arm 2 and onto port 2 of the ANA. The magnitude of the received signal at port 2 of the ANA is proportional to the magnitude of the reflection coefficient of the material sample under test. The measured dielectric constant (relative to the air) and conductivity for the different material samples are listed in Table 1. Samples No. 1, 2, and 3 shown in Table 1 were used for the calibration purpose. The comparison between the measured and known values of these samples demonstrates that the special reflectometer designed and fabricated in this study is capable of measuring dielectric properties with high accuracy.

Table 1. Measurement of Dielectric Property

Sample Number	Relative Dielectric Constant	Conductivity (S/m)
1	10.87 (10.8*)	0.68
2	2.28 (2.33*)	0.09
3	1.07 (1.02*)	0.00
4 (E-glass)	3.59	0.27
5 (Carbon Fiber)	14.66	2.49

* known values

Experimental Verification on FRP-Jacketed RC Columns

The effectiveness of the proposed EM imaging technology using focused EM waves and reflection analysis is investigated through experiments on FRP-jacketed RC columns. Three concrete columns of 16-in in diameter and 32-in in height were built. Two of these columns were built without reinforcing rebars and the third with No. 5 longitudinal rebars, in order to examine the influence of steel rebars on the detection. Each of the columns was wrapped with a three-layer glass FRP jacket. The thickness of each layer is 1.143 mm (0.045 in).

Various voids and debonding conditions were artificially introduced between the jackets and the columns and between the layers of the jackets. Some voids were caused by the holes on the concrete column surface which remained there although supposed to be filled before the application of jackets. Others were introduced by inserting a small block of Styrofoam in the bonding interface, which has the same dielectric property as that of the air.

Figure 11 is a photo showing one of the columns under testing. Two specially designed lenses are placed in 40 degrees with each other on a support that can slide up and down. One of them transmits and focuses the EM waves sent from the ANA (HP-8510) on the bonding interface of the jacketed column and the other receives the reflected waves. Two pieces of disks with smooth surfaces are installed on the bottom of each column, making it easily rotate. With the lenses sliding up and down and the column rotating, the entire surface of the jacketed column can be easily scanned without rotating the lenses and the ANA. For the future applications in the field, a portable compact device including an analyzer and the lenses will be developed and the scan mechanism will obviously be modified.

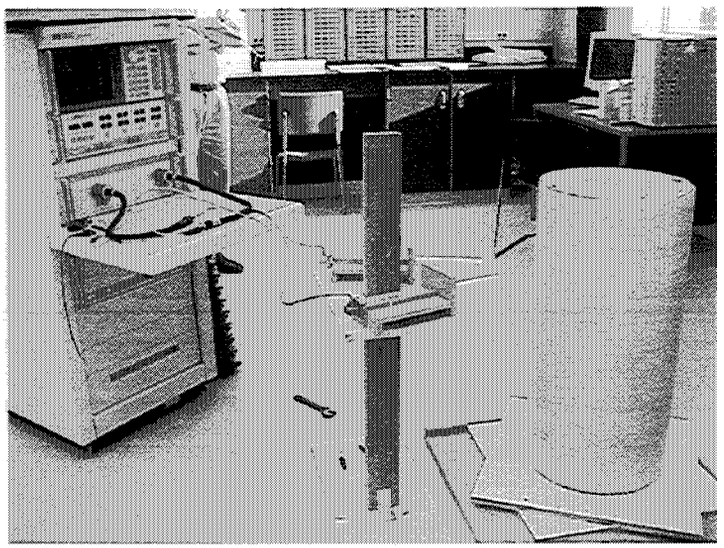

Fig. 11. FRP-Jacketed Concrete Columns under Testing

The ANA receives the reflected signals from one of the lenses and compares it with a reference signal representing a perfect bonding situation. Both time- and frequency-domain analysis can be performed. A computer program was developed especially for a PC to control the operation of the EM image scan. Signal processing for one point takes about half second.

A variety of EM waves with different frequencies ranging from 11.0GHz to 12.4GHz were tested. Figures 12(a) and (b) show 3D images scanned over an area of 110 mm by 110 mm in the surface of the jacketed concrete column, respectively using 11.0GHz and 12.4GHz waves. This area contains a hole in the concrete column surface. Although the air void cannot been seen from the outside of the jacket, the EM images produced in Figure 12 clearly identify the location and area of the void. The image produced using the higher frequency waves has a slightly better resolution. The voids and debonding at other locations were also successfully detected.

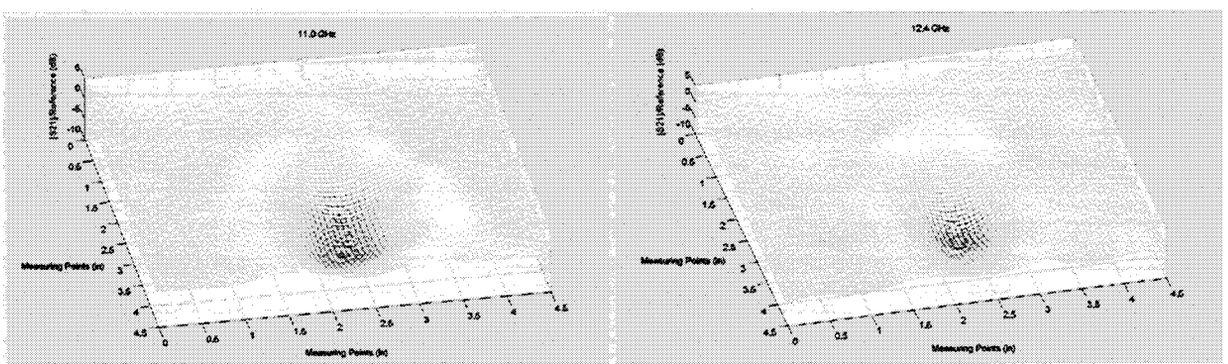

(a) 11.0 GHz Waves (b) 12.4 GHz Waves

Fig. 12. Scanned 3D Images of Bonding Interface

CONCLUDING REMARKS

The optical fiber sensors measuring acceleration, displacement, strain, and pressure developed in this study have innovative design based on interdisciplinary research effort, that makes them highly useful for monitoring large-scale civil engineering structures. These sensors are optically powered and transmit signals through optical fibers, thus eliminating all the practical problems associated with electrical cables of conventional sensors (electromagnetic interference, heavy weight, high cost, etc.). They represent a significant advancement over the currently available optical fiber sensors, because each durable sensor head consists of an oscillatory circuit and transforms a measured quantity into a frequency modulated (FM) signal with proven reliability even over a long-distance transmission. Extensive experimental studies performed in the laboratory and field demonstrated excellent performance of these sensors in terms of their accuracy, reliability, and ease of installation.

The NDE technology of using EM waves for detecting damage of jacketed RC columns also represents an innovative design based on interdisciplinary research efforts. The approach based on reflection analysis together with the use of special dielectric lenses and the time-gating technique has produced excellent results: The invisible voids and debonding conditions between an RC column and its FRP jacket have been successfully detected. A portable device suitable for field applications is currently under development.

By making condition monitoring and damage assessment of civil structures practical and reliable, the optical fiber sensors and the EM imaging NDE devices will make structural maintenance and management more cost-effective, and thus further enhance structural safety and reliability under natural and man-made hazards.

ACKNOWLEDGEMENTS

This work was supported by the National Science Foundation under Grants CMS-9501796, CMS-9812585 and CMS-9812856.

REFERENCES

Feng, M. Q. (1996). "An Experimental Study on an Electro-Optical Displacement Sensor", *Nondestructive Testing and Evaluation*,13, 5-14.

Feng, M. Q. (1998). "An Electro-Optical Accelerometer and Its Field Testing", *Journal of Engineering Mechanics, ASCE*, 124(5), 513-519..

Feng, M. Q. and Kim, J. M. (1998). "Identification of a Dynamic System Using Ambient Vibration Measurements", *Journal of Applied Mechanics, ASME*, 65(2), 1010-1023.

Feng, M. Q., Liu, C., He, X., and Shinozuka, M. (2000a). "Electromagnetic Image Reconstruction for Damage Detection", *Accepted for publication in Journal of Engineering Mechanics, ASCE.*

Feng, M.Q. De Flaviis, F., and Kim, Y.J. (2000b). "Application of Electromagnetic Waves in Damage Detection of Concrete Structures", *Proceedings of the International Symposium on Smart Structures and Materials, SPIE*, March 1-2, 2000, Newport Beach, CA.

Haroun, M. A. and Feng, M.Q. (1997). "Lap Splice and Shear Enhancements in Composite-Jacketed Bridge Columns", *Proceedings of the 3rd US-Japan Bridge Workshop*, Tsububa, Japan, 1997.

Session 2

Damage Assessment and Detection by Advanced Technologies

Chairs: A.E. Aktan and S. Masri

Advanced Accelerometers and Liquefaction Meters for Damage Assessment of Gas Distribution Systems

*Yoshihisa Shimizu[1)]

ABSTRACT

In order to achieve a more sophisticated real-time system of disaster mitigation, Tokyo Gas Co., Ltd., commenced preparation of what will be the world's most extensive ultra-high-density real-time seismic motion monitoring and disaster mitigation system in January 1998. Known as "SUPREME," the system employs the New SI (spectrum intensity) sensor and a district regulator remote surveillance system installed at about 3,600 locations in its supply area, which measures about 3,100 square kilometers. The New SI sensors are capable of measuring SI and ground acceleration, recording six earthquake wave-form acceleration trends on three (XYZ) axes, detecting liquefaction based on knowledge of the changes in acceleration waves, and control of regulators by means of settings for SI or acceleration. Tokyo Gas intends to harness the system for high-precision estimates of damage and detection of liquefaction in real time, and for investigation of seismic shaking amplication at various points based on wave-forms for small and medium earthquakes.

KEYWORDS

Real-time, Damage estimation, Damage mitigation, Earthquake monitoring, Liquefaction detection method, SUPREME, SI

INTRODUCTION

Tokyo Gas Co., Ltd. supplies gas to customers in metropolitan Tokyo area -- one of the world's most densely populated urban areas, and a major center of political, cultural and economic activity. We regard it as part of our responsibility to society as a gas supplier to assure safety even in the event of a major earthquake. Such preparations have long been an important concern of Tokyo Gas, and a range of hardware and software solutions is in place, including both the hardware of gas supply facilities and the software such as regulations or manuals relating to emergency response and efficiency of restoration work.

On 17 January 1995, an earthquake with a magnitude of 7.2 occurred directly under the Hanshin-Awajishima area of Japan. It resulted in unprecedented damage, especially in

[1)] *Senior Manager, Center for Disaster Management and Supply Control, Tokyo Gas Co., Ltd., Japan, 5-20, Kaigan 1-chome, Minato-ku, Tokyo 105-8527, Japan*

the city of Kobe, and subsequently became known as the "Great Hanshin Earthquake." As shown in Table 1, it also caused considerable damage to city gas supply facilities, and particularly low-pressure pipelines. The results reconfirmed the immensity of the threat posed by earthquakes and also underscored the importance of emergency response systems for gas supply facilities in the event of an earthquake (Agency of Natural Resources and Energy, 1996).

Table 1. Damage to gas facilities in the Great Hanshin Earthquake

Item	Details
1. Damage to pipelines	Medium-pressure pipelines 106 cases of leakage Low-pressure pipelines 26,459 cases of leakage
2. Number of cases of supply suspension	About 860,000
3. Number of days required for complete resumption	85 days

The Great Hanshin Earthquake provided graphic proof of how difficult it is to gather information on damage immediately after an earthquake, in spite of the crucial importance of obtaining such information. As a means of resolving this difficulty, systems for real-time estimation of earthquake damage are being planned or constructed by several agencies. To the same end, Tokyo Gas launched development of the Seismic Information Gathering & Network Alert System (SIGNAL) (Shimizu, Y., 1997) in 1986 and put it into operation in June 1994, about six months prior to the Great Hanshin Earthquake. With a view to achieving a higher level of safety in the event of major earthquakes, it began constructing another system in January 1998 for SUPer-dense REal-time Monitoring of Earthquakes (SUPREME). Based on installation of roughly 3,600 new seismometers (New SI sensors) over its supply area of roughly 3,100 square kilometers, the new system will feature the most intensive seismic monitoring of any in the world.

DEVELOPMENT OF THE NEW SI SENSORS

Micro-machining technology has made possible the adoption of ultra small acceleration pickups (manufactured by Sumitomo Precision Products Co., Ltd.), and the availability of low-cost, high performance CPU and RAM devices have resulted in the joint development together with Yamatake Co., Ltd. of a New SI sensor (see figure 1), which features high precision and high performance at a low price. The features are as follows:

Both Control and Measurement Functions, and Accommodation of Telemeter Equipment

The New SI sensors employ a voltageless relay contact point output for regulator shutoff, analog output of SI values and acceleration data for measurement, and an alarm (contact point output) for liquefaction. The analog output is of a highly general-purpose

nature; it has an operational range of 4 - 20 mA to accommodate various kinds of telemeter equipment.

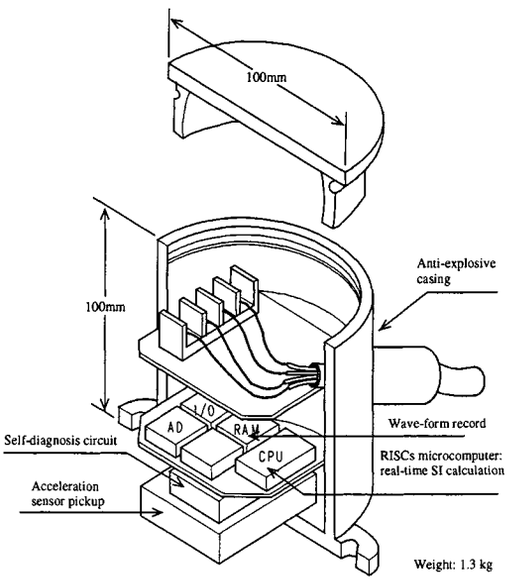

Figure 1. New SI sensor

The sensors are capable of measuring acceleration from plus 2,000 Gal to minus 2,000 Gal, and with a precision of less than plus or minus 5 percent. Moreover, the setting for issuance of alerts can be changed (in addition, the SI and acceleration settings can be selected as desired).

Wave-Form Data Storage

The New SI sensors are also equipped for storage of the earthquake wave-form data to permit their use in the formulation of disaster mitigation countermeasures and in related research. The data are stored on an internal memory together with header information for items such as six earthquake wave-forms on the X, Y, and Z axes, (listed beginning with the highest SI value) and the dates of occurrence. The sensors have a recording data sampling time of 1/100th of a second, a resolution of 1/8th of a Gal, and a wave-form recording duration of 50 seconds (from plus to minus 25 seconds) per seismic wave, centered around the wave with the highest SI value. Figure 2 shows the acceleration wave-form data actually stored for an earthquake which struck in the southern part of Ibaraki prefecture on 14 January 1998.

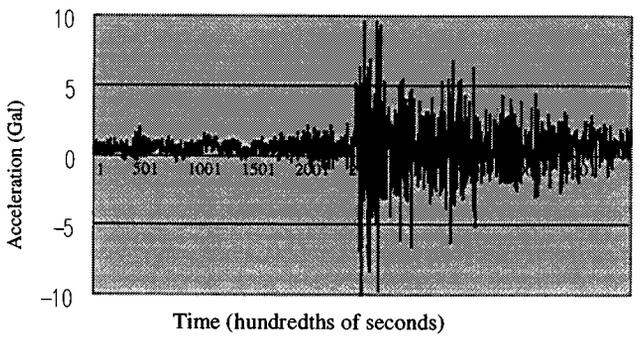

Figure 2. Seismic data, 1998/1/14 (Konan, Minato ward)

Self-Diagnosis

The SI units are equipped with a constantly available self-diagnostic function in the interest of more reliable action. In the event of abnormality, the situation can be promptly apprehended by abnormal output to the tele-metering device.

Liquefaction Judgment

Data on ground liquefaction are extremely important for estimating damage. Conventionally, the acquisition of such data has required large-scale boring. The New SI sensors make a judgment on the presence or absence of liquefaction from the changes in the acceleration wave-forms, and therefore make it extremely simple to apprehend ground liquefaction. As shown in Figure 3, the wave-form period for Port Island, where ground liquefaction occurred in the Great Hanshin Earthquake, is clearly longer than that for the Kobe Marine Meteorological Station.

The New SI sensors judge that ground liquefaction has occurred when the four conditions shown below have been met in respect of acceleration (A max), SI value, estimated displacement (D; $2SI^2/A$ max) (Towhata, I., J.K., Orense, R.P. and Kano, H., 1996), and estimated period (T), based on the change in seismic wave-form. The estimated period is equated with the time interval as defined by zero-cross, i.e., the time required for the wave-form trend measured by the sensor to cross the zero line.

(I) Amax > 100 gal
(II) SI value > 20 kine
(III) D > 10 cm
(IV) T > 2 sec

Recorded at Port Island (where severe liquefaction occurred)

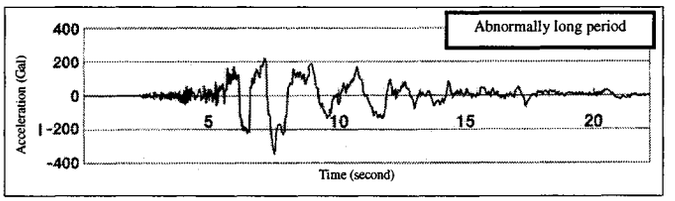

Recorded at the Kobe Marine Meteorological Station
(no liquefaction)

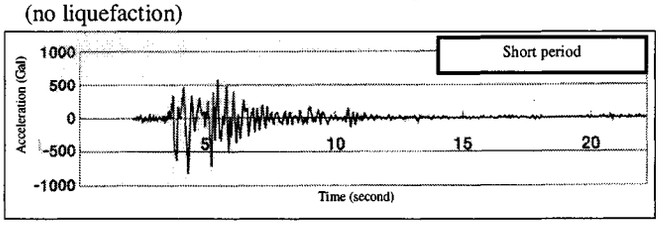

Figure 3. Seismic wave-forms for the Great Hanshin Earthquake

Figure 4 shows the results of the analysis of wave-forms and liquefaction judgment in the case of 70 past earthquakes. Among these 70 earthquakes, those which actually caused liquefaction were as follows (with areas of liquefaction noted in parentheses): the Central Sea of Japan Earthquake (Aomori, Hachirogata, and the Tsugaru Bridge), the Great Hanshin Earthquake (Amagasaki, Kobe harbor, Port Island, and the East Kobe Bridge), Superstition Hill (Wildlife) (Matasovic J. and Vucetic, M., 1993), and the Niigata Earthquake (Kawagishi-cho). Use of this newly developed measurement technique will enable determination of liquefaction in real time with an accuracy approaching 100 percent.

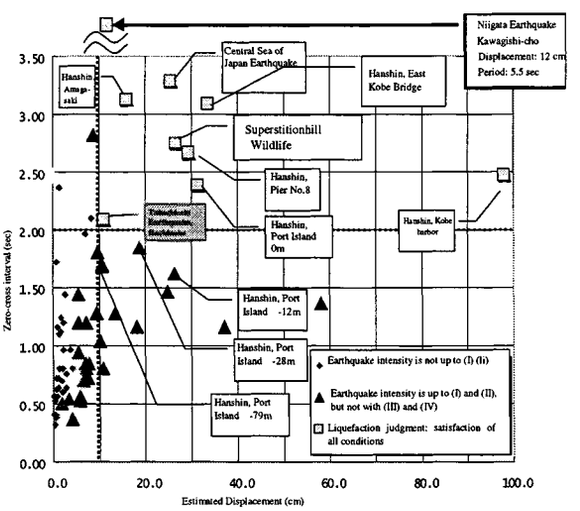

Figure 4. Results of liquefaction judgment

DEVELOPMENT OF THE NEW REAL-TIME DISASTER MITIGATION SYSTEM (SUPREME)

Outline of the New Real-Time Disaster Mitigation System (SUPREME)

Since the Great Hanshin Earthquake, numerous agencies have constructed systems for high-density monitoring of seismic motion and real-time damage estimation. Tokyo Gas is already operating the Seismic Information Gathering & Network Alert System (SIGNAL) based on installation of seismometers at 331 locations (see Figure 5). To raise the level of safety from disasters even higher, it embarked on construction of what will be the world's most extensive system for super-dense real-time monitoring of earthquakes (SUPREME) through installation of about 3,600 seismometers (New SI sensors) over its supply area, which measures about 3,100 square kilometers, beginning in January 1998. Figure 6 shows the distribution when all of the New SI sensors have been installed.

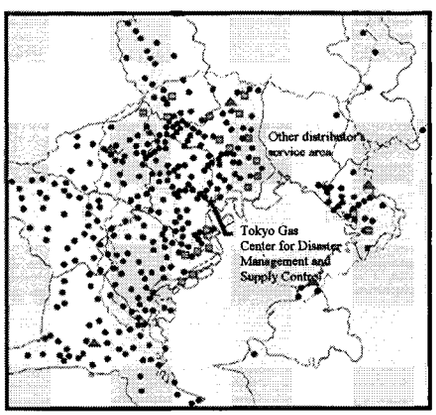

. 331 SI sensors . 20 Liquefaction sensors
. 5 ground seismometers

Figure 5. SI sensors in SIGNAL

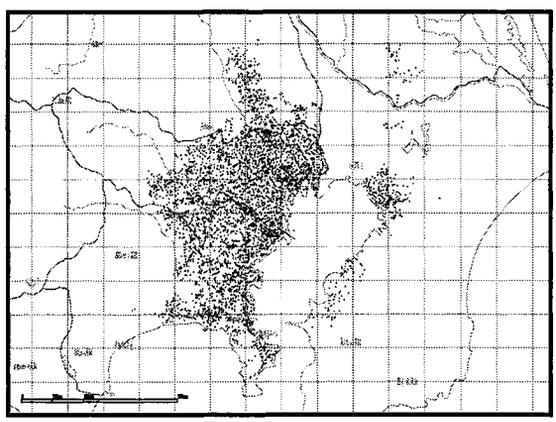

Figure 6. New SI sensors in SUPREME

Figure 7 shows the structure of the new real-time disaster mitigation system. Tokyo Gas is currently taking the opportunity presented by replacement of the former SI regulator shutoff sensors to install the New SI sensors and district regulator remote monitoring system (DCX) in about 3,600 district regulators. The linkage of this equipment with the command center through communications circuits will enable observation, and remote monitoring at the center, of various control items at the roughly 3,600 points in the supply area of roughly 3,100 square kilometers (for an average of one point every 0.9 square kilometers). These items include the SI value, PGA, pressure, regulator shut-off status, and liquefaction alert data.

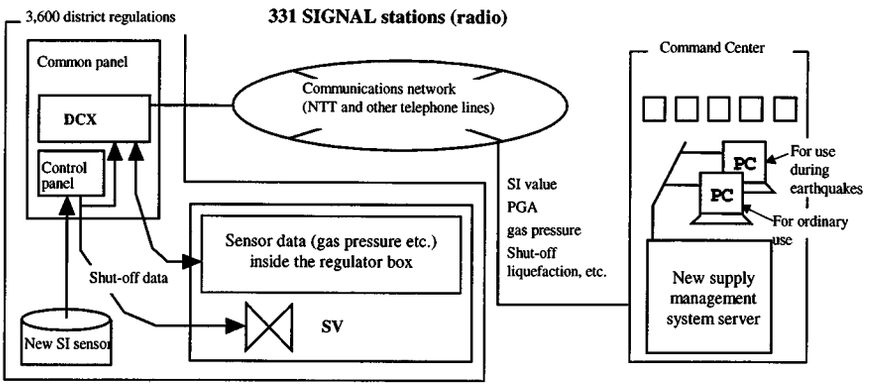

Figure 7. Composition of SUPREME

Approach to System Utilization

- The SI values, which are measured in ultra high density, and the GIS, which includes information on gas pipelines, soil and geography of the gas supply area, are used to make highly accurate estimations of the damage caused by an earthquake.
- Analysis of the yearly wave-form data on small and medium earthquakes in combination with GIS data will make it possible to determine the seismic shaking amplication at each of the roughly 3,600 points. Such information can be reflected in zoning plans and assist optimization of the setting of values for automatic shutoff of district regulators.
- In the event of a major earthquake, the system will not only automatically shut off the district regulators but also enable the command center to confirm the operation of the shutoff equipment. This will contribute to a more prompt and sure response to emergency situations.
- It is possible to monitor the gas pressure during critical events at approximately 3,600 points. Losses in gas pressure during an earthquake are indications of potential damage, and can be used to make early estimates of the extent of damage. Not only can realtime estimates of damage to major facilities be made, but a system is now being developed for the swift and accurate detection of actual damage.
- Detailed, realtime detection of liquefaction allows highly accurate estimates of damage, and the rapid execution of emergency measures

Release of Seismic Data

Data from 31 of the major points in the SIGNAL earthquake monitoring network are transmitted to Nippon Hoso Kyokai (NHK) and other mass media organs as well as public administrative institutions such as the Tokyo Metropolitan Government. Beginning in September 1996, it was decided to release data from all 331 SIGNAL points through

Internet within a very short time after occurrence in the case of earthquakes with a magnitude of 3 or more, in order to contribute to emergency response and research by numerous institutions (see Table 2). In addition, Tokyo Gas is promoting the sharing of data and research results with governmental bodies that are taking active approaches to real-time disaster mitigation. The transmission of data from the 331 SIGNAL points to the Yokohama municipal government beginning in 1998 is a part of this policy.

Table 2. Release of SIGNAL data through Internet

- ♦ Objective
  - Promotion of research for disaster mitigation through sharing of seismic data
  - Active use for initial mobilization
- ♦ Items of data release (for earthquakes occurring within the service area and having a magnitude of at least 3)
  - Earthquake name, time of occurrence, and epicenter
  - Location of the seismometer (name of location, latitude, and longitude)
  - SI value and maximum acceleration
- ♦ URL
  http//www.toyko-gas.co.jp

  Posted at the bottom of the Tokyo Gas web site

The new SUPREME real-time disaster mitigation system will record wave-form data (six earthquake wave-forms on three axes, listed from the highest SI value) for small and medium earthquakes at some 3,600 points. Earthquake wave-forms entail an immense load of data which cannot be collected in real time. However, the company plans to release data stored by CD-ROM once a year.

CONCLUSION

Real-time disaster mitigation came to the fore in the aftermath of the Great Hanshin Earthquake, and systems for real-time monitoring of seismic motion and damage estimation have since been installed or planned by many agencies. In SIGNAL, Tokyo Gas constructed one of the first systems of this type, and was commended for its foresight with selection for the 1996 Award for Civil Engineering and Development given by the Japan Society of Civil Engineering. In order to raise the level of safety from disasters even higher, Tokyo Gas began construction of a new SUPREME system for disaster mitigation based on installation of roughly 3,600 New SI sensors and a DCX system for remote monitoring of district regulators in January 1998.

It is hoped that the future will bring a sharing of seismic and geophysical data obtained from the systems of Tokyo Gas (i.e., the SUPREME disaster mitigation system

and SIGNAL) and the systems of other agencies, the promotion of related research by numerous institutions, and a sharing of the research results by all concerned.

REFERENCES

Agency of Natural Resources and Energy (1996), *Gas Industry Earthquake Countermeasures Study Report*, 7-11.

Matasovic J. and Vucetic, M. (1993), "Analysis of Seismic Records Obtained on November 24, 1987 at the Wildlife Liquefaction Array", *Research Report U.C.L.A.*

Shimizu, Y. (1997), "Soki Jishinji Higai Suitei Shisutemu - SIGNAL" (SIGNAL - An Early Earthquake Damage Estimation System)", *Keisoku to Seigyo* (Measurement and Control), Vol. 38, 41 - 44.

Towhata, I., J.K., Orense, R.P. and Kano, H. (1996), "Use of Spectrum Intensity for Immediate Detection of Subsoil Liquefaction", *Soils and Foundations*, Vol. 36, No 2, 29-44.

Detection of Damage Location and Extent of Water Supply Systems

*M. Shinozuka [1], Jianwen Liang [2] and Maria Q. Feng [3]

[1]*Fred Champion Professor, Department of Civil Engineering, University of Southern California, CA 90089-2531*
[2]*Porfessor, School of Civil Engineering, Tianjin University, Tianjin 300072, China*
[3]*Associate Professor, Department of Civil and Environmental Engineering, University of California, Irvine, CA 93697-2625*

ABSTRACT

This paper develops a methodology to identify location and severity of damage in a water delivery system by monitoring water pressure on-line at some selected positions in the water delivery system. Emerging supervisory control and data acquisition (SCADA) technology may well be used for this purpose. A neural network-based inverse analysis method is constructed for the damage identification based on the variation of water pressure. The neural network is trained by using analytically simulated data from the water delivery system with multiple locations of damage. However, this study considers, as an example, a water delivery system with single location of damage, and the trained neural network is validated by using a set of data that have not been used in the training. It is found that the method provides a quick, effective, and practical way in which the location and severity of the damage sustained by a water delivery system can be identified.

INTRODUCTION

Urban water delivery systems can be damaged by earthquakes or under severely cold weather. In the former situation, usually multiple pipelines are damaged together, but damaging earthquakes occur infrequently; while in the latter case, one or several pipes may be simultaneously damaged seasonally or even more often. In either case, the location and severity of breaks cannot easily be identified, especially immediately after the event.

In recent years, real-time damage estimation and diagnosis of buried pipelines attracted much attention of researchers focusing on establishing the relationship between damage ratio (breaks per unit length of pipe) and ground motion with taking the soil condition into consideration (Nishio, 1994; Takada and Ogawa, 1994; Yamazaki et al, 1994). Due to the uncertainty and complexity of the parameters that affect the pipe damage mechanism, it is not easy to estimate the degree of physical damage only with a few numbers of parameters. Eguchi et al (1994) put forward a method in which a nominal damage estimated through some earthquake parameters is updated gradually based on post-earthquake observation data. As an alternative, this paper develops a method to identify the location and severity of damage in a water delivery system by monitoring water pressures on-line at some selected positions in the water delivery system. For this purpose, a neural network-based inverse analysis method is used to carry out the identification based on water pressure variation before and after pipe breaks. As will be shown, this method provides a quick, effective, and practical tool to identify the damage location and severity.

In the city of Tianjin, China, a real-time water pressure monitoring system (Liang, 1996) was installed, in which the water pressure signals are transmitted to headquarters at certain time interval automatically. The pipe break data due to severely cold weather have been collected for several years, and they are used to construct an inverse analysis model to identify the possible locations and severity of damage.

This study explores the inverse analysis method to identify the location and extent of damage in the hope that the emerging SCADA technology will be able to provide pressure and possibly flow measurement data on-line and in real-time for actual water delivery systems. SCADA systems are recently being installed in water delivery networks to transmit, by means of wireless communication, water pressure/flow-rate data collected at remote sensor units to a control center for the purpose of surveillance and control of system function. Taking advantage of existing SCADA system for estimating location and extent of damage makes much more sense than using the ground motion information, since the water pressure and flow-rate data are more sensitive to damage of the water delivery network. The proposed method, however, presents a significant technical challenge due primarily to the limited number of SCADA sensor units placed in a spatial huge and functional complex water delivery network. In this respect, use of inverse analysis combined with neural network techniques as demonstrated in the present study appears to be promising to solve the technical difficulty.

DATABASE DEVELOPMENT

To establish a relationship between water pressure variation at monitoring stations and the damage location and severity in a water delivery system, a substantial input-output database is required. For a given water delivery system, there are basically two ways in which such a database can be developed; One is to collect the data actually monitored, and the other is to analytically simulate the data. Primarily for the purpose of demonstrating the efficiency of the proposed inverse analysis method, the simulation method is used in this study dealing with a system having only one location of damage and three monitoring stations. The multiple-damage case will be a cumbersome but straightforward extension of single-damage case, which will be the subject of another study (Shinozuka and Liang, 1999).

In the following, the severity of the damage is defined in such a way that the major damage represents a pipe rupture equivalent to the pipe cross-sectional area, through which the water leaks, and the minor damage equivalent to one hundredth (1/100) of the cross-sectional area. Other degrees of damage severity can be described by varying the equivalent rupture area. Each damage can be located by distance from the break point to the three monitoring stations. In fact, at least three monitoring stations are needed for this method of identification. For simplicity, the break is assumed to be located at the middle of a link between two directly connected nodes in the water delivery system.

The computer program developed by Tanaka et al (1993) is modified for the specific system used in this paper in order to perform hydraulic analysis of a water delivery system to generate the data needed.

NEURAL NETWORK MODEL

A back-propagation neural network is used to train the data obtained above. The neural network consists of three layers: input, hidden, and output layer (Figure 1). After input data are

fed into the neural network at the input layer, they are propagated through the hidden layer until output data are generated. The output data are then compared with the target output, and an error signal is computed for each output node. Then the error signals are transmitted backward from the output layer to each node in the intermediate and input layers that contributes directly to the output. This process is repeated until each node in the network has received an error signal that describes its relative contribution to the total error. Based on the error thus evaluated, connection weights are updated at all nodes forcing the network to converge to an acceptable state of performance measured in terms of the root-mean-square error defined as

$$E_{RMS} = SQRT\left[\frac{1}{M}\frac{1}{N}\sum_{i=1}^{M}\sum_{j=1}^{N}(out_{ij}^{t} - out_{ij}^{a})^2\right] \quad (1)$$

in which, out_{ij}^{t} and out_{ij}^{a} are the target and actual output, respectively, and M is the number of data set for training, and N is the number of nodes in output layer.

We train the neural network in this way: pressure variation at three monitoring stations as input, and location of break and damage index as output. In order to normalize the influence of input with different nodes and to prevent the saturation of the transfer function, the input and output are scaled based on the minimum and maximum values of the training data. Scaled values are (-1.0, 1.0) for input and (0.2, 0.8) for output.

RESULTS AND DISCUSSIONS

Figure 2 shows an example water delivery system with one supply station, consisting of 31 nodes and 50 pipe links. The length of each link is 1000m in N-S direction and 2000m in E-W direction, and diameters are between 0.3m to 0.6m and roughness coefficient is 140 for all links. The demand is assumed to be uniform throughout the water delivery system equal to 0.05 m^3/sec at each node. The water pressure at the source node is fixed at 52.0m. Three nodes (Figure 2) were selected as locations of water pressure monitoring and referred to as station-1, station-2, and station-3, respectively.

We generate 350 pairs of input-output data for 7 states of damage with respectively break area 0.01, 0.02, 0.05, 0.1, 0.2, 0.5, and 1.0 times cross-sectional area of the pipe. In the neural network training, therefore, the parameters M and N in equation (1) are equal to 350 and 4, respectively. Figure 3 shows the training curve expressing the relationship between RMS error and learning time. The training ends after 100,000 time units with the last RMS error being 0.00879.

The following analysis is performed to examine whether the neural network trained above can provide the results expected. The data used for training was fed to the neural network as the input to obtain the location and severity of the damage. The pipe links No.9, 20, 31, 42, 24, 25, 26, 27, and 28 are examined in Table 1. The numbers (except those in round brackets) in column 2 to 5 show the normalized distances to the three monitoring stations and the normalized severity index of the damage. (The normalized length for each pipe link is 0.247 in N-S direction and 0.340 in E-W direction based on the minimum and maximum values (500.0 and 6946.2) of the training data.) The numbers in round brackets indicate the relative error to the data that was used for training, and the minimum relative error is 0.42% and the maximum relative error is 20.5%. Looking at the link No.9, the normalized distances from the damage location to the three

monitoring stations are 0.371, 0.427, and 0.636, respectively, and the severity index is 0.545. The pipe links (any points in the links) at distance 0.371 to station-1 are the links No. 4, 9, 14, 20, 26, 32, 33, and 34. The links at distance 0.427 to station-2 are the links No. 7, 8, 9, 10, 16, 27, 38, 43, 42, 41, and 40, and the links at distance 0.636 to station-3 are the links No. 7, 8, 9, 10, 11, and 12. Only link No.9 satisfies the three conditions and, therefore, link No. 9 is judged to be the damaged link, as expected. Other links, No. 20, 24, 25, 26, 27, 28, 31, and 42, can be checked in the same way. Table 1 shows that the neural network trained above is sufficiently effective for the purpose of identification.

The same neural network trained above is now examined if it can identify the location and severity of damage well for the data never used for training. The results are shown in Table 2 also for links No. 9, 20, 24, 25, 26, 27, 28, 31, and 42, with the minimum and maximum relative errors being respectively 0.09%, and 25.8%, which are larger than the corresponding errors in Table 1 as expected. Table 2 shows that again only link No.9 is the damaged link, as also expected.

The following observations are made with respect to link No.31 which has the largest relative error. The links at distance 0.560 to station-1 are the links No. 2, 7, 18, 24, 30, 31, 37, 43, 44, and 45, and at distance 0.332 to station-2 are the links No. 18, 19, 20, 26, 29, 30, and 31, and at distance 0.359 to station-3 are the links No. 21, 30, 31, 33, 34, 35, 41, 42, 44, and 45. In this way, link No. 30 and 31 are judged to be potential candidates to be the damaged links. However, actually only link No.31 is the damaged link, and therefore link No.30 was mistakenly identified as a damaged link in addition to link No.31, though link No.31 is more consistent with what the data suggest. Actually, if the distance to station-2 is greater than 0.340 with relative error 14.2%, then link No.30 could be excluded from the candidate group of damaged links, which means that the relative error (16.3%) presently for the distance to station-2 is still not acceptable. The reason is that the RMS error in back-propagation neural network is an average error for all the data used for training in accordance with the learning rule, and not for each set of data or for each node in output layer. This problem can be resolved by additional training effort or reselecting the three monitoring stations, which will be studied further.

CONCLUSIONS

1. The purpose of this study is to develop a method to identify location and severity of damage in a water delivery system by monitoring water pressure on-line at some selected positions in the water delivery system. The method can also be applied in principle to other networks such as electric power systems.

2. A neural network-based inverse analysis method is developed for the stated purpose. The method is based on on-line water pressure variation before and after pipe breaks, and provides a quick, effective, and practical analysis tool to serve the purpose. The results also show that the number of monitoring stations can be less than one tenth of the number of nodes in a water delivery system.

ACKNOWLEDGEMENTS

This work was supported partially by U.S. National Science Foundation under Grant No. INT-9604614 and the Multidisciplinary Center for Earthquake Engineering Research under Grant No.R92249-A, and also supported by National Natural Science Foundation of China under

Grant No.59878032, which are gratefully acknowledged. This work was carried out when the second author visited University of Southern California.

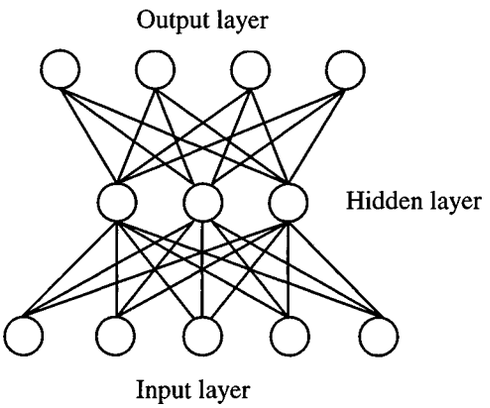

Figure 1. Back-propagation neural network model

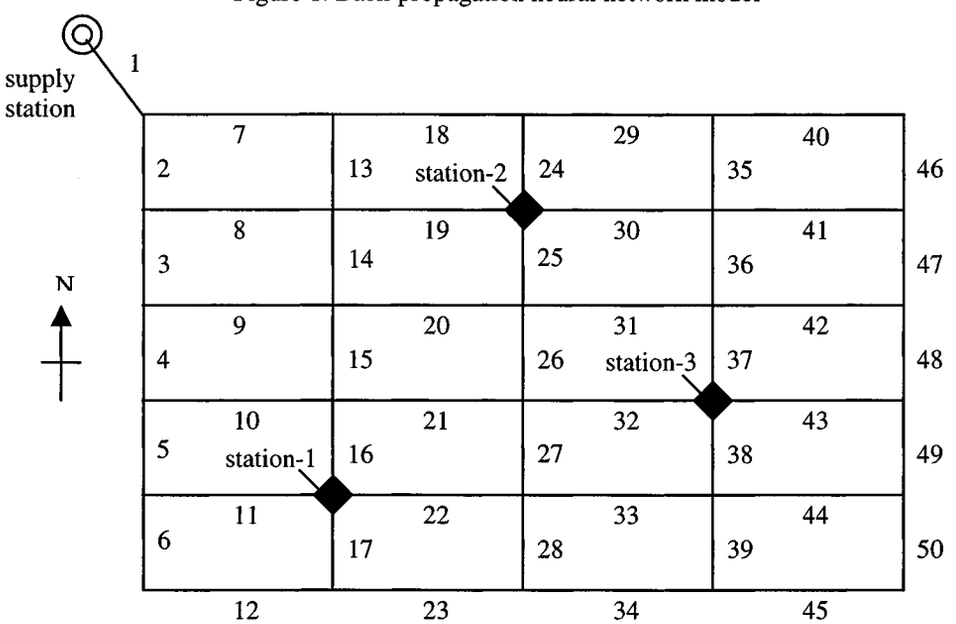

Figure 2. A water delivery system

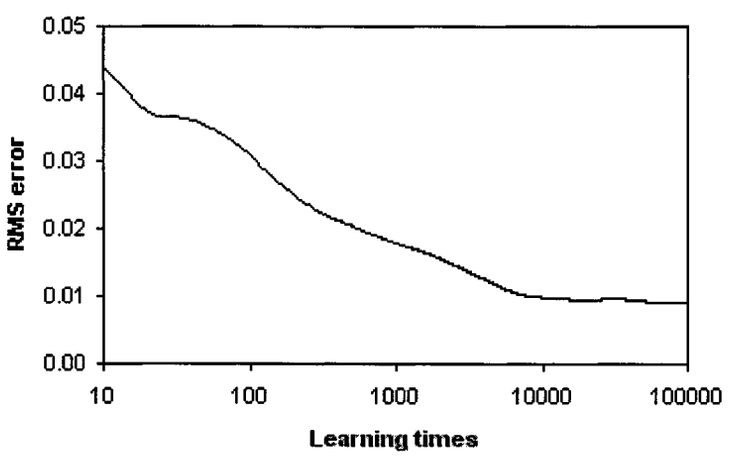

Figure 3. Training curve

Table 1. Damage output for data used for training

Link No.	Distance to Station-1	Distance to Station-2	Distance to Station-3	Severity Index
9	0.371	0.427	0.636	0.545
	(2.65%)	(4.86%)	(1.32%)	(9.08%)
20	0.363	0.268	0.428	0.480
	(2.77%)	(6.00%)	(4.47%)	(3.96%)
24	0.534	0.239	0.467	0.765
	(1.08%)	(19.4%)	(3.52%)	(7.83%)
25	0.433	0.228	0.373	0.713
	(4.01%)	(14.1%)	(3.42%)	(1.52%)
26	0.373	0.299	0.358	0.631
	(3.44%)	(2.05%)	(3.53%)	(11.1%)
27	0.359	0.367	0.355	0.690
	(4.03%)	(4.87%)	(2.81%)	(2.85%)
28	0.355	0.456	0.367	0.656
	(2.84%)	(4.84%)	(5.05%)	(7.64%)
31	0.565	0.343	0.324	0.274
	(15.6%)	(20.5%)	(13.6%)	(5.65%)
42	0.669	0.446	0.245	0.320
	(21.8%)	(0.42%)	(14.2%)	(10.2%)

Table 2. Damage output for data not used for training

Link No.	Distance to Station-1	Distance to Station-2	Distance to Station-3	Severity Index
9	0.413	0.471	0.676	0.467
	(14.1%)	(4.95%)	(7.69%)	(8.92%)
20	0.395	0.318	0.487	0.482
	(9.32%)	(11.4%)	(8.82%)	(5.93%)
24	0.562	0.239	0.480	0.797
	(6.33%)	(19.5%)	(6.36%)	(10.3%)
25	0.470	0.241	0.406	0.678
	(4.08%)	(20.4%)	(5.02%)	(6.05%)
26	0.361	0.293	0.359	0.645
	(6.60%)	(1.02%)	(4.03%)	(10.8%)
27	0.345	0.348	0.357	0.8143
	(0.09%)	(9.84%)	(3.30%)	(12.8%)
28	0.365	0.486	0.410	0.703
	(5.73%)	(14.2%)	(6.08%)	(2.60%)
31	0.560	0.332	0.359	0.369
	(14.4%)	(16.3%)	(25.8%)	(21.8%)
42	0.666	0.461	0.324	0.280
	(1.74%)	(2.95%)	(13.7%)	(7.63%)

REFERENCES

Eguchi, R. T., Chrostowski, J. D., and Till, C. W., (1994) "Early Post-Earthquake Damage Detection for Lifeline System." EQE Research Report prepared for National Science Foundation.

Liang, J. (1996) "A Comprehensive Framework for Post-Earthquake Rehabilitation Plan of Lifeline Networks," *ASME,* PVP-Vol.340, 283-289.

Nishio, N. (1994) "Damage Ratio Prediction for Buried Pipelines Based on the Deformability of Pipelines and the Nonuniformity of Ground ," *J. of Pressure Vessel Technology, ASME,* 116, 459-466.

Shinozuka, M., and Liang, J. (1999) "On-Line Earthquake Damage Identification of Water Supply Networks." Research Report, International Institute of Innovative Risk Reduction Research on Civil Infrastructure Systems, University of Southern California. (in print)

Takada, S., and Ogawa, Y. (1994) "Seismic Monitoring and Real Time Damage Estimation for Lifelines." *Proc. 4th U.S. Conf. on Lifeline Earthq. Engrg., ASCE,* 224-231.

Tanaka, S., Shinozuka, M., and Hwang, H. H. M. (1993) "LIFELINE-W(2) User's Guide: a Program for Connectivity and Flow Analysis of a Water Delivery System Under Intact and Seismically Damaged Conditions." Technical Report, Princeton University.

Yamazaki, F., Katayama, T., and Yoshikawa, Y. (1994) "On-Line Damage Assessment of City Gas Networks Based on Dense Earthquake Monitoring." *Proc. 5th U.S. Conf. on Earthq. Engrg., EERI*, Vol.4, 829-837.

SAR Technology Applications in Structural Damage Detection

Masanobu Shinozuka[1], Roger Ghanem[2], Babak Mansouri[3]and
Bijan Houshmand[4]

[1]*Prof., Dept. of Civ. Engrg., University of Southern California, Los Angeles, CA, USA.*
[2]*Assoc. Prof., Dept. of Civ. Engrg., Johns Hopkins University, Baltimore, MD, USA.*
[3]*PhD Student, Dept. of Civ. Engrg., USC, Los Angeles, CA, USA.*
[4]*Adj. Assoc. Prof., Dept. of Elec. Engrg., UCLA Los Angeles, CA, USA.*

ABSTRACT

Synthetic Aperture Radar (SAR) provides high quality images in all weather and all time conditions. It shows promise for acquiring spatial and temporal data for urban analysis. The objective of this study is to investigate the capability for damage and change diagnostic schemes based on simulated complex SAR images of pre- and post-events. SAR image is obtained from a coherent imagery system, it can be described as a three dimensional system, sometimes referred to as a complex imagery system, whereby two dimensions represent the spatial extent of the image and the third dimension represents the phase content of the image. The phase information is relevant to the detection of the finer details in the image.

INTRODUCTION

The purpose of this study is to demonstrate the application of SAR imagery technology to the detection of changes and damage in urban areas with particular emphasis on changes caused by a destructive earthquake. Rapid and efficient access to information on the spatial distribution, extent and nature of earthquake destruction can significantly help with disaster recovery efforts. The current investigation aims at extending remote sensing technologies to address this problem. Its aim is to produce a rapid assessment of the location and extent of urban seismic damage by identifying damage signatures in SAR images. It is hoped that this and similar studies will provide a more accurate catalogue of damage and help extend the knowledge base related to the valuation of property damage following natural disasters. Indeed, the authors are convinced that such a near-real time urban damage identification with the aid of SAR imagery is within a realm of the existing technology.

Electromagnetic wave propagation theory is first reviewed, followed by some background on SAR processing Simulation studies using a commercial electromagnetic wave simulation tool are then presented. The study area is part of the University of Southern California (USC) campus. In fact, SAR images of some buildings on the USC campus and other box-shaped structures with different resolutions, ranging from 15cm to 2m are developed with the aid of an electromagnetic computer simulation tool. Using the

properties of SAR imagery as a coherent 3-D complex imagery system, the location and extent of the simulated change/damage are extracted.

THEORETICAL BACKGROUND

SAR systems are based on electromagnetic waves governed by Maxwell's equations. The signal generated in SAR systems is usually frequency modulated and is referred to as a chirp signal when this modulation is a linear function of frequency. Most commonly, L-band (central wavelength ~ 25cm or central frequency ~ 1GHz), C-band (central wavelength ~ 6cm or central frequency ~ 5GHz) and X-band (central wavelength ~ 3cm or central frequency ~ 10GHz) SAR are used for the purpose of earth monitoring. A very desirable operational feature in this frequency range, particularly for spaceborne SAR systems, is the very high transmission ratio of the signals.

The ground features are usually modeled as a linear system characterized by its transfer function in the wave-number space. Measurements at the transmitter and receiver of the SAR system can then, in theory, provide a full characterization of this transfer function. A rough approximation of this function could clearly be obtained as the ratio of the Fourier transforms of the receiver signal to the transmitter signal. Given the finite resolution in the wave-number domain, over which the image is being reconstructed, though, a better approximation of the transfer function is obtained through filtering of the receiver signal. An optimal such filter, in the sense that it minimizes the signal to noise ratio in the received signal, can be shown to correspond to the so-called matched filter, whose impulse response function is equal to the transmitted signal. This procedure is equivalent to correlating the received signal with the transmitted signal. Thus, for example, starting with a chirp signal of the form,

$$S(t) = S_0(t)\exp[j2\pi(f_c t + \frac{At^2}{2\tau})] \tag{1}$$

$$S_0(t) = \begin{cases} 1 & nT - \frac{\tau}{2} < t < nT + \frac{\tau}{2} \\ 0 & otherwise \end{cases} \tag{2}$$

where. $f_c(t)$ denotes the carrier frequency of the radar, τ is the duration of the signal, and A its bandwidth, Figure 1 shows the propagation path from the transmitter to the ground point target and back to the airborne receiver.

It is clear from the figure that,

$$D(t) = \left[D_0^2 + \mathrm{v}^2 t^2\right]^{/2} = \left[H^2 + D_h^2 + \mathrm{v}^2 t^2\right]^{/2} \tag{3}$$

which upon using the approximation,

$$D(t) \approx D_0 + \frac{\mathrm{v}^2 t^2}{2D_0} \tag{4}$$

results in an expression for the phase of the echo at the point target of the form,

$$\phi(t) = \frac{2\pi}{\lambda} 2D(t) = \frac{4\pi D_0}{\lambda} + \frac{2\pi v^2 t^2}{\lambda D_0} \tag{5}$$

The received signal of the point target after eliminating the carrier frequency term is

$$S_{received}(t) = S_0 \exp\left[\frac{j2\pi v^2 t^2}{\lambda D_0}\right] \tag{6}$$

The reference signal echo from the same point as the point target must be the same as the received signal. Therefore the correlator output, defined as,

$$S_{correlator}(\tau) = \int_{-T/2}^{T/2} S_{received}(t).S^*_{reference}(t+\tau)dt \tag{7}$$

can be evaluated to be,

$$S_{correlator}(\tau) = aT \exp\left[-\frac{2\pi v^2}{\lambda D_0}\tau^2\right] Sinc\left[\frac{2\pi v^2}{\lambda D_0} T\tau\right] \tag{8}$$

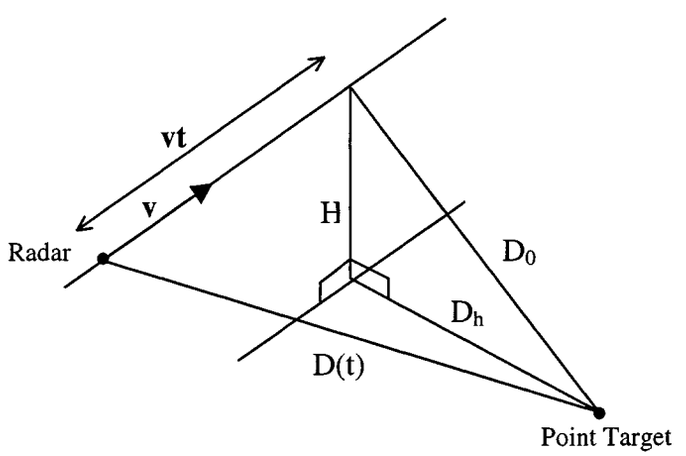

Fig. 1 – Point Target Detection

Thus the ground point target shown in Figure (1) is mapped into the distributed object given by equation (8). This function is often referred to as the spread function. The Sinc function decays very rapidly around zero from a value of 1, and the spread function is usually truncated beyond an effective range dimension of the target image. Ground targets that are separated by a distance greater than this effective dimension can be resolved by the SAR.

The most common algorithm for realizing SAR processing in remote sensing is the rectangular algorithm (Range-Doppler Processing). This is a two-dimensional correlation procedure. It is implemented by two one-dimensional matched filter operations. The first operating on single-pulse radar returns and the second operates on the phase of Doppler

shift due to the relative position between the target and the radar. More information on SAR processing techniques are found in the references.

Multiple SAR images of a scene are used to obtain information regarding changes in a scene during the period when the SAR images were acquired. Multiple SAR images are also used for producing the scene elevation model. The elevation or topography is derived by obtaining SAR images from two slightly separated view directions. For change detection applications, the SAR image is obtained from the same view direction. For interferometric SAR, the phase difference of the two SAR images is related to the scene elevation model or change detection. In this case, the phase difference image is called an interferogram.

SAR SIMULATION METHODOLOGY

Simulations of SAR measurements are useful for proper image interpretation and image understanding. In the algorithm adopted in this paper, a high frequency Shooting and Bouncing Ray (SBR) technique (Andersh et.al,1994) is used for the simulation of SAR measurements of buildings. It computes the scattering electromagnetic field from a scene which is represented by a geometrical model. Its operations can be divided into three segments: ray tracing based on geometrical optics, electromagnetic field computations and post processing. A particularly relevant post-processing step is the SAR image formation.

The computation typically starts by launching a bundle of parallel rays (plane wave approximation) from the source in a regular grid towards the scene. The Rays are traced based on geometrical optics. Scattered far-field is then computed by physical optics integration when rays exit the scene. Once the ray tracing is completed, the scattered field is computed either in the time or in the frequency domain. For SAR image formation, the ray tracing portion of the computation is carried out from each discretized antenna position (frequency domain algorithm). In order to reduce the computation time, an approximation is considered by using only one transmission direction (time domain algorithm). For this assumption to be valid the angular span is limited, thus restricting the azimuth resolution. This latter technique takes advantage of the fact that the simulated relative motion of the SAR system and the object creates a Doppler frequency with respect to hit-points. A hit-point is the intersection of the propagating ray with the geometry. Doppler frequency is proportional to the cross-range (azimuth or along track direction) position. Therefore, range and cross-range positions are defined and discriminated by the aid of the locations of the ray intersection with the scene. Taking into consideration the size of a real building, and the requisite computational resources, the time domain algorithm was used in this paper.

RESULTS

Our simulations are based on an X-band (central frequency of 10GHz or central wavelength of 3cm) SAR system. The average CPU time for a single, 256 bins by 256 bins simulated image of a real-sized building was about 10 hours. The particular building

used in this study consisted of the DRB building on the campus of the University of Southern California. Structures and their front edges are usually very well detectable. Reflections from the corner of structures are expected to result in the largest signal return to the SAR antenna. This effect is called corner reflection, and is clearly observed in our simulated results. Due to layover, the fact that higher objects appear closer in a radar, buildings are skewed in a predictable manner. Roofs appear shifted towards the SAR sensor but the building footprints look further away. We have shown that geometrical changes such as tilting, overturning or pancaking can be observed and measured by comparing SAR images before and after change.

Another characteristic of Radar or SAR images, namely shadowing, is clearly seen. Shadowing refers to the blockage of the radar signal by large objects. For this geometry, the shadowed region is not illuminated by the radar signal and appears as a dark region in the SAR image. The intensity of the image in the shadow region is an indication of the noise level in the SAR measurement system and of multiple scattering effects. Three case studies are considered next that demonstrate the above features.

Case one:

Figure 2 shows the geometrical set up of the SAR imagery. Two box-shaped structures each having a square footprint of 9 m^2, are placed 6m away from each other along one side. Orientations and the relative positions of the buildings and the SAR sensor are plotted. Angle **I** is the central incident angle and situated at the middle of the angular span. Slant Plane is identified by the central incident angle **I** and the direction of the SAR velocity vector **V**. Elevation, azimuth and ground squint angles are considered to be 10, 40 and 90 degrees respectively. The X-Y coordinate system shown in the figure refers to the target coordinates on the ground.

Figures 3.a and 3.b are the simulated SAR images based on the above mentioned geometry. These structures are isolated in free space and reflection from the ground is not considered. The taller structure is 15 meters high, and is twice the height of the second structure. Electromagnetic wave penetration is allowed within the structures. Sharp lines connecting the corners indicate the triangular facets and are overlayed on the corresponding SAR image. Up to five reflections of the radar signal are considered in this simulation. The resolution in both range and cross-range is assumed to be 0.15 meters. This required a bandwidth of 1 GHz. The angular span is 5.73 degrees. Figure 3.a shows the SAR image processed in the "Slant Plane" with range and cross-range coordinates projected in that plane. The entire square roof is illuminated as opposed to the footprint of the structure. The corner points are brighter than edges and well detected. In figure 3.b, the SAR process is performed in the ground level and similar observations are made.

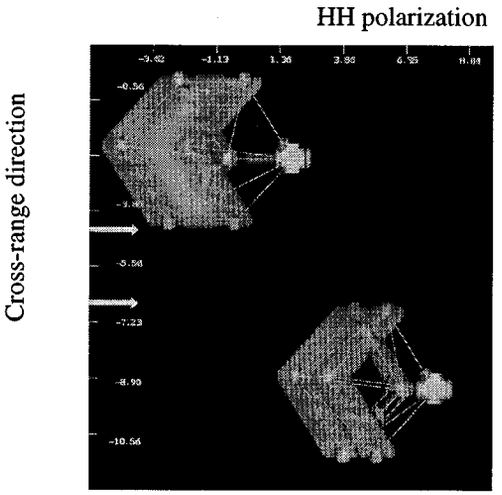

Fig. 3.a - SAR image in Slant Plane

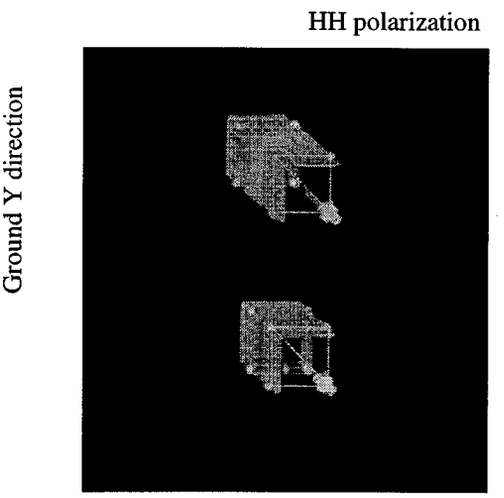

Fig. 3.b – SAR image projected on ground

Case two:

Figure 4.a is the simulated SAR image of the real-sized DRB building with 7.63m height. In here we used a more realistic resolution value of 2 meters. Elevation, azimuth and ground squint angles are 30, 40 and 90 degrees respectively. The angular span is 0.43 degrees and the signal bandwidth is 80 MHz. To reduce the computation time, we isolated the building in free space and did not consider any contribution to scattering from the ground. The front edges are well defined and basically two parallel bright contour-like regions are highlighted. The closer edge to the SAR sensor is from the roof. Corner reflector signature is seen along the front edge of the building footprint. The distance between these parallel edges can give estimates of building heights. In this case a flat roof was assumed.

In order to model the SAR image of the after event, some changes in the building geometry are introduced. Partial collapse, modeled as a 10 cm reduction in the height of six columns at the front entrance of the building, with the resulting inclination in the roof down towards the entrance. The simulated SAR image, Fig. 4.b, clearly shows the region of the geometrical changes.

Figure 4.c is obtained by subtracting the pre-event SAR image from the post-event SAR image. Unchanged regions are cancelled out and the remaining indicates the exact introduced changes in the building entrance.

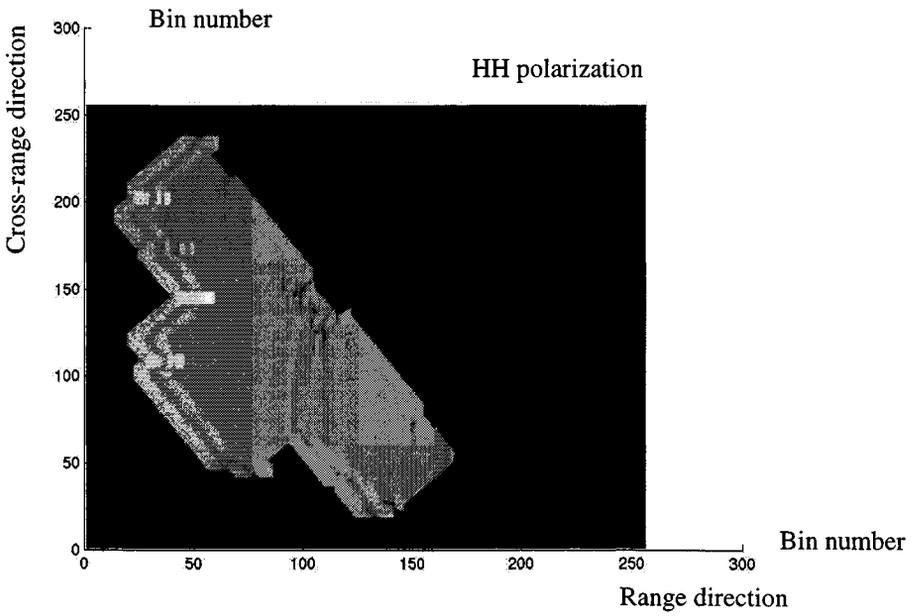

Fig. 4.a – SAR image of DRB building before change

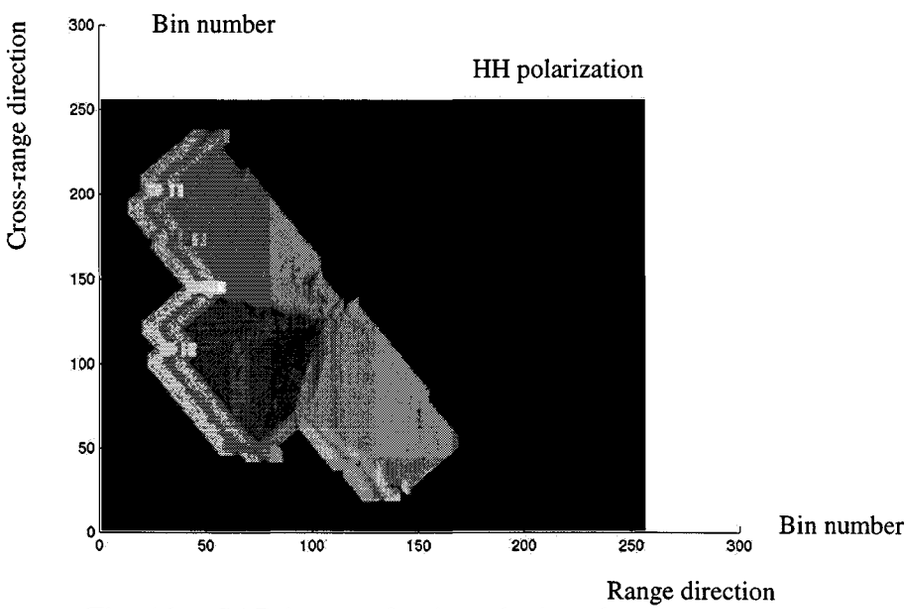

Fig. 4.b – SAR image after introducing changes

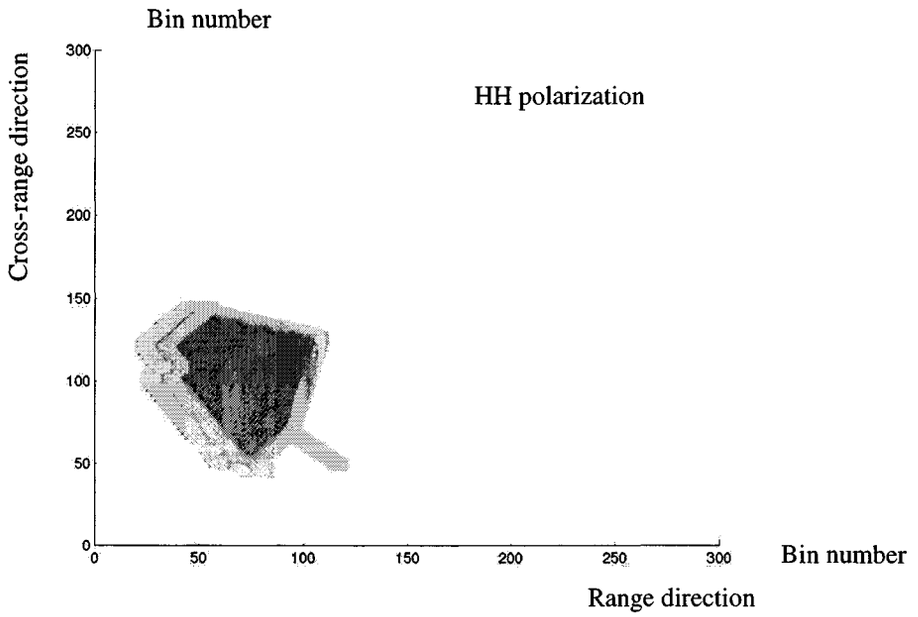

Fig. 4.c – Detected change in DRB building

***Case three*:**

This case study investigates a more complicated scene than the previous two. Specifically, scattering is considered from all three components in the model: DRB and KAP buildings as well as the flat ground surface. KAP building height is about 17.1 m as compared to 7.63 m for DRB. Building roofs are considered flat. Figure 5 is simulated with 2 m resolution in both range and cross-range directions. The elevation, azimuth and the ground squint angles are 30, 40 and 90 degrees respectively. The angular span of the scene is 0.43 degrees and the bandwidth is 80MHz. Difference in heights can be estimated by either the amount of the dislocation of the footprints and the roofs front edge or by comparing their shadows. Corner reflector effects are clearly seen in here as well. The front contour edges related to the building footprints are brighter than the roof.

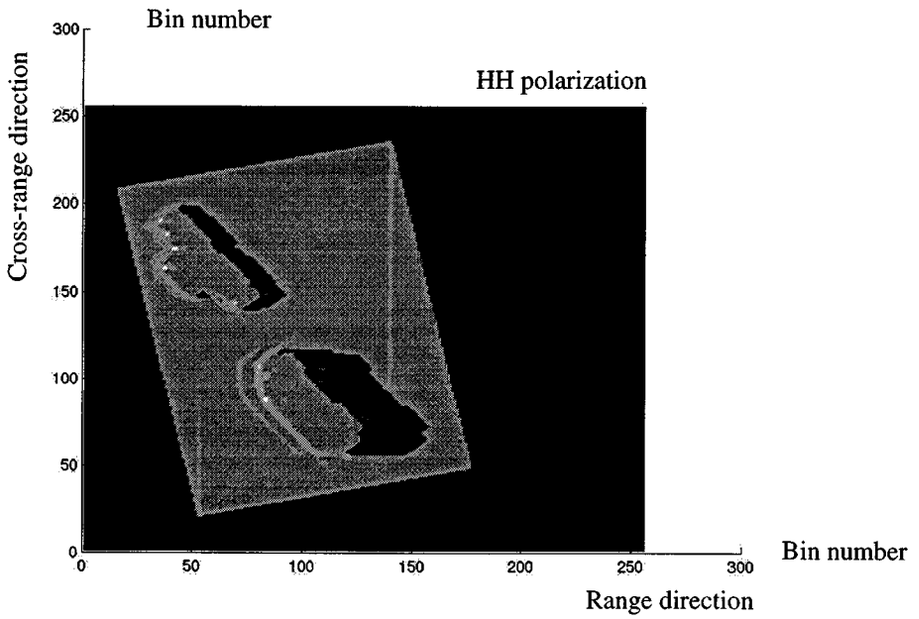

Fig. 5 – SAR image of DRB and KAP buildings and the flat ground (2 m resolution)

CONCLUSION

SAR technology provides a methodology for the rapid capture of reflectance and geometric information of a scene. In this paper an overview of the methodology for SAR image formation, and the underlying electromagnetic principles are presented. In addition, SAR imaging is used to demonstrate the possibility of detecting change in an urban environment. Such capability is useful to detect changes due to natural disasters such as earthquakes. In this paper, we have utilized the changes in SAR magnitude image to detect changes due to an event. We noted that the noise present in the imaging system can interfere with our change detection scheme. Our research is continuing with quantifying the change detection capability in the actual SAR images, in addition to use of interferometric phase related information. We anticipate the change detection in urban areas will be challenging due to the complex nature of the interaction of the radar signal with the urban environment, and system noise level. We are examining interferometric SAR measurements in addition to realistic SAR simulations to quantify the detectable urban changes via this technology.

REFERENCES

1. Fawwaz T. Ulaby, Richard K. Moore, Adrian K. Fung,(1982) "Microwave Remote Sensing Active and Passive – Volume II – Radar Remote Sensing and Surface Scattering and Emission Theory" Addison-Wesley Publishing Company, Inc.

2. Charles Elachi (1987) "Introduction to the Physics and Techniques of Remote Sensing" John Wiley & Sons Inc.

3. John C. Curlander (1991), Robert N. McDonough "Synthetic Aperture Radar Systems and Signal Processing" John Wiley & Sons Inc.

4. Howard A. Zebker, Paul Rosen, Richard M. Goldstein, Andrew Gabriel, and Charles L. Werner (1994) "On the Derivation of Coseismic Displacement Fields Using Differential Radar Interferometry : The Landers Earthquake," Journal of Geophysical Research, Vol.99, No. B10, Pages 19,617-19,634, October 10.

5. Dennis C. Ghiglia, Mark D. Pritt (1998) "Two-Dimensional Phase Unwrapping Theory, Algorithms, and Software," John Wiley & Sons Inc.

6. Didier Massonnet, Marc Rossi, Cesar Carmona, Frederi Adragna, Gilles Peltzer, Kurt Feigl and Thierry Rabaute (1993) "The Displacement Field of the Landers Earthquake Mapped by Radar Interferometry," Letters to Nature - Nature, Vol. 364, 8 July 1993.

7. Howard A. Zebker, Charles L. Werner, Paul A. Rosen, Scott Henseley (1994) "Accuracy of the Topographic Maps Derived from ERS-1 Interferometric Radar,"IEEE Transaction on Geoscience and Remote Sensing, Vol.32, No.4, July 1.

8. D. J. Andersh, M. Hazlett, S. W. Lee, D. D. Reeves, D. P. Sullivan, and Y. Chu (1994) "Xpatch: A High Frequency Electromagnetic-Scattering Prediction Code and Environment for Complex Three-Dimensional Objects," IEEE Antennas and Propagation Magazine, Vol. 36, No. 1 pp. 65-69.

Session 3

System Identification

Chairs: A. Mita and A. Smyth

Seismic Response Measurement and System Identification of Bridges

*Chin-Hsiung Loh

Professor, Department of Civil Engineering, National Taiwan University, Taipei, Taiwan, R.O.C.

Director, National Center for Research on Earthquake Engineering, Taipei, Taiwan, R.O.C.

ABSTRACT

Potential uses of structural identification to solve problems related to conditional safety assessment of bridge structure are proposed in this paper. Through the measurement of bridge for its critical global and local responses under moving truck and seismic loading, the dynamic characteristics of bridge structure was estimated using the time domain identification. Different identification algorithm was introduced in the analysis. The methods include: recursive least-square method, neural networks, empirical mode decomposition with Hilbert marginal spectrum and system realization using information matrix. The identification will concentrate not only on the global identification but also on the local structural system identification. This study provides some practical methods on bridge structure health monitoring.

INTRODUCTION

For the purpose of damage assessment of structures during strong ground excitation, it is desirable to identify severity of damage based on the input-output measurement. It is believed that structural identification application can lead to an understanding of the structural deterioration mechanism. A main disadvantage of structural identification has been the lack of experimental information on an actual structure. Both ambient vibration test and forced vibration test can provide information for structural system identification. Besides that strong motion instrumentation on structure to collect earthquake response can also provide valuable information for the safety assessment of the structure during earthquake excitation.

Much work has been done on structural identification of linear systems revealing in a number of efficient algorithms. The recursive least-square time-domain identification of structural parameters provides an on-line global identification method of linear system [Caravani et. al. 1977]. Damage identification based on nonlinear dynamic models has not yet been widely reported. The most common method to identify the nonlinear system with the prior information on nonlinear model is the application of Kalman filter technique [Hoshiya, 1984]. Identification

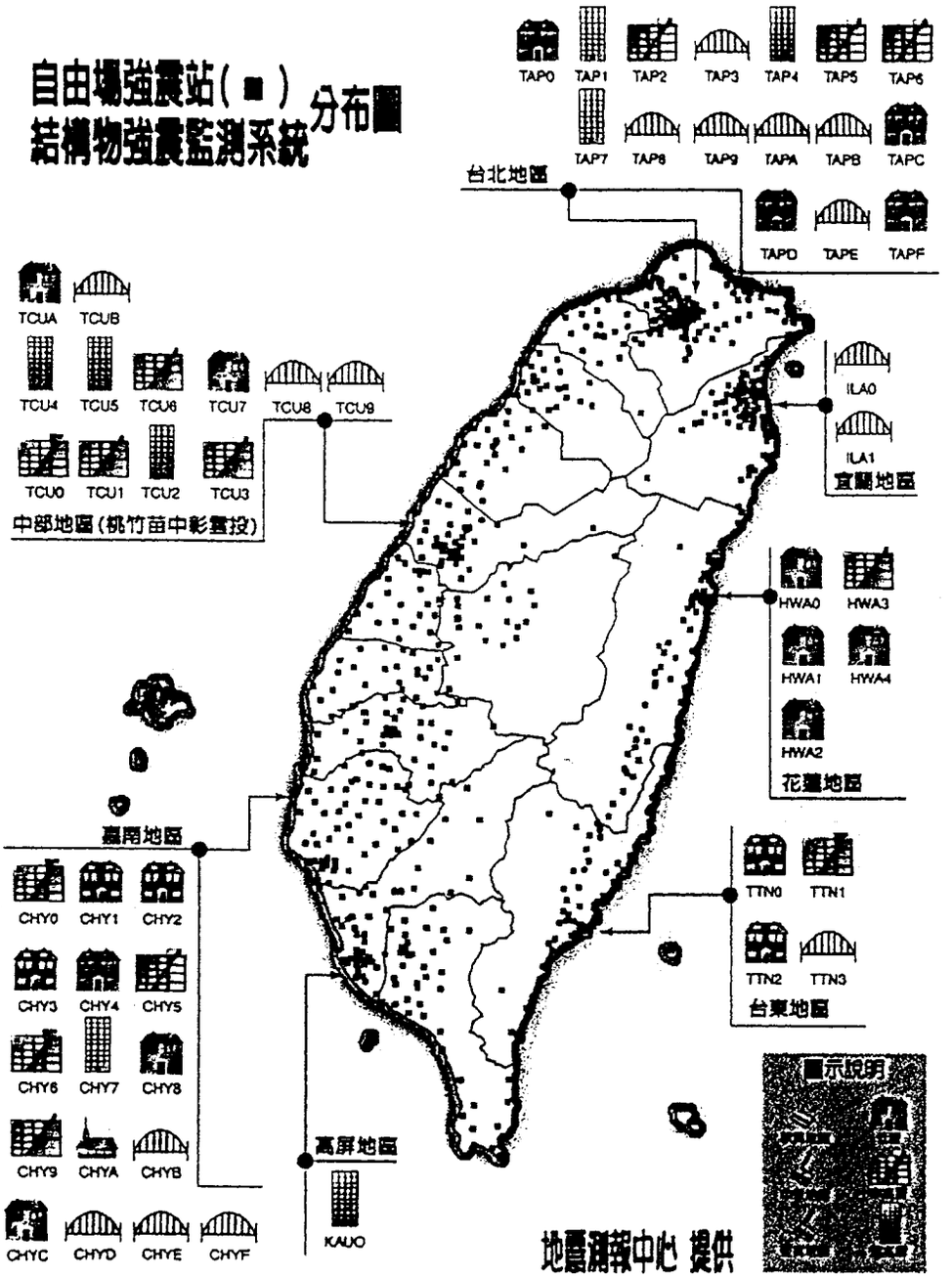

Fig.1: Distribution of free-field strong motion instrumentation and structural seismic Monitoring array under TSMIP (Taiwan Strong Motion Instrumentation Program, Central Weather Bureau).

of time-varying model parameters is also studied through adaptive model identification method [Ljung, 1982 and Goodwin, 1984]. The use of artificial neural networks in structural identification has been used in recent years [Elkordy et.al. 1993]. Due to the complex nature of civil infrastructure and noise-polluted measurement, and it becomes a challenging task to model the current structure for identification [Sato et. al. 1997 and 1999].

The purpose of this paper is to make a summary report on the use of different identification methods to identify the dynamic characteristics of bridge from its seismic response data. Work will concentrate the substructural identification using recursive least-square method, neural networks, and signal decomposition method. Seismic response data of the bridge structures from the Taiwan Strong Motion Instrumentation Program (TSMIP) will be used in this paper.

TAIWAN STRONG MOTION INSTRUMENTATION PROGRAM (TSMIP)

From 1991 the Central Weather Bureau develop a program called Taiwan Strong Motion Instrumentation Program (TSMIP). In this program the free-field strong motion array as well as structural seismic monitoring array was developed. Up to now there are over 600 free-field seismometers were deployed on the island and over 50 structures (including buildings and bridges) were instrumented with seismic monitoring system (at least 31 channels for each structure), as shown in Fig.1. In this program , for example, the New-Lian River Bridge had been instrumented with a strong motion array of 30 accelerometers along its deck, at its abutments and at a near-by free-field location, as shown in Fig. 2. This bridge is a continuous five-span pre-stress box-girder bridge located near the north-west coast of Taiwan. Up to the present time there were over six earthquake events triggered the recording system and provide valuable data for the identification of the bridge.

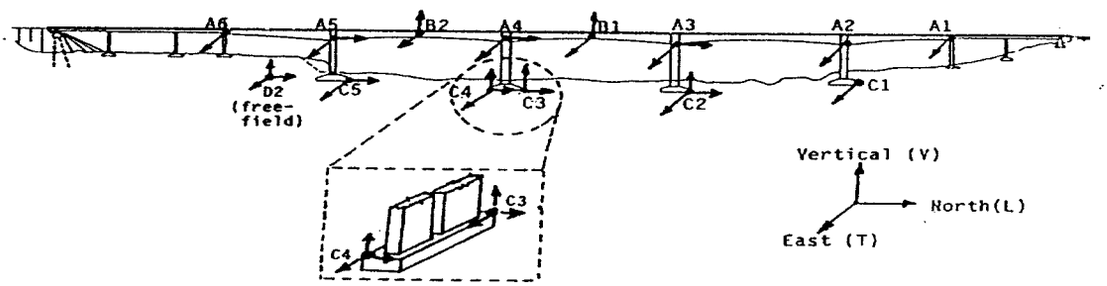

Fig.2 Instrumentation layout of New_Lian River Bridge

The measured responses from accelerometers on the bridge can be used not only for the safety evaluation of the bridge but also for the study of structural health monitoring technology. Based

on the recorded acceleration responses from the bridge structure, three different levels of response from weak motion to strong motion are specified. Some information (magnitude, depth, etc.) for these six earthquake events are listed in Table 1 and the peak acceleration response is also shown.

Table 1: Information of earthquake events

Index	*Excitation Level*	occuring date	Peak Acceleration(cm/sec2)				
			A3	A4	B1	B2	C4
L1	Low	1995.02.10	7.39	7.78	5.9	7.66	1.85
L2		1995.04.03	8.08	9.07	7.78	8.65	1.25
M1	Medium	1995.02.23	28.26	30.15	25.96	26.29	8.82
M2		1996.03.05	20.63	24.64	41.5	32.45	6.89
H	High	1995.06.25	483.24	252.47	221.61	212.12	50.79

Table 1: cont'd

Index	Latitude		Longitude		Magnitude	Depth	Epicentral distance	Hypercentral distance
	Degrees	Minutes	degrees	minutes		(km)	(km)	(km)
L1	23	45.65	121	55.18	5.16	24.61	138.18	140.36
L2	23	56.13	122	25.9	5.89	14.55	164.59	165.23
M1	24	12.22	121	41.22	5.78	21.69	84.93	87.66
M2	23	55.81	122	21.69	6.41	6	158.76	158.88
H	24	36.37	121	40.11	6.51	39.88	56.95	69.53

TIME DOMAIN SYSTEM IDENTIFICATION

The time domain identification of structural dynamic properties from its seismic response data , both discrete-time domain for linear time-invariant system as well as time-variant system can be used. The multi-variate ARX model was adapted in this study. Consider the ARX-model as:

$$\mathbf{y(t)} = \frac{\mathbf{B(q)}}{\mathbf{A(q)}}\mathbf{u(t)} + \frac{1}{\mathbf{A(q)}}\mathbf{e(t)} \tag{1}$$

where AR refers to auto-regressive part, **A(q)y(t)**, and X to the extra input, **B(q)u(q)**. Here **y(t)** and **u(t)** are ny- and nu- dimensional column vectors which refer to the multiple output/multiple input case. **A(q)** is an (ny x ny) matrix polynomial, and **B(q)** is an (ny x nu) matrix [Loh et.al. 1996], i.e.

$$\mathbf{A(q)} = \begin{bmatrix} \mathbf{a}_{11}(\mathbf{q}) & \cdots & \mathbf{a}_{1*ny}(\mathbf{q}) \\ \vdots & & \\ \mathbf{a}_{ny*1}(\mathbf{q}) & \cdots & \mathbf{a}_{ny*ny}(\mathbf{q}) \end{bmatrix} \tag{2}$$

where the entries a_{ij} are polynomials in the delay operator q^{-1}:

$$a_{kj}(q) = \delta_{kj} + a^{1}_{kj}q^{1} + \ldots\ldots + a^{nakj}_{kj}q^{-ngkj} \qquad (3)$$

Based on the recursive least-square method the modal parameters of ARX-model can be identified, and the system natural frequency and damping ratio of each structural mode can be estimated through the relationship between discrete form of equation of motion (modal equation) and ARX-model.

During strong earthquake excitaion, a structure may behave as a non-linear system or damage. In that situation the system modal parameters may change with respect to time during earthquake excitation. The traditional off-line identification method can not be applied in that case. The recursive least square method (RLS-method) with suitable choice on forgetting factor $\lambda(t)$ can then be applied to identify these data. This method can detect the time variant modal Pparameters.

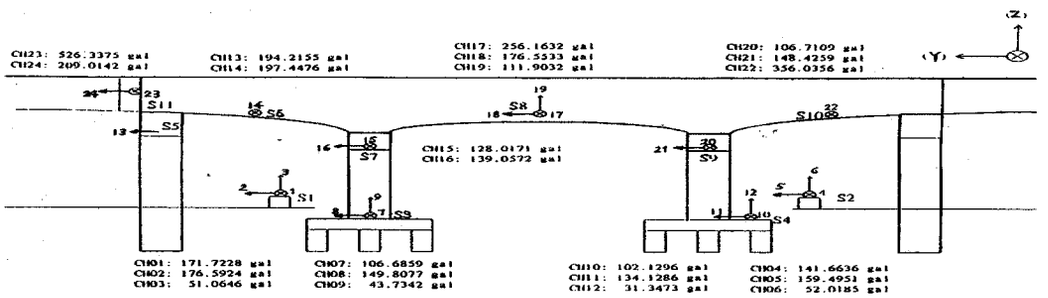

Fig. 3: A three-span bridge with base-isolation system at the top of bridge pier.

Example: Consider a three-span bridge with base-isolation at the top of the cap-beam, as shown in Fig. 3. The isolators were designed to absorb the energy in longitudinal direction during earthquake excitation. By using the ARX model with multiple inputs (motion at the top of two cap beams) and single output (motion at the center of the bridge girder) the dynamic characteristics of the isolators can be identified. Based on the sesimic response data of October 22, 1999 earthquake, the recursive least-square identification method was applied to identify the dynamic characteristics of the isolator. Fig. 4 shows the identified frequency response function between input and output. The first mode natural frequency and damping ratio of the isolation system in longitudinal direction are 6.32 rad/sec and 19.35%, respectively. The restoring force diagram of the isolation systen in longitudinal direction is also shown in Fig. 5. In transverse direction, the dynamic characteristics of the isolation system were difficult to be identified.

IDENTIFICATION OF MULTI-SUPPORTED STRUCTURAL SYSTEM

In the dynamic analysis of linear system to multi-support excitations, such as bridge

structure, the response of the structural system can be separated into quasi-static component $\mathbf{x}^s(t)$

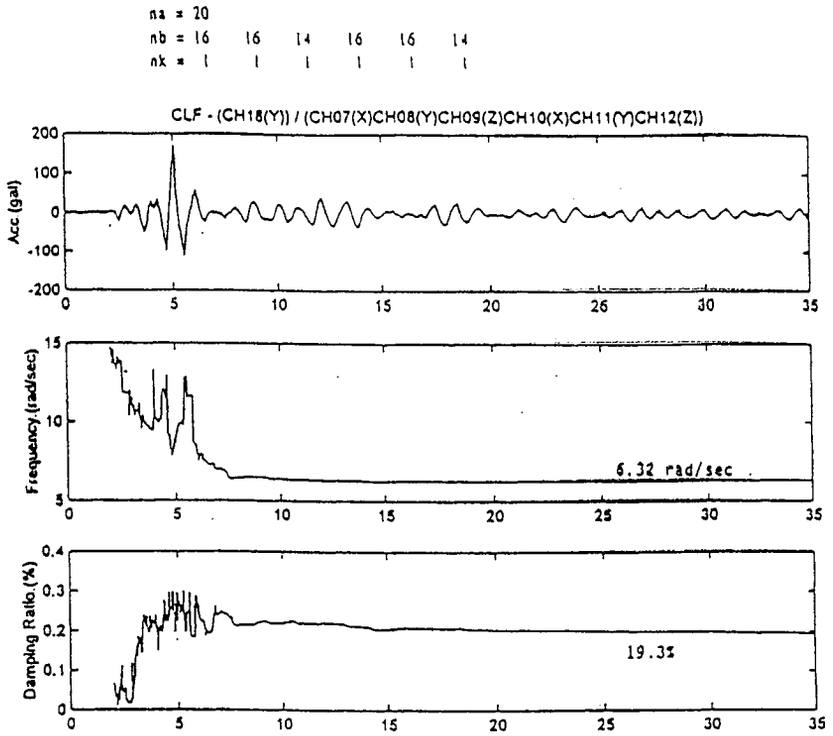

Fig.4: Identified natural frequency and damping ratio using recursive least-square ARX model.

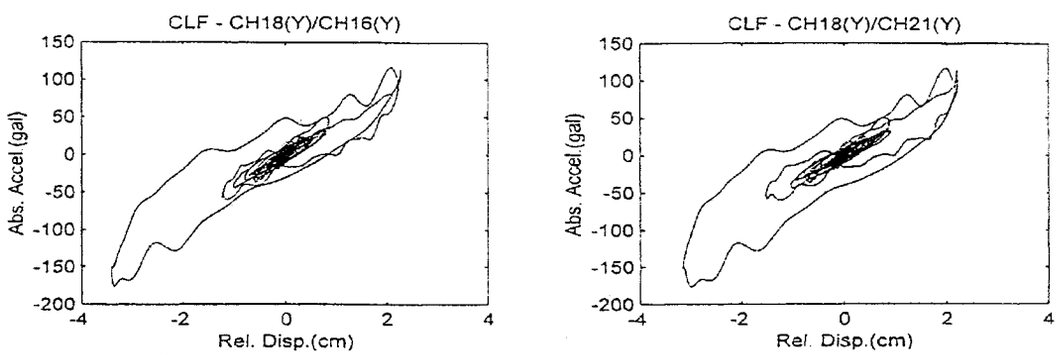

Fig.5: Plot of restoring force diagram of the bridge-isolator (1999-10-22 earthquake)

and dynamic component $\mathbf{x}^d(t)$. The generic response of interest z(t) can be expressed as a linear function of the model responses, i.e.,

$$\mathbf{z}(t) = \mathbf{q}^T (\mathbf{x}^s(t) + \mathbf{x}^d(t)) \qquad (4)$$

where $\mathbf{q}$ is a response transfer vector. In terms of the normalized modal responses, The response $\mathbf{z}(t)$ of i-th mode, $z_i(t)$, is expressed as:

$$z_i(t) = \sum_{k=1}^{m} a_k^i u_k(t) + \sum_{k=1}^{m}\sum_{j=1}^{n} b_{kj}^i s_{kj}(t) \qquad (5)$$

where $u_k(t)$ is the k-th prescribed support displacement, $s_{kj}(t)$ is the normalized modal response of j-th mode to k-th support input motion, a^i_k is the contribution factor of k-th support motion to i-th mode (contribution of quasi-static component).

Eq. (5) can be modified as the multi-input/single-output discrete time linear model and expressed in the following form:

$$z_i(t) = (\mathbf{B_1(q)/A_1(q)})u_1(t) + (\mathbf{B_2(q)/A_2(q)})u_2(t) + \ldots\ldots + (\mathbf{B_m(q)/A_m(q)})u_m(t) + \Sigma C_k u_k(t-d) + e(t) \qquad (6)$$

where $\mathbf{A(q)}=1+a_1q^{-1}+a_2q^{-2}+\ldots\ldots+a_nq^{-n}$ with order n and $q^{-1}[u(t)] = u(t-1)$, and $\mathbf{B_1(q)}$, $\mathbf{B_2(q)}$ .... are also polynomial in q^{-1} with respect to each input with order n_{k1}, ... ,n_{knu} , respectively. C_i corresponds to the contribution of quasi-static components. For the identification of sub-structural system it is necessary to include the quasi-static term (such as input motion $u_i(t)$) in the model. Application of the method will be shown in the following examples.

Example: Consider a 5-span continuous box-girder bridge, as shown in Fig. 2. The seismic response data from two earthquakes were used for the analysis (1995-2-23 and 1995-6-25 earthquakes). Consider the transverse motion of node B1 as output and the abutment motion at node C2 and C4 as output. The quasi-static contributions from supports were also used as inputs. Based on Eq.(6) the model parameters of the sub-structure were identified, as shown in Table 2. Then the natural frequency and damping ratio of each mode can be estimated. The identified natural frequencies consist with the designed value.

Table 2: Identified natural frequencies, damping ratios and quasi-static term
Using B1 as output and C2 and C4 as inputs (transverse direction).

B1/C2 (transverse dir.)			B1/C4 (transverse dir.)			
		Earthquake: 23 Feb. 1995				Error
ω	ξ (%)	a_j	ω	ξ	a_j	(%)
8·846	0·49		10·24	0·6		
		0·545			0·484	4·0
28·17	0·88		25·704	2·56		
		Earthquake: 25 June 1995				
9·037	0·91		8·89	0·63		
		0·436			0·582	3·8
11·76	0·90		12·47	1·02		

APPLICATION OF EMPIRICAL MODE DECOMPOSITION METHOD TO STRUCTURAL IDENTIFICATION

Different from the model identification by using both input and output data one can also analyze the structural response data using signal processing technique. Through signal analysis the abnormal of response data can be observed in which the change of modal prarameters can also be identified. Consider an arbitrary real-value function x(t), one may perform the following operation [Huang et.al. 1998]:

$$h_{11}(t) = x(t) - m_{11}(t) \tag{7}$$

where $m_{11}(t)$ is the mean of the lower and upper envelopes for x(t). Make the same shifting procedure for $h_{11}(t)$, that is:

$$h_{12}(t) = h_{11}(t) - m_{12}(t) \tag{8}$$

Keeping the same shiffting procrdure until $h_{1k}(t)$ converges, then, the subchannel signal $c_1(t)$ is defined as follows:

$$c_1(t) = h_{1k}(t) \tag{9}$$

Afterwards, the residual signal $\gamma_1(\mathbf{t})$, which is equal to x(t) minus $c_1(t)$, is treated as a new data and subjected to the same shifting process as defined above. Then, another sub-channel signal $c_2(t)$ is generated. Repeating those procedures, eventually, the original signal x(t) is decomposed as follows:

$$x(t) = \sum_{i=1}^{n} c_i(t) + \gamma_n(t) \tag{10}$$

applied Hilbert transform for each sub-channel $c_i(t)$:

$$d_i(t) = \frac{1}{\pi} \int_{-\infty}^{\infty} \frac{c_i(t')}{t - t'} dt' \tag{11}$$

and define $Z_i(t)$ as:

$$Z_i(t) = c_i(t) + d_i(t) j = a(t) e^{i\theta(t)} \tag{12}$$

Then the instantaneous frequency can be calculated:

$$\omega(t) = \frac{d\theta(t)}{dt} \tag{13}$$

The frequency-time-amplitude plot for each decomposed signal $c_i(t)$ can be plotted as:

$$\sum_{i}^{n} < t, \omega_i, a_i > \tag{14}$$

This spectrum provides high resolution in frequency-domain and time domain analysis of non-stationary signals. The dynamic characteristic of structural response can be observed through the

frequency-time-amplitude spectrum.

Example: Identification on Traffic Induced-vibration of Bridge Structure

Consider a truck (20 tons in weight) passing through a simply-supported bridge (dead load of the bridge deck is 150 ton). The vertical vibration signal (acceleration) was measured at the mid-span of the bridge. In the beginning the Fourier amplitude spectrum of ambient vibration signal of the bridge is shown in Fig. 6a. The dominant frequency of vertical vibration is at 4.11Hz. When the truck reached the mid-span of the bridge emergency brake was applied. From the bridge vibration data (Fig.7a) it is clear that the emergency brake was applied at t=16sec. The Fourier spectrum of the record (0~30sec) is also shown in Fig 6b. From the Fourier spectrum of the response data it was difficult to identify the dynamic characteristics of the bridge-vehicle interaction before and after the brake was applied. Now, empirical mode decomposition Hilbert transform is applied to the recorded data. The time-frequency-amplitude spectrum is calculated and shown in Fig.7b. Before the emergency brake (0~16sec), the dominant frequency of the bridge vibration is about 4Hz. At the moment of emergency brake the interaction between the truck and the bridge deck is significant (it acted as a mass system) and the system vibration frequency was changed. The vibration frequency of the system is then identified from the Hilbert marginal spectrum, defined as:

$$A(\omega) = \int \sum_{i}^{n} < a_i(\omega,t) > dt \tag{15}$$

Fig.7b shows the Hilbert marginal spectrum the recorded signal before and after the emergency brake of the truck. From this Hilbert marginal spectrum the dynamic characteristics of the bridge-vehicle interaction was clearly identified.

SYSTEM REALIZATION USING INFORMATION MATRIX

Based on the mathematical framework the system realization using information matrix (SRIM) is established [Junag, 1997]. The SRIM is derived using the state-space discrete-time linear equation to form a data correlation matrix for system identification. Based on the discrete-time ARX model the following matrix equality can be developed:

$$\alpha\, Y_p(k) = \beta U_p(k) \tag{16}$$

where

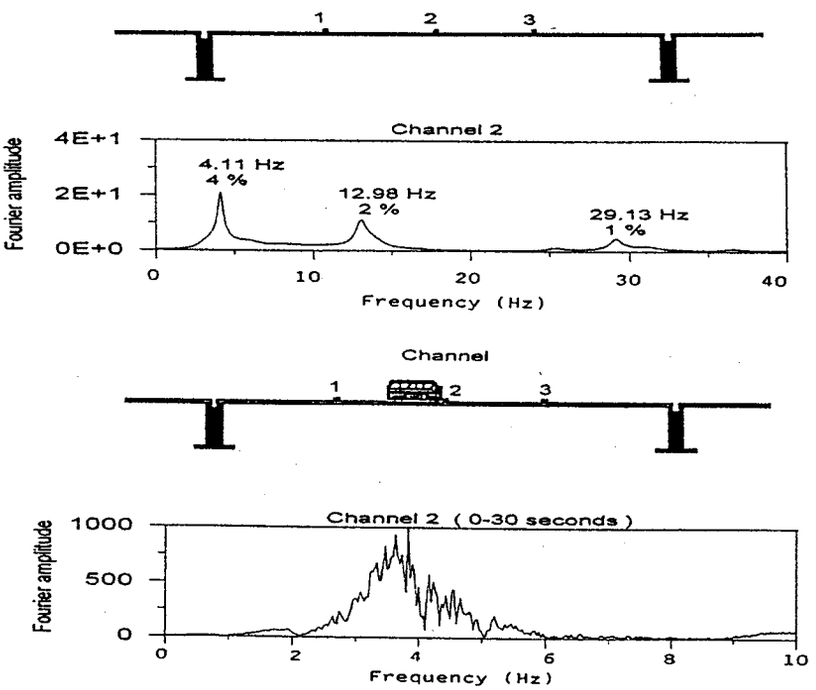

Fig.6: Plot of Fourier amplitude spectrum of ambient signals and vehicle-induced vibration at Channel 2 (vertical comp.)

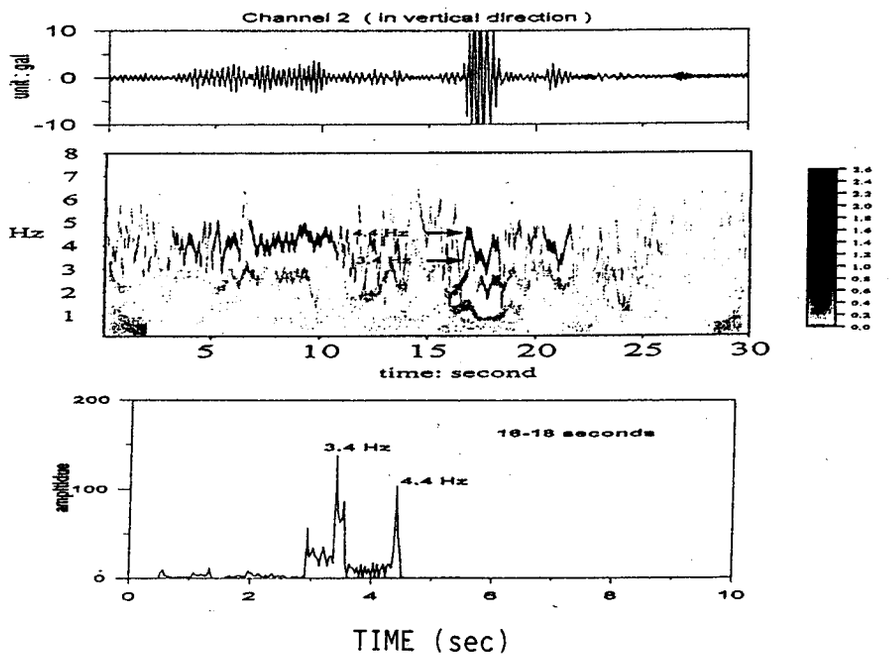

Fig. 7: Plot of vehicle-induced vibration of a simply-supported bridge structure. Based on empirical mode decomposition and Hilbert spectrum the frequency-time-amplitude spectrum of the signal is calculated. The Hilbert Marginal Spectrum is also shown.

$$\alpha = [\,\alpha_0 \quad \alpha_1 \quad \ldots\ldots \quad \alpha_{p-1}\,] \qquad \beta = [\,\beta_0 \quad \beta_1 \quad \ldots\ldots \quad \beta_{p-1}]$$

$$Y_p(k) = \begin{bmatrix} y(k) & y(k+1) & \cdots & y(k+N-1) \\ y(k+1) & y(k+2) & \cdots & y(k+N) \\ \vdots & \vdots & \ddots & \vdots \\ y(k+p-1) & y(k+p) & \ddots & y(k+p+N+2) \end{bmatrix}$$

$$U_p(k) = \begin{bmatrix} u(k) & u(k+1) & \cdots & u(k+N-1) \\ u(k+1) & u(k+2) & \cdots & u(k+N) \\ \vdots & \vdots & \ddots & \vdots \\ u(k+p-1) & u(k+p) & \ddots & u(k+p+N+2) \end{bmatrix} \tag{16a}$$

Post multiplying Eq.(9) by $U_p^T(k)$ one can obtained the correlation matrix:

$$\alpha\,[\,R_{yy} - R_{yu}\,R_{uu}^{-1}\,R_{uy}^{T}\,] = 0 \tag{17}$$

or

$$\alpha R_{hh} = 0_{m\,x\,pm} \tag{17a}$$

One may take a singular value decomposition to factor the matrix R_{hh} then the state matrix A can be obtained. With the computed matrix A the system dynamic characteristics can be estimated. For example: Consider the seismic response of the 5-story steel frame. Based on the seismic response data collected from the 8% excitation level of Kobe earthquake excitation, the above-mentioned SRIM's method was applied to identify the natural frequency and damping ratio of the isolated-bridge system. Fig.8a shows the comparison on the recorded and estimated bridge-deck acceleration response in longitudinal direction. The estimated equivalent natural frequency and damping ratio of the isolation system is 1.068 Hz and 18.9%, respectively. Fig.8b shows the estimation of deck response in transverse direction. The estimation in transverse direction is poor than in longitudinal direction. This method can be applied to the estimation dynamic characteristics of linear system using limited measurements and the noise measurement can also be minimized.

NEURAL MODELLING AND IDENTIFICATION APPLICATION

The complex nature of system makes it different to develop a proper parametric model which model parameters are having physical meanings. Therefore, non-parametric modeling approaches are giving more and more attentions in the system identification field. Neural-network-based approach is regarded as a kind of non-parametric method, and its capability will

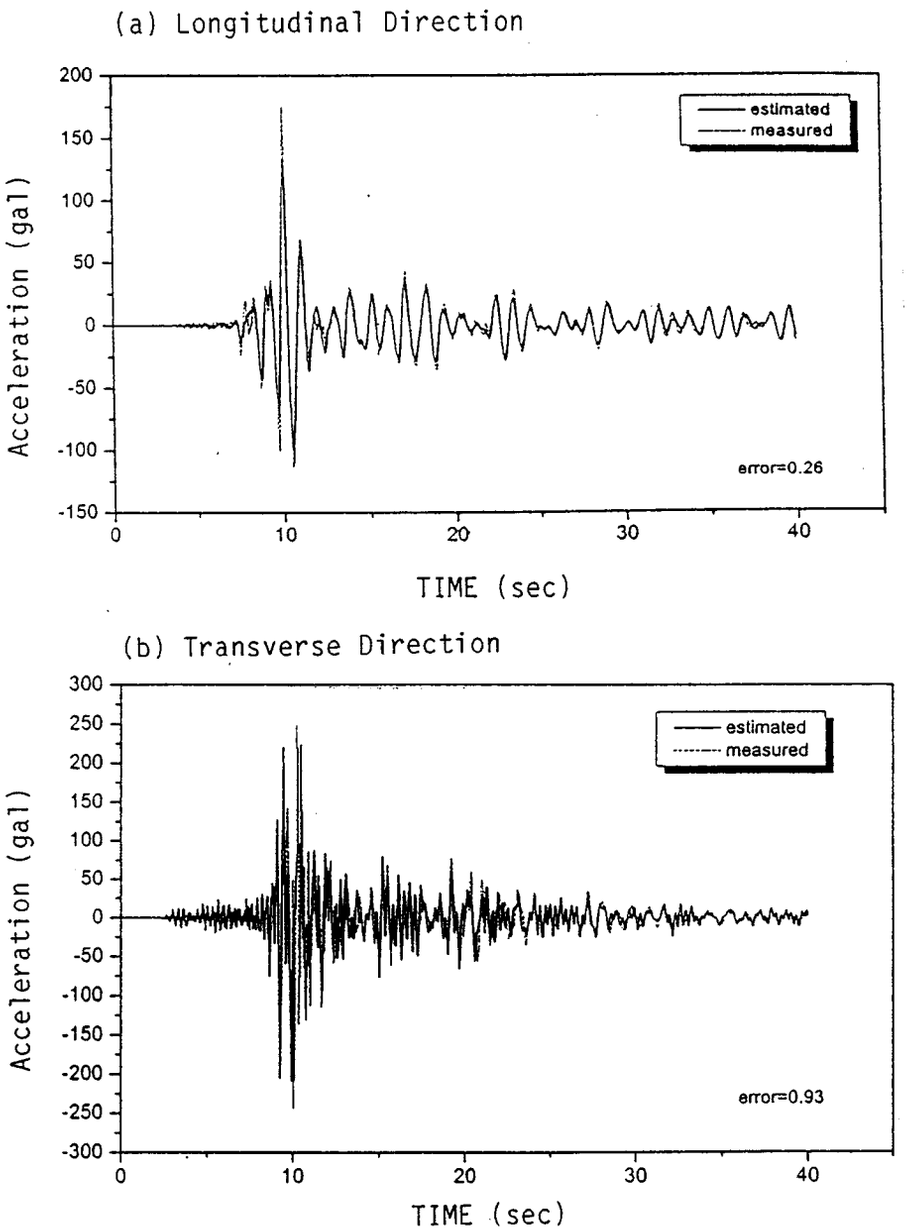

Fig. 8: Estimated deck response of the isolated bridge using system realization algorithm. (a) In longitudinal direction the estimated natural frequency and damping ratio of the isolation system is 1.068 Hz and 18.9%, respectively. (b)In transverse direction the estimated natural frequency and damping ratio of the isolation system is 1.192 Hz and 15.1%, respectively.

be discussed in this section. Generally, a wide class of discrete-time nonlinear system can be represented by the Nonlinear Auto Regressive Moving Average with eXogenous input (NARMAX) model. The capability of approximating a system within a desirable accuracy relies on a proper chosen set of known functions. Theoretical works performed by Cybenko and Funahashi (Cybenko 1989, Funahashi,1989) had proved that neural networks can approximate any contineous function even with a single hidden layer. Therefore, this gives the theoretical basis for modeling nonlinear systems by neural network (Chen 1990).

When the system responses exceed linear range, a nonlinear mathematical model is used. However, it is difficult to determine which nonlinear term should be included in the model, and the relation between system response is often not known. From the discussion above, the nonlinear activation function can be used to approximate any continuous function and is therefore suitable for this situation. The network was used as a model of the unknown nonlinearity for prediction of the system's responses to various excitations. For the identification of the internal (restoring) forces of some typical nonlinear structural system, the ANN's can be used. By putting $\bar{x}$, $\dot{\bar{x}}$ as input signals, $\ddot{\bar{x}}$ as output signal, the training procedure will use the nonlinear function mapping capability to avoid this nonlinear term selection (nonlinear model determination) problem. If the system exhibits hysteretic behavior, it is important to include the lagged information in the model to represent this energy-dissipating phenomenon. Based on a "Loss Function Table" proper delay term (n_y,n_u) can be determined. Note that if the system nonlinearity is known in advance, i.e. the nonlinear form is known, then neural network training procedure will just try to fit a model with a higher dimension than the necessary required.

Different from the identification of restoring forces, the network-based approach is also used for the detection of changes in the characteristics of structure-unknown systems. For example, consider the three-story structure again measured responses are acceleration at each floor and the mathematical description of these responses is not clear. By putting acceleration at one and third floor as input signals, second floor acceleration as output signal, hidden layer activation functions are either linear or nonlinear, the relation may still be established (if it exists) between these responses through the training process. It can be used as a tool for structural health monitoring. The underlying idea can be explained by the following procedures: (1) establish the neural networks from the structure under low level excitation and train the system to 'learn' the behavior of 'healthy' structure, (2) following step (1), by putting the current measured responses from the monitoring structure into the trained network . The deviation from the network output and structural response could be an indicator to the current condition of structure. Large deviation indicates that the damage has occurred in the structure or the structural behavior has changed. Similar idea can be found in (Masri 1996). This technique will be used in this study to identify the change of RMSE value of a bridge structure when subjected to earthquake

excitation.

Example: Health Monitoring of New-Lian River Bridge from Seismic Response Data

Part I Girder Substructure Model

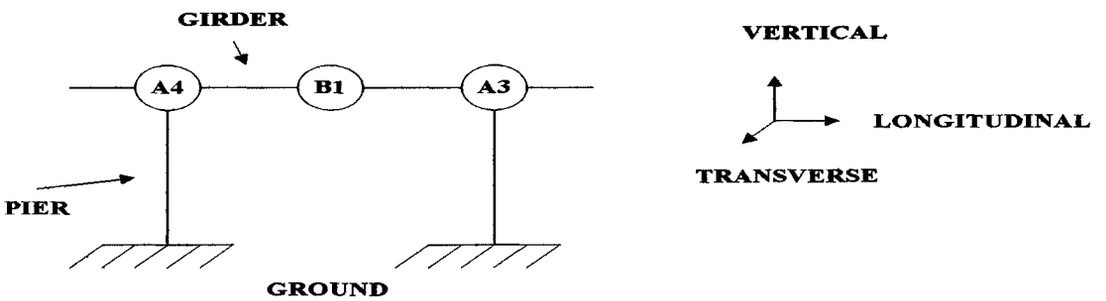

Fig.9 Girder substructure model (Model A)

Consider the girder substructure model of the bridge, as shown in Fig. 9. By assigning the transverse direction acceleration response at station B1 as output, the network was designed to establish the relation between this measurement and other information available at nearby station (A3,A4). The input information is chosen to be the current transverse displacement and acceleration response at A3, B1 and A4 station and immediate history of these quantities. The maximum values of delay time for displacement and acceleration at station A3, B1 and A4 are determined to be either 4 or 8 steps in delay time based on "loss function table". The network performance of the identified models is shown in Table 4. The results from linear model (Model A, B) show that lagged information is important and the networks trained with low-level response data (1995.02.10 and 1995.05.02 event) and medium-level response data (1995.02,23 and 1996.03.05 event) can produce the same or even smaller RMS errors for other low and medium level events. However, these trained linear networks can't predict the response for the high-level event (1995.06.25 event). On the contrary, linear network trained with high-level response data (1995.06.25 event) can predict the response from low to high level ones within 10% error. The trained nonlinear network (Model C, D) can not capture the response higher than the data used in training phase. On the contrary, nonlinear model (Model C, D) trained by high-level response data can alos model the system quite well from low-level to high-level situation. Note that satisfying performance can also be obtained from a simple linear model (Model B) with sufficient lagged input information.

Table 3 'Loss function table' for Girder substructure I/O mapping model
(based on response data during '1995.06.25' event)

Delay	$n_{A3T.v}$ $n_{B1T.v}$ $n_{A4T.v}$					
$n_{A3T.d}$ $n_{B1T.d}$ $n_{A4T.d}$	0	1	2	3	4	5
0	0.4885	0.3515	0.2923	0.2565	0.2394	0.2279
1	0.2619	0.1469	0.1303	0.1270	0.1262	0.1253
2	0.1954	0.1283	0.1269	0.1262	0.1252	0.1234
3	0.167	0.1268	0.1264	0.1230	0.1223	0.1216
4	0.1499	0.1254	0.1240	0.1224	0.1211	0.1184
5	0.1435	0.1243	0.1215	0.1214	0.1189	0.1050

Delay	$n_{A3T.v}$ $n_{B1T.v}$ $n_{A4T.v}$				
$n_{A3T.d}$ $n_{B1T.d}$ $n_{A4T.d}$	4	5	6	7	8
4	0.1211	0.1184	0.1157	0.1105	0.1038
5	0.1189	0.1050	0.1037	0.1031	0.0989
6	0.1106	0.1043	0.1007	0.0987	0.0968
7	0.1038	0.1019	0.0991	0.0948	0.0932
8	0.0975	0.0962	0.0961	0.0931	0.0924

Note: $n_{A3T.d}$, $n_{B1T.d}$, $n_{A4T.d}$ are the maximum values of displacement delay time for A3, B1 and A4 station in transverse direction, respectively. $n_{A3T.v}$, $n_{B1T.v}$, $n_{A4T.v}$ are the maximum values of velocity delay time for A3, B1 and A4 station in transverse direction, respectively.

Part II. Pier-Girder Substructure Model

Consider the pier-girder substructure model, as shown in Fig. 10. The network model was designed to establish the relation between the displacement at A4 and other available

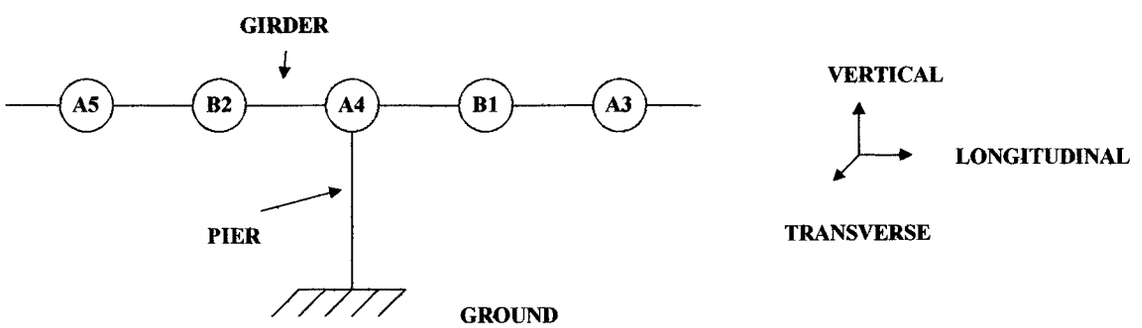

Fig.10: Pier-Girder substructure model (Model B)

Table 4: Identified I/O mapping model

Model A	Linear Type	$\mathrm{B1T.a(k)} = \sum_{i=0}^{8} a_i \times \mathrm{A3T.d(k-i)} + \sum_{j=0}^{8} b_j \times \mathrm{B1T.d(k-j)} + \sum_{s=0}^{8} c_s \times \mathrm{A4T.d(k-s)} + \sum_{t=0}^{8} d_t \times \mathrm{A3T.a(k-t)} + \sum_{q=0}^{8} e_q \times \mathrm{A4T.a(k-q)}$
	Nonlinear Type	$\mathrm{B1T.a(k)} = \sum_{m=1}^{9} w_m \times f(\sum_{i=0}^{8} a_{im} \times \mathrm{A3T.d(k-i)} + \sum_{j=0}^{8} b_{jm} \times \mathrm{B1T.d(k-j)} + \sum_{s=0}^{8} c_{sm} \times \mathrm{A4T.d(k-s)} + \sum_{t=0}^{8} d_{tm} \times \mathrm{A3T.a(k-t)} + \sum_{q=0}^{8} e_{qm} \times \mathrm{A4T.a(k-q)})$
Model B	Linear Type	$\mathrm{A4T.a(k)} = \sum_{i=0}^{8} a_i \times \mathrm{B2T.d(k-i)} + \sum_{j=0}^{8} b_j \times \mathrm{A4T.d(k-j)} + \sum_{s=0}^{8} c_s \times \mathrm{B1T.d(k-s)} + \sum_{n=0}^{8} d_n \times \mathrm{C4T.d(k-n)} + \sum_{t=0}^{8} e_t \times \mathrm{B2T.a(k-t)} + \sum_{q=0}^{8} f_q \times \mathrm{B1T.a(k-q)} + \sum_{m=0}^{8} g_m \times \mathrm{C4T.a(k-m)}$
	Nonlinear Type	$A4T.a(k) = \sum_{z=1}^{9} w_z \times f(\sum_{i=0}^{8} a_{iz} \times B2T.d(k-i) + \sum_{j=0}^{8} b_{jz} \times A4T.d(k-j) + \sum_{s=0}^{8} c_{sz} \times B1T.d(k-s) + \sum_{n=0}^{8} d$ $\sum_{t=0}^{8} e_{tz} \times \mathrm{B2T.a(k-t)} + \sum_{q=0}^{8} f_{qz} \times \mathrm{B1T.a(k-q)} + \sum_{m=0}^{8} g_{mz} \times \mathrm{C4T.a(k-m)})$

Note: A3T.a, B1T.a, A4T.a, B2T.a, C4T.a are the acceleration response for A3, B1, A4, B2, C4 station in transverse direction, respectively, and A3T.d, B1T.d, A4T.d, B2T.d, C4T.d are the displacement response for A3, B1, A4, B2, C4 station in transverse direction, respectively.

information at nearby stations (B1, A3, B2 and A5). The input information is therefor chosen to be the current transverse displacement response at A3, B1, B2 and A5 station and immediate history of these quantities. The identified models are shown in Table 4 and based on the loss function table the maximum values of delay time at these stations are determined to be either 4 or 8 steps. The performance of the identified models is shown in Table 5. As the same situations mentioned above, the linear model with sufficient lagged information can perform well and the nonlinear model trained with high-level response data can model the system response from low to high level response situations. The results discussed above show that the response of bridge could be modeled with a linear or nonlinear model. The proposed model can not indicate whether the structural behavior is linear or nonlinear and whether the damage has occurred or not during strong earthquake event (1995.06.25 event). However, it still can be used as an indicator to the monitoring of current condition of bridge.

CONCLUSIONS

Base on the seismic response data of bridge structures (data from TSMIP) the time-domain identification methods were used to estimate the dynamic characteristics of bridges. In the Table

5a: RMS Error of model A for linear type

Linear Type		Events for Training				
		L1	L2	M1	M2	H
Events for Testing	L1	*0.0394*	0.0512	0.0590	0.0677	0.1664
	L2	0.0234	*0.0126*	0.0210	0.0191	0.1421
	M1	0.0330	0.0234	*0.0156*	0.0263	0.1451
	M2	0.0211	0.0143	0.0087	*0.0037*	0.1183
	H	0.1712	0.1823	0.1828	0.2374	*0.0769*

Table 5b: RMS Error of model A for nonlinear type

Nonlinear Type		Events for Training				
		L1	L2	M1	M2	H
Events for Testing	L1	*0.0977*	0.1758	0.1632	0.2397	0.4199
	L2	0.0747	*0.0513*	0.0711	0.0635	0.3327
	M1	0.1091	0.1070	*0.0818*	0.1311	0.3591
	M2	0.1587	0.0282	0.0407	*0.0165*	0.2473
	H	1.0952	0.5104	0.5619	0.5574	*0.1644*

Table 5c: RMS Error of model B for linear type

Linear Type		Events for Training				
		L1	L2	M1	M2	H
Events for Testing	L1	*0.0804*	0.1115	0.1200	0.1096	0.1928
	L2	0.0467	*0.0317*	0.0464	0.0428	0.0892
	M1	0.0559	0.0520	*0.0276*	0.0487	0.0794
	M2	0.0402	0.0217	0.0194	*0.0074*	0.0462
	H	0.1492	0.1730	0.2625	0.1533	*0.0531*

Table 5d: RMS Error of model B for nonlinear type

Nonlinear Type		Events for Training				
		L1	L2	M1	M2	H
Events for Testing	L1	*0.1328*	0.2585	0.3512	0.1897	0.4350
	L2	0.0906	*0.0717*	0.1246	0.0698	0.2991
	M1	0.1631	0.1672	*0.1410*	0.0950	0.3215
	M2	0.2547	0.0649	0.0785	*0.0132*	0.2175
	H	0.7443	0.6095	0.5666	0.4154	*0.1778*

beginning the discrete-time ARX model was used to represent the bridge substructure with multiple inputs. From which the system natural frequency and damping ratio can be identified. The system realization method using information matrix provides a systematic identification method with limited measurements and noise-polluted signals.

A modeling and identification method has been developed for discrete-time nonlinear hysteretic system based on a neural network approach. The capability of neural network is

explained and its applications to simulated and real structural system have been demonstrated. The results suggest that the proposed method is an effective approach to the input-output mapping problem, especially for structure-unknown problem.

The success of health-monitoring system relies on its ability to detect the minor damage of structures. The modeling capability of neural network makes itself suitable for the implementation of on-line monitoring of real structures and further research in this field is worth pursuing.

ACKNOWLEDGEMENTS

The authors wish to express their thanks to Central Weather Bureau as well as National Science Council (Grant NO. NSC88-2211-E-002-006) for the support of this research.

REFERENCES

1. Billings, S. A., Jamaluddin, H. B., and Chen, S. (1992). "Properties of neural networks with applications to modeling non-linear dynamical systems." *International Journal of Control*, 55, 193-224.
2. Caravani, P., Watson, M.L. and Thomson, W.T., "Recursive Least-Square Time Domain Identification of Structural Parameters," *J. of Applied Mechanics*, March, 1977, pp. 135–150.
3. Chassiakos, A. G., and Masri, S. F. (1996). "Modeling unknown structural systems through the use of neural networks." *Earthquake Engineering and. Structural Dyn*amics, 25, 117-128.
4. Chen, S., and Billings, S. A. (1989). "Representation of non-linear systems: the NARMAX model." *International Journal of Control*, 49, 1013-1032.
5. Chen, S., Billings, S. A., and Grant, P. M. (1990). "Non-linear system identification using neural networks." *International Journal of Control*, 51, 1191-1214.
6. Cybenko, G. (1989). "Approximations by superpositions of a sigmoidal function." *Mathematics of Control, Signals and Systems*, 2, 303-314.
7. Elkordy, M. F., Chang, K. C., and Lee, G. C. (1993). "Neural networks trained by analytically simulated damage states." *Journal of Computing in Civil Engineering*, ASCE, 7(2), 130-145.
8. Funahashi, K. (1989). "On the approximate realization of continuous mappings by neural networks." *Neural Networks*, 2, 183-192.
9. Goodwin, G.C. and Sin, K.S., *Adaptive Filtering, Prediction and Control*, Englewood Cliffs, NJ: Prentice-Hall, 1984.
10. Hagan, M. T., Demuth, H. B., and Beale, M. (1996). *Neural Network Design*. Boston: PWS

Pub.

10.Hoshiya, M., and Sato, E., "System Identification for Extended Kalman Filter," ASCE, *J. of Engineering Mechanics*, 112(12), 1984,

11.Huang, Norden E. et.al. "the Empirical Mode Decomposition and the Hilbert Spectrum for Nonlinear and Non-stationary time Series Analysis," *Proc. R. Soc. Lond*, 454, 1998, 903-995.

12.Ljung, L. and Söderström, T., "Theory and Practice of Recursive Identification," MIT Press, Cambridge, MA, 1983.

13.Loh, C.H., H.M. Lin and T.S. Wu "Discussion on the Identification of Seismic Response Data of Building," *The Chinese Journal of Mechanics*, Vol.12, No3, Sept. 1996, 339-351.

14.Loh, C. H. and Lee, Z. K. "Seismic monitoring of a bridge : assessing dynamic characteristics from both weak and strong excitation." *Earthquake Engineering and Structural Dynamic*, Vol. 36, 1997, 269-288.

15.Masri, S. F., Chassiakos, A. G., and Caughey, T. K. (1993). "Identification of nonlinear dynamic systems using neural networks." *Journal of Applied Mechanics*, 60, 123-133.

16.Masri, S. F., Nakamura, M., Chassiakos, A. G., and Caughey, T. K. (1996). "Neural network approach to detection of changes in structural parameters." *Journal of Engineering Mechanics*, ASCE, 122(4), 350-360.

17.Nakamura, M., Masri, S. F., Chassiakos, A. G., and Caughey, T. K. (1998). "A method for non-parametric damage detection through the use of neural networks." *Earthquake Engineering Structural. Dynamics*, 27, 997-1010.

18.Safac, A., "Adaptive Modeling, Identification and Control of Dynamic Structural Systems, I: Theory," ASCE, *J. of Engineering Mechanics*, 115(11), 1989, pp. 2386–2405.

19.Sato, T. and Takei, K., "Real Time Robust Algorithm for Structural System with Time-Varying Dynamic Characteristics," *Proc. of SPIE's Symposium on Smart Structures and Materials*, San Diego, CA, USA, 1997, pp. 393–404.

20.Sato, T. and Qi, K., "Adaptive H_∞ Filter: Its Application to Structural Identification," ASCE, *J. of Engineering Mechanics,* Vol.124, No.11, Nov. 1998 1233-1240.

NON-LINEAR STRUCTURAL IDENTIFICATION USING ROBUST AND ADAPTIVE KALMAN FILTER

*Tadanobu SATO[1] and Keisuke KAJI [2]

[1] *Professor, Disaster Prevention Research Institute, Kyoto University, Japan*
[2] *Graduate Student, School of Civil Engineering, Kyoto University, Japan*

ABSTRACT

Structural system identification using the concept of back analysis was categorized into non-linear optimization problems without constraint conditions because the system transfer equation of a structural system is intrinsically expressed by a non-linear differential equation. To apply a linear optimization technique to system identification problems we developed a method to linearize the observation equation which has intrinsic non-linear characteristics. To identify the non-stationary dynamic change of structural parameters we used an adaptive Kalman filter scheme, in which the function of memory fading for past observation data was added to the Kalman filter that is widely used as a time marching identification algorithm. We also assigned robustness to the adaptive Kalman filter to eliminate the effect of abnormal signals contained in the observed structural response. This identification scheme can be used to identify structural hysteresis characteristics without any information on the constitutive relationship of the structural elements. For the case that the hysteresis is defined by Versatile model all the shape parameters, including the power parameter, can be identified.

INTRODUCTION

The purpose of this research was to develop robust algorithms for structural system identifications. In discussions of the seismic capacity of structural systems, the nonlinear response characteristics of the system are essential, especially the hysteretic characteristics of structural elements. The capacities of plastic deformation and hysteretic energy absorption are important factors for evaluating structural safety and preventing structural collapse. In structural response control technologies that use active, semi-active and passive devices a key issue is the real time grasp of nonlinear dynamic characteristics of the structural system. We here define structural identification in terms of grasping dynamic characteristics of the structural system. To identify the hysteretic characteristic of the system a constitutive model is usually needed but it is not an easy task to define a general constitutive relationship. The non-parametric system identification techniques are therefore necessary for a real time evaluation of the dynamic nonlinear characteristic of structural response. Many methods for the nonlinear system identification have been developed in the past decade. Noteworthy recent publications in this field are the works of Safac (1989), Masri et al. (1991), Peng and Iwan (1992), Stry and Moak (1992), Loh and Chung (1993), Benedettini et al. (1995), Chassiakos et al. (1998), Sato et al. (1998a,c), and most recently Smyth et al. (1999). These are classified into developments of non-parametric identification schemes, applications of sequential prediction-error method (Ljung, 1987) and Kalman filter (Kalman 1960) as well as H_∞ filter (Takaba and Katayama 1996) techniques.

To assign adaptability to Kalman and H_∞ filters we introduced a parameter to control forgetting rate of past observation data (Sato et al. 1998a,c). In the first part of this paper the applicability of the developed adaptive Kalman filter is checked to identify the hysteretic characteristics of a structure by the use of the incremental linearization technique. Stiffness and damping matrices of the equation of motion expressed by an incremental formula are identified for each sampling interval.

In the second part of the paper a linearization technique is developed to identify of the Versatile constitutive

relationship of the restoring force (Wen 1976). Identification studies done with this constitutive model showed instability because a power term in the constitutive parameters; therefore, this power parameter is assumed to be given apriori (Sato and Kikukawa 1998b). To overcome this drawback we defined a new multi-dimensional Versatile model and developed a method to linearize the observation equation even when the power parameter included in the constitutive relationship. The developed adaptive Kalman filter technique was used to identify the constitutive parameters of the Versatile model, but the accuracy of the identified results becomes unstable if the signal used for identification is contaminated by abnormal noise. A technique to evaluate the efficiency of observed data (Sato and Takei 1998a), robust to abnormal signals, is introduced into the adaptive Kalman filter to eliminate the effect of abnormal signals

CONCEPT OF THE ADAPTIVE KALMAN FILTER

We explain briefly the algorithm with a memory fading function in the Kalman filter. The state transfer equation from the time step $t-1$ to t is assume to be given by

$$z_t = \Phi_{t-1} z_{t-1} + \Gamma_{t-1} w_{t-1} \tag{1}$$

in which z_t is the state vector, Φ_t the state transfer matrix, w_t the system noise vector, Γ_t the state transfer matrix for system noise. Several state variables are assumed to be observed as defined by the observation equation;

$$y_t = H_t z_t + v_t \tag{2}$$

in which y_t is the observation vector, H_t the observation matrix, v_t the observation noise vector.

The adaptive Kalman filter algorithm is defined by the following six steps:

Step 1. Define the initial value of state vector $\hat{z}_0$ and its covariance matrix P_0 as well as the covariance matrix of the observation noise R.

Step 2. Calculate the pre-estimation of state vector $\bar{z}_t$ and its covariance matrix M_t using

$$\bar{z}_t = \Phi_{t-1} \hat{z}_{t-1} + \Gamma_{t-1} \overline{w}_{t-1} \tag{3}$$

$$M_t = \Phi_{t-1} P_{t-1} \Phi_{t-1}^t + \Gamma_{t-1} Q_{t-1} \Gamma_{t-1}^t \tag{4}$$

Step 3. Calculate the post-estimation of covariance matrix P_t of the state vector by

$$P_t = \left(\lambda_t M_t^{-1} + H_t^T R^{-1} H_t\right)^{-1} \tag{5}$$

Step 4. Calculate the Kalman gain G_t by

$$G_t = P_t H_t^T R^{-1} \tag{6}$$

Step 5. Calculate the most likely-hood (or post-) estimation of the state vector $\hat{z}_t$ by

$$\hat{z}_t = \bar{z}_t + G_t \left(y_t - H_t \bar{z}_t\right) \tag{7}$$

Step 6. Return to step 1 after renewal of the time step.

λ_t is called the forgetting factor and has the constraint $\lambda_t \leq 1.0$. The forgetting rate of past observed data becomes larger as the value chosen decreases. If $\lambda_t = 1.0$ this adaptive Kalman filter coincides with the normal Kalman filter. Because the weights of past observed data are equal and unit in the normal Kalman filter we can not use this filter to identify non-stationary dynamic characteristics of a structural system.

NON-LINEAR STRUCTRAL SYSTEM IDENTIFICATION BASED ON THE INCREMENTAL LINEARIZATION ALGORITHM

Incremental Linearization

By applying the equivalent linearization technique, the non-linear response of a structural system can be identified at a certain level (Sato and Takei 1998). The equivalent damping coefficient and the stiffness at each time step are identified by using the adaptive Kalman filter. The applicability of equivalent linearization, however, is limited to weak non-linear systems. This defect is overcome by using the incremental linearization technique. The concept is shown in schematically in Figure 1. A linear system is assumed between time steps $t-1$ and t for the

case of stepwise linearization. The equation of motion for an n degree of freedom system is

$$M\left(\Delta\ddot{x}_t + \Delta\ddot{x}_{g,t}\right) = -C\Delta\dot{x}_t - K\Delta x_t \tag{8}$$

in which $\boldsymbol{M}$, $\boldsymbol{C}$, and $\boldsymbol{K}$ are the mass, damping and stiffness matrices between time steps $t-1$ and t, x_t is the relative displacement of the structural system to ground displacement, $\ddot{x}_{g,t}$ the ground acceleration, and Δ the difference operator defined by

$$\Delta x_t = x_t - x_{t-1} \tag{9}$$

If the new notations for components of damping and stiffness matrices are defined as

$$\boldsymbol{C} = \begin{bmatrix} c_{11} & c_{12} & \cdots & c_{1n} \\ c_{21} & \ddots & & \vdots \\ \vdots & & \ddots & \vdots \\ c_{n1} & \cdots & \cdots & c_{nn} \end{bmatrix} = \begin{bmatrix} \boldsymbol{c}_1 \\ \boldsymbol{c}_2 \\ \vdots \\ \boldsymbol{c}_n \end{bmatrix} \tag{10}$$

$$\boldsymbol{K} = \begin{bmatrix} k_{11} & k_{12} & \cdots & k_{1n} \\ k_{21} & \ddots & & \vdots \\ \vdots & & \ddots & \vdots \\ k_{n1} & \cdots & \cdots & k_{nn} \end{bmatrix} = \begin{bmatrix} \boldsymbol{k}_1 \\ \boldsymbol{k}_2 \\ \vdots \\ \boldsymbol{k}_n \end{bmatrix} \tag{11}$$

the observation equation is obtained by substituting equations (10) and (11) in equation (8), assuming that absolute acceleration responses are given at all the mass points:

$$\begin{Bmatrix} m_1\left(\Delta\ddot{x}_1 + \Delta\ddot{x}_g\right) \\ m_2\left(\Delta\ddot{x}_2 + \Delta\ddot{x}_g\right) \\ \vdots \\ m_n\left(\Delta\ddot{x}_n + \Delta\ddot{x}_g\right) \end{Bmatrix} = \begin{bmatrix} h & \mathbf{0} & \cdots & \mathbf{0} \\ \mathbf{0} & h & & \vdots \\ \vdots & & \ddots & \vdots \\ \mathbf{0} & \cdots & \cdots & h \end{bmatrix} \begin{Bmatrix} c_1^T \\ k_1^T \\ \vdots \\ c_n^T \\ k_n^T \end{Bmatrix} \tag{12}$$

in which h is defined by

$$h = \left\{\Delta\dot{x}_1 \quad \cdots \quad \Delta\dot{x}_n \quad \Delta x_1 \quad \cdots \quad \Delta x_n\right\} \tag{13}$$

By applying the adaptive Kalman filter, the components of damping and the stiffness matrices are identified at each time step.

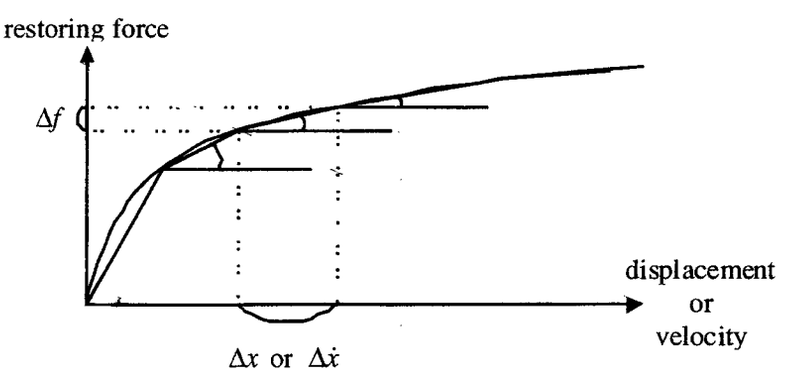

Fig. 1 Concept of incremental Linearization

Analytical Model

A two degree of freedom structural model (Figure 2) is used to demonstrate non-linear structural identification. The non-linear restoring force between the mass points $i-1$ and i is assumed to be expressed by the Versatile model as defined by

$$\dot{f}_i = k_i \dot{u}_i - \alpha_i \left| \dot{u}_i \right| f_i \Big|^{n_i - 1} f_i - \beta_i \dot{u}_i \left| f_i \right|^{n_i} \tag{14}$$

in which f_i is the restoring force, u_i the relative displacement between the mass points $i-1$ and i, k_i the initial stiffness, and α_i, β_i, n_i are the shape parameters of the Versatile model. The response of this structure was simulated using El Centro (1940 NS) scaled to a maximum acceleration of 25 gal. The fourth order Runge-Kutta time integration scheme was used. The time step in the numerical analysis was 0.01 sec. Pink noise with a frequency band from 0 to 25Hz was added as observation noise, which level is defined by

$$v = \frac{\sigma_{noise}}{\sigma_{resp}} \times 100 \quad (\%) \tag{15}$$

in which σ_{resp} is the standard deviation of the response without noise, and σ_{noise} the standard deviation of the white noise added to the simulated response.

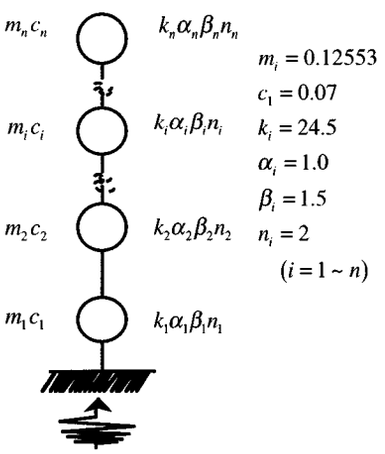

Fig.2 N degrees of freedom model

In the identification we assume that each nodal mass, m_i, is given. The increment of relative displacement, velocity to the ground, and absolute acceleration of each mass point, $\Delta x_i, \Delta \dot{x}_i, \Delta \ddot{x}_i + \Delta \ddot{x}_g$ also are assumed to be observed. The initial value of c_{ij} is assumed to be 50% of the exact value and k_{ij} to be 50% of the exact initial stiffness of the Versatile model. The initial value of the state transfer vector composed of another parameters is assumed to be given by

$$\begin{aligned} \hat{z}_0 &= \{c_{11} \quad c_{12} \quad k_{11} \quad k_{12} \quad c_{21} \quad c_{22} \quad k_{21} \quad k_{22}\}^T \\ &= \{0.07 \quad -0.035 \quad 24.5 \quad -12.25 \quad -0.035 \quad 0.035 \quad -12.25 \quad 12.25\}^T \end{aligned} \tag{16}$$

In addition, the initial value of the covariance matrix of the state transfer vector, P_0, and that of the noise covariance matrix, R, are assumed to be given by

$$P_0 = 0.01 \times diag\{\cdots \quad z_{0i}^2 \quad \cdots\} \tag{17}$$

$$R = rI \tag{18}$$

in which z_{0i} is the ith component of the vector, $\hat{z}_0$, and r=0.00001. The method assigning the initial value of the state transfer vector and its covariance matrix, as well as the covariance matrix of the noise vector is given elsewhere (Sato and Takei 1998).

Results and Discussion

Structural parameters were identified for v=1% in equation (15). An example of the observation time history of acceleration at mass point one is shown in Figure 3. To track the dynamic characteristics of nonlinear system a small value of the forgetting factor, $\lambda_t = 0.825$ was assumed. The effective number of observation time steps is 6 because this number is given by $1/(1-\lambda)$. The time histories of the identified damping and stiffness matrix components are shown in Figures 4 and 5.

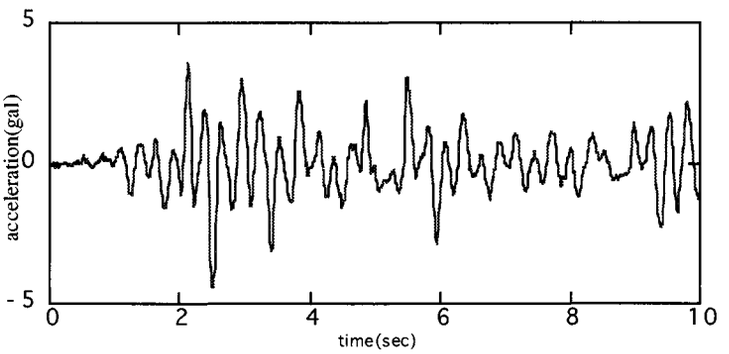

Fig.3 Observed time history of acceleration (mass point 1)

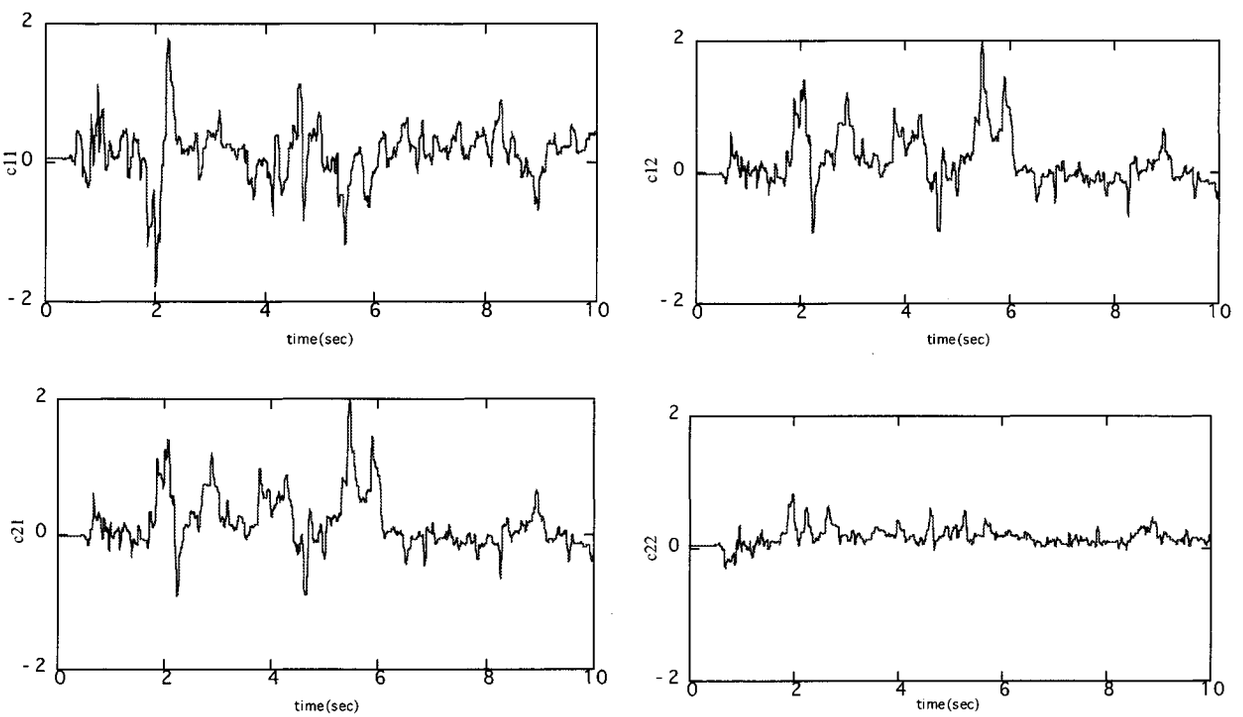

Fig. 4 Time histories of identified damping matrix components (noise level 1%, $\lambda_t = 0.825$)

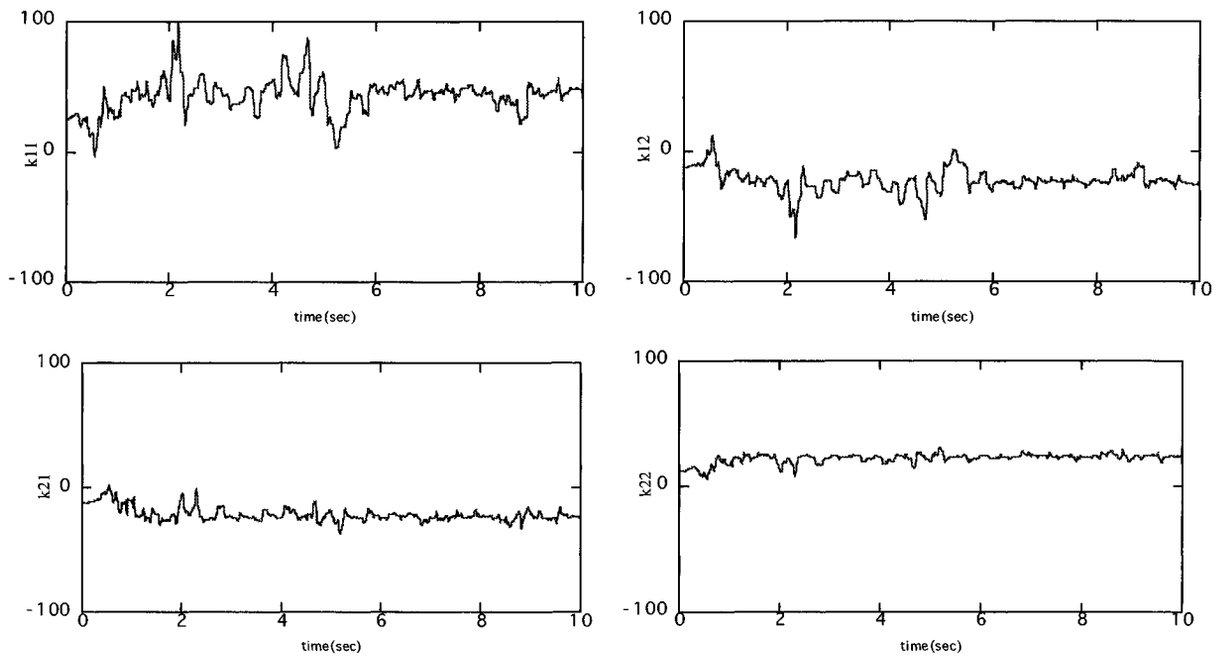

Fig. 5 Time histories of identified stiffness matrix components (noise level 1%, $\lambda_t = 0.825$)

System responses were resimulated using the identified parameters. The following explanation is derived by using the Newmark β method

$$\Delta x_t = \dot{x}_{t-1}\Delta t + \frac{1}{2}\ddot{x}_{t-1}\Delta t^2 + \beta\Delta\ddot{x}_t\Delta t^2 \tag{19}$$

$$\Delta\dot{x}_t = \ddot{x}_{t-1}\Delta t + \frac{1}{2}\Delta\ddot{x}_t\Delta t \tag{20}$$

$$\Delta\ddot{x}_t = -M^{-1}C_t\Delta\dot{x}_t - M^{-1}K_t\Delta x_t - \Delta\ddot{x}_{g,t} \tag{21}$$

in which we adapt β=1/6. The resimulated hysteresis loops of the first layer was compared and agreed well with the observed (Figure 6). The next example is the case of v =3%. The forgetting factor chosen was $\lambda_t = 0.825$. The bold line in Figure 7 is the resimulated displacement at mass point 1 using the identified non-stationery structural parameters, and the broken line the time history used for identification. The resimulated displacement can not trace the original time history after the time of 5sec, when development of residual displacement is seen. To reduce the effect of noise on the identified results, the number of effective time steps must be as large as possible, but to maintain tracking ability a small value is assigned to the forgetting factor. Because of this, identified parameters affected by noise and the resimulated response diverged from the real response. The resimulated hysteresis loop also diverged from the real one as seen by comparing Figures 6 and 8. We introduced the local repetition scheme (Hoshiya and Saito 1991; Takimoto and Hoshiya 1997) to the adaptive Kalman filter. The state transfer vector and its covariance matrix identified using the observed data at time step t are assumed to be those at time step $t-1$, and the identification is repeated using observed data at time step t. Usually it is repeated three times at the maximum within one time step from time $t-1$ to t, and the covariance matrix of the state transfer vector at each repetition step is multiplied by a weight as defined in the following equations

$$\hat{\boldsymbol{z}}_{t-1}^{(j)} = \bar{\boldsymbol{z}}_t^{(j-1)} \tag{22}$$

$$\boldsymbol{P}_{t-1}^{(j)} = w\boldsymbol{P}_t^{(j-1)} \tag{23}$$

in which j is the local repetition number and w the local weight.

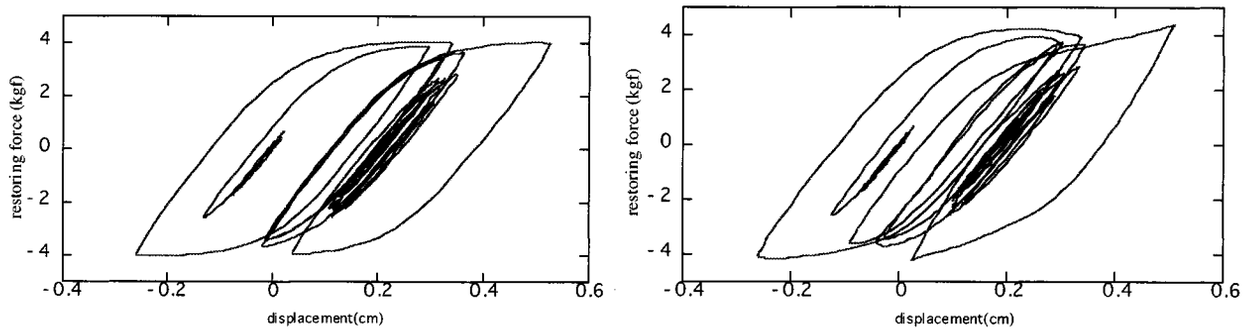

(a)Observed hysteresis loop of the first layer (b)simulated hysteresis loop of the first layer

Fig.6 Hysteresis loop (noise level 1%, $\lambda_1 = 0.825$)

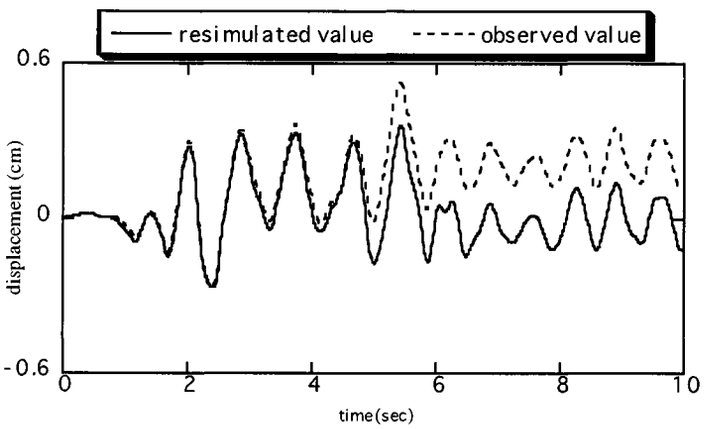

Fig.7 Comparison of simulated and observed displacements

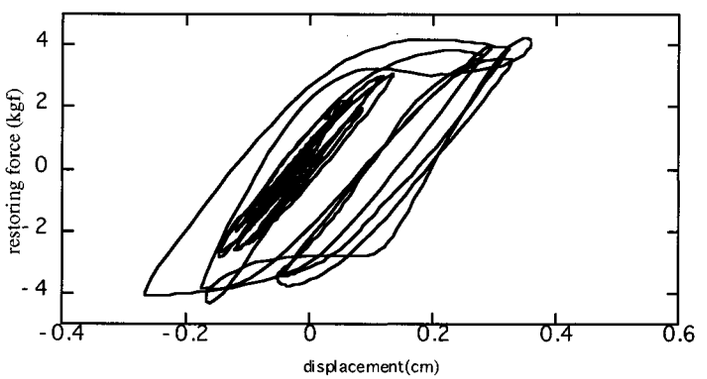

Fig.8 Simulated hysteresis loop (noise level 3%, $\lambda_1 = 0.825$)

The resimulated displacement response of mass point 1 is shown in Figure 9 together with the real response. The number of local repetitions is two and the weight used at each repetition $w = 1.0$. No improvement in tracking ability for the residual displacement can be seen. The value of the weight is changed to $w = 1.05$ and the identification performed. The result is shown in Figure 10. Tracking ability is improved dramatically, and due to this the resimulated hysteresis loop also agrees well with the real one (Figure 11).

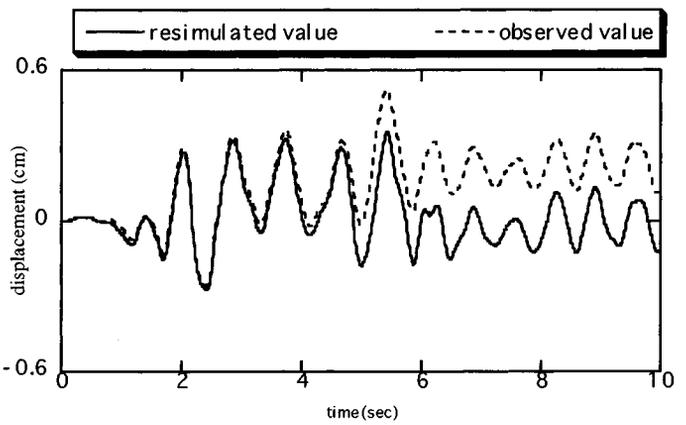

Fig.9 Comparison of simulated and observed displacements(noise level 3%, $\lambda_t = 0.825$, local iteration=2, w=1.0)

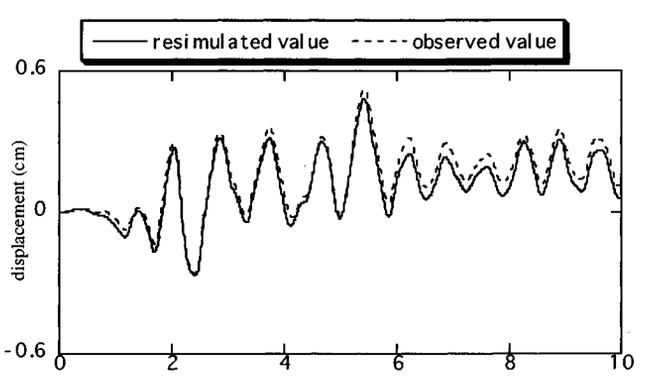

Fig.10 Comparison of simulated and observed displacements (noise level 3%, $\lambda_t = 0.825$, local iteration=2, w=1.05)

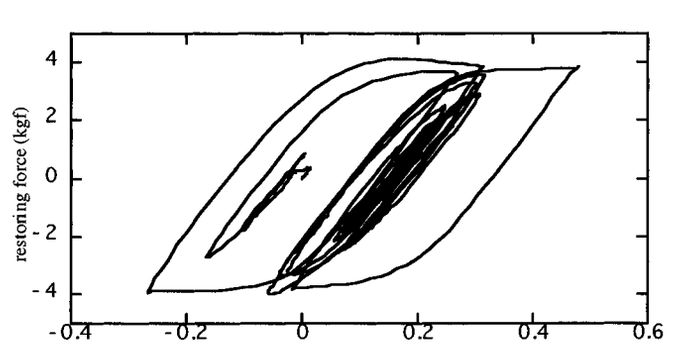

Fig.11 Simulated hysteresis loop of the first layer (noise level 3%, $\lambda_t = 0.825$, local iteration=2, w=1.0)

IDENTIFICATION OF VERSATILE MODEL PARAMETERS

Derivation of the Observation Equation

The nonlinear equation motion of an n degrees of freedom structure at the i mass point is

$$m_i(\ddot{x}_i + \ddot{x}_g) + c_i\dot{u}_i + f_i - (1-\delta_{in})(c_{i+1}\dot{u}_{i+1} + f_{i+1}) = 0 \tag{24}$$

in which m_i is mass at the ith mass point, x_i the relative displacement of the ith mass point to the ground, c_i the damping coefficient of the ith layer, u_i the relative displacement at the ith layer expressed by $u_i = x_i - x_{i-1}$ with the condition $x_0 = 0$, δ_{in} the Kronecker delta, f_i the Versatile restoring force of the ith layer expressed by Eq. (14).

In former analyses (Sato and Takei 1998a; Sato and Kikukawa 1998b) the power parameter n_i in the Versatile model was assumed to be given. To identify not only the nonlinear parameters controlling the shape of the hysteresis loop but this power parameter as well, we define the multi-dimensional Versatile model by

$$\dot{f} = k_i \dot{u}_i - \sum_{j=1}^{m} \left\{ \alpha_{ij} |\dot{u}_i| |f_i|^{j-1} f_i + \beta_{ij} \dot{u}_i |f_i|^j \right\} \tag{25}$$

in which m is the maximum natural number to sum up each Versatile restoring force with power parameter j, α_{ij} and β_{ij} are the shape parameters of the Versatile model with the jth order power parameter for the ith layer. When this multi-Versatile model is used for identification, m times of α_i and β_i must be identified. The restoring force at the ith layer is obtained from Eq. (24) when the absolute acceleration, $\ddot{x}_i + \ddot{x}_g$, and relative velocity to the ground, $\dot{x}_i$, at each mass point are assumed to be observed;

$$f_i = -c_i \dot{u}_i - \sum_{j=1}^{n} m_j \left(\ddot{x}_j + \ddot{x}_g \right) \tag{26}$$

in which the mass of each node, m_j, is assume to be given.

The observation equation for this case is derived by integrating Eq. (25) with respect to time;

$$\begin{aligned} \Delta f_i(t) = {} & \frac{1}{2} k_i \{ \dot{u}_i(t) + \dot{u}_i(t-1) \} \Delta t \\ & - \sum_{j=1}^{m} \left[\frac{1}{2} \alpha_{ij} \left\{ |\dot{u}_i(t)| |f_i(t)|^{j-1} f_i(t) + |\dot{u}_i(t-1)| |f_i(t-1)|^{j-1} f_i(t-1) \right\} \Delta t \right. \\ & \left. + \frac{1}{2} \beta_{ij} \left\{ \dot{u}_i(t) |f_i(t)|^j + \dot{u}_i(t-1) |f_i(t-1)|^j \right\} \Delta t \right] \end{aligned} \tag{27}$$

in which $\Delta f_i(t)$ is the increment of the restoring force at time t.

If Eq. (27) is used as the observation equation, all the shape parameters of the multi-dimensional Versatile model appear as linear coefficients of the terms in the summation formula on the right hand side of Eq. (27). It is necessary to use this equation to identify the incremental formula of the restoring force. The equation of motion defined by Eq. (24) is rewritten

$$m_i \left(\Delta \ddot{x}_i + \Delta \ddot{x}_g \right) + c_i \Delta \dot{u}_i - (1 - \delta_{in}) c_{i+1} \Delta \dot{u}_{i+1} = -\Delta f_i + (1 - \delta_{in}) \Delta f_{i+1} \tag{28}$$

Substituting Eq. (27) in Eq. (28) gives the observation equation;

$$\begin{Bmatrix} m_1 \left(\Delta \ddot{x}_1 + \Delta \ddot{x}_g \right) - c_1 \Delta \dot{u}_1 + c_2 \Delta \dot{u}_2 \\ m_2 \left(\Delta \ddot{x}_2 + \Delta \ddot{x}_g \right) - c_2 \Delta \dot{u}_2 + c_3 \Delta \dot{u}_3 \\ \\ m_n \left(\Delta \ddot{x}_n + \Delta \ddot{x}_g \right) - c_n \Delta \dot{u}_n \end{Bmatrix} = \begin{bmatrix} \boldsymbol{h}_1 & -\boldsymbol{h}_2 & \boldsymbol{0} & \cdots & \cdots & \cdots & \boldsymbol{0} \\ \boldsymbol{0} & \boldsymbol{h}_2 & -\boldsymbol{h}_3 & \boldsymbol{0} & & & \vdots \\ \vdots & & \ddots & \ddots & & & \vdots \\ \vdots & & \boldsymbol{0} & \boldsymbol{h}_i & -\boldsymbol{h}_{i+1} & \boldsymbol{0} & \vdots \\ \vdots & & & & \ddots & \ddots & \boldsymbol{0} \\ \vdots & & & & \boldsymbol{0} & \boldsymbol{h}_{n-1} & -\boldsymbol{h}_n \\ \boldsymbol{0} & \cdots & \cdots & \cdots & \cdots & \boldsymbol{0} & \boldsymbol{h}_n \end{bmatrix} \begin{Bmatrix} \boldsymbol{d}_1 \\ \vdots \\ \boldsymbol{d}_i \\ \vdots \\ \boldsymbol{d}_n \end{Bmatrix} \tag{29}$$

$$\boldsymbol{h}_i = \begin{Bmatrix} K_i & A_{i1} & B_{i1} & \cdots & A_{ij} & B_{ij} & \cdots & A_{im} & B_{im} \end{Bmatrix} \tag{30}$$

$$d_i = \{k_i \quad \alpha_{i1} \quad \beta_{i1} \quad \cdots \quad \alpha_{ij} \quad \beta_{ij} \quad \cdots \quad \alpha_{im} \quad \beta_{im}\}^T \tag{31}$$

$$K_i = \frac{1}{2}\{\dot{u}_i(t) + \dot{u}_i(t-1)\}\Delta t \tag{32}$$

$$A_{ij} = \frac{1}{2}\left\{|\dot{u}_i(t)||f_i(t)|^{j-1} f_i(t) + |\dot{u}_i(t-1)||f_i(t-1)|^{j-1} f_i(t-1)\right\}\Delta t \tag{33}$$

$$B_{ij} = \frac{1}{2}\left\{\dot{u}_i(t)|f_i(t)|^j + \dot{u}_i(t-1)|f_i(t-1)|^j\right\}\Delta t \tag{34}$$

The adaptive Kalman filter is used to identify the parameters of the Versatile model; k_i ,α_{ij} and β_{ij} . Because the suffix *j* corresponds to the *j*th power parameter there are *m* times of α and β . Through the process of identification, the values of α_{ij} and β_{ij} , however, converge to the values of α and β with the exact power parameter.

Analytical Model

The structural model used here is the same as that shown in Figure 2, and the observation noise level is 1%. The absolute acceleration response, $\ddot{x}_i + \ddot{x}_g$, relative velocity to the ground, $\dot{x}_i$, and the increments $\Delta\ddot{x}_i + \Delta\ddot{x}_g$,$\Delta\dot{x}_i$ are assumed to be observed. The mass and the damping coefficient are assumed to be given, a multi-dimensional Versatile model with $m = 5$ is considered. The initial condition of k_i is 50% of the exact value and that for α_{ij} , β_{ij} is assigned 0.0. The initial state transfer vector is given by

$$d_{i0} = \{12.25 \quad 0 \quad \cdots \quad 0\}^T \tag{35}$$

The initial covariance matrix of the state transfer vector is defined as Eq. (17), but the initial value ofα_{ij} andβ_{ij} is 0.0 therefore the value of z_{0i} in terms of α_{ij} andβ_{ij} is assumed to be 1.0. The covariance matrix of the observation noise is assumed to be defined by Eq. (18).

Analytical Results and Discussion

Time histories of the Versatile model parameters α_{ij} and k_i for the first layer of a two degree of freedom system are shown in Figure 12. The value of α_{ij} is large for *j*=1, 2 and 3, whereas for the other *j* values it converges almost to zero. The value of k_i converges to its exact value at about 2.0 sec. The hysteresis loop of the first layer resimulated using identified parameters α_{ij} , β_{ij} and k_i , obtained after the first step identification, is shown in Figure 13. Because of the fluctuating nature of the identified parameters their average values between 8.0 and 10 sec are used to resimulate the hysteresis loop. Comparing this result with the exact hysteresis shown in Figure 6, we conclude that the multi-dimensional Versatile model has high flexibility for simulating an arbitrary hysteresis loop. No identification of the power parameter is possible after the first step identification because several α_{ij} andβ_{ij} have non-zero values (Figure 12). A global identification scheme therefore is used to reduce the number of parameters. After the first step in the global identification process, parameters with values less than 30% of the maximum absolute value of the concerned parameter are eliminated from the multi-dimensional Versatile model. The second global identification then is performed. The maximum absolute value of α_{1j} after the first identification process is $|\alpha_{11}| = 0.4145$ and 30% of this value, 0.1244 is the threshold value for elimination. The parameters α_{14} and α_{15} are candidates for elimination in the second step of global identification, but the only value of β_{1j} concerned, β_{15}, is a candidate for elimination. Therefore, the nonlinear parameters related only to $n_i = 5$, α_{15}, and β_{15} are eliminated in the second global identification process. For parameters α_{2j} and β_{2j} , the parameters related to $n_i = 4$ and 5 are eliminated in the second step of global identification. The initial condition of the parameters for the *l*th step of global identification is assigned as the identified values in the *l-1*th step. The covariance matrix of the parameters is redefined by Eq. (17) in each global identification step. Table 1 shows the parameters remaining in each global

identification step up to step four. After this step the parameters of the Versatile model with $n_l = 2$ remain and the value of identified parameters converge to the exact values.

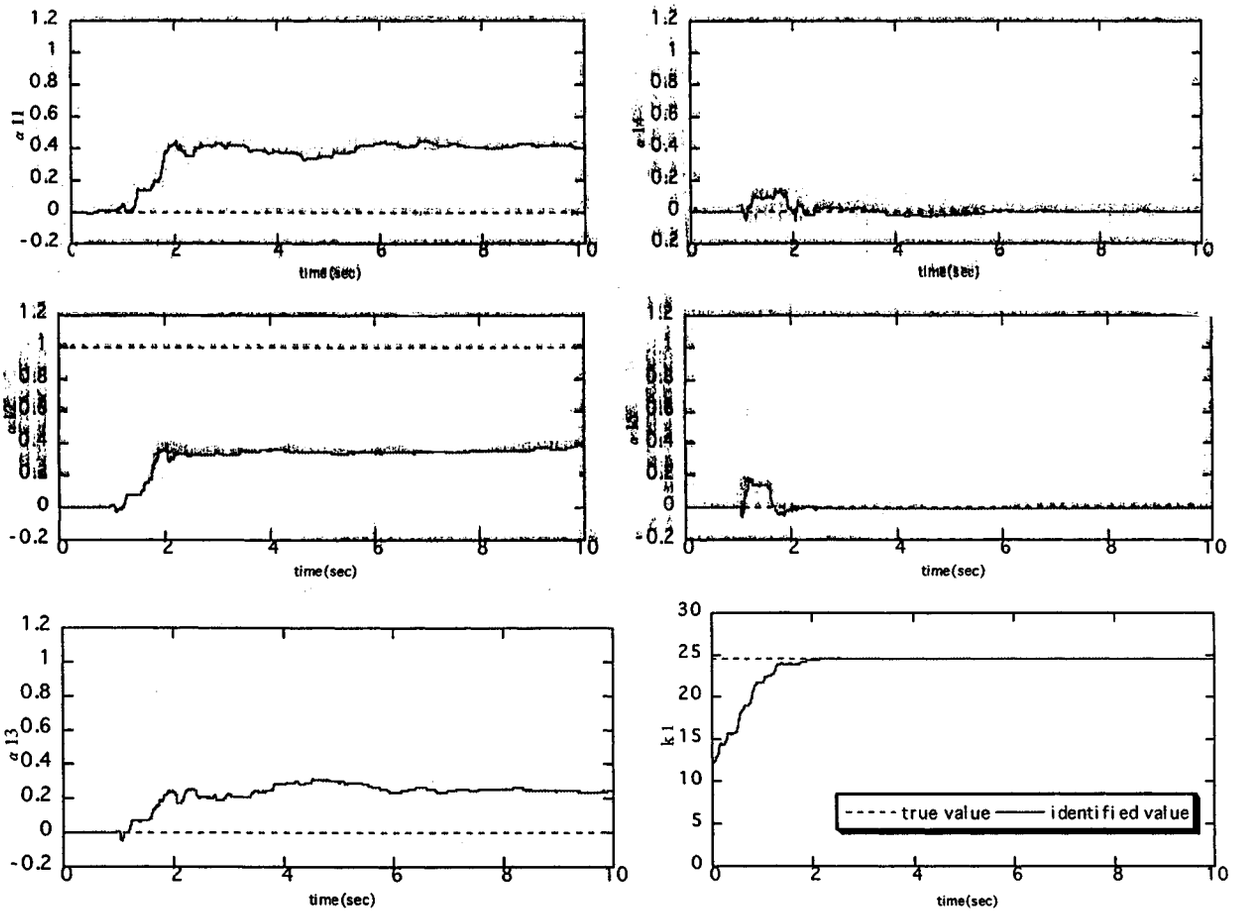

Fig.12 Time histories of identified Versatile model parameters α_{1j}, k_1 (first layer)

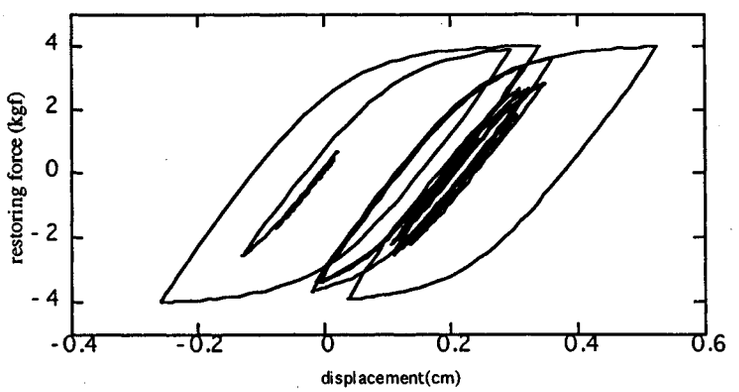

Fig.13 Simulated hysteresis loop of the layer (using identified parameters after step identification)

Table 1. Identifid parameters in each global identification step

parameter	number of iterations		1	2	3	4	Exact value
α_1	n_i	1	0.4145	0.3760	-0.0905		
		2	0.3636	0.3743	1.315	1.0057	1.0000
		3	0.2465	0.3241	-0.0308		
		4	0.0011	-0.0506			
		5	-0.0084				
	elimination level		0.1243	0.1128	0.3395		
α_2	n_i	1	0.3318	0.3283	0.1548		
		2	0.4962	0.0384	0.9474	1.0200	1.0000
		3	0.3445	0.0573			
		4	0.1057				
		5	0.0114				
	elimination level		0.1489	0.2191	0.2842		
β_1	n_i	1	0.1350	0.2401	0.0675		
		2	0.2296	0.3185	0.4188	0.5046	0.5000
		3	0.2306	0.0127	0.0213		
		4	-0.0951				
		5	0.0141				
	elimination level		0.0692	0.0956	0.1256		
β_2	n_i	1	0.1416	0.1201	-0.0690		
		2	0.1872	0.2894	0.4928	0.4621	0.5000
		3	0.1132	0.0528			
		4	-0.00226				
		5	-0.00261				
	elimination level		0.0562	0.0868	0.1478		
k_1			24.5472	24.9514	24.5669	24.5638	24.5000
k_2			24.4046	24.4185	24.4008	24.4221	24.5000

The global identification process for an eight degree of freedom system is shown in Tables 2 and 3. To simulate the structural response the same values of $n_i = 2$, $\alpha = 1.0$ and $\beta = 0.5$ were assigned for all the stories. The remaining power parameter, *n*, after each global identification step is shown in Table 2. Values for parameters α and β and the remaining n values after the fifth global identification step are given in Table 3. The Versatile model parameters for layers 2 to 6 converged to the exact values, whereas those for layers 1, 7, and 8 have values for other n values as well as $n_i = 2$. The observed force-displacement relationships for layers 7 and 8 show almost linear behavior. Even when the non-linear parameters exist the response force-displacement relationship shows linear behavior in the small range of external excitation force. This is why good convergence could not be obtained for layers 7 and 8.

Table 2. Remaining power parameters in each global identification step

layer	Number of iterations				
	1	2	3	4	5
1st	1,2,3	1,2	1,2	1,2	1,2
2nd	1,2,3	2	2	2	2
3rd	1,2,3,	2	2	2	2
4th	2,3,4	2	2	2	2
5th	1,2,3,4	1,2	2	2	2
6th	1,2,3,4	1,2	1,2	2	2
7th	1,2,3,4	1,2	1,2	1,2	1,2
8th	1,2,3,4,5	1,2,3,4,5	1,2,3,4,5	1,2,3,4,5	1,2,3,4,5

Table 3. Identified parameters after the 5th global identification step

layer	n	α	β	layer	n	α	β
1st	1	0.0280	0.2018	7th	0	-0.1668	0.1342
	2	1.0185	0.4377		2	1.0916	0.3990
2nd	2	1.0324	0.4863	8th	1	0.0013	0.1103
3rd	2	1.0177	0.5047		2	0.0357	0.3846
4th	2	1.0446	0.4535		3	0.8455	0.0143
5th	2	0.9868	0.5190		4	0.1374	-0.3856
6th	2	0.9939	0.4893		5	-0.1627	0.1764

Introduction of Robustness

The robust characteristic of the adaptive Kalman filter to an unusual signal is assigned by changing the explanation of the error covariance matrix given by Eq. (5) and the Kalman gain defined by Eq. (6) as follows:

$$\boldsymbol{P}_t = \left(\lambda_t \boldsymbol{M}_t^{-1} + \boldsymbol{H}_t^T \boldsymbol{W}_t \boldsymbol{R}^{-1} \boldsymbol{H}_t\right)^{-1} \tag{36}$$

$$\boldsymbol{G}_t = \boldsymbol{P}_t \boldsymbol{H}_t^T \boldsymbol{W}_t \boldsymbol{R}_t^{-1} \tag{37}$$

in which $\boldsymbol{W}_t$ is a diagonal matrix with diagonal components that is used to evaluate the reliability of the observed values. Each component is determined using the residual between the observed and estimated values, $\boldsymbol{v}_t = \boldsymbol{y}_t - \boldsymbol{H}_t \hat{\boldsymbol{x}}_t$, as given by

$$w_i = \begin{cases} \left\{1 - \left(\dfrac{v_i}{as}\right)^2\right\}^2 & |v_i| < as \\ 0.0 & |v_i| \geq as \end{cases} \tag{38}$$

in which w_i and v_i are the ith component of matrices of $\boldsymbol{W}_t$ and $\boldsymbol{v}_t$, and s is a scale constant expressing the standard value of the residual. The a is a constant used to evaluate the observation data. For the case of $\lambda_t = 1.0$ and $w_i = 1.0$ the proposed adaptive Kalman filter becomes the usual Kalman filter.

The response of the nonlinear two degree of freedom system is simulated as described in the preceding section. After a standard noise signal of γ=1% is added, a train of unusual pulses is mixed in the simulated response of the structure. This train of unusual pulses is composed of ten pulses selected randomly from a time series of white noise with five times the standard deviation of the simulated structural response. An example of contaminated time histories of the structural response is shown in Figure 14 (first floor acceleration response).

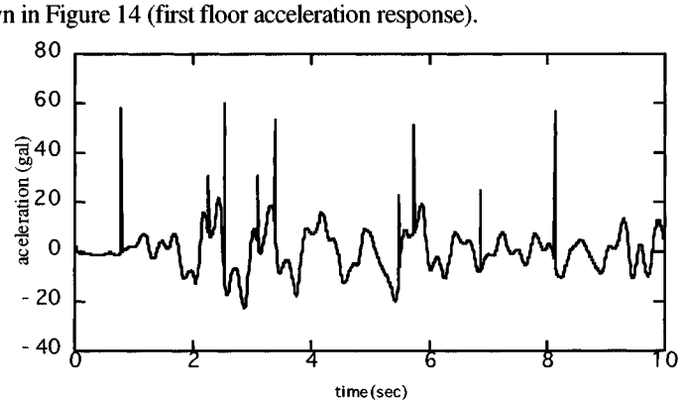

Fig. 14 Contaminated time histories of acceleration (mass point 1)

The value $\lambda_r = 1.0$ was used for the identification because the nonlinear structural parameters to be identified do not have time varying characteristics. The initial condition of the parameters and the error covariance matrix of the parameters are defined as described in the preceding section. The order of the multi-Versatile model is set at $m = 5$. The scale constant s is selected as the central value of the past ten time steps of the corresponding value's residual, $a = 10$ is assigned.

The identified time history of parameter α_{11} (Figure 15) was obtained using the normal Kalman filter. A comparison of this with the result from the robust Kalman filter (Figure 16) shows that the abrupt fluctuation of the identified parameter in Figure 15 is eliminated in the case of the robust Kalman filter algorithm. The identifying process using the global repetition of identification is given in Table 4. The parameters converge to exact values, including the power parameter, after four repetitions of global identification.

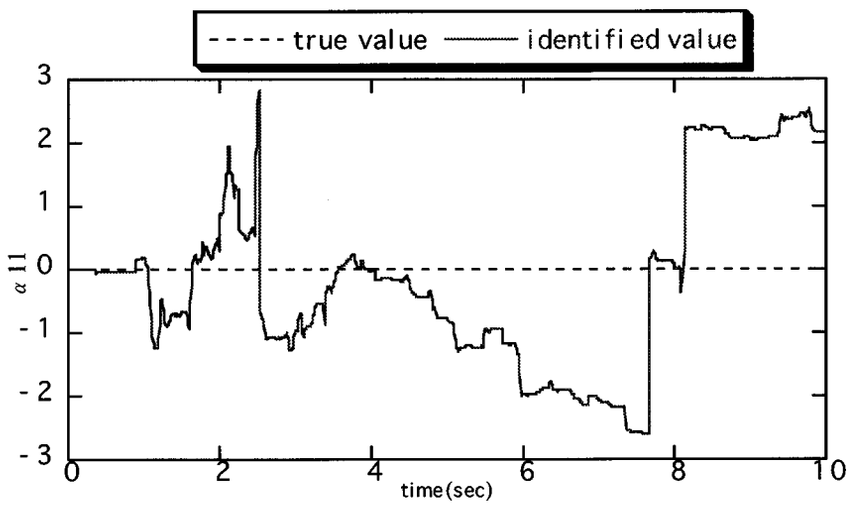

Fig. 15 Identified time history of parameter a_{11} (using the Kalman filter)

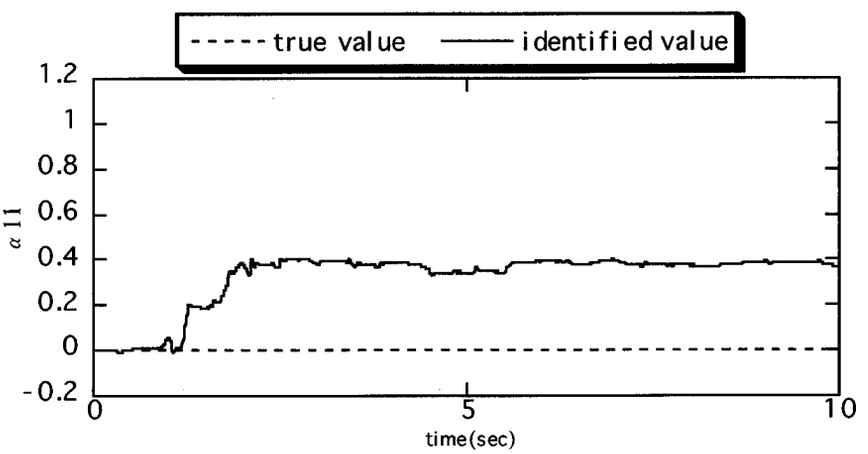

Fig.16 Identified time history of parameter a_{11} (using the robust Kalman filter)

Table 4. Identified parameters in each global identification step

parameter	number of iterations		1	2	3	4	Exact value
α_1	n_i	1	0.3797	-0.0916			
		2	0.3858	1.1464	1.0023	1.0024	1.0000
		3	0.2655	-0.0361			
		4	-0.0200				
		5	-0.0041				
	elimination level		0.1157	0.3438			
α_2	n_i	1	0.3361	0.1672	0.1072		
		2	0.4839	0.9581	0.9679	1.0177	1.0000
		3	0.3268	-0.0089			
		4	-0.0934				
		5	0.0102				
	elimination level		0.1452	0.2874	0.2903		
β_1	n_i	1	0.2428	0.079			
		2	0.2524	0.229	0.5058	0.5060	0.5000
		3	0.0310	0.0208			
		4	0.0180				
		5	-0.0031				
	elimination level		0.0757	0.1269			
β_2	n_i	1	0.1170	0.1187	-0.0365		
		2	0.1796	0.3182	0.4833	0.4670	0.5000
		3	0.1235	0.0462			
		4	0.0122				
		5	-0.0082				
	elimination level		0.0539	0.0955	0.1450		
k_1			24.5430	24.5647	24.5536	24.5500	24.5000
k_2			24.3999	24.4504	24.4212	24.4273	24.5000

CONCLUSIONS

After a brief introduction of the adaptive Kalman filter we introduced robustness into this filter. The results obtained are as follows:

(1) A non-parametric linear identification algorithm was developed based on the incremental linearization of the motion equation. Nonlinear responses of the structure system were well simulated by using the identified non-stationary time history of incremental stiffness and damping matrices.

(2) A linear algorithm to identify the parameters controlling Versatile model that includes the power term was developed by defining a new multi-dimensional Versatile model. A numerical example showed the efficiency of the developed algorithm.

(3) A robust Kalman filter with adaptive function was developed to eliminate the effect of abnormal signals that are contained in observation time histories on identified results. An application of the developed algorithm to identify the Versatile model parameters including the power parameter worked well.

APPENDIX I. DEDUCTION OF THE ADAPTIVE KALMAN FILTER

To briefly introduce the Kalman, the expression given by Kato (Kato 1987) is used because it is very simple and easy to understand. The discrete system transfer and observation equations are expressed by

$$z_t = \Phi_{t-1} z_{t-1} + \Gamma_{t-1} w_{t-1} \tag{39}$$

$$y_t = H_t z_t + v_t \tag{40}$$

in which z and y are the state variable and observation vector in $z \in R^n, y \in R^m$; w and v the system and observation noise vectors in $w \in R^r, v \in R^m$; Φ is the system transfer matrix; Γ the matrix evaluating system noise ; and H the observation matrix. Noise is assumed to be Gaussian white noise with the characteristics

$$E[w_t] = 0, \quad E[v_t] = 0 \tag{41}$$

$$E\left[\begin{Bmatrix} w_t \\ v_t \end{Bmatrix} \{w_\tau \quad v_\tau\}\right] = \begin{bmatrix} Q_t & \mathbf{0} \\ \mathbf{0} & R_t \end{bmatrix} \delta_{t\tau} \tag{42}$$

The initial values of the state variable vector and its covariance matrix are defined by $\hat{z}_0$ and P_0. If the maximum likelihood estimator of the state variable vector and its covariance matrix obtained from the observation data up to time $t-1$ are given by

$$E[z_{t-1}] = \hat{z}_{t-1} \tag{43}$$

$$E\left[(z_{t-1} - \hat{z}_{t-1})(z_{t-1} - \hat{z}_{t-1})^T\right] = P_{t-1} \tag{44}$$

then the maximum likelihood estimation of the state variable vector and its covariance matrix at time t are obtained by the following Kalman filter scheme: The pre-estimators of the state variable vector and its covariance matrix (i.e. pre-information) calculated from Eq. (39) before the observation data are

$$\bar{\mathbf{z}}_t = \Phi_{t-1}\hat{\mathbf{z}}_{t-1} \tag{45}$$

$$M_t = f?_{t-1}P_{t-1}f?^T_{t-1} + f_{i-1}R_{t-1}f_{i-1}^T \tag{46}$$

Applying the Bayes theorem, the probability distribution function of the state variable vector z_t is expressed by equation (47) under the constrain of the observation vector y_t

$$p(z_t \mid y_t) = \frac{p(y_t \mid z_t)p(z_t)}{p(y_t)} = \frac{1}{p(y_t)\sqrt{(2\pi)^{m+n}|R_t||M_t|}} exp(-J_t) \tag{47}$$

in which

$$J_t = \frac{1}{2}(y_t - H_t z_t)^T R_t^{-1}(y_t - H_t z_t) + \frac{1}{2}(z_t - \bar{z}_t)^T M_t^{-1}(z_t - \bar{z}_t) \tag{48}$$

The value of z_t to maximize Eq. (47) is called the maximum likelihood estimator, or the post-estimator of state variable vector. This value is obtained by minimizing the quadratic evaluation function given by Eq. (48) with respect to z_t

$$\hat{z}_t = \bar{z}_t + P_t H_t^T R_t^{-1}(y_t - H_t \bar{z}_t) \tag{49}$$

$$P_t = \left(M_t^{-1} + H_t^T R_t^{-1} H_t\right)^{-1} \tag{50}$$

In the Kalman filter the rate of modification of the pre-estimator of the state variable vector, $\bar{z}_t$, depends on the relative magnitude of the difference between the covariance matrix of the state variable and that of the observation noise as shown in Eq. (49) and (50). The adaptability of the state variable vector to non-stationary change therefore is evaluated by putting the relative weight between them. This is done by replacing R_t and M_t with $a_t R_t$ and $b_t M_t$, in which a_t and b_t are arbitrary constants.

$$R_t \to a_t R_t, \quad M_t \to b_t M_t \tag{51}$$

Defining a new scalar parameter λ_t

$$\lambda_t = \frac{a_t}{b_t} \tag{52}$$

and substituting Eq. (51) into Eqs.(47) and (48) gives

$$p(z_t \mid y_t) = \frac{\sqrt{\lambda_t^n}}{p(y_t)\sqrt{(2\pi a_t)^{m+n}|\boldsymbol{R}_t||\boldsymbol{M}_t|}} exp\left(-\frac{J_t}{a_t}\right) \tag{53}$$

$$J_t' = \frac{1}{2}(y_t - \boldsymbol{H}_t z_t)^T \boldsymbol{R}_t^{-1}(y_t - \boldsymbol{H}_t z_t) + \frac{1}{2}\lambda_t (z_t - \bar{z}_t)^T \boldsymbol{M}_t^{-1}(z_t - \bar{z}_t) \tag{54}$$

Minimizing Eq. (54) with respect to z_t gives the following equations with which to calculate the maximum likelihood estimator of the state variable vector and its covariance matrix;

$$\hat{z}_t = \bar{z}_t + \boldsymbol{P}_t \boldsymbol{H}_t^T \boldsymbol{R}_t^{-1}(y_t - \boldsymbol{H}_t \bar{z}_t) \tag{55}$$

$$\boldsymbol{P}_t = \left(\lambda_t \boldsymbol{M}_t^{-1} + \boldsymbol{H}_t^T \boldsymbol{R}_t^{-1} \boldsymbol{H}_t\right)^1 \tag{56}$$

The scalar parameter, λ_t, is called the forgetting factor because this value controls the fading rate of the pre-information effect on the post-estimator of the state variable vector obtained by taking into account the observation data at the present time.

APPENDIX II. INTRODUCTION OF ROBUSTNESS INTO THE ADAPTIVE KALMAN FILTER

The adaptive Kalman filter was derived by minimizing the following evaluation function with respect to z_t

$$J_t' = \frac{1}{2}(y_t - \boldsymbol{H}_t z_t)^T \boldsymbol{R}_t^{-1}(y_t - \boldsymbol{H}_t z_t) + \frac{1}{2}\lambda_t (z_t - \bar{z}_t)^T \boldsymbol{M}_t^{-1}(z_t - \bar{z}_t) \tag{57}$$

in which z_t is the state variable vector to be identified, y_t the observation vector, $\bar{z}_t$ the pre-estimation of the state vector, $\boldsymbol{H}_t$ the observation matrix, $\boldsymbol{R}_t$ the covariance matrix of the observation noise, $\boldsymbol{M}_t$ the covariance matrix of the estimation error of $\bar{z}_t$, λ_t the forgetting factor.

Robustness is introduced by multiplying a weighting matrix $\boldsymbol{W}_t$ and the quadratic term of observation error residual as follows;

$$J_t'' = \frac{1}{2}(y_t - \boldsymbol{H}_t z_t)^T \boldsymbol{W}_t \boldsymbol{R}_t^{-1}(y_t - \boldsymbol{H}_t z_t) + \frac{1}{2}\lambda_t (z_t - \bar{z}_t)^T \boldsymbol{M}_t^{-1}(z_t - \bar{z}_t) \tag{58}$$

in which the weighting matrix $\boldsymbol{W}_t$ is a diagonal matrix in which each component is proportional to the relative importance of observation values. In this paper $\boldsymbol{W}_t$ is defined by Eq. (38). Minimizing the variation of Eq. (58) with respect to z_t the maximum likelihood estimate $\hat{z}_t$ is obtained form Eq. (36) and the Kalman gain $\boldsymbol{G}_t$ is given by Eq. (37).

REFERENCES

Benedettini, F., Capeccchi, D., and Vestroni, F. (1995). "Identification of hysteretic oscillators under earthquake loading by nonparametric models." *J. Engrg. Mech. Div, ASCE*, 121(5), 606-612.

Chassiakos, A. G., Masri, S. F., Smyth, A. W., and Caughey, T. K. (1998). "On-line identification of hysteretic systems." *J. Appl. Mech.*, 65(March), 194-203.

Hoshiya, M. and Saito, E. (1991). *Data Analyses and Applications*, Kajima Press (in Japanese)

Kato, K. (1987). *Introduction to Optimal Control*, Tokyo University Press (in Japanese)

Kalman, R. E. (1960). "A new approach to linear filtering and prediction problem." *J. Basic Engrg. Trans.*, 82D(1), 34-45.

Ljung, L. (1987). *System identification*, Prentice-Hall, New Jersey.

Loh, C. H. and Chung, S. (1993). "A three-stage identification approach for hysteretic systems." *Earthquake Engrg. And Struct. Dynamics*, 22, 129-150.

Masri, S. F., Miller, R. K., Traina, M. J. and Caughey, T. K. (1991). "Development of bearing friction models from experimental measurements." *J. Sound and Vibration*, 148(3), 455-475.

Peng, C. Y. and Iwan, W. D. (1992). An identification methodology for a class of hysteretic structures." *Earthquake Engrg. And Struct. Dynamics*, 21, 695-712.

Safac, A. (1989), "Adaptive modeling, identification and control of dynamic structural systems, I. Theory." *J. Engrg. Mech. Div., ASCE*, 115(11), 2386-2405.

Sato, T. and Takei, K. (1998a). "Development of a Kalman Filter with Fading Memory", *Structural Safety and Reliability*, 387-394

Sato, T. and Kikukawa, M. (1998b). "A Linear Algorithm to Identify the Nonlinear Structural System Equation", *Proc. Part of the SPIE Conference on Mathematics and Control in Smart Structures*, 3323, 154-166

Sato, T. and Qi, K. (1998c). "Addaptive H_∞ filter: Its applicatiln to structural identification." H *J. Engrg. Mech. Div., ASCE*, 124(11), 1233-1240.

Smyth, A. W., Masri, S. F., Chassiakos, A. G. and Caughey T. K. (1999). "On-line parameter identification of MDOF nonlinear hysteretic systems." *J. Engrg. Mech. Div., ASCE*, 125(2), 133-142

Stry, G. and Moak, D. J. (1992). "An experimental study of nonlinear dynamic system identification." *Nonlinera Dynamics*, (3), 1-11.

Takaba, K. and Katayama, T. (1996). "Discrete-time H_∞ algebraic Riccati equation and parametrization of all H_∞ filters." *Int. J. Control*, 64(6), 1129-1149.

Takimoto, M. and Hoshiya, M. (1997). "Identification of Nonlinear Structures by the Kalman Filter" , *J. Struct. Mech. and Earthquake Engrg. Japan Society of Civil Engineers* , No556/ I -38 , 179-187

Wen, Y. K. (1976). "Method for random vibration of hysteretic systems.", *J. Engrg. Mech. Div., ASCE*, 102(2), 249-263.

Session 4

Application of SCADA (Supervisory Control and Data Acquisition) Systems for Lifeline Networks

Chairs: T.C. Chang and F. De Flaviis

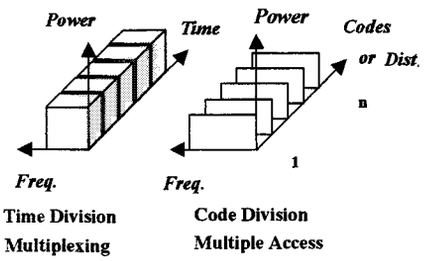

Fig.4. Principles of time division multiplexing (TDM) and code division multiple access (CDMA) techniques.

Table 1. Specifications of the radio systems used in the experimental system.

Link	Freq. (MHz)	Bandwidth	Output Power	Modulation	Mod. Rate
Upper Layer Polling System - TDM					
Up	2289.9	< 200kHz	1W	π/4-shift QPSK	288kbps
Down	2109.9	< 200kHz	1W	π/4-shift QPSK	288kbps
Lower Layer Polling System - LPRS					
Up/Down	429.250-429.737	< 8.5kHz	< 10mW	MSK	1200bps (4800bps)
Lower Layer Polling System - TD-CDMA					
Reverse (Up)	2482	< 1.5MHz	< 10mW	DQPSK/DS*	9.6ksps
Forward (Down)	2402	< 1.5MHz	< 10mW	DBPSK/DS*	19.2ksps

*** DS: direct spreading**

IV. DATA FLOW IN THE EXPERIMENTAL SYSTEM

a. 430MHz LPRS

Data flow between a LPG (liquefied petroleum gas) meter to a DB in relay-DB station via a 430MHz LPRS unit is depicted in Fig.5. In this system design, the 430MHz LPRS, which is a standard technology existing on the market, is applied to monitoring and control of the LPG meter.

Digital data generated in the LPG meter equipped with a micro-computer comprises 8 words (7 bits/word) for monitoring and control signals, 8 words for meter reading signal, and 4 words for identification codes. The 20 word (7 bits/word) data is translated into 20 byte (B) data in an interface unit placed between the radio system and the RDB.

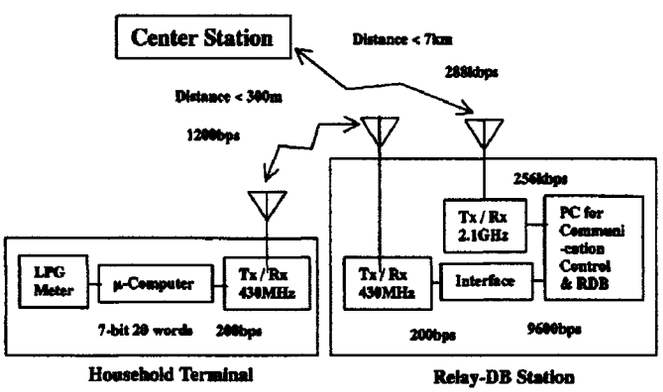

Fig.5. A block diagram of household terminal and relay-DB station connected by 430MHz LPRS.

A word-and-bit assignment for the monitoring/control signals, including such signals as excessive gas flow rate (b1 of w1), emergency gas valve shut-off (b3 of w2) and ground motion above threshold (b3 of w5), is shown in Table 3 [JGIA 1997, JWSIA 1998].

Table 3. Word/bit assignment of the monitoring/control signals in the LPG meter equipped with micro-computer.

		Bit						
		Start	b1	b2	b3	b4	b5	Stop
Word	* 1	0	Excess Flow Rate Valve Shut Off	Cont. Use Time Limit Valve Shut Off	Slow Leak Warning	Battery Voltage	0	1
	* 2	0	External Sensor Valve Shut Off	Center-Command Valve Shut Off	Emergency Valve Shut Off	Valve Shut Off Malfunction	0	1
	* 3	0	Container Replacement	Continuous Use Time Pre-set	Valve Shut Off Test	Valve Open	0	1
	* 4	0	LPG Level Warning 1	LPG Level Warning 2	LPG Level Warning 3	Electronics Reset Request	0	1
	* 5	0	Gas Leak Alarm Activated	Pressure Sensor Activated	Seismic Motion Detector Activated	AC Line Unplugged / Signal Short Circuited	0	1
	* 6	0	Meter Capacity Category 1	Meter Capacity Category 2	Meter Capacity Category 3	Meter Capacity Category 4	0	1
	* 7	0	Not Used	Abnormal Pressure Behavior	External Equipment 1	External Equipment 2	0	1
	8	Character 0						

b. 2.4GHz TD-CDMA Radio System

Data flow between meters to a DB in the relay-DB station via a 2.4GHz TD-CDMA radio unit is depicted in Fig.6. The transmitter (Tx)/receiver (Rv) unit of TD-CDMA is referred to as the base station in the present work. The system is designed to monitor and control up to 3 meters, i.e., LPG, NG (natural gas supplied through pipelines) and water meters, and also to accept additional input signals. The 2.4GHz TD-CDMA radio system was developed for use in the experimental lifeline system and installed in April 1999, aiming to improve the data acquisition time. The CDMA radio unit in the base station of Fig.6 can give access to 8 HTs simultaneously using

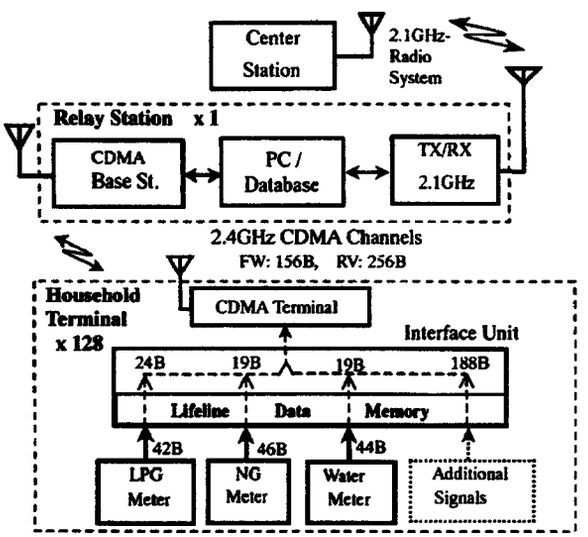

Fig.6. A block diagram of household terminal and relay-DB station connected by 2.4GHz TD-CDMA radio system.

orthogonal spreading codes. Then, 32 groups of HTs, each consisting of those 8 HTs, are interrogated by the base station in turn to send out lifeline data in response. This allows the base station to give access to 256 HTs in a cell. Hence, the system is called TD-CDMA system. The time required to collect 256B data from 256 HTs is 10.24 seconds [Fujiwara 2000, 2000]. This system can handle a total of 256B data per HT as compared to 20B/HT in the 430MHz LPRS.

Perhaps it should be pointed out here that the use of the spreading codes provides a powerful tool with the data acquisition system to prevent from unauthorized wiretapping and entry into the system.

c. 2.1GHz TDM Radio System

As mentioned earlier, a 2.1GHz TDM radio system is employed to connect the center station and the 1024 (or 2048) relay-DB stations. A block diagram of the radio channels is shown in Fig.7. The modulation rate on radio waves is at 288kbps to support a data rate at 256kbps. The differential decoding technique is used [Stein 1969]. Signals are transmitted in block codes designated by (n,k). The interrogation and response signals transmitted via the down-link and up-link are represented by (152,120) and (4248,4216), respectively. 32-bit CRC (Cyclic Redundancy Check) codes are employed to detect errors incurred in the transmission of data. Probability of errors escaping from this CRC check is estimated at levels below 10^{-20} [Boudreau 1994].

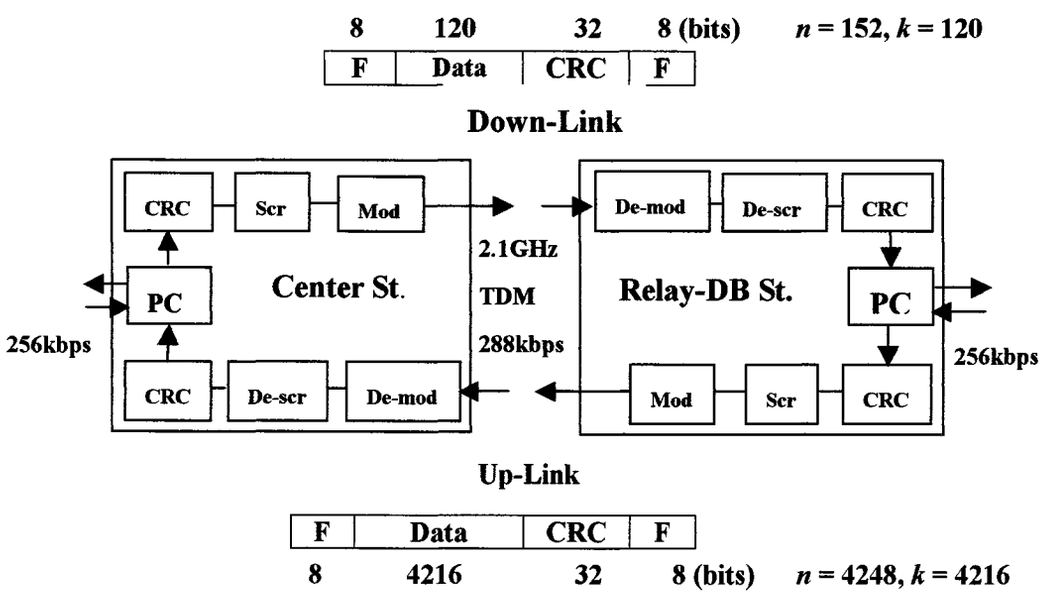

Fig.7. A block diagram of 2.1GHz TDM radio channels. Mod: modulator. Scr: scrambler. De-mod: de-modulator. De-scr: de-scrambler. CRC: cyclic redundancy check.

V. PERFORMANCE TEST RESULTS

a. Data Collection-and-Update Time in Lower Layer Polling Systems

Results of performance tests on the data collection-and-update times in the lower layer polling systems are presented in Table 4.

Table 4. Data collection-and-update time in the lower layer polling system.

	Data	Data Collection-and-Update Time
430MHz LPRS	20B/HT × 256 (1200bps, 200bps)	23.6 (min)
	20B/HT × 128 (4800bps, 4800bps)	6.8 (min)
2.4GHz TD-CDMA	256B/HT × 128 (with 50% time slots idle)	10.24 (sec)
	256B/HT × 256 (with no time slots idle)	10.24 (sec)

b. Data Collection-and-Update Time in Upper Layer Polling System

Results of performance tests on the data collection-and-update times in the upper layer polling system are presented in Table 5.

Table 5. Data collection-and-update time in the 2.1GHz TDM, upper layer polling system.

Data (B/Cell)*		Network Configuration	Data (B/HT)	Data Collection-and-Update Time (min.)
Urgent	*512*	256HT/Cell × 1024Cells	*2*	*1.1*
		128HT/Cell × 2048Cells	2	1.4
Detailed	2560	128HT/Cell × 2048Cells	20/2	4.2
	4096	256HT/Cell × 1024Cells	256/16	6.0
	5120	256HT/Cell × 1024Cells	*20*	*7.4*

Italic: measured

*** Data (B) collected from a relay-DB station in 1 cycle of polling.**

the round-trip path through relay-DB station 2, p_{r2}, was 8.1×10^{-7}. This value is quite close to 6.99×10^{-7} given in Table 6. A comment may be due here that $p_r = 7\sim8 \times 10^{-7}$ is a typical value for a wireless communication system operating in 2GHz range.

The above results show that the 2.1GHz TDM radio system is readily applicable to lifeline data acquisition system with satisfactory performance characteristics that can be predicted from theoretical considerations.

VII. RELIABILITY OF ACQUIRED DATA

a. Communication Failure and Database Update

Communications through the wireless system fail according to the probabilities discussed in the previous section. When the data transmission from a particular relay-DB station fails in a particular polling cycle, the database in the system waits for new data to be transmitted from that station in the next polling cycle for updating of its content, while retaining the data of the previous cycle. In this manner, continuity of lifeline data is maintained.

b. Reliability of Acquired Data

All the lifeline data acquired by the center station DB has cleared the CRC (32 bits) during the transmission through the wireless system. Consequently, the probability of error of the acquired data is bound by the probability of errors escaping the CRC, which is estimated at levels less than 10^{-20}, as discussed previously.

VIII. DAMAGE ASSESSMENT

a. Time-Course Record of Urgent Data

The main DB in the center station stores the urgent data over the last hours, say, 24 hours, to form a time-course record. Since the urgent data is updated continuously at an interval, say, 7 minutes, it provides a running-time-course record of lifeline performance observed at individual household terminals distributed across city. Sudden changes in supply conditions in certain areas, which can be detected instantly from the running data, can be taken as signals of damages inflicted on lifeline in those areas. Furthermore, a retrospective analysis of the record is expected to reveal that the lifeline supplies at which terminals have been shut-off since when. Results of such analysis will be displayed on a computer screen such as GIS (geographic

information system) terminal.

b. Detailed Data

When the areas of severe damages are identified by an analysis of urgent data, the detailed data can be collected selectively from those areas for further analysis.

IX. READINESS OF SYSTEM

The lifeline monitoring system must be kept ready for an unpredictable earthquake. The readiness of system operation is guaranteed by keep running it all times. This calls for the dual use of the system for purposes useful in normal times, such as remote meter reading.

X. DISCUSSION

The system reported in this paper can be regarded as a SCADA system in broad sense, since it can control the gas-valves of individual households by a command from the center station as described in Section V.d., but is different in usual sense from most of the existing SCADA systems [McDaniel 2000, Nakao 2000, Coolidge 2000, Shimizu 2000]. SCADA systems usually use a configuration that comprises the center station and some designated crucial points within the entire lifeline network. The center monitors these points and decides what to control accordingly. The primary task in the system reported in this paper, however, is to monitor lifeline supply conditions at the individual households. The number of data gathering points is much larger in the reported system than in the existing SCADA systems, and as a consequence, the former can readily be modified to accommodate additional monitoring points on top of the household terminals. In fact, it has been discussed in our group to introduce arrays of water-pressure meters and ground motion sensors into the lifeline data acquisition system at some strategic points of lifeline network, taking advantage of its ability to gather data from a large number of points quickly. Such data acquired from dense arrays of sensors in near-real time is expected to allow one to make inference of damage locations of underground network with a high degree of precision. Results of the analysis can be checked against the lifeline performance data at the individual households.

In short, it is conceivable to develop a new system that would allow the adaptive control of operation of lifeline network and the assessment of lifeline performance at individual households in near-real time by combining the SCADA and the household data acquisition techniques.

XI. CONCLUSION

An experimental wireless data acquisition system is described. The system comprises 430MHz LPRS, 2.4GHz TD-CDMA radio, and 2.1GHz TDM radio systems to connect household terminals distributed over a city to a center station through 1024 relay-DB stations. PCs equipped with an RDB are used for communication control, data processing, storage, and assessment of lifeline performance. Results of this experimental investigation has shown that wireless and computer technologies are available to build a wireless data acquisition system capable of monitoring some 260k household terminals at a repetition interval of about 7 minutes. Acquired urgent data of lifeline is stored in the database of center station in a form of running-time-course record of lifeline performance. Assessment of damages inflicted on lifeline can be made by analyzing the time-course record of the urgent data first, and then the detailed data can be collected from the areas of sever damages for further analysis. It was also demonstrated that the gas valves of all or designated household terminals were successfully shut off by a command transmitted in a broadcasting or terminal designating mode from the center station, respectively. It is recommended that the system should be kept running all times to maintain its readiness for an unpredictable earthquake.

It was suggested that a new system that would allow the adaptive control of operation of lifeline network and the assessment of lifeline performance at individual households in near-real time could be developed by combining the SCADA and the household-data acquisition techniques.

ACKNOWLEDGEMENTS

This work was conducted in a project run by the Telecommunications Advancement Organization (TAO) and was funded by the Ministry of Posts and Telecommunications of Japan. It is acknowledged with thanks that the work was carried out in collaboration with HAMANEN, OKI, NEC, IBI, TOYO KEIKI, and TG I-NET. The authors also thank to M.Hirata and T.Mitsugi of TAO for their encouragement and help..

REFERENCES

[1] Association of Radio Industries and Businesses, Ed. (1998). *Telemetry/Tele-control Radio Equipment for Special Low Power Radio Station, ARIB Standard RCR STD-16A*, ARIB, Tokyo.

[2] Boudreau,P.E., Bergman,W.C., and Irvin,D.R. (1994): "Performance of a Cyclic Redundancy Ckeck and Its Interaction with a Data Scrambler", *IBM Journal of Research & Development*, 38(6), 651-658.

[3] Coolidge,A.P. and Wiesman, R.M. (2000). Proceedings of MEDAT-1, Los Angeles, CA, March 2-3, 2000, paper No.12.

[4] Fujiwara,T., Shimazaki,Y., Toyoshima,H.,Ito,S., Sugiura,M., Atsumi,M., Watanabe,T., and Mizushina,S. (2000). "A TD-CDMA Data Collection System for City Lifeline Monitoring", accepted for presentation at the IEEE Vehicular Technology Conference 2000, May 15-18, 2000, Tokyo.

[5] Fujiwara,T., Ikeda,A., Ito,S., Sugiura,M., Atsumi,M., Mizushina,S., Watanabe,T., Shimazaki,Y., Toyoshima,H., and Adachi.A. (2000). "Experimental TD-CDMA System for City Lifeline Monitoring", accepted for presentation at the IEEE International Conference on Third Generation Wireless Communications, June 14-16, 2000, Silicon Valley, USA.

[6] Ito,S., Sugiura,M., Atsumi,M., Toyoshima,H., Adachi,A., Watanabe,T. , and Mizushina,S. "A 2GHz Polling System for Lifeline Data Gathering", Proceedings of the 1999 Asia Pacific Microwave Conference, Singapore, November 30 – December 3, 1999, 754-757.

[7] Japan Gas Instrument Association, Ed. (1997): *Specifications of Interface between Micro-computerized Gas Meter and Communication Equipment, JGIA9709*, Tokyo.

[8] Japan Water Supply Instrument Association, Ed. (1998): *Specifications of 8 bit Communication Interface between Micro-computerized Water Meter and Communication Equipment,* Tokyo.

[9] Kasano,H., Ed. (1997). *Communications Protocol Dictionary*, ASCII, Tokyo.

[10] Kroenke,D.M. (1996). *Database Processing, Fundamentals, Design, and Implementation,* 5th Ed., Japanese Edition, Prentice-Hall/Toppan, Tokyo.

[11] McDaniel,J.B., Yonnotta,J.G, and Dekermenjian (2000). "Los Angeles Department of Water and Power Water Services Organization SCADA System", Proceedings of MEDAT-1, Los Angeles, CA, March 2-3, 2000, paper No.10.

[12] Mizushina,S, Sugiura,M., Ito,S., Atsumi,M., Adachi,A., and Watanabe,T. (1999). "A Wireless Data Collection System for Monitoring and Control of City Lifelines", 1999 IEEE MTT-S International Microwave Symposium Digest, Anaheim, CA, USA, June 13-19, 1999, 1855-1858.

[13] National Land Agency, Ed.(1996). *1996 White Paper on Disaster Planning and Response*, 46-50, Government Printing Office, Ministry of Finance, Tokyo, Japan.

[14] Nakao,M.J. (2000). "SCADA Application for Los Angeles DWP Power System", Proceedings of MEDAT-1, Los Angeles, CA, March 2-3, 2000, paper No.11.

[15] Ogawa,A.: "Development of Infrastructure-DBMS Applicable to Both Operational and Managerial Information Systems", Final Reports, Information Technology Promotion Agency, Tokyo, 1998, 27-32.

[16] Ogawa,A.(1999): US Patent No.S.N.09/025,834.

[17] Shimizu,Y. (2000). "Advanced Accelerometers and Liquefaction Meters for Damage Assessment of Gas Distribution Systems", Proceedings of MEDAT-1, Los Angeles, CA, March 2-3, 2000, paper No.4.

[18] Stein,S. and Jones,J.J. (1969): *Modern Communication Principles, With Application to Digital Signaling*, McGraw Hill, New York.

[19] Viterbi,A.J. (1995). *CDMA : Principles of Spread Spectrum Communication*, Addison-Wesley, Reading, MA.

Water Services Organization SCADA System

James B. McDaniel, James G. Yannotta, Hampik Dekermenjian

Professional Engineers, Los Angeles Department of Water and Power

ABSTRACT

The Water Services Organization (WSO) of the City of Los Angeles, Department of Water and Power serves water to over 3.5 million residents within the city through 700,000 plus services. Its water distribution system includes one filtration plant, 16 open reservoirs, 78 tanks, 78 pumping stations, 96 priority regulator stations, 26 water treatment facilities, and 7100 miles of pipe that serve water in 101 pressure zones.

WSO monitors and controls the entire water system using multiple SCADA systems, which will soon be merging into a unified system. The new system is designed to allow operators to monitor and remotely control facilities such as pumping stations, regulator stations, tanks, reservoirs, and critical trunkline locations. The new system will also be the critical component during emergency operations.

Currently, there are six different systems within the Water Services organization. These systems are:

LAWSDAC: Monitor and remote control of water distribution facilities in the city of Los Angeles
DCS: Los Angeles Aqueduct Filtration Plant monitoring and control system
REMOS: Chlorine Station Monitoring and control system
REOS: Open distribution reservoir water quality monitoring system
LIMS: Laboratory information monitoring system
RUGID: Intellution system, which monitors the aqueduct.

There are multiple reasons for upgrading the existing systems. Primarily, these systems operate independently of each other. Sharing information between these systems is difficult and restrictive. Back-up control rooms for monitoring and remote control of water treatment and distribution facilities do not presently exist, but are necessary for reliability of the Water System. And current and future water quality regulations, i.e., Surface Water Treatment Rule, Disinfection Byproducts, etc., will result in having less in-city regulatory storage. SCADA systems must have the ability to more closely monitor and have better system wide control of water quality and the distribution of water throughout the city.

LAWSDAC, the system that monitors and controls distribution facilities in the city was developed in the mid 1980's. It is the most critical SCADA system that is used during emergencies. Its technology is outdated and furthermore, its legacy code will require specialized programming if any changes or upgrades are to be made. It was estimated that just upgrading the graphics of the system would cost in excess of $400 thousand. Reporting capabilities are almost non-existent therefore no valuable information is gathered to learn from for future emergency operations. And most critical

is that LAWSDAC has no back up control center to activate if the primary location became inaccessible during an emergency.

This upgrade will provide the Water Services Organization with a unified SCADA system with "open" structure allowing for easy upgrades and improvements in the future. It will also provide a simplified information sharing capabilities with a consistent high-level security measures. All control and operational activities will be preformed with knowledge of the entire system not just the one component. Furthermore, it will also provide a consistent hardware and equipment structure, reducing costs of maintaining the SCADA system.

During emergency operations, the new SCADA system will provide a single point and complete supervisory control of the entire Water System facilities. There will also be a back up control center that will be able to duplicate all functions. Furthermore, all facilities will be equipped with Uninterrupted Power Supplies (UPS). This will maintain local control at each facility if all communication with a control center is lost. These facilities will then operate using independent preset parameters.

Critical points in the distribution system that require monitoring of water quality parameters, pressure, and flow will be identified. Monitoring pressures at high elevations and areas that serve critical customers would help operators to identify major problems and to take corrective actions. They will have the ability to isolate facilities or place portions of a facility out of service and to activate a work around solution. This solution can be implemented through manipulation of valves within the system or by dispatching crews.

Another component of emergency operations is the monitoring and control of old, large diameter trunk lines in the distribution system. There are about six old riveted trunk lines that pose a high risk of failure. The installation of about a dozen remote controlled shutoff valves would allow operators to minimize property damage if there were a break in one of these lines. A recent major pipe break flooded the freeway primarily because of the time it took to report the break and for crews to identify the isolation valves and to close them. If these control systems were in place, the break would have been known immediately due to pressure drops in that pipe and the system would have isolated that pipe preventing the flood. Many of these old pipelines are structurally incapable of handling static pressures. The new system will prevent pressure built up in these pipes, past preset thresholds.

Key regulator stations that require remote monitoring and control will also be identified. There are about a dozen major regulator and flow control stations that shift supplies among the major pressure zones. During an emergency where storage or pumping facilities may be rendered inoperable, these stations will require frequent and drastic adjustments to balance water supply. A single point of control will allow an operator to view and consider the entire system prior to making drastic changes at these stations.

The operations strategy during emergencies will be based on existing hydraulic models and water control experience. These models will be used to develop multi-point decision-making and multi-point control scenarios. These scenarios may initially be implemented as auto-control program for the PLCs or central system to activate without intervention of operators. During an emergency, many of these scenarios may be used to assist operators in their decision-making.

In conclusion, the implementation of the new SCADA system will provide a complete monitoring and control capabilities of the entire water system from redundant control centers. This level of control will allow operators to see and make informed decisions responding to emergencies immediately. And this response will minimize damage and facilitate a rapid restoration of water service in the city of Los Angeles.

Los Angeles Dept. of Water and Power

Water Services Organization
SCADA Systems

LADWP Water System

- Over 3.5 Million Residents
- Over 700,000 Services
- 101 Pressure Zones
- 16 Open Reservoirs
- 78 Pumping Plants
- 78 Tanks
- 26 Water Treatment Facilities
- 96 Priority Regulator Stations

Existing Water Services Organization Electronic Monitoring Systems

- LAWSDAC - Monitor and remote control of water distribution facilities in the city (Most critical during emergencies)
- DCS - Los Angeles Aqueduct Filtration Plant monitoring and control system
- REMOS -Chlorine station monitoring and control system
- REOS - Open distribution reservoir water quality monitoring system
- LIMS - Laboratory information monitoring system
- RUGID - Aqueduct monitoring system

Major Driving Forces

- Inconsistent hardware and software of multiple platforms
- Difficult to share data
- Inconsistent security measures
- Lack of a back up control center for LAWSDAC
- Aged legacy technology that will require specialized programming for simple enhancements (LAWSDAC was developed in 1984)
- High cost of improving the existing system ($400,000 for a graphics upgrade of LAWSDAC)
- Lack of reporting capabilities
- High cost of operating multiple systems

Advantages Of New System

- Unified SCADA system with "open" architecture
- Simplified information sharing capabilities
- Integrated with existing Windows NT network via firewall
- System with consistent high-level security measures
- Consistent hardware, software and equipment
- Multiple consistent and redundant system control centers
- Consistent operator interface and training

Emergency Operations Framework

- The new system will allow the option of a single point of control and monitoring during emergencies
- Back up control center will be available and fully functional
- Failures will be evident at monitoring location and control center operator will be able to make system changes and dispatch field personnel immediately
- Resource allocation will be based on actual conditions rather than uniform predetermined response
- All critical facilities will be equipped with uninterrupted power supplies (UPS)
- Accurate reports of facility conditions after an emergency
- Increased ability to forecast recovery timeframe

Emergency Operations

- Remotely isolate broken, large diameter pipes and other facilities to prevent further damage
- Capability to remotely operate pumping plants to maintain pressure grades
- Capability to isolate tanks to prevent water loss in case of major damage to surrounding pipe network
- Critical regulator stations can be remotely adjusted to shift water supply throughout the city
- Dispatch crews to respond to critical points of damage

Questions?

SCADA Application for Los Angeles DWP Power System

Mark J. Nakao
Los Angeles Dept. of Water & Power

Abstract

This presentation will focus on the SCADA systems used by Los Angeles Department of Water and Power to monitor and control the Department's power system. An overview of the SCADA system will be provided; including, communication requirements and data subsystems. In addition, discussion will focus on the benefits of the SCADA system during the 1994 Northridge Earthquake. The future of the DWP SCADA system and the potential for Substation Automation will be considered.

Introduction

- DWP - 12 Years.
- SCADA system - 12 Years
- Remote Terminal Unit Section

DWP SCADA System: Overview

- Energy Control Center - 2 Mainframe Computers
  - –Sub transmission: Below 34.5 KV
  - –Transmission: Above 34.5 KV
- Power Stations - Remote Terminal Unit
  - –Supervisory Control and Data Acquisition

DWP SCADA System: Communications

- Four-wire telecommunication line
- Asynchronous communication
- Frequency Shift Keying
- 1200 Baud
- 32-bit message structure

DWP SCADA System: Subsystems

- Analog
- Control
- Status
- Accumulators
- Automatic Generation Control
- Analog Output

DWP SCADA System: Analog Subsystem

- MW/MV
- Voltage
- Frequency
- Tap Changer position

DWP SCADA System: Control Subsystem
- Circuit breaker control - Open/Close
- Tap changer control - Raise/Lower

DWP SCADA System: Status Subsystem
- Circuit breaker indication
- Station alarms

DWP SCADA System: Accumulators
- MWH

DWP SCADA System: Automatic Generation Control
- Generator Control - Raise/Lower

DWP SCADA System: Analog Output
- Synchronous Condenser control

1994 Northridge Earthquake: System condition
- Major damage to DWP facilities
- Entire Power Grid de-energized

1994 Northridge Earthquake: DWP Response
- SCADA System - Allows dispatchers to evaluate system condition and take appropriate action.
  - Monitor Power Flow
  - Monitor Critical Alarms
  - Remotely control field circuit breakers
  - Control Generation
  - Dispatch trouble crews to adversely affected areas

1994 Northridge Earthquake: Problems
- Communication Infrastructure damaged (I.e. Communication circuits).
  –Loss of communication between Energy Control Center and power stations

Future DWP SCADA System
- New mainframe computer
- Substation Automation
- VAR Dispatch
- LAN/WAN

Future DWP SCADA System: Mainframe computer
- Maintain larger database
- ISO software
- Scheduling/Marketing support

Future DWP SCADA System: Substation Automation

- PLC-based data concentrator
- Intelligent Electronic Devices (IED) interfaced to PLC
- Human Machine Interface (HMI) located at each power station

Future DWP SCADA System: VAR Dispatch

- Automatic Capacitor control

Future DWP SCADA System: LAN/WAN

- LAN - Network for local areas
  - –Data access to affected power stations in the area
- WAN - Network for central office personnel
  - –Data access for sections needing specific data

Conclusion

- SCADA System Reliability
  - –99% Up-time
- Timely and reliable information
- Efficient power system operation

SCADA Application for Los Angeles DWP Power System

Mark J. Nakao

Los Angeles Department of Water and Power

ABSTRACT

This presentation will focus on the SCADA systems used by Los Angeles Department of Water and Power to monitor and control the Department's power system. An overview of the SCADA system will be provided; including, communication requirements and data subsystems. In addition, discussion will focus on the benefits of the SCADA system during the 1994 Northridge Earthquake. The future of the DWP SCADA system and the potential for Substation Automation will be considered.

Introduction

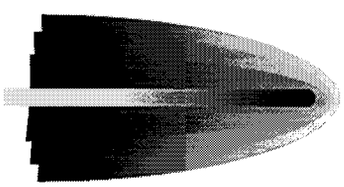

- DWP - 12 Years.
- SCADA system - 12 Years
- Remote Terminal Unit Section

DWP SCADA System: Overview

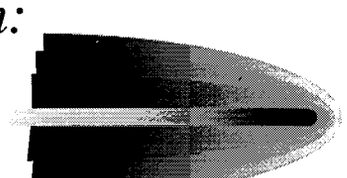

- Energy Control Center - 2 Mainframe Computers
  - Subtransmission: Below 34.5 KV
  - Transmission: Above 34.5 KV
- Power Stations - Remote Terminal Unit
  - Supervisory Control and Data Acquistion

DWP SCADA System: Communications

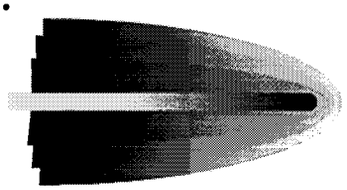

- Four-wire telecommunication line
- Asynchronous communication
- Frequency Shift Keying
- 1200 Baud
- 32-bit message structure

DWP SCADA System: Subsystems

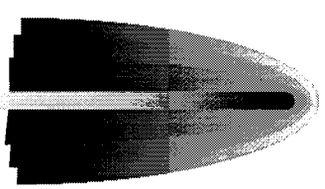

- Analog
- Control
- Status
- Accumulators
- Automatic Generation Control
- Analog Output

DWP SCADA System: Analog Subsystem

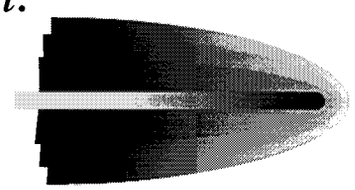

- MW/MV
- Voltage
- Frequency
- Tap Changer position

DWP SCADA System: Control Subsystem

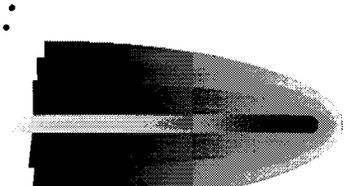

- Circuit breaker control - Open/Close
- Tap changer control - Raise/Lower

DWP SCADA System: Status Subsystem

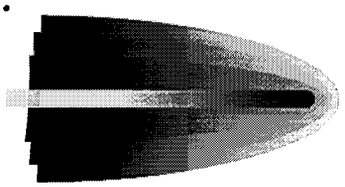

- Circuit breaker indication
- Station alarms

DWP SCADA System: Accumulators

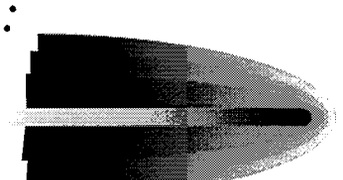

- MWH

DWP SCADA System: Automatic Generation

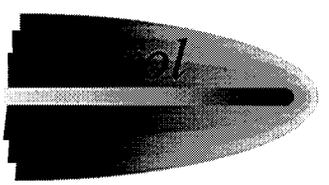

- Generator Control - Raise/Lower

DWP SCADA System: Analog Output

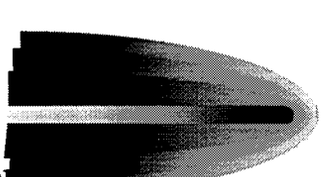

- Synchronous Condenser co

1994 Northridge Earthquake: System condition

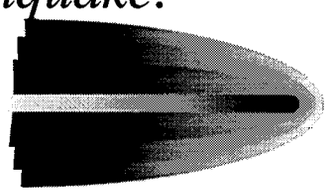

- Major damage to DWP facilities
- Entire Power Grid de-energized

1994 Northridge Earthquake: DWP Response

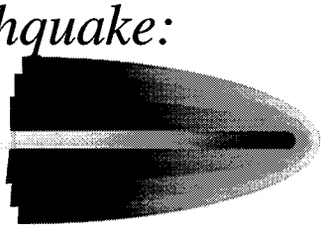

- SCADA System - Allows dispatchers to evaluate system condition and take appropriate action.
  - Monitor Power Flow
  - Monitor Critical Alarms
  - Remotely control field circuit breakers
  - Control Generation
  - Dispatch trouble crews to adversely affected areas

1994 Northridge Earthquake: Problems

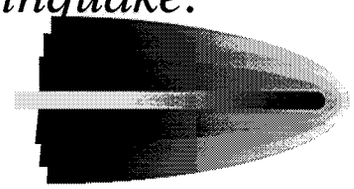

- Communication Infrastructure damaged (I.e. Communication circuits).
  - Loss of communication between Energy Control Center and power stations

Future DWP SCADA S[illegible]n

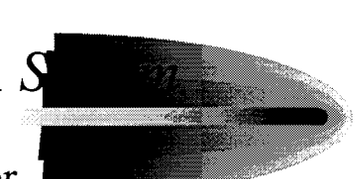

- New mainframe computer
- Substation Automation
- VAR Dispatch
- LAN/WAN

Future DWP SCADA System: Mainframe computer

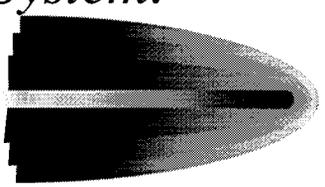

- Maintain larger database
- ISO software
- Scheduling/Marketing support

Future DWP SCADA System: Substation Automation

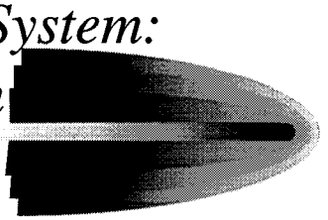

- PLC-based data concentrator
- Intelligent Electronic Devices (IED) interfaced to PLC
- Human Machine Interface (HMI) located at each power station

Future DWP SCADA System: VAR Dispatch

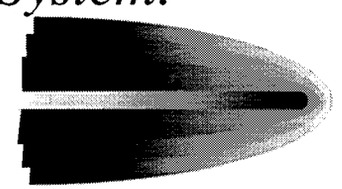

- Automatic Capacitor control

Future DWP SCADA System: LAN/WAN

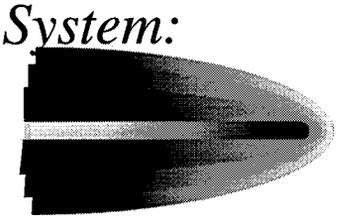

- LAN - Network for local areas
  - Data access to affected power stations in the area
- WAN - Network for central office personnel
  - Data access for sections needing specific data

Conclusion

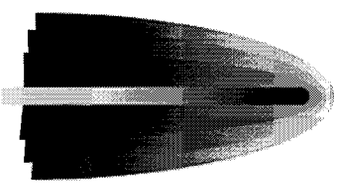

- SCADA System Reliability
  - 99% Up-time
- Timely and reliable information
- Efficient power system operation

SCADA Applications for Power Distribution Systems Intelligent, Distributed Sensor Networks

Aaron P. Coolidge[1] and *Richard M. Wiesman[2]

[1] *Senior Engineer, Foster-Miller, Inc., Waltham, Massachusetts, US*
[2] *Vice President, Foster-Miller, Inc., Waltham, Massachusetts, US*

ABSTRACT

Present uses of voltage and current sensors are generally confined to substations where the measurements are incorporated into SCADA systems. Barriers to the greater use of current and voltage sensors throughout distribution systems include: the cost of the sensors and the related necessary equipment; the cost of installation of sensors and associated equipment; and the cost of communications of sensed data including communications equipment, infrastructures and recurring communications costs. Foster-Miller and GridCom have developed and tested a family of low cost and easily installed intelligent, communicating powerline sensors for both underground and overhead medium and low voltage applications.

INTRODUCTION

New forms of automation in the electric power distribution industry are required to extend the service life of aging infrastructures; reduce operations and maintenance costs; and improve service. In addition, the power distribution industry is undergoing a fundamental change in market dynamics. Regulation is being diminished and competition between utilities for customers is intensifying. This is a time, at electric utilities, when cost-effectiveness, functionality, and quality are becoming the most important criteria for choosing a product, a process or a supplier rather than the reasons that arose from regulatory logic. Utilities need to invest in effective operations and maintenance technologies and services that can give them a competitive edge.

Foster-Miller and GridCom have developed a family of low cost and easily installed intelligent power line sensors for both underground and overhead medium and low voltage applications. The underground sensors were initially developed for Consolidated Edison Company of New York's Secondary Underground Network Distribution Automation System (SUNDAS) and are the result of five years of development and testing. The objective was to develop a comprehensive sensing system that would be relatively inexpensive to purchase, install, operate and maintain (inexpensive in quantities). The sensors measure current and voltage waveforms and can be equipped to measure and/or detect a number of additional conditions or quantities including temperature, moisture, specific substances, light, acceleration, and vibration. Underground sensors utilize two-way power line carrier communications over the existing power lines and overhead sensors communicate through two-way low power RF systems.

The sensors utilize on-board intelligence to perform data processing and analysis at each sensor. In typical applications the sensors calculate true rms voltage and current, power factor, harmonic content and a number of other quantities. Peak rms quantities and distribution system fault recognition capabilities can also be employed. The sensors report by exception, when polled, or at determined times and since data is processed at the sensors, communications bandwidth require-

ments are relatively low. Only processed data or observed data related events (like faults, voltage dips, or high current limits) are reported — not extensive strings of raw data.

Consolidated Edison has tested experimental versions of the low voltage underground sensors in their Battery Park City and Harlem networks. These tests demonstrated the capabilities of these sensors to monitor power line conditions and to detect variations in line conditions associated with circuit limiter loss, arcing faults, changes in network protector relay status and unusual changes in power flow patterns. Based on the performance of the experimental sensors, Con Edison will install GridCom sensors throughout the Hunter network with installations beginning in spring 2000. Overhead sensors have gone through extensive laboratory testing and evaluation versions of these devices have been tested at six utilities in North America.

Typical functions of these sensors (both overhead and underground) include:

- Detection and location of faults
- Measurement of power quality
- Identification of grounding and cable insulation issues
- Detection of non-technical losses
- Detection of unanticipated loads
- Confirmation of recloser, sectionalizer and other switch operations
- Support capacitor switching algorithms
- Monitoring distributed generation

TECHNICAL DISCUSSION

The Need for Power Distribution Information

Present uses of voltage and current sensors are generally confined to substations where the measurements are incorporated into SCADA systems. At substations these sensors supply information on the utilization of individual feeders; the occurrence of faults; and the operational status of feeders, switches and sectionalizers. Sensors can also be employed at switched capacitor banks to track the need for and the effects of "switching in" capacitance at a particular site.

In safety related functions current and voltage sensors are used to verify switch status and line status to insure that lines are dead when service on lines and attached equipment is required.

In industrial applications, current and voltage sensors are employed in submetering, process control, and safety related applications. In submetering applications sensors are used to track the consumption of energy and to understand how various functions and processes account for the overall use of energy at a particular site. In process controls these sensors are used to directly regulate process parameters which may relate to functions like motor speeds (pumps, blowers, mixers, etc.), temperature (ovens, heaters, chillers, etc.), and actuator currents (motor torque, pressure, force, etc.).

The electric power distribution industry is facing a number of changes in both the condition and utilization of infrastructures for distribution and the markets that this industry serves. Demands for electric power are increasing at the same time most distribution companies are faced with aging and deteriorating infrastructures. The costs of large-scale infrastructure replacements are generally prohibitive. This is particularly true in denser population areas like urban and suburban environments. Many larger urban areas, throughout the world, utilize either partial or complete underground power distribution systems. In these situations, in particular, one can imagine the difficulty

and expense in replacing a distribution infrastructure. New forms of automation and monitoring are required to extend the service life of these aging infrastructures; reduce operations and maintenance costs; and improve service.

In addition, the power distribution industry is undergoing a fundamental change in market dynamics, largely brought on by deregulation. Competition between utilities for customers is intensifying and this is driving utilities to incorporate effective operations technologies and services that can give them a competitive edge.

Present Sensing Technology

For power distribution applications, current and voltage sensors have traditionally been current transformers and potential transformers. Potential transformers can be either capacitive or inductive. Since these devices supply proportional analog outputs of their respective waveform measurements, remote terminal units (RTU's) are generally installed in close proximity to the sensors to convert analog signals to digital measurements. Once digitized at the RTU's, the current and voltage measurements can be stored or transmitted to remote utility databases as "raw" measurements of the respective waveforms. Additionally, it may be desirable to process raw current and voltage measurements at the RTU. Such processing might typically consist of the calculation of root mean square (RMS) values and the detection of current and voltage values passing above or below alarm thresholds.

Current and voltage distribution sensors are commercially available for overhead applications. Sensors for underground applications are just becoming available. In addition to sensors intended for permanent "pole-top" installation there are instantaneous measurement probes available for hot stick use. These devices are useful for quick measurements at specific locations within a distribution network.

There have been three significant barriers to the greater use of current and voltage sensors in electric power distribution. Those barriers are: the cost of the sensors and the related equipment necessary for use of the sensors; the cost of installation of sensors and associated equipment; and the cost of communications of sensed data including communications equipment, infrastructures and recurring communications costs. Additionally, the lack of sensors for underground distribution systems has been a barrier to sensing in these networks.

Foster-Miller Power Line Sensor System

Foster-Miller and GridCom have developed a family of low cost and easily installed intelligent, communicating power line sensors for both underground and overhead medium and low voltage applications. The underground sensors were initially developed for Consolidated Edison Company of New York's Secondary Underground Network Distribution Automation System (SUNDAS) and are the result of five years of development and testing. The objective was to develop a comprehensive sensing system that would be relatively inexpensive to purchase, install, operate and maintain (inexpensive in quantities).

The underground and the overhead systems each has hardware variations to accommodate the voltage category (low and medium voltage) in which the sensor will be applied. Responding to feedback and interest of the utilities the development work being done now is for:

- Overhead sensor systems for the 4 kV to 69 kV phase to phase range and
- Underground sensor systems for low voltage (up to 600 Volts)

Overhead Sensor System The overhead sensor system includes Line Mounted Monitors, one for each phase, mounted on the distribution lines with clamps. The design is such that one lineman with proper gloves or using a hot stick can easily install them. These Line Mounted Monitors pick up and process the line data, which is then transmitted to the Utility Control Station through a digital cellular modem. The overhead sensor system is shown pictorially in Figure 1

Figure 2 shows a Line Mounted Monitor that is used on a distribution line. The particular device shown is one of the evaluation units, which have been tested by six utilities in North America. A complete system of three Line Mounted Monitors installed at a single location provides full three-phase sensing. The transmission of the data to the Utility Control Station is done using the UCA™ V2.0 protocol or some other protocol that may be preferred by the utility and is accomplished through a digital cellular modem.

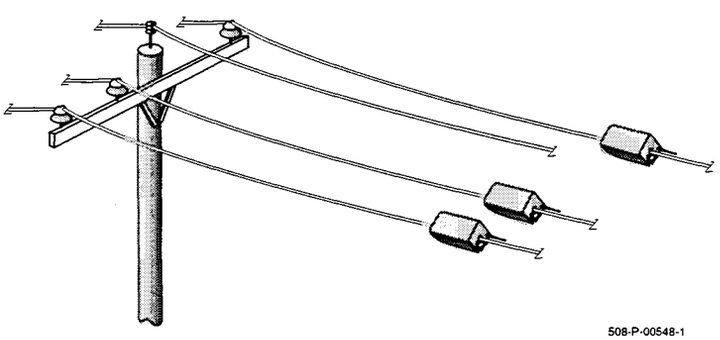

Figure 1. The Overhead Sensor System

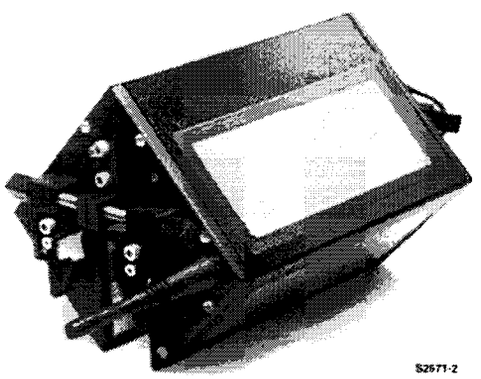

Figure 2. Line Mounted Monitor

Underground Sensor System The Underground Sensor System includes Line Pick-Up Clamps, mounted one on each phase line and neutral, connected to a Monitor Station. The Monitor Station processes the data and transmits it through a power line modem to a Collector Station. The Underground Sensor System is shown schematically in Figure 3.

Figure 4 shows the Underground Sensor System Control and Communication Architecture. The selected architecture is a hybrid hierarchy. This sort of hybrid architecture is structured hierarchi-

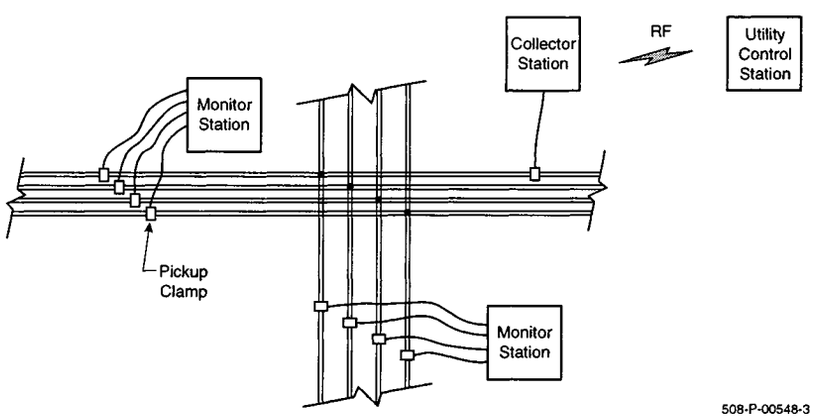

Figure 3. The Underground Sensor System

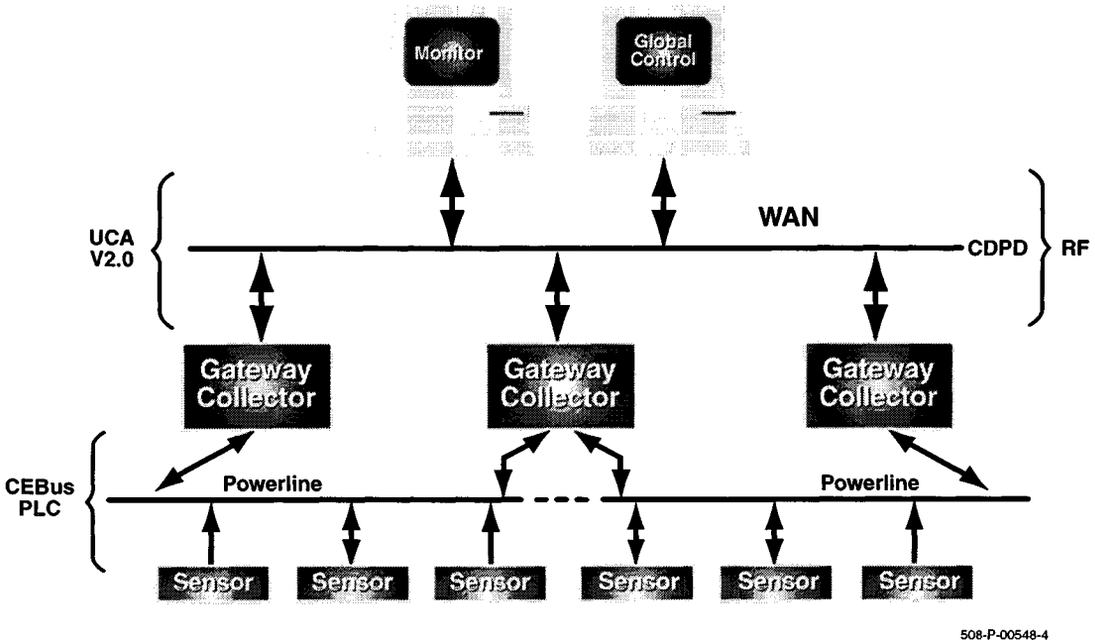

Figure 4. Underground Sensor System Control and Communication Architecture.

cally for control functions, but communication among nodes on the same level is possible. The lowest level of the system is made up of the actual power lines being monitored. Power line carrier communications are used for two-way communications with each sensor system. Gateway collectors are distributed spatially throughout the system. Each gateway collector may communicate with a number of sensor systems and it is likely that each sensor system will be within functional communication range of more than one collector.

A key feature of the sensors is the use of CEBus power line carrier (PLC) communications to carryout two-way communications between the underground sensors and the collectors via the power lines. CEBus was selected after several years of testing in actual Consolidated Edison networks and because it is an "open" communication standard for which any group is free to build hardware. CEBus standards describe a complete communications system including the physical layer (a particular CEBus form of spread spectrum power line carrier), protocols and all other parameters for defining a complete communications system. By adhering to the CEBus standards with both the sensors and the collectors GridCom can assure that the sensors and collectors will communicate with all existing and future CEBus systems and devices. Similarly, the utility is assured that the system they are implementing will have communication compatibility with any existing or future devices they may want to introduce to their distribution automation system.

Successful communications with PLC, as with other communications mediums, requires that adequate signal-to-noise ratios be maintained during communications. Powerline communications can present some unique challenges, and powerline communications on a distribution grid can be particularly interesting. We have observed, during more than 5 years of testing, time varying noise conditions and somewhat nonintuitive impedance's that can exist from time-to-time and in different locations around a distribution network. A seemingly short path on power lines between a sensor and a collector may not allow communications because of some localized interfering noise or because of some signal suppressing impedance drops. Furthermore, a clear path of communica-

tions at one moment may be obscured by noise only seconds later. We have observed communications on the powerline to be clear and reliable over distances of two to three blocks (or more) while communications between a vault and an adjacent manhole, only 40 or 50 feet away, were obscured.

To help to maintain reliable and optimized PLC communications CEBus supports a dynamic rerouting capability for communications between collectors and devices. Foster-Miller utilizes this dynamic rerouting capability to greatly improve the robustness of communications when sensors are deployed on a distribution grid. A basic description of a dynamic rerouting scenario is the following: When a sensor attempts to communicate to the collector that the sensor has been historically reporting to and because of some dynamic event (like noise, line damage, impedance changes, etc.) the collector does not receive and acknowledge the communication, then any other collector which has heard the communication attempt and has not heard the acknowledgment from the intended receiver will acknowledge the communication and report its identity as the successful new receiver. Future communications attempts from the sensor will be addressed to the new receiver. The new receiving collector will also report this "reassignment" or rerouting to the central control station so that communications back to the sensor are properly rerouted. Without dynamic rerouting when communications over the power lines are interrupted there is no method to redirect communications or even allow another collector to acknowledge a communication that it has received if that communication was not directed to it.

From the collectors back to the utility central control station the utility's preferred protocol is used over whatever wireless WAN is the most effective in the area of operation. These WAN's will generally utilize existing infrastructures and include systems like CDPD, PCS digital data and GSM digital data. Consolidated Edison has selected the DNP 3.0 protocol over the CDPD physical communications network. CDPD is a RF to Internet data service that Con Edison used in previous tests in the Harlem Network. DNP 3.0 is the current version of an open protocol that is used by some utilities for data communications.

The most basic function of the collectors is to receive CEBus communications from the sensors, convert those communications to the desired protocol and send them along via an appropriate RF physical layer to the utility central control station. The reverse takes place when the utility central control sends messages down to the sensors.

Figure 5 shows a mock-up of the installed underground sensor system.

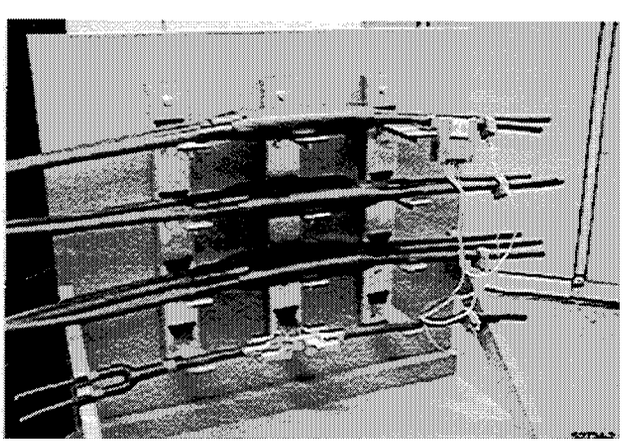

Figure 5. Mock-up of an Underground Sensor System Installation

Sensing and Data Processing The Monitor Stations of the underground and overhead sensing systems have DSP-based architectures. The use of a DSP processor allows high sampling rate with accurate waveform measurement for multiple inputs. The voltage and current wave forms are monitored and processed and the following values are calculated and reported by the Monitors:

- Voltage (phase to neutral underground, phase to ground overhead, three phases) reported in Volts RMS.
- Current (three phases and neutral underground) reported in Amps RMS.
- Temperature (of the Monitor Station) reported in Degrees Celsius.
- Instantaneous Current (three phases and neutral underground). Pulses of 20,000+amps lasting less than 0.5 microsecond are accurately measured.
- Power Factor (three phases).
- Harmonic Distortion (three phases and neutral underground)
- Reactive Power (three phases) reported in VAR.
- Real Power (three phases) reported in Watts.
- Voltage (phase to phase, three combinations) underground.
- Current Rate Change (three phases and neutral underground). This value is calculated for internal exception detection and is presently not available over the communications link.

The underground and overhead Monitor Stations sample the lines continuously and can transmit the data by three reporting modes:

- Report unsolicited messages when an exception occurs. When values exceed alarm limits, the Monitor Station will alert the operations station that an exception occurred. The alarm limits can be remotely pre-set and modified through the two-way communications.
- Report the data sampled at time intervals. The time intervals for reporting can be remotely set and modified through the two-way communications.
- Report the data sampled only when requested by the control station.

Utility Control Station The Utility Control Station is required to have:

- A convenient graphic user interface (GUI)
- A data base for collecting data, archiving data and allowing that data to be researched.
- An interface for communications from the control center to the collectors and the monitors. This communications path is used to set or change monitor alarm points; to set or change timed reporting intervals; to poll collectors and monitors; and to set or change any other adjustable parameters at the collectors and the monitors.

SENSOR TECHNOLOGY DEMONSTRATIONS AND TESTS

Consolidated Edison SUNDAS – Battery Park City Network

The initial demonstration of the underground sensor system started mid-June in 1996. This demonstration utilized pre-prototype sensors and was carried out in Consolidated Edison's Battery Park City Network. Figure 6 shows a simplified map of the Battery Park City secondary distribution network. Each letter designates a transformer vault or set of vaults. Manholes and cable runs are also displayed. Six sensors were demonstrated at various locations. Figure 7 shows the typical installation conditions in one of the transformer vaults. A single gateway collector was placed in a meter room near vault "B". A leased telephone line was utilized for the WAN.

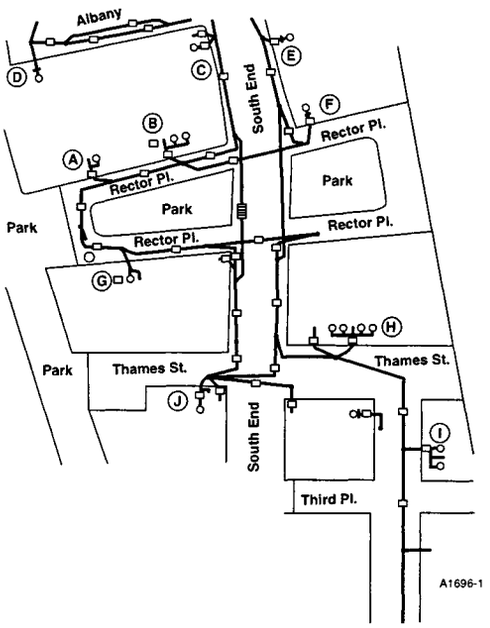

Figure 6. Battery Park City Secondary Network

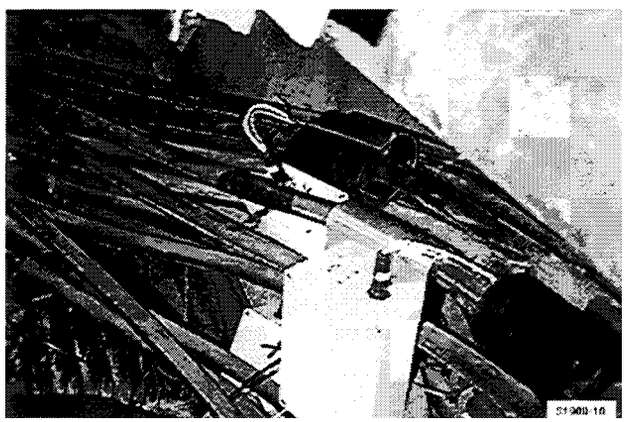

Figure 7. Typical Pre-Prototype Sensor Test Installation

Tests at Battery Park City verified the effectiveness of power line communications and displayed real time data on continuous operation of secondary power lines. Figure 8 shows typical 24-hour voltage and current conditions in a secondary distribution line as monitored by one of the sensors.

Consolidated Edison SUNDAS – Harlem Network

In 1997, during the summer, a demonstration of the underground sensor system began in Consolidated Edison's Harlem network. This demonstration used 28 sensors and 3 gateway collectors. CDPD was first used for the WAN physical communications in this test and CEBus power line communications was also utilized.

Real-time data from the ongoing tests was delivered to a Foster-Miller server via an Internet link from the CDPD WAN. The server posted real-time data, status and archived data on the Internet. Figure 9 shows a section of the test area map as displayed by the server. Sensors actively communicating were displayed at their respective locations in green. Sensors not communicating were displayed in purple. Gateway collectors are shown as larger circles (two are shown in this figure).

Figure 10 shows a typical sensor data table as displayed by the server. The table shows actively reporting sensors (at that time); the active collectors; collector CDPD signal strength; voltage and current information at each respective sensor; power flow direction; and the number of consecutive communication packets received from each reporting sensor. Figure 11 displays, for a particular sensor, recorded voltage and current for that particular 24-hour period and recorded voltage and current from that sensor during the previous 24-hour period.

Figure 12 presents detailed current and voltage records from a single sensor in the Harlem tests.

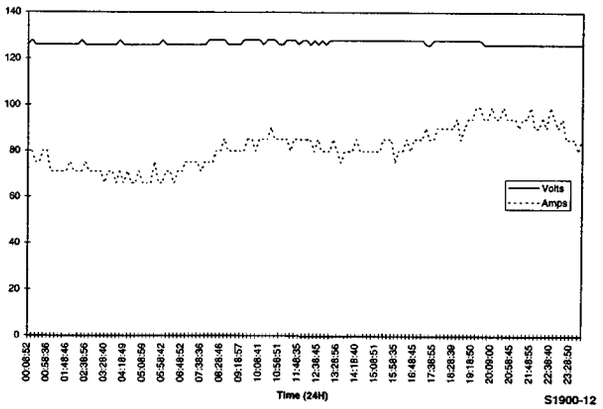

Figure 8. 24-hour voltage and current conditions in a secondary distribution line

Figure 9. Harlem Network Demonstration Location Map

Collector	Date	Time	Signal (dB)
0001	10/22/97	13:42:35	-75
0002	10/22/97	13:44:46	-84

Address	Type	Time	Volts	Amps	Flow	Packets	Collector
0001:8003	r	13:40:59	125	177	-	58	0001
0001:8004	r	13:41:35	125	97	-	200	0001
0001:8005	r	13:41:23	126	43	-	197	0001
0001:8007	r	13:40:51	125	93	-	60	0001
0001:800A	r	13:41:29	126	30	-	199	0001
0001:800B	r	13:43:34	125	28	+	86	0002
0001:800C	r	13:43:35	121	72	-	91	0002
0001:8011	r	13:41:17	126	96	+	255	0001
0001:8012	r	13:41:38	125	186	-	201	0001
0001:8013	r	13:43:00	123	70	-	1	0002
0001:8015	r	13:41:24	126	33	+	188	0001
0001:8017	r	13:43:58	125	12	+	92	0002
0001:801A	r	13:41:21	125	93	+	175	0001
0001:801D	r	13:41:35	125	18	-	431	0001
0001:801E	r	13:41:34	126	108	-	197	0001

S2101-2

Figure 10. Real-Time Sensor Data

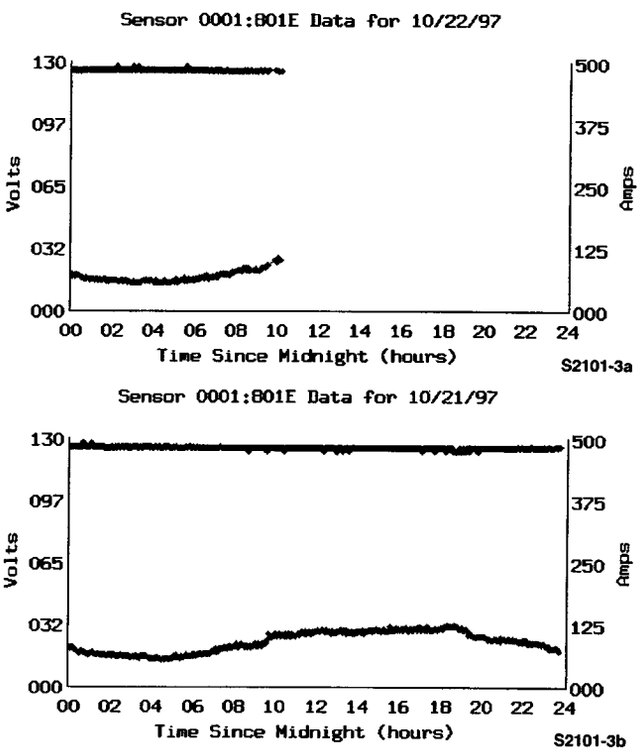

Figure 11. 24-hour Recorded Current and Voltage from a Sensor

Figure 12 illustrates an event which occurred at sensor 8004 around 1:00 AM on 10/15/97. A near instantaneous rise in current is seen at this sensor. This event is typical of the redirection of power on the underground grid due to the change-in-state of a network protector relay at a near-by transformer.

Overhead Sensor Evaluations

Following extensive laboratory testing, field tests with evaluation-level overhead sensors began in early November 1998. An evaluation overhead sensor is shown in Figure 2. These tests have

shown that the overhead sensing system can accurately measure medium voltage distribution line currents and voltages: can compute the desired power line quantities; can reliably communicate measured and computed quantities; and can be deployed efficiently by utility line technicians. Figure 13 shows the comparison of unscaled voltage measurements from the Foster-Miller sensor with unscaled voltage measurements from a nearby potential transformer. Temperature and local weather conditions are also displayed. The test shows excellent agreement between the two measurements.

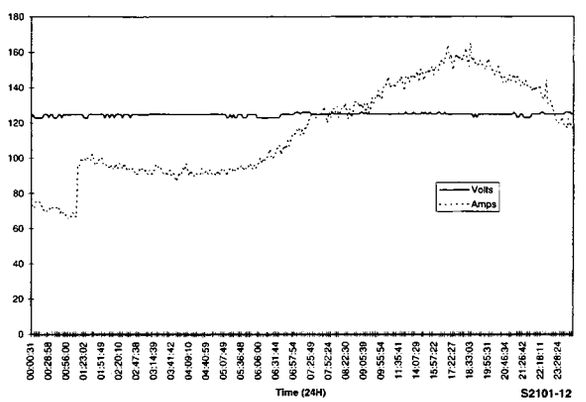

Figure 12. Sensor Measurements from the Harlem Network Tests

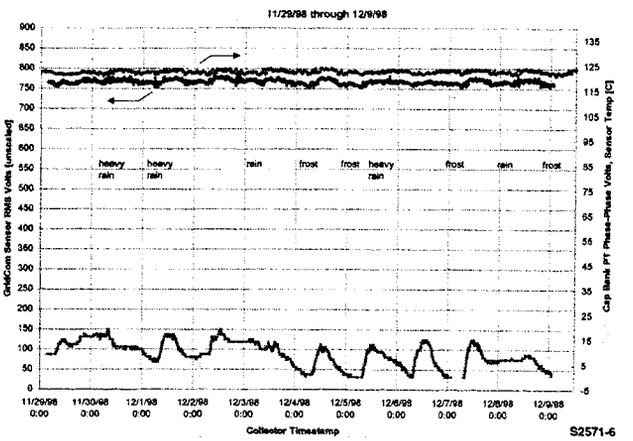

Figure 13. Overhead Evaluation Tests - Voltage

CONCLUSIONS

Versions of the Foster-Miller low voltage underground sensors have been tested by Consolidated Edison in their Battery Park City and Harlem networks. These tests demonstrated the capabilities of the sensors to monitor, in real-time, power line conditions and to detect variations in line conditions associated with circuit limiter loss, arcing faults, changes in network protector relay status and unusual changes in power flow patterns. Based on the performance of the experimental sensors, Con Edison will install GridCom sensors throughout their Hunter network with installations beginning in spring 2000.

Field tests of evaluation versions of the overhead sensors have also shown the sensors to accurately measure medium voltage distribution line currents and voltages; compute the desired power line quantities; and reliably communicate measured and computed quantities to monitoring facilities.

The Foster-Miller power line sensor systems have demonstrated the importance of moving much of the data processing and system "intelligence" from traditional central processing stations out to the actual points of sensing. This approach can improve the overall sensing system reliability; greatly reduce communications requirements; and can allow a sensing system to utilize existing communications infrastructures. Use of existing communications infrastructures can be key in providing an overall cost effective sensing system. For the electric power distribution industry these low cost, intelligent, communicating power line sensors can enable widespread real-time monitoring of distribution system health and operation.

Session 5

GIS and Remote Sensing

Chairs: J. Wilson and E. A. Johnson

The Marmara Earthquake: A View from Space
By R. Eguchi, C.K. Huyck, B. Houshmand, B. Mansouri, M. Shinozuka, F. Yamazaki, M. Matsuoka and S. Ulgen

Remote Sensing Technologies for Earthquake Damage Detection: Examples for Kobe, Japan and Luzon, the Philippines
By M. Matsuoka and F. Yamazaki

Advanced GIS Applications for Earthquake Disaster Mitigation: Development of Spatial-Temporal Information System
By S. Kakumoto, M. Hatayama, H. Kameda and Y. Oda

PURPOSE OF THE TRIP

This reconnaissance trip had three main objectives:

1. To conduct high level reconnaissance using satellite imagery, differential Global Positioning Systems (GPS), and in-field GPS-GIS interfaces
2. To validate damage information contained in early U.S. State Department Damage Maps
3. To reinforce the collaborative activities between MCEER and EDM.

The collaboration with EDM has been ongoing since the 1994 Northridge Earthquake in the U.S. and the Kobe Earthquake in Japan (1995). Both Centers have committed substantial resources to explore the use of advanced technologies for natural disaster management. The investigation of the Marmara Earthquake represents the latest collaboration between these two organizations.

The investigation team consisted of seven researchers. Owing to the diverse research interests of the two centers, the investigation team was multidisciplinary and focused on various aspects of the earthquake. The team is listed below for each center:

MCEER:

- Ronald T. Eguchi, EQE International (Team Leader)
- Charles K. Huyck, EQE International (GIS)
- Bijan Houshmand, Jet Propulsion Laboratory and the University of California at Los Angeles (Remote Sensing)
- Babak Mansouri, the University of Southern California (Radar Imagery)
- Gary Webb, the Disaster Research Center at the University of Delaware (Social Impacts)

EDM:

- Fumio Yamazaki, Tokyo University and the Earthquake Disaster Mitigation Research Center (Team Leader)
- Mashashi Matsuoka, EDM (Remote Sensing)

In addition to this research team, several Turkish companies provided invaluable support.

Collaborators in Turkey:

- Süha Ülgens, Interactive Media and Geographic Information Systems (IMAGINS)
- Serkan Bozkurt, IMAGINS
- Turgay Türker, Türker Engineering (Structural Engineering)

ITINERARY

The itinerary for the trip was established several weeks before departing for Turkey. The trip consisted of meetings with Turkish researchers and investigators, and brief field visits to several of the hardest hit areas. The details of the field visits are discussed in more detail later in this section. Provided below are brief summaries of the meetings that were held during the first two days of this trip. Table 1 summarizes the itinerary for this trip.

During our visit with Professor Mustafa Erdik at the Kandilli Observatory and Earthquake Research Center of Bogazici University, the research team was able to ask general questions about the extent of damage to Western Turkey. We found that although the earthquake was initially named after one of the cities closest to the main shock (i.e., Izmit), damage in this area was not as severe as other areas further away from the epicenter. We were told that Golcuk (located on the southern side of Izmit Bay and roughly 80 kilometers east of Istanbul) and Adapazari (located roughly 125 kilometers east of Istanbul) had experienced far more damage than the town of Izmit.

Table 1 Itinerary

Date	Meeting/Visit
9/30/99	▪ Mustafa Erdik, Kandilli Observatory and Earthquake Research Institute, Bogazici University ▪ Field Visit to Avcilar
10/1/99	▪ Tubitak: Earth Sciences Research Institute ▪ Tubitak: Space Technologies Group ▪ Field Visit to Seymen ▪ Field Visit to Golcuk
10/2/99	▪ Field Visit to Adapazari
10/3/99	▪ Field Visit to Seymen ▪ Field Visit to Golcuk

We were also shown preliminary ground motion records from this event, learning that the peak ground acceleration in Adapazari reached about 40 percent g. At the time of our visit, a number of portable instruments were being installed in order to record ground motions from large aftershocks. Before leaving this facility, the MCEER/EDM team was given a tour of the Kandilli Observatory Laboratory where we viewed other ground motion data that was being collected.

At Tübitak (a government research organization), several different meetings were held. The first meeting was with the Earth Sciences Research Institute where the team met with Dr. M. Namik Yalcin, the Director of the Marmara Research Center at the Earth Sciences Institute at

2. The ERS-1 and ERS-2 data proved to be useful once the MCEER/EDM team left the field and returned home. Although these data were available before the trip, it was difficult to process this information because of map registration problems, and because the data contained more than just image data. We are now beginning to work with these data to explore how useful they are in detecting damage through interferometric techniques. We speculate that correlation or coherence maps developed from an analysis of pre- and post-earthquake images will result in the best use of these data and could possibly detect areas where significant damage (e.g., collapsed buildings) has occurred.

3. The use of GPS equipment was essential in documenting the activities of the team. Precise coordinates were established for important damage sites. This information was crucial in relating satellite imagery data to on-ground observations. Also, when connected to the portable laptop computer, many critical analyses were possible in real-time. There was also a significant difference in results when differential GPS was available. In Avcilar, geographical coordinates were accurate to within one (1) meter. In Adapazari, where differential GPS measurements were not possible, coordinates were accurate to within 30 meters. This difference could be critical when attempting to document damage to individual buildings.

4. Having access to in-field GIS software made the documentation process extremely efficient. Many of the records – such as the Adapazari survey – would not have been possible had it not been for the GPS-GIS setup. The actual survey that was discussed in the previous section took less than 4 hours. If paper maps or other manual methods of documenting damage had been employed, it would have taken at least several days to accomplish what was done in half a day using these new mapping technologies.

5. One important piece of equipment – which was used by investigation team members for the first time – was a digital camera. The advantages to using such a camera is that the images that are taken are immediately viewable, they can be downloaded immediately for transmission to some other site, and when connected to a GPS unit (which was not done on this trip), could produce more reliable documentation of an event.

ACKNOWLEDGMENTS

The MCEER/EDM team would like to acknowledge the Multidisciplinary Center for Earthquake Engineering Research for its generous support of this investigation. In addition, we would like to thank the following individuals and organizations for their help in making this a unique and productive trip. Without this support, many of the activities mentioned above would not have been possible.

- Dr. Betlem Rosich, ESA/ESRIN
- Mr. Serkan Bozkurt, IMAGINS
- Mr. Turgay Türker, Türker Engineering
- Professor Mustafa Erdik, Kandilli Observatory
- Dr. M. Namik Yalcin, Tübitak
- Dr. Semih Ergintav, Tübitak

- Dr. Hülya Yildirim, Tübitak
- Mr. Ismail Baris, Mayor of Gölcük
- Mr. Larry Roeder, U.S. State Department
- Dr. Charles Scawthorn, EQE
- Ms. Hope A. Seligson, EQE

Remote Sensing Technologies for Earthquake Damage Detection: Examples for Kobe, Japan and Luzon, the Philippines

Masashi Matsuoka[1] and Fumio Yamazaki[2]

[1] *Chief Research Engineer, Earthquake Disaster Mitigation Research Center, RIKEN, Japan.*
[2] *Team Leader, Earthquake Disaster Mitigation Research Center, RIKEN, Japan.*

Abstract

Several satellites have on-board optical sensors and/or synthetic aperture radar (SAR), with which the Kobe area before and after the 1995 Hyogoken-Nanbu (Kobe) earthquake in Japan was observed. Since a part of the damage survey results of this earthquake is maintained as GIS data, a quantitative analysis on the surface changes in the damaged areas is possible. In this paper, pixel values in the images, such as the digital number, intensity and phase information of the area damaged by the earthquake, were investigated using Landsat and JERS images taken before and after the earthquake to examine the possibility of extracting earthquake damage distribution by satellite remote sensing. According to the difference in the pixel values from the pre- and post-event images, we found that the spectral characteristics and backscattering property of damaged areas exhibit significant variation. We further demonstrated an example of ground settlement due to the 1990 Luzon, Philippine earthquake detected from satellite optical sensors.

INTRODUCTION

To gather information on damage due to natural disasters, several methods exist, such as field survey, aerial videography and photography, and satellite imagery. Satellite remote sensing, by which a large area is easily monitored, may provide effective information at the time of recovery activity, e.g., developing a restoration plan, if it is possible to determine the distribution of damage due to disasters at an early stage. Several satellites observed the Kobe area before and after the 1995 Hyogoken-Nanbu (Kobe) earthquake, which occurred on January 17, 1995 (Sudo et al., 1995). Multispectral characteristics were different between the images of liquefied areas and burned areas taken by airborne remote sensing just after the earthquake occurred (Mitomi and Takeuchi, 1995). A study (Inanaga et al., 1995) suggested the possibility of interpreting the damaged area based on the spectral pattern changes between optical satellite images taken before and after this earthquake.

Synthetic aperture radar (SAR) observations can be performed night and day and are not influenced by weather conditions. This feature could be useful for effective postdisaster damage assessment when optical remote sensing, such as multispectral scanning and aerial photography, or a field survey for a large area is difficult. Earth observation satellites equipped with SAR, containing information on the amplitude and phase of microwave backscattering from the objects on the earth's surface, observed the areas hit by recent damaging earthquakes. Massonnet et al. (1993) introduced a SAR interferometric analysis using phase information to estimate the distribution of ground displacement due to the 1992 Landars earthquake and Ozawa et al. (1997) applied the same technique for the Kobe earthquake. For the estimation of building damaged areas, studies on interpreting damage distribution due to the Kobe earthquake were reported using ERS/SAR amplitude information (Yonezawa and Takeuchi, 1998a) and phase information (Yonezawa and Takeuchi, 1998b). The approach to use the phase information, which is more

sensitive than the intensity value, could reproduce a good relationship between the damaged area and phase information using JERS/SAR images (Rosen et al., 1999).

Applications of satellite remote sensing to identify the damaged areas were attempted, but no quantitative approach was found for examining the relationship between the spectral characteristics and backscattering properties of the damaged area using satellite images and detailed damage survey results. Since a part of the damage survey results of the Kobe earthquake was maintained as GIS data, a quantitative analysis of the surface changes in the damaged area is possible. In this paper, the spectral characteristics from Landsat and the amplitude of backscattered echoes from JERS/SAR of the damage due to this earthquake were investigated. We also examined the coherency from interferometric analysis using JERS/SAR images obtained at different acquisitions.

According to the Kobe study, we found that the difference in the pixel values from the pre- and post-event images relates to the surface changes due to the earthquake. We further demonstrated an example of ground settlement due to the 1990 Luzon, Philippine earthquake detected from satellite optical sensors.

THE 1995 KOBE, JAPAN EARTHQUAKE

Earthquake Damage Survey Data

Liquefaction and building damage were focused on as forms of earthquake damage in this study. Sand deposits boiled by the earthquake were digitized by the authors on the 1/50,000-scale ground-failure survey map (Hamada et al., 1995) and used as liquefied area data. The building damage data based on detailed survey results compiled by AIJ (the Architectural Institute of Japan) and CPIJ (the City Planning Institute of Japan), and digitized by BRI (Building Research Institute, Ministry of Construction) were utilized as GIS data. In the GIS data, the building damage level was classified into five categories: damage by fire, severe structural damage, moderate damage, slight damage and no damage, and the number of damaged buildings was totaled for each city block of the city (Building Research Institute, 1996).

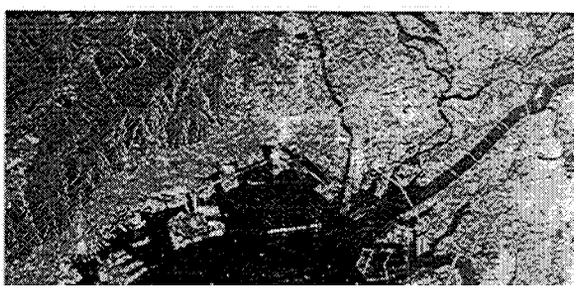

Fig. 1 Intensity image of JERS/SAR taken after the Kobe earthquake

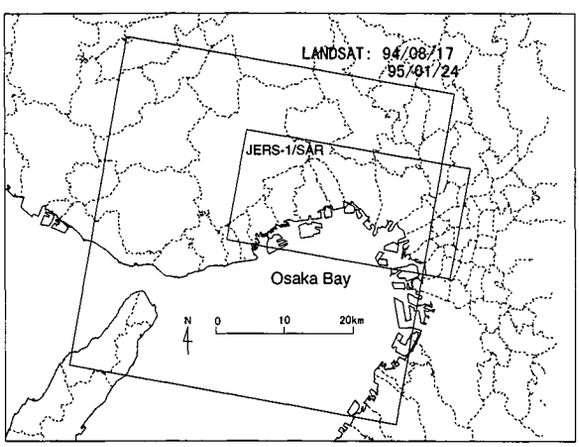

Fig. 2 Area of Kobe study

Satellite Data

In this study, we prepared several satellite images taken after the Kobe earthquake. The Landsat/TM, which is an optical sensor, was used to observe the area of interest on January 24, 1995. Because the sensitivity of the sensor equipped on the SPOT satellite is low to detect earthquake damage in spite of its spatial high

resolution (Matsuoka and Yamazaki, 1998), the SPOT image was not used in this study. We used the images taken on August 17, 1994 by Landsat for the data before the earthquake, and aimed to examine the change in the spectral characteristics of the damaged area. We used the JERS/SAR image observed on February 5, 1995, 20 days after the Kobe earthquake, and also used five pre-event images taken on September 8, 1992, October 22, 1992, May 30, 1993, November 22, 1993 and February 18,1994 to examine the change in the backscattering characteristics of the damaged area. SAR systems have the capability of recording complex signals including the amplitude (intensity) and phase of backscattered echoes from the objects on the earth's surface. We obtained complex signals using a processing software from SAR Level 0 signal data (Ono and Yamanokuchi, 1997). The backscattered intensity image taken after the earthquake and the area covered by the satellite images are shown in Fig. 1 and Fig. 2, respectively.

OPTICAL IMAGE CHARACTERISTICS OF THE KOBE ERATHQUAKE

Registration and Geometric Correction

Because the digitized values in the satellite images were different depending on the observation and surface conditions, digital number (DN) normalization is required before starting this study. The characteristics of the reflection of electromagnetic waves from the surface differ depending on the observation season, because the altitude of the sun, the strength of sunlight and distribution of vegetation are variable. One common technique to eliminate this influence is the band ratioing, which is defined as the ratio of the DN of each band to the DN of a reference band (Campbell, 1996). We calculated the normalized DN (NDN) based on the band ratioing using band 6 as a reference band. The pre- and post-event images, from which the NDN values were calculated, were subjected to the affine geometric correction using ground control points (GCP) and were registered. The correlation coefficients between the two sets of images were calculated using a 5 x 5 pixel-window filter, and were also used as characteristic indices.

Spectral Characteristics of the Damaged Areas

First, clouds and cloud shadows covering the area were removed using proper threshold values of several spectral bands in order to select pixels in the damaged areas, for an accurate analysis using the Landsat images. Areas with vegetation were also excluded from these images, based on the normalized difference vegetation index (NDVI), because the reflection characteristics of the leaves of plants differ seasonally.

The pixels that represent the areas of liquefaction, burning, and heavy damage, slight damage and no damage of buildings were selected from the images to examine the characteristics of DN in the earthquake-damaged area. The liquefied class contained pixels included in the liquefaction data. The pixels for the burned class were selected from the city blocks where all buildings burnt down. Pixels were also selected from the city blocks where all buildings were determined to have severe or moderate structural damage and slight damage, and categorized into heavy and slight damage classes, respectively. The nondamaged class includes the pixels of buildings that show no exterior evidence of damage according to the field survey data.

The ratios of mean values of the NDN in the post-event and pre-event images for the classified damaged areas are shown in Fig. 3. Like the liquefied area, the ratio is high for all bands. For the burned area, the ratio in the blue-light range of band 1 was especially low in comparison with the nondamaged area. These results are in good agreement with those of the damage survey performed by airborne multispectral scanner remote sensing (Mitomi and Takeuchi, 1995). The ratio in the

heavy damage area, which was similar to that in the liquefied area, did not greatly differ from the values in the nondamaged area.

The ratio of the NDN in the liquefied area was high in the range from the visible to mid-infrared bands because of the higher reflectance of sand than the surface of asphalt. It is also conceivable that the ratio was raised in infrared bands in the heavy damage area due to the exposure of soil under mud walls and roofing tiles upon the collapse of old wooden dwellings.

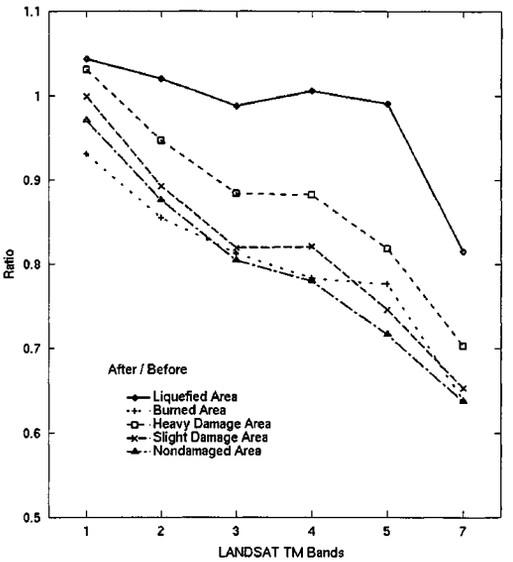

Fig.3 Ratio of digital numbers of Landsat/TM bands for damaged areas before and after the earthquake

SAR IMAGE CHARACTERISTICS OF THE KOBE ERATHQUAKE

Registration and Geometric Correction

We overlaid the sets of two SAR images and calculated the complex coherence, which is described in the next section, for the area of the 7 x 7 pixel window around the initial position. Then matched positions were shifted pixel by pixel within the 15 x 15 pixel window to find the position at which the two images match best. By this procedure, the optimum pixel pair was determined at the position that yields the highest coherence and used to match all SAR images using the nearest neighbor transformation. The pixel pairs were also used as a ground control point (GCP) for the affine geometric correction to overlay SAR images with the damage survey data.

Interferometric Analysis

The coherence, which is the correlation calculated from the phases of the backscattering echoes of two co-registered complex SAR images, is a suitable and sensitive parameter for change detection and land use classification. The complex coherence γ of two complex signals z_1 and z_2 is defined in equation (1) for N signal measurements,

$$\gamma = \frac{\sum_{i=1}^{N} z_{1i} z_{2i}^{*}}{\sqrt{\sum_{i=1}^{N} |z_{1i}|^2} \sqrt{\sum_{i=1}^{N} |z_{2i}|^2}} \quad , \qquad (1)$$

where i is the sample number. This approach is usually adopted between two co-registered complex images acquired under slightly different geometrical configurations. However, decorrelated areas exist in the coherence image. The main sources of decorrelation are spatial and temporal decorrelation. The spatial decorrelation is derived from the difference in the geometry of observation between two acquisitions, which is called baseline length B, as shown in Fig. 4. The temporal decorrelation is related to an atmospheric effect such as moisture and/or surface changes in two acquisitions.

The time intervals and the baseline between two observations in our dataset are listed in Table 1. Four pairs were selected to calculate the degree of coherence and N is defined as 81 pixels in

under the condition of a long baseline. Generally, because superficial changes may occur during a long time interval between two acquisitions, the coherence becomes low. The relationship between the coherence of nondamaged areas and the value of the baseline length times the time interval is shown in Fig.6 (b). As the value increases the coherence becomes low, which is in agreement with the recent studies. It is considered that the long baseline brought about the decorrelation and low sensitivity of pair-A2 in spite of a short time interval.

From the pair of pre-event images, we observed small differences of coherence in each damage class in pair-B1. However, there is quite a large variation in pair-B2 with a very short baseline. We currently lack definite information on this result and a further investigation is necessary to identify coherency characteristics in an urban area. However the degree of coherence shows that it is possible to capture changes such as building damage from SAR images in spite of a large standard deviation observed in each damage category.

THE 1990 LUZON, PHILIPPINE EARTHQUAKE

Ground Subsidence and Satellite Images

The Luzon, Philippine earthquake on July 16, 1990, shook an area of approximately 20,000km^2, caused extensive liquefaction in the area along Lingayen Gulf. Because of liquefaction-induced lateral spreads and land subsidence, several villages, such as Narvacan and Alaska, sunk into the sea after the earthquake. Figure 7 shows photographs of Narvacan village taken 1 month after the earthquake at low tide and 9 years after at high tide, respectively. The village has completely sunk into the sea in the recent picture although the effect of the tidal level in this area is significant.

In this study, the SPOT/XS, which is an optical sensor, observed the area of interest on March 27, 1991. Although the post-earthquake image was taken 8 months after the event, basic evaluation is possible on the potential of satellite remote sensing to detect affected areas. A pre-event image (March 29, 1987) and one more post-event image (on March 6, 1994) were used to identify the surface change caused by the earthquake. We determined to select SPOT high-resolution images in spite of its low sensitivity because the damaged area exists locally. The target area covered by the SPOT images is shown in Fig. 8.

(a) Photograph taken on Aug. 20, 1990

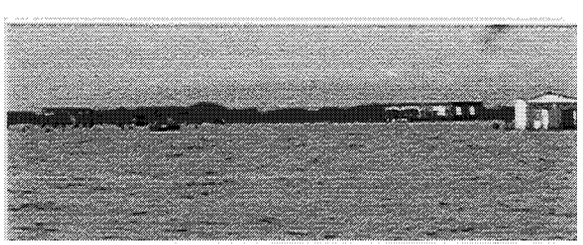

(b) Photograph taken on June 29, 1999

Fig. 7 Narvacan village at two time periods after the Luzon earthquake

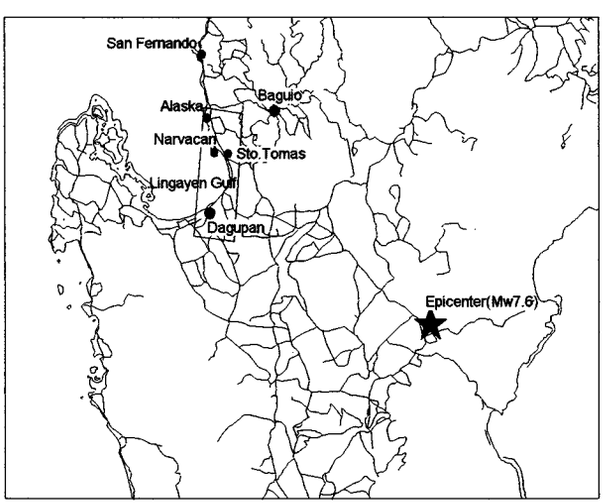

Fig. 8 Area of this study
(Rectangle indicates area for SPOT/XS)

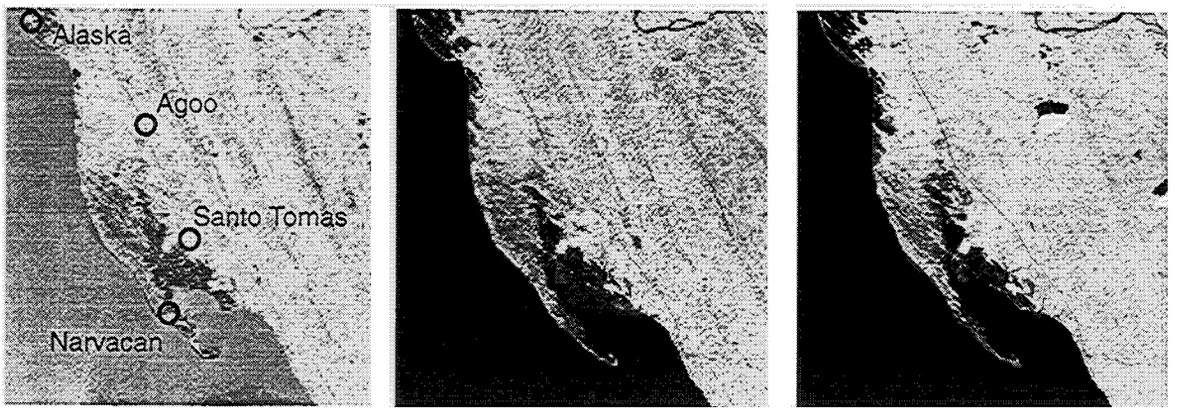

(a) Image on 3/29/1987 (before) (b) Image on 3/27/1991 (after) (c) Image on 3/6/1994 (after)

Fig. 9 SPOT/XS band 3 images of Santo Thomas area before and after the Luzon

Though the correction of the DN is necessary to compare satellite images of different acquisitions, it was omitted in this case because the images were taken in the same season. The zoom-up images of the surrounding of Santo Thomas on the three acquisitions are shown in Fig. 9. The form of a sand bar is observed to become thinner in Fig. 9 (b) and (c), which were taken after the earthquake, in comparison with Fig. 9 (a), taken before the event. Narvacan and Alaska villages, which were located in the middle and in the northern part of the sand bar, respectively, are depicted in the pre-event image shown in Fig. 9 (a).

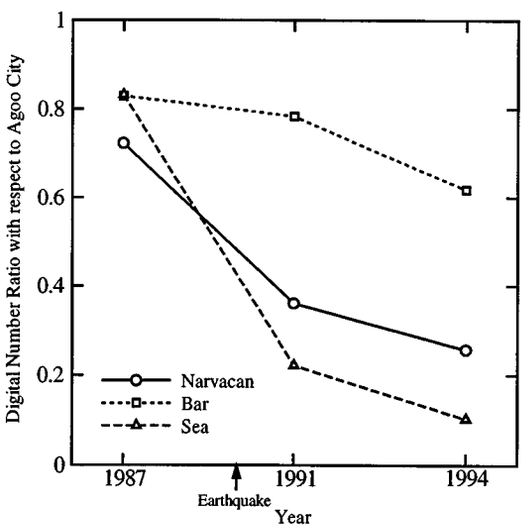

Fig. 10 Changes in the digital number ratios of SPOT/XS Band 3 for the selected areas

Characteristics of Digital Number in the Damaged Areas

The pixels that represent the areas of Narvacan village, the sand bar near Narvacan village and sea were selected from the three images to examine the characteristics of the DN in the damaged or nondamaged areas. The mean DN of ratio with respect to Agoo City for the selected areas before and after the event is shown in Fig. 10. In this figure, the ratio values for the selected areas are almost the same level before the event in 1987. The ratio value in Narvacan became much smaller than that in the sand bar after the event in 1991 and almost equal to the value in the sea. The same trend was observed in the image of 1994. Thus it may be concluded and verified from the satellite images that the area of Narvacan sunk into the sea due to the 1990 Luzon earthquake.

CONCLUSIONS

Using satellite images, this paper reported the quantitative evaluation on the spectral characteristics and the backscattering properties of the areas damaged by the 1995 Kobe earthquake, to examine the possibility of capturing earthquake damage distribution. In the Landsat optical images, the digital numbers of liquefied areas were high in the range of visible to mid-infrared bands, whereas those of burned areas became low in the visible light range. The heavily damaged area showed a trend similar to that of the liquefied area. The relationship between the building damage level and the satellite SAR images was found to show a clear trend; as the damage level increases, the ratio of backscattered intensity, the correlation and the complex coherence of the pre- and post-event images become low. In case of the 1990 Luzon earthquake, the areas of Narvacan and Alaska villages were found to sink into the sea area after the event, based on the comparison between the pre- and post-event images from SPOT satellite. In spite of these results regarding the mean characteristics of satellite images, a large degree of randomness still exists in each damage category. Hence, a further study is necessary until a practical use of satellite images for an earthquake damage detection is realized.

ACKNOWLEDGMENTS

We thank Prof. Saburoh Midorikawa of Tokyo Institute of Technology and Ms. Asako Inanaga of Remote Sensing Technology Center of Japan (RESTEC) for their helpful advices and the staff of Philippine Institute of Volcanology and Seismology (PHIVOLCS) for the cooperative survey and research. We also thank Mr. Ronald T. Eguchi of EQE International, Inc. for his helpful advice on detecting earthquake damage of man-made structures based on the interferometric approach. The Landsat, SPOT and JERS images used in this study are owned by Space Imaging EOSAT, SPOT Image and Ministry of International Trade and Industry (MITI) and National Space Development Agency of Japan (NASDA), respectively. These images are used in cooperation with NASDA. JERS/SAR image processing was conducted using the programs coded by Mr. Makoto Ono of RESTEC.

REFERENCES

Building Research Institute (1996). *Final Report of Damage Survey of the 1995 Hyogoken-Nanbu Earthquake* (in Japanese).

Campbell, J. B. (1996). *Introduction to Remote Sensing*, Taylor & Francis.

Hamada, M., Isoyama, R. and Wakamatsu, K. (1995). *The 1995 Hyogoken-Nanbu (Kobe) Earthquake, Liquefaction, Ground Displacement, and Soil Condition in Hanshin Area*, Association for Development of Earthquake Prediction.

Inanaga, A., Tanaka, S., Takeuchi, S., Takasaki, K. and Suga, Y. (1995). "Remote Sensing Data for Investigation of Earthquake Disaster", *Proceedings of the 21st Annual Conference of the Remote Sensing Society*, pp.1089-1096.

Massonnet, D., Rossi, M., Carmona, C., Adragna, F., Peltzer, G., Fiegl, K. and Rabaute, T. (1993). "The Displacement Field of the Landars Earthquake Mapped by Radar Interferometry", *Nature*, 364, pp.138-142.

Matsuoka, M. and Yamazaki, F. (1998). "Identification of Damaged Areas due to the 1995 Hyogoken-Nanbu Earthquake Using Satellite Optical Images", *Proceedings of the 19th Asian Conference of Remote Sensing*, pp.Q9/1-6.

Mitomi, Y. and Takeuchi, S. (1995). "Analysis of Spectral Feature of the Damaged Areas by

Liquefaction and Fire Using Airborne MSS Data", *Proceedings of the 18th Japanese Conference on Remote Sensing*, pp.117-118 (in Japanese).

Ono, M. and Yamanokuchi, T. (1997). "Image Reconstruction of JERS-1 SAR Data with PC or EWS", *Proceedings of Joint Earth, Planet and Space Meeting*, p.298 (in Japanese).

Ozawa, S., Murakami, M., Fujiwara, S. and Tobita, M. (1997). "Synthetic Aperture Radar Interferogram of the 1995 Kobe Earthquake and Its Geodetic Inversion", *Geophysical Research Letters*, Vol. 24, No. 18, pp.2327-2330.

Rosen, P. A., Hensley, S., Peltzer, G. Rignot, E. and Werner, C. (1999), "JERS-1 Synthetic Aperture Radar Interferometry Applications, - Mapping of Rain Forest Environment and Crustal Deformation Studies", *JERS-1 Science Program '99 PI Reports, Global Forest Monitoring and SAR Interferometry*, Earth Observation Research Center, NASDA, pp.179-184

Sudo, N., Tada, T., Nakano, R., Cho, K., Shimoda, H. and Sakata, T. (1995). "Multi Stage Remote Sensing on the Great Hanshin Earthquake Disaster Survey", *Proceedings of the 18th Japanese Conference on Remote Sensing*, pp.115-116 (in Japanese).

Yonezawa, C. and Takeuchi, S. (1998a), "Detection of Damaged Built-up Areas by the 1995 Hyogoken-Nanbu Earthquake Using ERS-1/SAR Intensity Images", *Photogrammetric Engineering and Remote Sensing*, Vol. 37, No. 4, pp.57-61 (in Japanese).

Yonezawa, C. and Takeuchi, S. (1998b), "Change Detection of Backscattering Characteristics on the Ground in SAR Imagery - Comparison between Intensity and Coherence -", *Proceedings of 24th Japanese Conference on Remote Sensing*, pp.119-120 (in Japanese).

Herein, the requirement to share information is viewed from the point of collecting information from objected region. As the data about individual privacy is involved in the citizen's information used in local government, this will become a disadvantage if all geographic information is shared.

The data sharing method can be break down into 3 categories, based on characteristics of the geographic information as shown in figure 3.

1) Data sharing method for like the case of inside in the local government
   Intra-net is suitable to share common geographic information, which make exchanging and sharing updated data possible with keeping securities of individual attribute data.

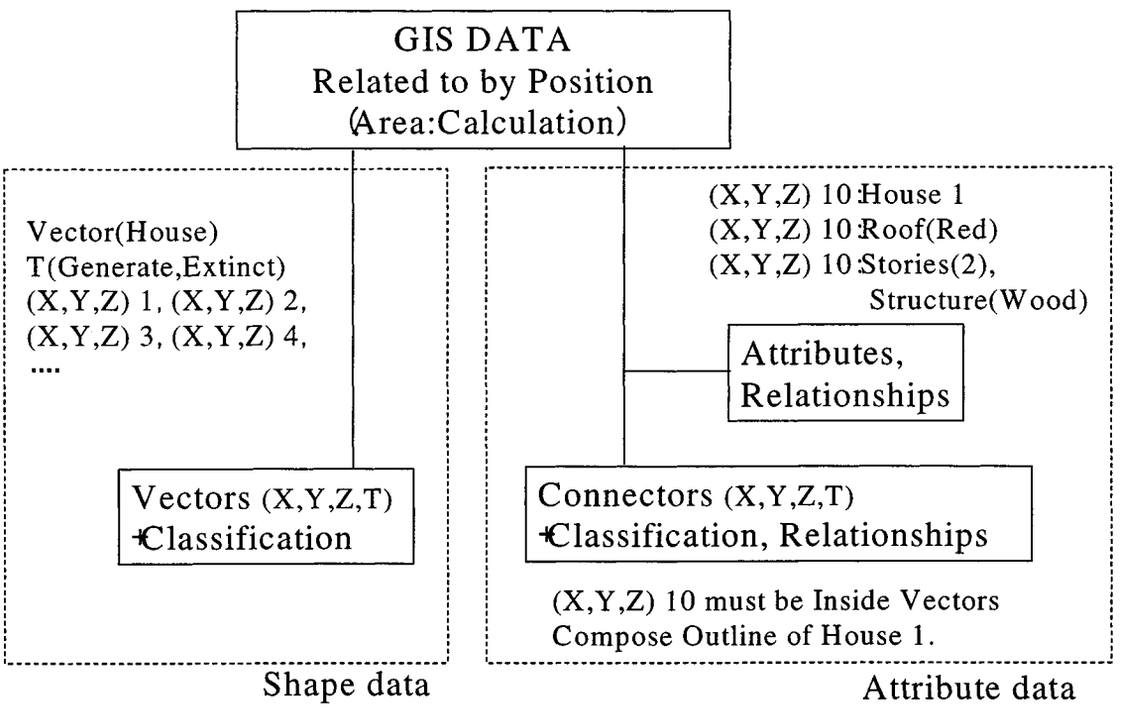

Figure 2 Data description with shape data and attribute data

Geographic information has to manage as spatial temporal data to keep consistency in relationship between objects and attributes. Update data can be used in different division soon after the change has made at the division where responsible to data maintenance.

2) Data sharing method for utilizes unspecified user
   Internet is suitable to exchange geographic information that is opened to public. Here, treatment of geographic information of basis that is made based on surveying and attached attribute data has to be differentiated. Update has to be done more carefully with basis information than attached attribute data. Objects or features described as geographic information of basis has to manage as spatial temporal data to allow combining attribute data with keeping consistency.
3) Data sharing method for specific purposes such as a car navigation system
   Geographic information suitable to the application is combined together into a unit and stored in such as CD-ROM or DVD. These data are provided with application system or can be purchased at a store, similar to music CD. Update data can be provided as log data of changes by telecommunication or Internet. Latest information such as point of interest can be also distributed same way. Spatial temporal data management is also necessary to allow combining additional data or deleting data.

4. Sharing data via Network

Network is effectively applicable for geographical information to share information. However it is needed to meet the characteristic of geographical information and its purpose. For the basic data of geographical information, the specific data is normally used repeatedly and for long period. Therefore it can increase its usability by capturing and storing the data previously into user's information systems.

The updated data and attribute information as required is obtained via Internet, thereby it requires for the data to be capable of location matching. Relating the representative points represented by the location of topological space with respective information, it will be possible to make relationship with information. In that case, it is expected to enhance the accuracy of locating by using the same basic data. It is essential to be capable of time

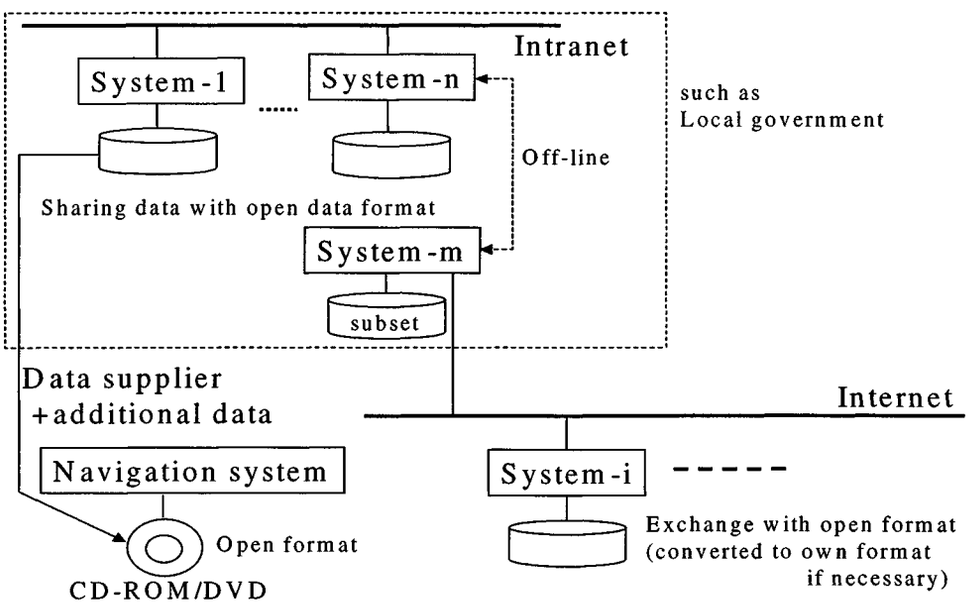

Figure 3 Data sharing with open format data

matching by relating it with respective information. So it is needed to keep the information using the location of spatial temporal information which is integrated with the location of, topological space and time. For the location of time, it is important to keep the information whether the target object exists or not. The criteria of the accuracy as a location information of topological space are basically to be within allowable deviation. In considering homogeneous polygon, it makes it easier to decide whether it exists within the allowable range on the corresponding lines and points, so it can avoid making uncertain decision.

It is rather needed for shared geographical data to be stored in each system than to download from servers very often. In this case, the data exchange should be made in the specified standard open format. In terms of its efficiency, it is better to convert the data into original format only when it's necessary. If this open format is suitable enough for execution, it can be used for application program directly without modification. It also makes it possible to realize the structure easier for open format data such that has been considered at the ISO/TC211.

5. Exchange Information through Network

When natural disaster happened in urban area, spatial data of the area just before disaster and information of damages are needed for analysis and decision making to support rescue and planning for recovery. Here, a local government manages latest spatial data of the area which is mainly used for connecting and visualizing regional attribute data such as address, house number, structure of building and so on. On the other hand, latest specialized systems for analyzing disaster or simulating the situation of damage are usually managed and updated by special research organization or consultant companies (Data analysis center) where regional information is not managed.

When disaster happens, latest spatial information and specialized system has to be combined as soon as possible. There are three possibilities,

1)Local government where latest regional data is managed prepares specialized system.
Weak points are difficulty of updating the system to latest version and make officer to operate sophisticated system in confusion by disaster.

2)Data analysis centers where keeping latest system for analysis keep latest regional data.
Weak point is centers, which are responsible for analyzing hardly gather all regional data of latest.

3)Exchange spatial through network when regional data has to be analyzed.

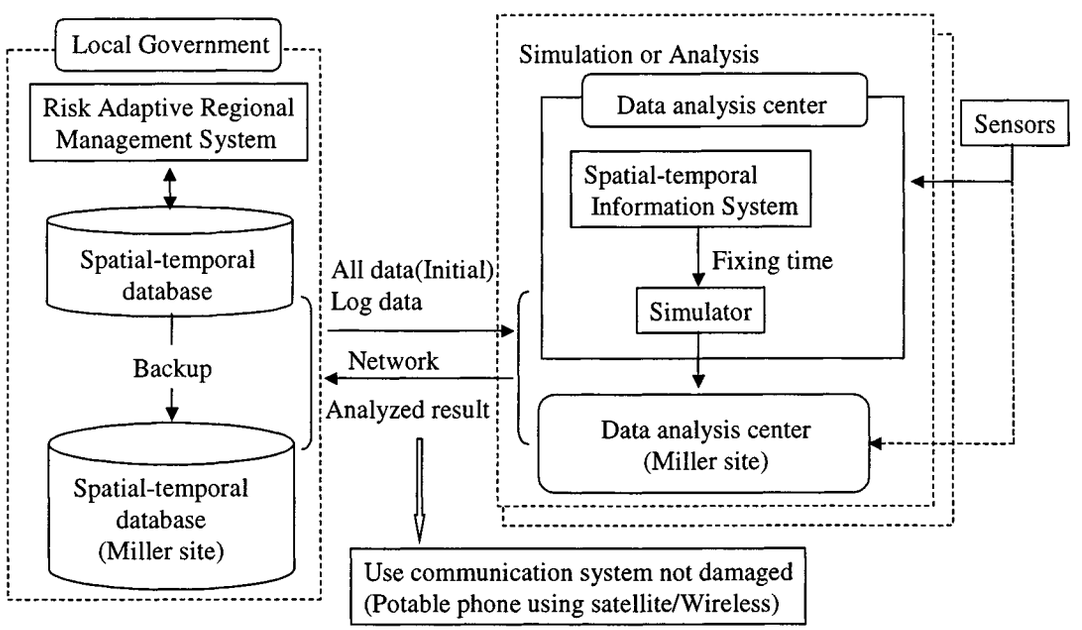

Figure 4 Exchanging disaster information using Spatial-Temporal Information System

This is realistic way however mechanism to avoid breaking down when local government and/or data analysis center.

Figure 4 shows a structure of exchanging disaster information. To avoid problem pointed above, using miller sites is proposed. At the beginning, all regional data has to be sent from local government or it's miller site to the data analysis center. Disaster information is sent occasionally as temporal data by log data form or difference data. Fixing time in a

spatial-temporal data-handling unit carries out simulation or analysis for spatial data without temporal data treatment function.

Reference

[1]Kakumoto et al 'Occasional Data Update and Data Sets Unification using Spatial-temporal Data with Implicit Topology Description': Proceeding of DMGIS'99 at Beijing (1999)

[2]Kakumoto et al 'Disaster Management through Normal-Service GIS based on Spatial-Temporal Database': Proceeding of GIS'99 at Vancouver (1999)

[3]Hatayama et al 'Development of Rescue Support System and its Application to Disaster Drill in Nagata Ward, Kobe City': Proceeding of GIS'99 at Vancouver (1999)

Appendix A

Workshop Discussions

Discussion Session One
Chairs: W. Hayes and D.J. Inman
Minutes of the Forum Session - Day One
By A. Smyth

Discussion Session Two
Chairs: L. Lund and A. Zeizel
Minutes of the Forum Session - Day Two
By L. Graham

A.1. MINUTES FROM DAY ONE
March 2rd, 2000

Discussion Session
Chairs: W. Hayes and D. J. Inman

Discussion in the afternoon session was conducted by providing commentary on each of the talks given throughout the day. A summary of the comments is provided below, for each of the papers:

G. C. Lee:
The focus on response to user's needs in this work, as opposed to generating a new technology and subsequently fitting it to an application, was seen as a very positive aspect of this paper. There was further agreement that there is too much emphasis on devices, in that researchers create a device and then apply it. A more rational process is to identify the needs of the structure and then create a device to address this need.

I. Juran:
The author suggested that contractors should be responsible for the performance of their system, not for meeting a set of design criteria. This was well received by the group, as this would encourage contractors to take more interest in new technology and using them to find better ways to address the performance needs of geotechnical systems. It was also suggested in discussion that better publicity of the issues in earthquake engineering is needed, in order to generate more support for exploring this area.

M. Feng:
The audience enjoyed many aspects of this work, including that it is quite "avant garde" in this field, and that the column jacket retrofitting technology has the capability to be applied to a wide range of systems, such as pipelines. Further, the work incorporates interdisciplinary researchers, industrial partners, and government agencies. By getting this full range of engineers involved at the early stages, the technology is more likely to be adopted in practice. The interdisciplinary nature and wider applicability of the research generated discussion of the need to break down barriers between Civil Engineering and other disciplines. There exists a need to develop an approach to such new areas in the framework of the technology, not in the framework of specific disciplines. It was further pointed out that Civil Engineering researchers will need to continue to expand their work in this way, or risk losing students to more challenging and relevant fields. The major need of this work that was cited by the group was addressing how the technology would be implemented in practice.

Y. Shimizu:
This work was praised extensively for its aggressive advance in the state of the art in implementing sensor technology in gas pipelines. Some of the issues that arose in discussion were the need to try combining networks for gas with those for water,

electric, or other lifelines, rather than leaving each industry to take care of its own technology. Such a combination would generally require a consortium of members from each of these industries, as well as a full understanding of the legal implications of sharing the sensor data. Finally, it was suggested that the authors provide some economic analysis of this work. This would help the group to address important economic issues when requesting resources for earthquake engineering research.

M. Shinozuka:
The audience applauded the fact that the researchers addressed the social, economic, and planning aspects of this work, as this is the best way to get policy makers involved and interested in this work. The other issue in getting these policy makers involved is to demonstrate the feasibility of using this reverse engineering in the decision-making process. A positive aspect of the research is that it is very cost-effective, which will be attractive in developing policy. It was suggested that we begin including social scientists in this research at this stage, in order to help provide incentives to move this discipline forward. Finally, one member of the audience suggested that PEER and PG&E are performing tests to obtain fragility curves for transformers, which may be of interest to these researchers.

R. Ghanem:
All agreed that this is a young technology that has tremendous promise for the future. SAR has distinct advantages in that it can penetrate clouds and that it has improved resolution over traditional aerial photography. It is important that the integration of this technology with land-based technology be addressed. It was further pointed out that this work has great potential to direct emergency response and relief; FEMA's distribution of resources after the Northridge earthquake was proposed as an example of how there is room for improvement in this area.

C. H. Loh:
The use of data from the Chi-Chi earthquake was seen as an excellent example of how quickly we can gather information from an earthquake to demonstrate the benefits of new technology. Further, the data obtained from this earthquake provides a great opportunity to perform "blind tests" to check bridge and structural damage. It was suggested that the authors add comments regarding the benefits and economic costs of this technology.

T. Sato:
This work is extremely challenging, and the audience agreed that there exists a need to address the complexities of controlling non-linear structures. The group also appreciated that this research addressed prevention of earthquake hazard, as much of the current work is focussed on response to earthquake hazard. This work clearly fills an important purpose in this area. Some suggestions were to indicate results that can be used for disaster mitigation and how they can be used. The author indicated that the results can identify damage time during the earthquake and that they can identify the weak point of the structure.

A.2. MINUTES FROM DAY TWO
March 3rd, 2000

Discussion Session
Chairs: L. Lund and A. Zeizel

These minutes are organized based on the comments on each paper:

On Mizushina Paper

Shinozuka was very interested in the collection of data from the customer meters. From the viewpoint of SCADA, Shinozuka wanted to know if it was truly a SCADA.

Mizushina acknowledged that he neglected to describe how his data collection system fits into the SCADA system.

Wiesman pointed out that the AMR (Automatic Meter Reading) community deals with similar issues raised in the paper. He listed several companies that have experience in the AMR. He also mentioned that SCADA has a lot of similarities with the AMR concept. AMR has traditionally been involved in this for revenue collection, and that the author should investigate similarities.

Lund: asked how the Hamamatsu experiment was organized.

Mizushina explained that his organization is called TAO (Telecommunications Adv. Organization). The Japanese Ministry of Post and Telecommunications invites proposals for new applications in telecommunications. They funded this 5 years ago. There are 30 similar research centers funded by the Ministry of Telecommunications.

Zeizel wanted to know if this system would be applicable in other cities.

Mizushina still hasn't finished in Hamamatsu, so agencies have not been fully convinced.

Shinozuka wonders how they enticed customers to install the devices.

Mizushina says that this was not a big problem.

McDaniel Paper:

Lund: wanted to know about the time frame, staffing, organization, etc. of enhanced system.

McDaniel: wanted to simplify administrative organization. Three staff members are required to run servers and provide support and the same applies to instrumentation mechanics. Funding for the first phase will come out of savings from cancelled upgrade to the old system. It is a $5 million project spread out over 5 years.

Zeizel wanted to know if other hazards were considered.

McDaniel hasn't had much of a problem with debris flow or flooding. However, wind storms have been a problem. He is looking into wireless communication for the system. Large open reservoirs in the Santa Monica mountains are getting by-pass pipelines so this would avert problem with mudslides into reservoirs.

Lund wondered about the conservation elements of the emergency plan.

McDaniel expects a 70% reduction of water for short periods of time if there is a trunk line break.

Nakao Paper: (Nakao was not present for discussion)

Shinozuka mentioned that Nakao indicated that SCADA was very useful during the Northridge earthquake, but wasn't clear on how (in some concrete ways).

McDaniel believes the system isn't that capable of control. But managers can see the whole system.

Zeizel: wanted to know about the interface between water and power needs.

McDaniel said that there is already coordination. This is done by a radio and telephone system.

Wiesman Paper:

Zeizel: wondered about the collocation of different types of utilities.

Wiesman said that older infrastructures were not planned well (rather haphazardly). If one is building a new infrastructure, then one could plan SCADA systems etc. to be collocated. Funding limits rate of progress.

Eguchi Paper:

Lund asked regarding liquefaction in Turkey whether ground water maps can be incorporated in order to focus areas.

Zeizel: thinks that there should be a lot of on-ground verification.

Eguchi thinks that Ghanem's work is valuable. Believes that the repeat pass time is a problem which is very important ... can be overcome with additional satellites.

Shinozuka notes that SAR is just one technology. Notes that "Data Fusion" is still important. DOD technology may help (XPATCHT). This allows any resolution in simulation. This tells you what your requirements must be for damage detection.

Zeizel said there should be a linkage between us and DOD.
Hayes mentioned that one should contact Darryl Heard at USGS on this point.

Bardet: mentions that the military was used for the Turkey reconnaissance trip. They were given estimates of casualties. He calls for midrange technologies (i.e. not too close and not too far away).

Eguchi mentioned that airborne systems would be good. The SAR data is from airborne source. LIDAR also gives better resolution, but is very expensive.

Bardet said that he agrees that "Before" pictures should be of better resolution so that good comparisons can be made.

Craig Davis wanted to see if any baseline studies have been done, i.e. have 2 photos been compared with no damage.

Eguchi mentioned that a good example was a study of Las Vegas area that studied the population growth. Denver also has a lot of available data for it because many of the sensing companies are located there.

Eguchi would like to know what the role of government is.

Hayes said that there is a lack of champions.

Zeizel said that the Federal Government needs to put funding to this area, but believes that there needs to be more public private collaboration.

Shinozuka gave some closing remarks and wrap-up.

Appendix B

Workshop Information

Agenda

Participants Roster

Program Chairs and Speakers

Program for Workshop on Mitigation of Earthquake Disaster by Advanced Technologies (MEDAT-1)

Radisson Hotel Midtown, Los Angeles

March 2 (Thursday) and 3 (Friday), 2000

Sponsors: Multidisciplinary Center for Earthquake Engineering Research (MCEER)
National Science Foundation (NSF)
International Institute for Innovative Risk Reduction Research on Civil Infrastructure Systems (I^3R^3CIS)

Conference Co-Chairs: **M. Shinozuka, D. J. Inman and T. D. O'Rourke**

March 1, 2000

18:00- 19:30 **Icebreaker**

March 2, 2000

9:00 - 9:30 **Registration**

9:30 – 10:00 **Opening Remarks - C.L. Wellford, T. D. O'Rourke and M. Shinozuka**

10:00 - 11:30 **Session 1 Condition Monitoring and Response Control**
Chairs: **M. Bruneau and M. Zako**

Paper 1 "Advanced Energy Dissipation Technologies for Seismic Protection of Civil Structures" by **G.Lee**

Paper 2 "Soil Reinforcement for Seismic Retrofitting and Liquefaction Mitigation" by **I. Juran**

Paper 3 "Advanced Sensors for Condition Monitoring and Damage Assessment for Civil Structures" by **M. Feng**

11:30 – 13:00 **Lunch**

13:00 - 14:00 **Session 2 Damage Assessment and Detection by Advanced Technologies**
Chairs: **A.E. Aktan and S. Masri**

Paper 4 "Advanced Accelerometers and Liquefaction Meters for Damage Assessment of Gas Distribution Systems", by **Y. Shimizu**

Paper 5 "Detection of Damage Location and Extent of Water Supply Systems" by **M. Shinozuka**

Paper 6 " SAR Technology Applications in Structural Damage Detection" by **R. Ghanem**

14:30 - 15:30 **Session 3 System Identification**
Chairs: **A. Mita and A. Smyth**

Paper 7 "Seismic Response Measurement and System Identification of Bridges" by **C. H. Loh**

Paper 8 "Nonlinear System Identification" by **T. Sato**

15:30 – 16:00 **Break**
16:00 – 18:00 **Discussion Forum**
Chairs: **W. Hayes and D. J. Inman**

19:00 - 21:00 **Banquet at the Radisson Hotel**
End of Day 1

March 3, 2000

9:30 - 11:30 **Session 4 Application of SCADA (Supervisory Control and Data Acquisition) Systems for Lifeline Networks**
Chairs: **T.C. Chang and F. De Flaviis**

Paper 9 "Wireless Data Acquisition and Assessment of Post-Earthquake Lifeline Performance" by **S. Mizushina**

Paper 10 "LAWSDAC for Los Angeles DWP Water System" by **J. McDaniel**

Paper 11 "SCADA Applications for Los Angeles DWP Power System", by **M. Nakao**

Paper 12 "SCADA Applications for Power Distribution Systems", by **R. Wiesman**

11:30 – 13:00 **Lunch**
13:00 - 14:30 **Session 5 GIS and Remote Sensing**
Chairs: **J. Wilson and Eric Johnson**

Paper 13 " Remote Sensing Technologies for Urban Earthquake Disaster Assessment ; Earthquakes in USA and Turkey " by **R. Eguchi**

Paper 14 " Remote Sensing Technologies for Urban Earthquake Disaster Assessment ; Earthquakes in Japan and Taiwan" by **M. Matsuoka**

Paper 15 " Advanced GIS Applications for Earthquake Disaster Mitigation" by **S. Kakumoto**

14:30 – 15:00 **Break**

15:00 – 17:00 **Discussion Forum**
Chairs: **L. Lund and A. Zeizel**

17:00 - 17:15 **Closing Remarks - D. J. Inman and M. Shinozuka**

End of Day 2

MEDAT-1
Participants List

Atsushi Adachi
Hamamutso Research Center
Phone: 81-53-445-3221
Fax: 81-53-445-3222
email: a-adachi@tcp-ip.or.jp

A. E. Aktan, Director
Drexel Intelligent Infrastructure and Transportation Safety Institute
John Roebling Professor of Infrastructure Studies
Drexel University
3201 Arch Street, Suite 240
Philadelphia, PA 19104
Phone: 215-895-6134, 6135
Fax: 215-895-6131
email: aaktan@mail.drexel.edu
URL:
http://www.drexel.edu/academics/institutes/di3

Michel Bruneau, Deputy Director
Multidisciplinary Center for Earthquake Engineering Research (MCEER)
Professor, Department of Civil, Structural and Environmental Engineering
105 Red Jacket
State University of New York at Buffalo
Buffalo, New York 14261-0025
Phone: (716) 645-3391 x104
Fax: (716) 645-3399
email: bruneau@acsu.buffalo.edu
URL:
http://www.civil.buffalo.edu/cie/people/faculty/bruneau/bruneau.html

Ruchira Buragohain
University of Southern California
3620 S. Vermont, Kaprielian Hall
KAP210
Los Angeles CA, 90089-2531
Phone: 213-740-4582
Fax: 213-740-4045 Fax
email: buragoha@usc.edu

F. Necati Catbas
Drexler University
Phone: 215-895-5947
Fax: 215-895-6121 Fax
email: fnc23@mail.drexel.edu

T. C. Cheng, Lloyd F. Hunt Professor
Electrical Engineering/Electrophysics
Department of Electrical Engineering
University of Southern California
Los Angeles, CA 90089-0271
Phone: 213-740-4712
Fax: 213-740-8677
email: cuason@mizar.usc.edu

Howard Chung
University of Southern California
3620 S. Vermont, Kaprielian Hall
KAP210
Los Angeles CA, 90089-2531
Phone: 213-740-6132
Fax: 213-740-4045 Fax
email: hungchic@usc.edu

Andrea S. Dargush, Assistant Director for Education and Research Administration
Multidisciplinary Center for Earthquake Engineering Research (MCEER)
107 Red Jacket Quadrangle
State University of New York at Buffalo
Buffalo, New York 14261-0025
Phone: 716-645-3391 ext. 106
Fax: 716-645-3399
email: dargush@acsu.buffalo.edu

Franco De Flaviis, Assistant Professor
Department of Electrical and Computer Engineering
Room 416C, Engineering Tower
University of California
Irvine, CA 93697-2625
Phone: 949-824-5631
Fax: 949-824-2321
email: franco@uci.edu

Xuejiang Dong
University of Southern California
3620 S. Vermont, Kaprielian Hall
KAP210
Los Angeles CA, 90089-2531
Phone: 213-740-4245
Fax: 213-740-4045 Fax
email: xdong@usc.edu

Ronald Eguchi, Vice President
Image Cat Inc.
Union Bank of California Building
400 Oceangate, Suite 305
Long Beach, CA 90802
Phone: 562-628-1675
Fax: 562-628-1676
email: rte@imagecatinc.com

Asadollah Esmaeily
University of Southern California
3620 S. Vermont, Kaprielian Hall
KAP210
Los Angeles CA, 90089-2531
Phone: 213-740-0575
Fax: 213-744-1426 Fax
email: esmaeily@usc.edu

Amir Hossein Fassihi
University of Southern California
3620 S. Vermont, Kaprielian Hall
KAP210
Los Angeles CA, 90089-2531
Phone: 323-735-1470
Fax: 213-744-1426 Fax
email: fassihi@usc.edu

Maria Q. Feng, Associate Professor
Dept. of Civil & Environmental Eng.
E4139, Engineering Gateway
University of California
Irvine, CA 92697-2175
Phone: 949-824-2162
Fax: 949-824-2117
email: mfeng@uci.edu

Roger Ghanem, Associate Professor
Department of Civil Engineering
The Johns Hopkins University
201 Latrobe Hall
Baltimore, MD 21218
Phone: 410-516-7647
Fax: 410-516-7473
email: ghanem@jhu.edu

Lori Graham, Professor
Department of Civil Engineering
University of Virginia
Charlottesville, VA 22903
Phone: 804-924-3930
Fax: 804-982-2951
email: graham@virginia.edu
llg3s@cms.mail.virginia.edu

Walter Hays, Senior Program Manager
Technical and International Activities
ASCE World Headquaters
1801 Alexander Bell Drive
Reston, VA 20191-4400
Phone: 703-295-6054
email: whays@asce.org

Howard H. M. Hwang, Research Professor
Center for Earthquake Research &
Information
University of Memphis
3890 Central Ave
Memphis, TN 38152
Phone: 901-678-4830
Fax: 901-678-4734
email: hwang@ceri.memphis.edu

Daniel Inman, Herrick Professor of
Engineering Science and Mechanics
219 Norris Hall
Virginia Polytechnic Institute
Blacksburg, VA 24061-0219
Phone: 540-231-4709
Fax: 540231-4574
email: Dinman@vt.edu

Xianhe Jin
University of Southern California
Phone: 213-740-4920
Fax: 213-740-8877
email: xianjin@usc.edu

Erik A. Johnson, Assistant Professor
Department of Civil Engineering
University of Southern California
Los Angeles CA 90089-2351
Phone: 213-740-0610
email: Johnsone@usc.edu

Ilan Juran, Professor and Director
Dept. of Civil & Environmental Eng
Polytechnic University of NY
6 Metrotech Center
Brooklyn, NY 11201
Phone: 718-260-3633
Fax: 718-260-3433
email: ijuran@poly.edu

Shigeru Kakumoto, Visiting Researcher
Disaster Prevention Research Institute
Kyoto University
Chief Researcher
Hitachi Ltd. Central Research Laboratory
1 - 280 Higashikoigakubo, Japan
Phone: 81-42-323-1111 X 3640
Fax : 81-42-327-7825
email: kaku@aa.mbn.or.jp

Nick Kezman, Superintendent Substation
Protection and RTU
Los Angeles Department of Water and
Power
Phone: 213-367-7295
Fax: 213-367-7614

Chul-Young Kim
Myongji University, Korea
Phone: 335-33-6413
Fax: 335-336-9705 Fax
email: cykim@wh.myongji.kr

Hokyung Kim, Visiting Scholar
University of Southern California - RRI -
Phone: 213-740-9756
Fax: 213-740-4045
email: hokyoungk@mizar.usc.edu

George Lee, Director
Multidisciplinary Center for Earthquake
Engineering Research (MCEER)
S.P. Capen Professor of Engineering
State University of New York at Buffalo
Red Jacket Quad
Buffalo, NY 14261-0025
Phone: 716-645-3391
Fax: 716-645-3399
email: gclee@mceermail.buffalo.edu

Ching-Hsiung Loh, Director
National Center for Research on Earthquake
Engineering
Professor, Department of Civil Engineering
National Taiwan University
Taipei, Taiwan ROC
Phone: 02-3623356
Fax:02-3631558
email: Lohc@ncree.gov.tw

LeVal Lund
3245 Lowry Road
Los Angeles, CA 90027
Phone: 213-664-4432
email: Lundasan@earthlink.net

Sami Masri, Professor
Department of Civil Engineering
University of Southern California
Los Angeles, CA 90089
Phone: 213-740-0602
Fax: 213-744-1426
email: masri@vivian2.usc.edu

Masashi Matsuoka
Earthquake Disaster Mitigation Research Center
Mikiyama 2465-1, Fukui, Miki
Hyogo 673-0433, Japan
Phone: (+81) 794-83-6632
Fax: (+81) 794-83-6695
email: matsuoka@miki.riken.go.jp
URL:
www.miki.riken.go.jp/pages/staff_e.html

James McDaniel, Director of Water Quality and Operations
Los Angeles Department of Water and Power
Phone: 213-367-1050
Fax: 213-367-0038
email:
James.McDaniel@water.LADWP.com

Najmedin Meshkati, Associate Professor
Department of Civil Engineering
University of Southern California
Los Angeles, CA 90089-
Phone: 213-740-8765
Fax: 213-740-8789
email: meshkati@mizar.usc.edu

Akria Mita
Institute of Technology
Shimizu Corporation
3-4-17 Etchujima, Koto-Ku
Tokyo 135-8530, Japan
Phone: 81-3-3820-5536
Fax: 81-3-3820-5959
email: mita@sit.shimz.co.jp

Shizuo Mizushina, Director
Hamamatsu Lifeline Research Center
Professor Emeritus, Shizuoka University
800-8 Tomitsuka-cho, Hamamatsu-city
Shizuoka Prefecture 432-8002, Japan
Phone: +81 53 471 2441
Fax: +81 53 471 2446
email: smizu@mail.yaramaika.ne.jp

Farzad Naeim
John A. Martin Association Inc.
Phone: 213-483-6490
Fax: 213-483-3048 Fax
email: farzad@johnmartin.com

Mark Nakao, RTU Field Supervisor
Los Angeles Department of Water and Power
Phone: 213-367-7614
Fax: 213-367-7302
email: mnakao@dwp.ci.la.ca.us
mark nakao/isf/ladwp@ladwp.com

Thomas D. O'Rourke, Professor
School of Civil & Envir. Engrg
265 Hollister Hall
Cornell University
Ithaca, NY 14853-3501
Phone: 607-255-6470
Fax: 607-255-9004
email: tdo1@cornell.edu

Takayosh Rachi
Tokyo Gas Company
Phone: 81-3-5322-8225
Fax: 81-3-5322-8215 Fax
email: rachi@tg-inet.co.jp

Ali Rejaie, Research Assistant
International Institute for Innovative Risk Reduction Research on Civil Infrastructure Systems (I^3R^3CIS)
Department of Civil Engineering
University of Southern California
Los Angeles, CA 90089-2531
Phone: 213-740-4582
Fax: 213-740-4045
email: rejaiesh@usc.edu
URL: www-scf.usc.edu/~rejaiesh

Tadanobu Sato, Professor
Disaster Prevention Research Institute
Kyoto University
Uji, Kyoto 611-0011, Japan
Phone: +81-774-38-4065
Fax:+81-774-38-4070
email: sato@catfish.dpri.kyoto-u.ac.jp

Yoshihisa Shimizu, Senior Manager
Center for Disaster Management and Supply Control
Tokyo Gas Co., Ltd.
5-20 Kaigan 1-chome
Minato-ku, Tokyo 105-8527 Japan
email: yshimizu@tokyo-gas.co.jp

Masanobu Shinozuka, Director
International Institute for Innovative Risk Reduction Research on Civil Infrastructure Systems (I^3R^3CIS)
Fred Champion Professor
Department of Civil Engineering
University of Southern California
Los Angeles, CA 90089-2531
Phone: 213-740-9528
Fax: 213-740-9529
email: shino@usc.edu

Andrew Smyth, Assistant Professor
Department of Civil Engineering and Engineering Mechanics
Columbia University
New York, N.Y. 10027
Phone: 212-854-3369
Fax: 212-854-6267
email: smyth@civil.columbia.edu

Pol Spanos
Rice University
Phone: 713-348-4909
Fax: 713-348-5191 Fax
email: spanos@rice.edu

Shahram Taghavi
University of Southern California
3620 S. Vermont Kaprielian Hall
KAP210
Los Angeles CA 90089-2531
Phone: 213-740-2036
Fax: 213-744-1426 Fax
email: taghavia@usc.edu

Farzad Tasbihgo
University of Southern California
3620 S. Vermont Kaprielian Hall
KAP210
Los Angeles CA 90089-2531
Phone: 213-740-2036
Fax: 213-744-1426 Fax
email: tasbihgo@usc.edu

Carter L. Wellford, Professor and Chairman
Department of Civil Engineering
University of Southern California
Los Angeles, CA 90089-2531
Phone: 213-740-0609
Fax: 213-744-1426
email: wellford@alnitak.usc.edu

Richard Wiesman
Foster - Miller Inc.
350 Second Avenue
Waltham, MA 02451
Phone: 981-684-4387
email: rwiesman@foster-miller.com

John Wilson, Chairman
Department of Geography
University of Southern California
Los Angeles, CA 90089
Phone: 213-740-1908
Fax: 213-740-0056
email: uscgeog@usc.edu

James G. Yannotta
LADWP
Phone: 213-367-1001
Fax: 213-367-1061 Fax
email: James.Yannotta@water.ladwp.com

Shy-Chin Yeh
National Center for Research on Earthquake Engineering
Phone: 8862-2732-6607
Fax: 8862-2732-2223 Fax
email: luke@email.ncree.gov.tw

Masaru Zako, Professor
School of Engineering
Osaka University
2-1, Yamada-oka
Suita-shi, Osaka-fu 565, Japan
Phone: 81-6-6879-7563
Fax: 81-6-6879-7570
email: zako@mapse.eng.osaka-u.ac.jp
URL: http://www.mapse.eng.osaka-u.ac.jp/w8/

Farzin Zareian
University of Southern California
3620 S. Vermont Kaprielian Hall
KAP210
Los Angeles CA 90089-2531
Phone: 213-740-2036
Fax: 213-744-1426 Fax
email: zareian@usc.edu

Arthur J. Zeizel, Director
Center For Disaster Loss-Reduction
Futures Institute For Sustainable
Development
Washington, D.C.
Phone: 301-229-2378
email: azeizel@att.net

Ruichong Zhang, Assistant Professor
Division of Engineering
Colorado School of Mines
Golden, CO 80401-1887
Phone: 303-273-3671
Fax: 303-273-3602
email: rzhang@mines.edu
URL:
http://www.mines.edu/fs_home/rzhang

Program Chairs and Speakers

March 2, 2000

Carter L. Wellford	Opening Remarks
Daniel J. Inman	Opening Remarks
Masanobu Shinozuka	Opening Remarks
Micheal Bruneau	Chair, Sesion 1
Masaru Zako	Chair, Session 1
George C. Lee	Speaker, Paper 1
Ilan Juran	Speaker, Paper 2
Maria Feng	Speaker, Paper 3
A. Emin Aktan	Chair, Sesion 2
Sami Masri	Chair, Sesion 2
Yoshihisa Shimizu	Speaker, Paper 4
Masanobu Shinozuka	Speaker, Paper 5
Roger Ghanem	Speaker, Paper 6
Akira Mita	Chair, Session 3
Andrew Smyth	Chair, Session 3
Chin H. Loh	Speaker, Paper 7
Tadanobu Sato	Speaker, Paper 8
Walter Hayes	Chair, Discussion Forum
Daniel J. Inman	Chair, Discussion Forum
Andrew Smyth	Transcriptions

March 3, 2000

T. C. Cheng	Chair, Session 4
Franko De Flaviis	Chair, Session 4
Shizuo Mizushina	Speaker, Paper 9
James McDaniel	Speaker, Paper10
Mark Nakao	Speaker, Paper 11
Richard Wiesman	Speaker, Paper12
John Wilson	Chair, Session 5
Erik A. Johnson	Chair, Session 5
Ron Eguchi	Speaker, Paper 13
Masashi Matsuoka	Speaker, Paper 14
Shigeru Kakumoto	Speaker, Paper 15
Leval Lund	Chair, Discussion Forum
Arthur J. Zeizel	Chair, Discussion Forum
Lori Graham	Transcriptions
Masanobu Shinozuka	Closing Remarks

MULTIDISCIPLINARY CENTER FOR EARTHQUAKE ENGINEERING RESEARCH

A National Center of Excellence in Advanced Technology Applications

University at Buffalo, State University of New York
Red Jacket Quadrangle ▪ Buffalo, New York 14261-0025
Phone: 716/645-3391 ▪ Fax: 716/645-3399
E-mail: mceer@acsu.buffalo.edu ▪ WWW Site: http://mceer.buffalo.edu